VOLUME 87 NO. ST6
AUGUST 1961

JOURNAL of the

Structural Division

PROCEEDINGS OF THE

AMERICAN SOCIETY
OF CIVIL ENGINEERS

BASIC REQUIREMENTS FOR MANUSCRIPTS

Original papers and discussions of current papers should be submitted to the Manager of Technical Publications, ASCE. Authors should indicate the technical division to which the paper is referred. The final date on which a discussion should reach the Society is given as a footnote with each paper. Those who are planning to submit material will expedite the review and publication procedures by complying with the following basic requirements:

1. Titles must have a length not exceeding 50 characters and spaces.

2. A summary of approximately 50 words must accompany the paper, a 300-word synopsis must precede it, and a set of conclusions must end it.

3. The manuscript (an original ribbon copy and two duplicate copies) should be double-spaced on one side of 8½-inch by 11-inch paper. Three copies of all illustrations, tables, etc., must be included.

4. The author's full name, Society membership grade, and footnote reference stating present employment must appear on the first page of the paper.

5. Mathematics are recomposed from the copy that is submitted. Because of this, it is necessary that letters be drawn carefully, and that special symbols be properly identified. The letter symbols used should be defined where they first appear, in the illustrations or in the text, and arranged alphabetically in an Appendix.

6. Tables should be typed (an original ribbon copy and two duplicate copies) on one side of 8½-inch by 11-inch paper. Specific illustrations and explanation must be made in the text for each table.

7. Illustrations must be drawn in black ink on one side of 8½-inch by 11-inch paper. Because illustrations will be reproduced with a width of between 3-inches and 4½-inches, the lettering must be large enough to be legible at this width. Photographs should be submitted as glossy prints. Explanations and descriptions must be made within the text for each illustration.

8. The desirable average length of a paper is about 12,000 words and the absolute maximum is 18,000 words. As an approximation, each full page of typed text, table, or illustration is the equivalent of 300 words.

9. Technical papers intended for publication must be written in the third person.

10. The author should distinguish between a list of "Reading References" and a "Bibliography," which would encompass the subject of his paper.

This Journal is published bi-monthly by the American Society of Civil Engineers. Publication office is at 2500 South State Street, Ann Arbor, Michigan. Editorial and General Offices are at 33 West 39 Street, New York 18, New York. $4.00 of a member's dues are applied as a subscription to this Journal. Second-class postage paid at Ann Arbor, Michigan.

The index for 1959 was published as ASCE Publication 1960-10 (list price $2.00); indexes for previous years are also available.

Vol. 87 No. ST 6

Journal of the
STRUCTURAL DIVISION
Proceedings of the American Society of Civil Engineers

CONTENTS

August, 1961

Papers

(over)

The three preceding issues of this Journal are dated March 1961, April 1961, and June 1961.

DISCUSSION

Journal of the
STRUCTURAL DIVISION
Proceedings of the American Society of Civil Engineers

TORSIONAL BEHAVIOR OF SUSPENSION BRIDGE TOWERS

By Frank Baron,[1] F. ASCE and Anthony G. Arioto,[2] A. M. ASCE

SYNOPSIS

An interpretive study is presented of the influences of different variables on the torsional behaviors of suspension bridge towers. General and specific classes of towers are considered. Among the variables are the numbers of struts, proportions of panels, and relative sizes of legs and struts. Dimensionless ratios are used to relate the behaviors.

INTRODUCTION

The torsional characteristics of suspension bridge towers are of interest in studies dealing with the effects of (a) traffic loads on one side of the roadway, and (b) aerodynamic forces which tend to twist the roadway of a bridge. Each of these loading conditions produces a torque at the top of a tower about the longitudinal axis of the tower. The torque produces an angle of twist and it is the result of the unbalanced horizontal components of cable tension at the top of the tower. Its magnitude is dependent on the characteristics of the loads and of the bridge. With reference to those of the bridge, the torque on a tower is dependent on the torsional rigidity of the tower and on the relative resistances of the side and center span cables to displacements at the top of the tower.

The torsional rigidities of the towers can influence the deformations of the towers, the roadway, the stiffening trusses, and the bracing elements of

Note.—Discussion open until January 1, 1962. To extend the closing date one month, a written request must be filed with the Executive Secretary, ASCE. This paper is part of the copyrighted Journal of the Structural Division, Proceedings of the American Society of Civil Engineers, Vol. 87, No. ST 6, August, 1961.

[1] Prof. of Civ. Engrg., Univ. of California, Berkeley, Calif.
[2] Assoc. Civil Engr., County of Santa Clara, Calif.

the roadway system of a bridge. The influence of these factors has been presented in (a) a report of the Chief Engineer[3] of the Golden Gate Bridge, and (b) in the reports of the Boards of Engineers[4] appointed to study the causes of failure in the first Tacoma Narrows Bridge. A summary of these studies was given in a previous paper by the writers.[5]

The torsional rigidities of towers and with the distributions of bending moments, twisting moments, and shears in the legs and struts of the towers are analyzed. Two groups of towers are considered. One group consists of actual towers, specifically those of the Golden Gate Bridge, the first Tacoma Narrows Bridge, and the Walt Whitman Bridge. The other group consists of hypothetical towers. Among the variables are the height to width ratio of a tower, the number of struts in the tower, and the flexural and torsional rigidities of the legs and struts.

Results obtained from an analytical procedure, presented elsewhere,[5] for determining the torsional characteristics of towers are given. The procedure consists of beginning at the base of a tower and obtaining successive statical and geometrical relationships at each section of the tower until the top of the tower is reached. For the actual towers, the procedure was adjusted to consider the effects of the vertical saddle reactions at the tower tops, variations in I and J of the legs, and variations in the horizontal distances between the legs.

The notations are the same as those listed previously,[5] except for a few modifications where necessary. The notations for the actual towers and the hypothetical towers are illustrated in Figs. 1(a) and 1(b), respectively. The most significant notations are as follows:

b = horizontal distance between center lines of legs or center lines of cables.

h_s = total height of tower;

h_{01} = height of a panel at the base of a tower;

r = number of struts in a tower;

E = Young's modulus = 30×10^3 k in.$^{-2}$;

$G = \frac{E}{2(1 + \mu)}$ = shearing modulus, in which μ is Poisson's ratio ($\mu = 0.3$);

I = moment of inertia (Subscripts designate axis, location of section, or kind of member);

$G\,J$ = torsional rigidity of a member, in which J is taken about the appropriate axis of the member;

---

3 "The Golden Gate Bridge," by Joseph B. Strauss, Bd. of Directors, Golden Gate Bridge and Highway Dist., California, September, 1937, pp. 90–107.

4 "The Failure of the Tacoma Narrows Bridge," Texas Engrg. Experiment Sta., Bulletin No. 78, 1944. Part (a): Report to John M. Carmody by Bd. of Engrs., Othmar H. Amman, Theodore von Kármán, and Glenn B. Woodruff, March 28, 1941, pp. 61, 62, 125, and 133. Part (b): Reports to Paul Carew by Bd. of Narrows Bridge Loss Committee, Clifford E. Paine, Chmn., Hardy Cross, Shortridge Hardesty, Holton D. Robinson, and Wilbur M. Wilson, June 2, 1941, pp. 42–48. Part (c): Report to James A. Davis by Bd. of Investigation, Tacoma Narrows Bridge, L. J. Sverdrup, Chmn., Francis Donaldson, and Russell G. Cone, Part 1, February 2, 1941 to March 4, 1941; Part 2, June 26, 1941; Part 3, January 26, 1941.

5 "Torsional Analysis of Suspension Bridge Towers," by Frank Baron and Anthony G. Arioto, Proceedings, ASCE, Vol. 86, No. ST 1, January, 1960, pp. 143–169.

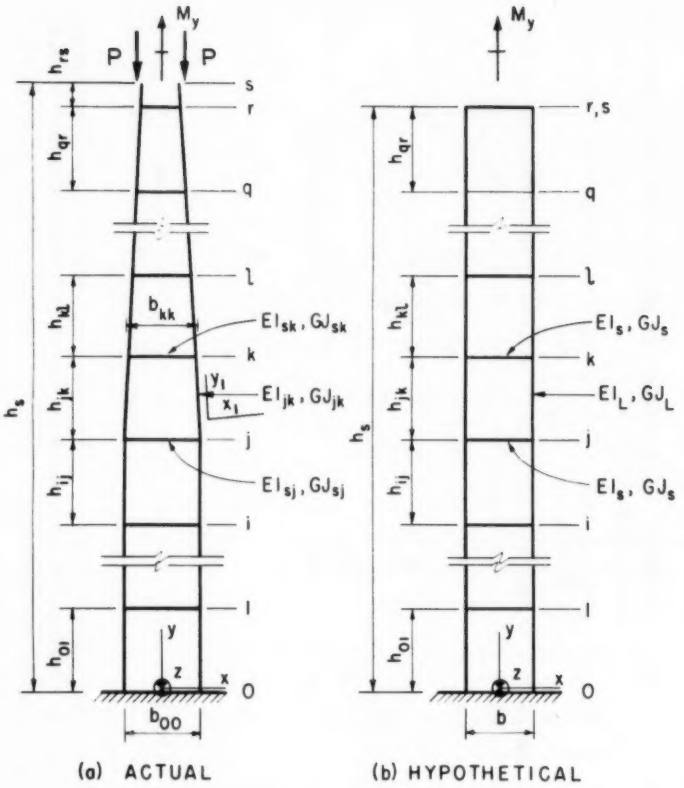

FIG. 1.—DIMENSIONS

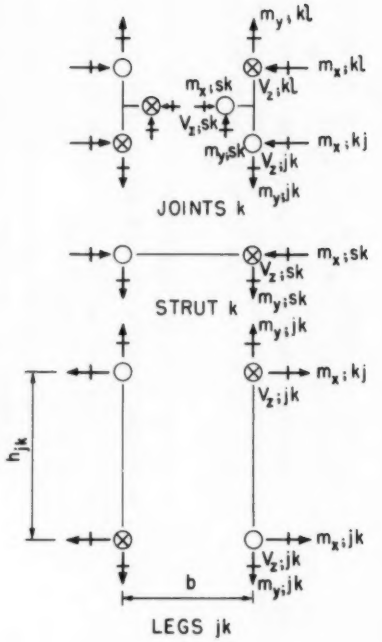

FIG. 2.—SIGNS

EI = flexural rigidity of a member, in which I is taken about the appropriate axis of the member;

$G J_{tow} = \frac{M_y h_s}{\psi_y}$ = torsional rigidity of the entire tower;

v_z = transverse shear along the z-axis (Additional subscripts designate the section or member);

m_x, m_y = bending moments or twisting moments about x and y axes, respectively, depending on whether the member is a leg or a strut (Additional subscripts designate the section or member);

M_y = torque about the longitudinal axis of the tower;

P = vertical reaction at each saddle of the tower;

P_{DL} = vertical reaction at each saddle, caused by the dead load of the suspended system;

P_e = an Euler buckling load selected as a reference for each leg of a tower (The buckling load is for a leg fixed at the base and free at the top. Bending is about the x-axis);

Δ_z = deflection of a saddle, relative to the base and in the z-direction; and

ψ_y = angle of twist of a horizontal chord at the top of the tower, relative to the base and about the y-axis.

In the section of the paper which deals with the hypothetical towers, additional notations are used, giving dimensionless ratios as follows:

$$a_1 = \frac{E I_L}{G J_L} \quad \ldots\ldots\ldots\ldots\ldots \quad (1a)$$

$$a_2 = \frac{E I_s}{E I_L} \quad \ldots\ldots\ldots\ldots\ldots \quad (1b)$$

$$a_3 = \frac{G J_s}{G J_L} \quad \ldots\ldots\ldots\ldots\ldots \quad (1c)$$

and

$$a_4 = \frac{h}{b} \quad \ldots\ldots\ldots\ldots\ldots \quad (1d)$$

In Eq. 1, the subscripts s and L refer to the struts and legs of the towers, respectively. Note that h is the same for each panel of an hypothetical tower, h/b is the height-to-width ratio of the panel, an h/s = r h for an hypothetical tower.

The sign convention is illustrated in Fig. 2. The shears are represented as force vectors along the z-axis and the moments are moment vectors about the

x and y-axes. A positive angle of twist ψ_y is associated with a positive torque M_y.

TORSIONAL CHARACTERISTICS OF ACTUAL TOWERS

The towers are those of the Golden Gate Bridge, the first Tacoma Narrows Bridge, and the Walt Whitman Bridge. These towers were selected for study because of the wide range which they represent in tower parameters. The only comparisons that are made are those concerning the torsional characteristics

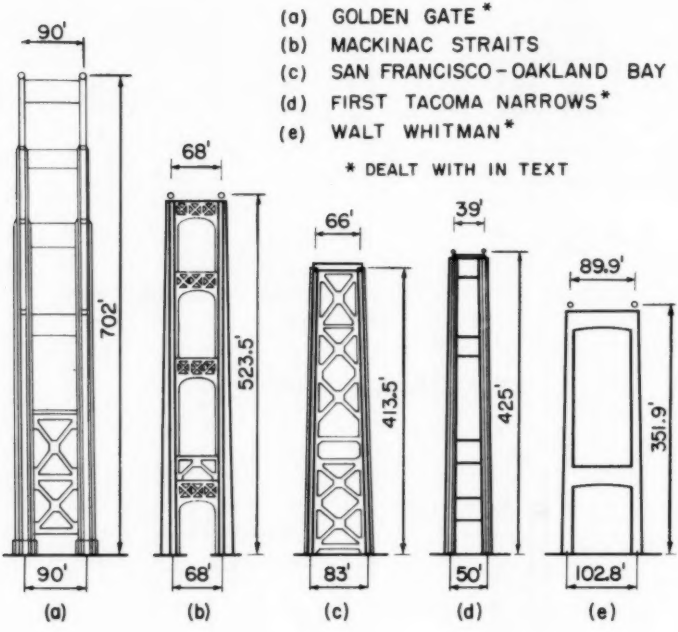

FIG. 3.—OUTLINES

of the three towers. Obviously, the design of each tower is based on many considerations besides those of torsion.

Description of the Towers.—The outlines and over-all dimensions of the three towers are shown in Fig. 3. If additional details are desired, the reader is referred to the plates and figures which are given elsewhere.[6,7,8] Each

6 "The Golden Gate Bridge," by Joseph B. Strauss, Bd. of Directors, Golden Gate Bridge and Highway Dist., California, September, 1937, pp. 90-107, Plates V to IX.

7 "The Failure of the Tacoma Narrows Bridge," Texas Engrg. Experiment Sta., Bulletin No. 78, 1944, Part (c), Figs. 2, 5, 5(a); Part (b), Fig. 2.

8 "Anchorages and Superstructure of Walt Whitman Bridge," by Homer R. Seely, Civil Engineering, February, 1956, pp. 52-57.

tower is composed of legs which are vertical and two or more horizontal struts. The legs of each tower are cellular in form and vary in cross-section from the base to the top of the tower. The cross-sections at the bases of the towers are illustrated in Fig. 4. The variation in cross-section along the length of a tower is affected in two ways; first, by a change in the thickness of the plates and in the sizes of the angles; second, (a) by a change in the number of cells for the Golden Gate towers, (b) by a change in the transverse dimensions of the legs and a change in the number of cells for the first Tacoma Narrows

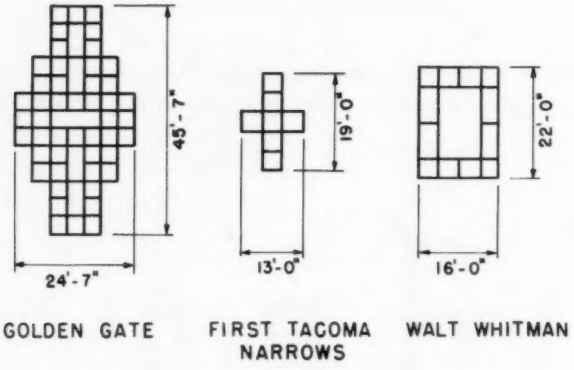

FIG. 4.—CROSS-SECTIONS OF LEGS

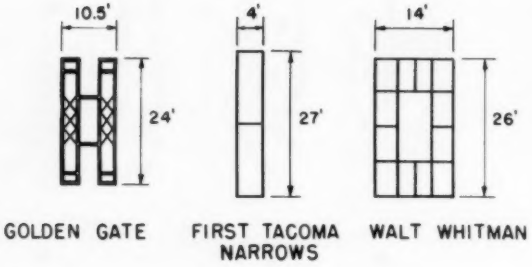

FIG. 5.—CROSS-SECTIONS OF STRUTS

towers, and (c) by a change in the transverse dimensions of the legs for the Walt Whitman towers.

The numbers and cross-sections of the struts are different for the three towers and are illustrated in Figs. 5 to 8. The struts of the Golden Gate towers are composed of trusses, whereas those of other towers are composed of thin-walled cells. The trusses of the three top struts of the Golden Gate Bridge towers are laced together in pairs. It is reported[3] that the lacing of the web members was increased as a result of an investigation of the effects of a torsion.

Dimensions and Properties of Towers.—A summary is given in Table 1 of the panel proportions and of the horizontal and vertical dimensions of the towers.

Other factors which influence the torsional characteristics of the towers are the values of E I and G J of the various members. The values of E I and G J are

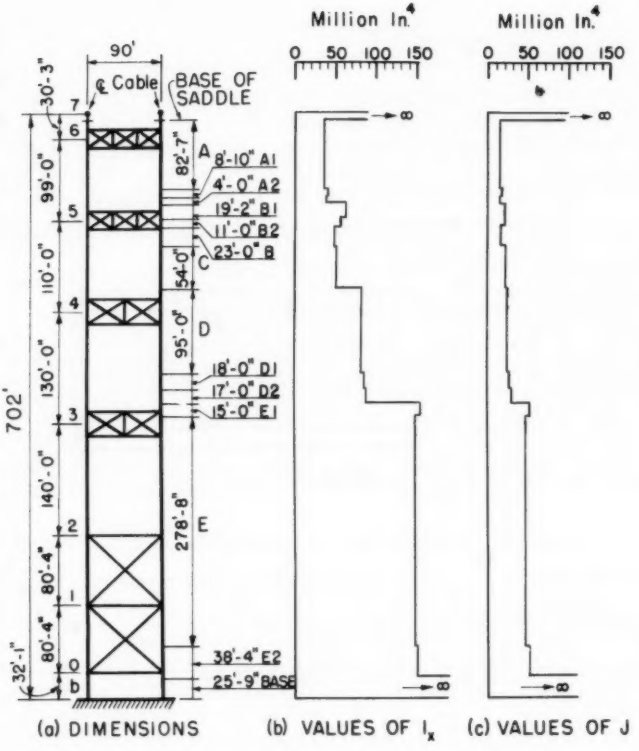

FIG. 6.—GOLDEN GATE TOWERS

measures of the flexural and torsional stiffnesses of an element of a member to unit deformations. They are evaluated as follows: For a leg

$$E I_{x1} = \frac{m_{x1}}{\frac{\Delta \phi_{x1}}{ds}} \quad \ldots\ldots\ldots\ldots\ldots \quad (2)$$

and

$$G J_{y1} = \frac{m_{y1}}{\frac{\Delta \phi_{y1}}{ds}} \quad \ldots\ldots\ldots\ldots\ldots \quad (3)$$

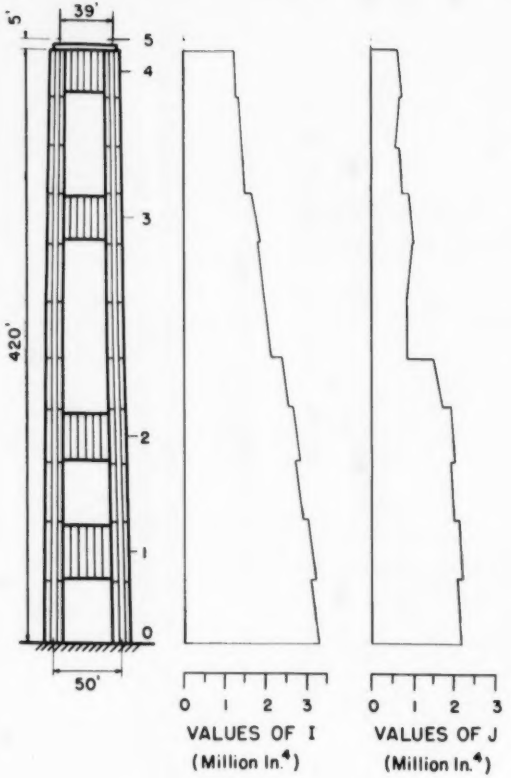

FIG. 7.—TACOMA NARROWS TOWERS

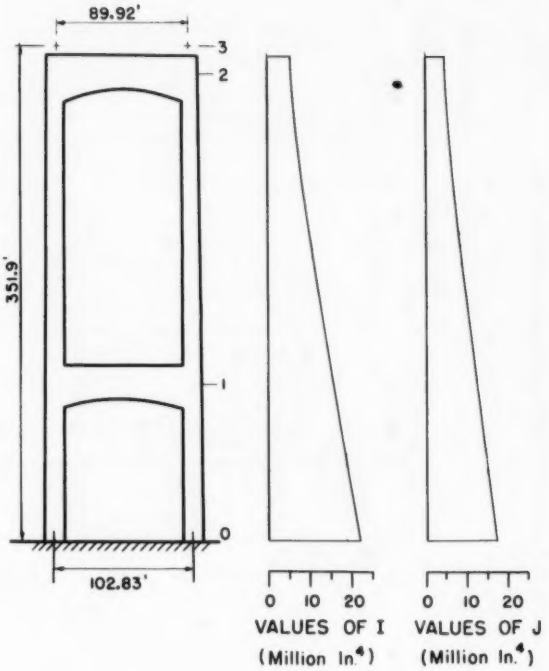

FIG. 8.—WALT WHITMAN TOWERS

and for a strut

$$E I_y = \frac{m_y}{\frac{\Delta \phi_y}{ds}} \quad \ldots\ldots\ldots\ldots\ldots (4)$$

and

$$G J_x = \frac{m_x}{\frac{\Delta \phi_x}{ds}} \quad \ldots\ldots\ldots\ldots\ldots (5)$$

In Eqs. 2 to 5, the subscripts refer to the axes that are shown in Fig. 1.

Values of A, I, and J were computed for the top and bottom sections of every tier in the legs (Figs. 6 to 8), and for the ends and center cross-sections

TABLE 1.—SUMMARY OF TOWER DIMENSIONS

Towers	Heights, in ft				Widths, in ft		Ratios	
	h_s	h_{01}	h_{qr}	h_{rs}	b_{base}	b_{cable}	$\frac{h_{01}}{b_{base}}$	$\frac{h_{qr}}{b_{cable}}$
(1)	(2)	(3)	(4)	(5)	(6)	(7)	(8)	(9)
Golden Gate	702.0	80.3	99.0	30.3	90.0	90.0	0.89	1.10
First Tacoma Narrows	425.0	64.2	103.2	21.3	50.0	39.0	1.28	2.65
Walt Whitman	351.9	111.5	220.3	20.0	102.8	89.9	1.09	2.46

TABLE 2.—REPRESENTATIVE VALUES OF I AND J

Towers	Legs				Struts			
	Sec. 01 (Bottom) Values of		Sec. rq (Top) Values of		Strut 1 (Bottom) Values of		Strut r (Top) Values of	
	I_x (10^6in.^{4})	J (10^6in.^{4})	I_x (10^6in.^{4})	J (10^6in.^{4})	I_y (10^6in.^{4})	J (10^6in.^{4})	I_y (10^6in.^{4})	J (10^6in.^{4})
(1)	(2)	(3)	(4)	(5)	(6)	(7)	(8)	(9)
Golden Gate	148.	48.2	30.3	11.7	0.445	1.04	0.200	0.466
First Tacoma Narrows	3.31	2.21	1.35	0.683	0.257	0.386	0.204	0.290
Walt Whitman	22.2	16.9	6.60	5.37	12.3	18.7	5.77	10.7

of the struts. The distributions of the values of I and J along the legs of the towers are indicated in Figs. 6 to 8; and representative values of I and J are listed in Table 2. The representative values are for the midsections of the top and bottom struts, and for the top and bottom sections of the legs. Figs. 6 to 8 show that the values of I_L and J_L are greatest for the legs of the Golden Gate towers, and smallest for the legs of the first Tacoma Narrows towers. Table

2 shows that the stiffnesses of the struts relative to the stiffnesses of the legs are greatest for the Walt Whitman towers, and smallest for the Golden Gate towers.

The computations of I are based on the gross areas of the cross-sections. The computations of J are based on the gross areas of the sections minus one-half of the areas of the stiffener angles. In Table 2, equivalent values of I and J are given for the trussed struts of the Golden Gate towers.

The computations for J are based on the assumptions of the ordinary theory of torsion, and on the application of Bredt's formula[9,10] to each section of the towers. For example, consider the section that is shown in Fig. 9. The section is subjected to a total torque T, and is composed of walls of equal thickness and of five equal cells. The walls are so thin in proportion to the transverse dimensions of the cells that the shearing stresses f/t can be assumed uniformly

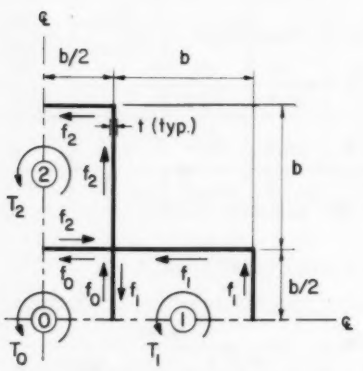

I/4 OF CROSS-SECTION IS SHOWN

FIG. 9.—TORQUE OF SECTION

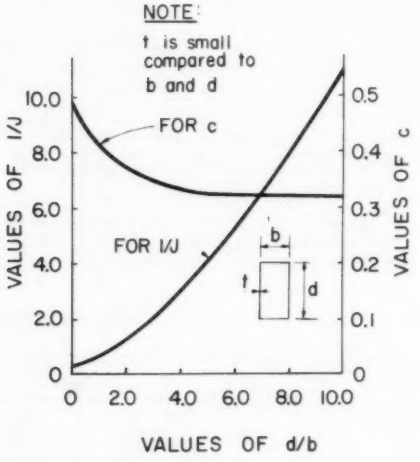

FIG. 10.—SINGLE CELL

distributed across the thicknesses of the walls. Buckling of the walls is not included in this study. A distribution of forces f per unit of length as shown in the figure satisfies the requirements of static equilibrium because the quantity of force f flowing into a junction equals the quantity of force f flowing away from the junction. In Fig. 9, torques are

$$T_0 = 2 f_0 b^2 \quad \ldots\ldots\ldots\ldots\ldots \quad (6)$$

$$T_1 = 2 f_1 b^2 \quad \ldots\ldots\ldots\ldots\ldots \quad (7)$$

9 "Theory of Elasticity," by S. Timoshenko, McGraw-Hill Book Co., New York, 1934, pp. 265–273.

10 "Torsion of Multiconnected Thin-Walled Cylinders," by Frank Baron, Journal of Applied Mechanics, ASME, June 1942, pp. A72–A74.

and

$$T_2 = 2 f_2 b^2 \quad \ldots\ldots\ldots\ldots\ldots \quad (8)$$

Because of the symmetry of the section, $T_1 = T_2$ and

$$T_{tot} = T_0 + 4 T_1 \quad \ldots\ldots\ldots\ldots\ldots \quad (9)$$

Bredt's formula is based on Hooke's Law and on the requirement of continuity of deformations along a closed path such as the periphery of a cell. The formula is given by

$$\oint \frac{f}{t} ds = 2 G a A_c \quad \ldots\ldots\ldots\ldots\ldots \quad (10)$$

in which A_c is the area within a closed circuit and α is a measure of the angle of twist per unit of length.

TABLE 3.—RELATIVE VALUES OF I AND J

Towers	Legs				Struts			
	Sec. 01 (Bottom) Values of		Sec. rq (Top) Values of		Strut 1 (Bottom) Values of		Strut r (Top) Values of	
	$\frac{I_x}{J}$	$\frac{EI_x}{GJ}$	$\frac{I_x}{J}$	$\frac{EI_x}{GJ}$	$\frac{I_y}{J}$	$\frac{EI_y}{GJ}$	$\frac{I_y}{J}$	$\frac{EI_y}{GJ}$
(1)	(2)	(3)	(4)	(5)	(6)	(7)	(8)	(9)
Golden Gate	3.07	7.99	2.58	6.71	0.427	1.11	0.429	1.11
First Tacoma Narrows	1.50	3.90	1.97	5.11	0.666	1.73	0.702	1.83
Walt Whitman	1.31	3.40	1.23	3.20	0.659	1.71	0.529	1.37

TABLE 4.—RANGES IN VALUES OF C AND I/J

Tower (1)	Legs		Cellular Struts	
	Values of c_x (2)	Values of I_x/J (3)	Values of C_y (4)	Values of I_y/J (5)
Golden Gate	$0.254 \leqq C_x \leqq 0.306$	$2.20 \leqq \frac{I_x}{J} \leqq 3.11$	...	...
First Tacoma Narrows	$0.234 \leqq C_x \leqq 0.263$	$1.35 \leqq \frac{I_x}{J} \leqq 2.40$	$0.475 \leqq C_y \leqq 0.485$	$0.666 \leqq \frac{I_y}{J} \leqq 0.704$
Walt Whitman	$0.331 \leqq C_x \leqq 0.347$	$1.22 \leqq \frac{I_x}{J} \leqq 1.31$	$0.345 \leqq C_y \leqq 0.358$	$0.534 \leqq \frac{I_y}{J} \leqq 0.654$

Application of Bredt's formula to each cell of the given section (Fig. 9) yields but two independent equations, namely

$$4 T_0 - 4 T_1 = 4 G a b^3 t \quad \ldots\ldots\ldots \quad (11)$$

and

$$4 T_1 - T_0 = 4 G a b^3 t \quad \ldots\ldots\ldots\ldots \quad (12)$$

TABLE 5.—SUMMARY OF MOMENTS AND SHEARS

Towers	Members		Case A			
			Values of			
			$\frac{m_x}{M_y}$	$\frac{bv_z}{M_y}$	$\frac{m_y}{M_y}$	$\frac{m_x}{M_y}$
(1)	(2)		(3)	(4)	(5)	(6)
Golden Gate	Leg	Sec. 01	1.32	0.184	0.408	0.432
		Sec. rq	-0.309	0.484	0.258	0.517
	Strut	Bot. (1)	0.006	-0.080	-0.040	0.864
		Top (r)	0.027	0.516	0.258	0.853
First Tacoma Narrows	Leg	Sec. 01	0.836	0.462	0.269	0.600
		Sec. rq	-0.268	-0.004	0.502	0.892
	Strut	Bot. (1)	0.068	-0.338	-0.169	1.31
		Top (r)	0.288	1.01	0.507	1.45
Walt Whitman	Leg	Sec. 01	0.851	0.615	0.193	0.523
		Sec. rq	0.245	0.368	0.316	0.633
	Strut	Bot (1)	0.411	-0.230	-0.115	1.33
		Top (r)	0.468	0.732	0.366	0.856

Solving these equations for T_0 and T_1, and substituting the results into Eq. 9 yields

$$T_{tot} = \frac{28}{3} G \alpha b^3 t \quad \ldots\ldots\ldots\ldots\ldots\ldots (13)$$

in which the angle of twist per unit of length is defined by

$$\alpha = \frac{T_{tot}}{G J} \quad \ldots\ldots\ldots\ldots\ldots\ldots (14)$$

Consequently, the value of J for the section is given by

$$J = \frac{28}{3} b^3 t \quad \ldots\ldots\ldots\ldots\ldots\ldots (15)$$

The determination of J because increasingly complex as the number of cells in a section increases, because of the corresponding increase in the number of simultaneous equations that must be solved.

Estimating the Properties of Other Towers.—Relationships were obtained between A, I, and J for the various sections of the towers. The relationships can be useful in estimating the properties of other towers and are summarized in Tables 3 and 4. In Table 3, the representative sections shown are the same as those in Table 2.

For the various sections, the values of I can be estimated by means of the equation

$$I = A r^2 \quad \ldots\ldots\ldots\ldots\ldots\ldots (16)$$

(P = 0) (BASED ON ACTUAL MOMENTS OF INERTIAS)

Case B		Case C			Case D		
Values of		Values of			Values of		
$\frac{bv_z}{M_y}$ (7)	$\frac{m_y}{M_y}$ (8)	$\frac{m_x}{M_y}$ (9)	$\frac{bv_z}{M_y}$ (10)	$\frac{m_y}{M_y}$ (11)	$\frac{m_x}{M_y}$ (12)	$\frac{bv_z}{M_y}$ (13)	$\frac{m_y}{M_y}$ (14)
0.968	0.016	2.05	0.234	0.383	7.81	1.00	0
0.945	0.027	-0.308	0.234	0.383	-0.366	1.00	0
0	0	. . .	. . .	. . .	. . .	. . .	. . .
0.054	0.027	0.028	0.766	0.383	. . .	. . .	. . .
0.922	0.039	0.336	0.013	0.493	10.9	1.28	-0.141
0.713	0.144	-0.229	0.010	0.495	-0.555	1.01	-0.004
-0.064	-0.032	. . .	. . .	. . .	. . .	. . .	. . .
0.297	0.149	0.325	0.998	0.499	. . .	. . .	. . .
0.910	0.045	0.900	0.356	0.322	3.91	1.14	0.072
0.672	0.164	0.249	0.343	0.329	-0.223	1.10	-0.050
-0.206	-0.103	. . .	. . .	. . .	. . .	. . .	. . .
0.428	0.214	0.473	0.756	0.378	. . .	. . .	. . .

in which r is the radius of gyration that corresponds with I. The value of r can be stated in the same way as for sections that are ordinarily used for columns; that is

$$r = c\,d \quad \ldots\ldots\ldots\ldots\ldots\ldots (17)$$

in which c is a coefficient and d denotes the depth of the section normal to the axis of I. The coefficient c depends on the distribution of the material in the section. Its value is between 0 and 1/2 and it is practically an invariant for a given kind of section.[11] In Table 4, ranges of values are given for c_x of the legs and c_y of the cellular struts. Note that the values of c_x are about the strong axes of the legs, and the values of c_y are about the weak axes of the struts.

The values of J for the cellular sections can be estimated by means of the ratios between I_x (or I_y) and J. The ranges of values for I_x/J of the legs and I_y/J of the cellular struts are given in Table 4.

An additional aid is given in Fig. 10 for estimating values of c and I/J of multi-cellular thin-walled sections. The cross-section shown in Fig. 10 is rectangular. It is composed of a single hollow cell, and has a constant wall thickness t which is small relative to the lateral dimensions b and d. In estimating the values of c and I/J for a multicellular section, the values of Fig. 10 can be used by substituting an average rectangular cross-section for the multicellular section.

Torsional Behaviors of the Towers.—Four cases of each tower are studied for the condition of a torque about the y-axis with the vertical saddle reactions

11 "Structural Design in Steel," by T. C. Shedd, John Wiley and Sons, Inc., New York, 1934, Table II, p. 421.

TABLE 6.—SUMMARY OF DISPLACEMENTS AND TORSIONAL-RIGIDITIES

Towers	$\frac{EI_L}{GJ_L}$	Case A: Δ_z, in in.	Case A: ψ_y, in 10^{-3} Rad.	Case A: GJ_{tow}, in 10^{12} lb in.^{2}	$\frac{GJ_{tow}}{EI_L}$	Case B: Δ_z, in in.	Case B: Δ_y, in 10^{-3} Rad.	Case B: GJ_{tow}, 10^{12} lb in.^{2}
(1)	(2)	(3)	(4)	(5)	(6)	(7)	(8)	(9)
Golden Gate	8.08	1.07	1.98	459.0	0.104	0.042	0.078	11,700
First Tacoma Narrows	3.77	5.10	21.8	25.3	0.255	1.45	6.21	82.2
Walt Whitman	3.33	0.774	1.44	318.0	0.477	0.323	0.600	760

equal zero. The cases are designated by A, B, C, and D. Case A is the actual tower (Figs. 6, 7, and 8). In Cases B, C, and D, the legs are identical to those of Case A but the struts are different from those of the actual tower. In Case B, the struts are the same in number as in Case A but the values of I_s and J_s are infinite. In Case C, the tower is braced with only the top strut of the actual tower. In Case D, the tower is braced with no strut.

The results of the analyses are summarized in Figs. 11 to 13 and Tables 5 and 6. The distributions of m_x/M_y, m_y/M_y, and $b\ v_z/M_y$ along the legs of the towers are indicated in Figs. 11 to 13. Representative values of these same ratios are listed in Table 5. The representative values of $m_x,/M_y$, m_y/M_y, and $b\ v_z/M_y$ are for sections at the ends of the top and bottom struts, and for sections at the tops and bottoms of the legs (Fig. 1 for the locations of sections rq and 01). The values of the moments and shears in a tower are dependent on the relative magnitudes, not on the absolute magnitudes, of E I and G J of the various members of the tower.

In Table 6, a summary is given of the deflections and chord rotations at the tops of the towers, and the torsional rigidities of the towers. These factors depend on the over-all dimensions of the towers and on the absolute values of E I and G J of the various members of the towers. The values of the deflections and chord rotations in Table 6 are for values of $M_y = 108$ by 10^6 in. lb, $E = 30 \times 10^6$ lb in.$^{-2}$, and $E/G = 2.6$. Further, the values of the torsional rigidities are independent of the values of M_y, because the torsional rigidity of each tower is defined by

$$G J_{tow} = \frac{M_y\ h_s}{\psi_y} \qquad (18)$$

and ψ_y is proportional to M_y.

The variables listed elsewhere[5] are based on the assumption of uniform mements of inertia in bending and torsion for each strut and tower leg segment. The actual distributions of moments of inertia shown in Figs. 6, 7, and 8 would indicate that this assumption is valid for the Golden Gate towers, but

(P = 0) (BASED ON ACTUAL MOMENTS OF INERTIAS)

	Case C					Case D		
	Values of				Values of			
$\frac{GJ_{tow}}{EI_L}$ (10)	Δ_z, in in. (11)	ψ_y, in 10^{-3} Rad. (12)	GJ_{tow}, 10^{12} lb in.^{2} (13)	$\frac{GJ_{tow}}{EI_L}$ (14)	Δ_z, in in. (15)	ψ_y, in 10^{-3} Rad. (16)	GJ_{tow}, in 10^{12} lb in.^{2} (17)	$\frac{GJ_{tow}}{EI_L}$ (18)
2.64	1.29	2.39	381.0	0.086	4.49	8.32	109.0	0.025
0.828	5.43	23.2	23.8	0.240	124.0	524.0	1.05	0.011
1.14	0.866	1.60	284.0	0.426	4.56	7.69	59.3	0.089

questionable for the first Tacoma Narrows and Walt Whitman towers. Furthermore, the effect of the saddle reaction at the tower top on the longitudinal bending of the tower legs is neglected in the simplified analysis given elsewhere.[5] The analysis was modified to include these factors and a study was made to determine the degree of approximation that is inherent in the assumptions of the simplified analysis. Tables 7 and 8 show the relative values for several items compared to those given in Tables 5 and 6. The relative values of Table 7 are for Case A of each tower when the saddle reactions, P, are equal to zero. These values are based on the assumption of average but uniform moments of inertia in torsion and bending for each strut and tower leg segment.

The relative values in Table 8 are for Cases C and D of each tower with the saddle reactions $P = 0.4\ P_e$, and for Case A of the Walt Whitman tower with $P = P_{DL}$. The actual moments of inertias are considered in Tables 5, 6, and 8. Table 8 shows (a) the influence of the vertical saddle reactions is appreciable for Case D (when only the longitudinal bending of the tower legs is involved), (b) a major change occurs in this influence as soon as the top strut of a tower is introduced, and (c) the influence of the vertical saddle reactions on the torsional behaviors of the actual towers is practically negligible. Although the results of Table 8 are based on a deflection theory, superposition holds, provided that the values of P are held constant.[12]

Tables 5, 6, and 8 also show the differences that exist in the torsional and flexural rigidities of each tower (Cases A and D). Note particularly the torsional and flexural rigidities of the first Tacoma Narrows towers, and the values of P_{DL} and P_e for these towers. The flexural rigidities of these towers with $P = P_{DL}$ are almost nil.

RESULTS FOR ACTUAL TOWERS

The results of the actual towers are explained, considering the results of the hypothetical towers. The reader may wish to compare at a later stage the

12 "Theory of Elastic Stability," by S. Timoshenko, McGraw-Hill Book Co., New York, 1936, pp. 1-36.

results of both groups of towers, selecting in each instance an hypothetical tower that is considered to be the most representative of an actual tower.

Statical Relationships.—For Case A, the values of m_{x01}/M_y are greatest for the Golden Gate towers (1.32) and smallest for the first Tacoma Narrows towers (0.836). These values are principally dependent on the values of a_1 and are in agreement with those obtained for the hypothetical towers. To verify this statement, locate at a later stage the groups or sets of hypothetical towers which have two or more struts and which have values of a_1 and a_4 that are approximately the same as those of the actual towers. The values of a_1 are 7.99 and 3.90 for the base sections of the Golden Gate and first Tacoma Narrows towers, respectively. The average values of a_4 are approximately 1.0 and 1.21 for the same towers, respectively. Now obtain the values of m_{x01}/M_y for the corresponding hypothetical towers. The latter values should check within reason the values for the actual towers.

TABLE 7.—RESULTS BASED ON UNIFORM MOMENTS OF INERTIA; CASE A, P = 0

Items Compared		Relative Values, Assuming Values In Tables 5 and 6 As 1.00		
		Golden Gate	First Tacoma Narrows	Walt Whitman
(1)		(2)	(3)	(4)
Legs	m_{x01}	1.00	0.971	0.931
	m_{y01}	1.00	1.01	0.995
	m_{xrq}	1.00	1.00	1.18
	m_{yrq}	1.00	0.994	1.02
Top Strut	m_x	1.00	0.965	1.05
	m_y	1.00	0.984	0.883
	ψ_y	1.00	0.957	0.940
	GJ_{tow}	1.00	1.04	1.06

This illustrates the procedure to be followed in correlating the results of the hypothetical and the actual towers. It does not imply that complete agreement will be obtained in each instance between the two sets of results.

In Figs. 11 to 13, it will be observed that the distributions of the bending moments m_x/M_y along the legs of the towers are uniform for the Golden Gate towers, whereas, they are non-uniform for the first Tacoma and Walt Whitman towers. The principal causes for these differences are the number and kinds of struts that are used in each tower. For example, there are six flexible struts for the Golden Gate towers, whereas, there are two stiff struts for the Walt Whitman. Also note the influences of the panel proportions and the values of $\left(\frac{E\,I}{G\,J}\right)_L$ on the bending moments along the legs of the towers. The latter influences are particularly large for the first Tacoma Narrows towers.

For the struts of the various towers, the values of the bending moments $(m_y/M_y)_s$ and the twisting moments $(m_x/M_y)_s$ are biggest for the Walt Whitman towers and smallest for the Golden Gate towers. This is principally because of the differences in the relative stiffnesses of the struts and the legs of the towers. For each tower the biggest values of $(m_y/M_y)_s$ and $(m_x/M_y)_s$ occur in the top strut of the tower. This is most apparent for the top struts of the Walt Whitman and the first Tacoma Narrows towers. (It is assumed in this analysis that the bottom strut of a tower is adequate to resist the bending and torsional deformations at the base of the tower.)

TABLE 8.—RELATIVE EFFECTS OF VERTICAL SADDLE REACTIONS (BASED ON ACTUAL MOMENTS OF INERTIAS)

Item (1)		Golden Gate (2)		First Tacoma Narrows (3)		Walt Whitman (4)		
P_{DL}		33.86 x 10^6 lb		7.13 x 10^6 lb		18.0 x 10^6 lb		
P_e		138. x 10^6 lb		7.40 x 10^6 lb		63.7 x 10^6 lb		
0.4 P_e		55.2 x 10^6 lb		2.96 x 10^6 lb		25.5 x 10^6 lb		
P_{DL}/P_e		0.245		0.964		0.283		
$0.4P_e/P_{DL}$		1.63		0.415		1.42		
Item Compared		Relative Values, Assuming Values in Tables 5 and 6 As 1.00						
		Case C	Case D	Case C	Case D	Case A	Case C	Case D
		P = 0.4 P_e	P = 0.4 P_e	P = 0.4 P_e	P = 0.4 P_e	P = P_{DL}	P = 0.4 P_e	P = 0.4 P_e
Legs	m_{x01}	1.00	1.49	0.894	1.52	1.02	1.03	1.50
	m_{y01}	1.13	1.00	1.02	1.00	1.03	1.08	1.00
	m_{xrq}	1.20	1.92	1.02	1.87	1.01	1.10	1.87
	m_{yrq}	1.13	1.00	1.02	1.00	1.04	1.07	1.00
Top Strut	m_x	1.17	. . .	1.04	. . .	1.03	1.08	. . .
	m_y	1.13	. . .	1.02	. . .	1.03	1.06	. . .
ψ_y		1.13	1.65	1.02	1.65	1.04	1.07	1.64
GJ_{tow}		0.822	0.605	0.977	0.605	0.963	0.931	0.611

The values of $b\,v_z/M_y$ and $2\,m_y/M_y$ are of particular interest for the top and bottom tiers of the towers. Because the values of $2\,m_y/M_y$ are related to those of $b\,v_z/M_y$, the succeeding study is restricted to the values of $b\,v_z/M_y$. This value indicates for a panel the proportion of the total torque which is resisted by the transverse shears in the legs of the panel. For the top panels of the three towers, the values of $b\,v_z/M_y$ are biggest for the Golden Gate

towers (48.4%) and smallest for the first Tacoma Narrows towers (almost 0%). These values are in agreement with those of a set of hypothetical towers which have a single strut and values of a_1 through a_4 that are about the same as those of the top panels of the actual towers.

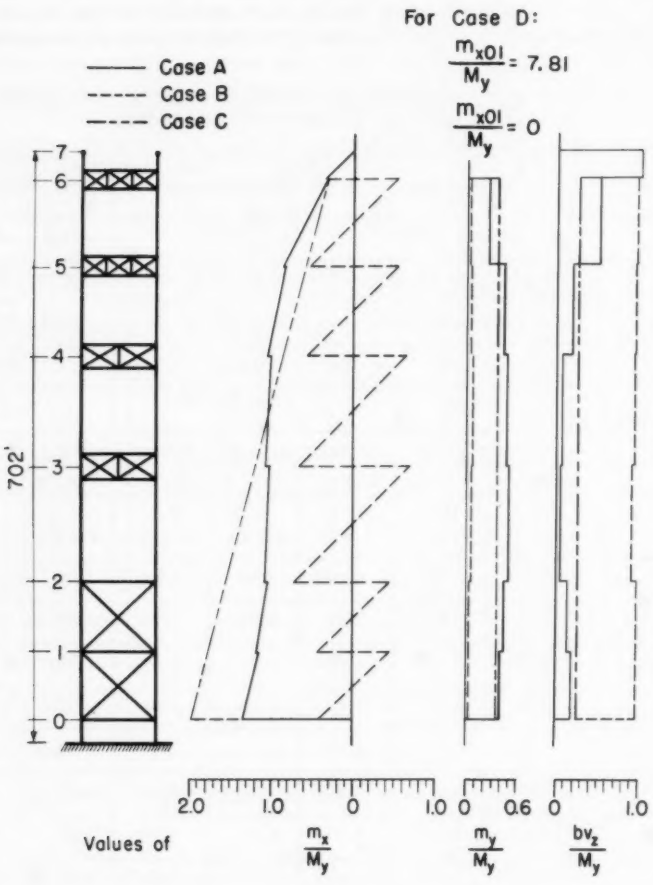

FIG. 11.—MOMENTS AND SHEARS IN GOLDEN GATE BRIDGE TOWERS

For the bottom panels of the three towers, the values of $b\,v_{z01}/M_y$ are 0.615 for the Walt Whitman towers, 0.462 for the first Tacoma Narrows towers, and 0.184 for the Golden Gate towers. These values are decreased by an increase in the number of struts and, to a lesser extent, by a decrease in the sizes of struts. The same relationships are obtained for the hypothetical towers.

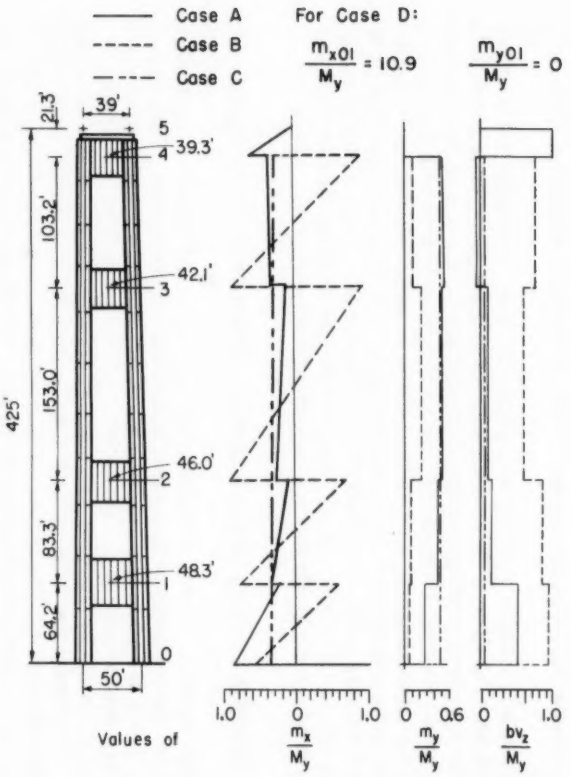

FIG. 12.—MOMENTS AND SHEARS IN FIRST TACOMA NARROWS TOWERS

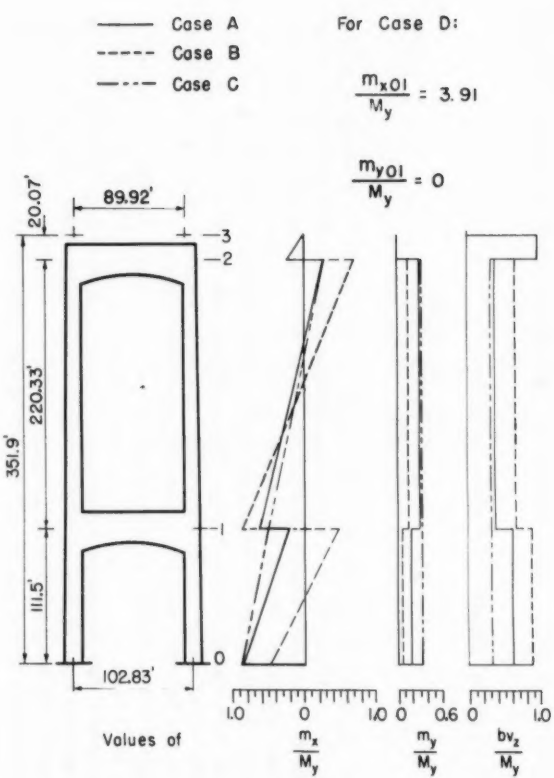

FIG. 13.—MOMENTS AND SHEARS IN WALT WHITMAN TOWERS

Torsional Rigidities and Displacements.—The angle of twist at the top of a tower is defined by

$$\psi_y = \frac{2\,\Delta_z}{b} \quad \ldots\ldots\ldots\ldots\ldots \quad (19)$$

and the torsional rigidity of a tower is defined by

$$G\,J_{tow} = \frac{M_y\,h_s\,b}{2\,\Delta_z} \quad \ldots\ldots\ldots\ldots \quad (20)$$

in which Δ_z is the displacement at the top of a saddle and b is the width between cables. The values of Δ_z, ψ_y, and $G\,J_{tow}$ for the actual towers are summarized in Table 6. This table shows that for a value of M_y = 108 by 10^6 in. lb the displacement Δ_z of the Golden Gate tower is 1.07 in., and the corresponding displacement for the Walt Whitman and first Tacoma Narrows towers are 72% and 477% of this value, respectively. This comparison does not show all of the characteristics of the towers subjected to a torque, because of the large differences in the heights, widths, and makeups of the towers.

Further comparisons of the three towers are given in Table 6, in which values of $G\,J_{tow}$ and $G\,J_{tow}/(E\,I_L)$ are listed. The value of $E\,I_L$ at the base of each tower is selected as a reference. The values of $G\,J_{tow}/(E\,I_L)$ for the actual towers are decreased by an increase in the value of a_1. The same relationship is obtained for a similar group of hypothetical towers. However, the absolute values of $G\,J_{tow}/(E\,I_L)$ for the two groups are not the same because of the variations in $G\,J_L$ and EI_L along the legs of the actual towers.

In Case B, the towers are the same as in Case A, except the struts of Case B are infinite. The results of Case B are at complete variance with those of Case A.

The statical relationships for the towers of Case C are appreciably different from those of Case A. The torsional deformations, however, are about the same for the corresponding towers of Cases A and C. Therefore, the torsional rigidity of a tower can be approximated as if it were braced with its top strut only. This approximation may be surprising to some readers. It is possible because of the similarities in the distributions of m_x/M_y along the legs of the towers for Cases A and C. For example, compare the distributions of m_x/M_y in Figs. 11 to 13. In each figure, the straight line defining the distribution of m_x/M_y for Case C closely follows the corresponding line for Case A.

TORSIONAL CHARACTERISTICS OF HYPOTHETICAL TOWERS

In this section, a more detailed study is given of the influence of different factors on the torsional behaviors of suspension bridge towers. The analysis is for a group of hypothetical towers in which the dimensions and properties of the towers are varied.

Description of the Towers.—An outline of an hypothetical tower is shown in Fig. 1(b). The tower is comprised of two parallel legs, r struts, and is subjected to a torque M_y. The legs are prismatic and the values of $E\,I_L$ and $G\,J_L$ are constant. All struts are identical, equally spaced, and have values of $E\,I_s$ and $G\,J_s$ which are constant. The struts divide the tower into r panels, each panel having a height-to-width ratio of h/b.

Dimensions and Properties of the Towers.—In the succeeding study, the dimensions and properties that are varied are the heights of the towers, the number of struts in a tower, the panel proportions, and the flexural and torsional rigidities of the members. The properties of a tower are defined by

$$r = \frac{h_s}{h} \quad \ldots\ldots\ldots\ldots\ldots\ldots \quad (21a)$$

$$a_1 = \frac{E I_L}{G J_L} \quad \ldots\ldots\ldots\ldots\ldots\ldots \quad (21b)$$

$$a_2 = \frac{E I_s}{E I_L} \quad \ldots\ldots\ldots\ldots\ldots\ldots \quad (21c)$$

$$a_3 = \frac{G J_s}{G J_L} \quad \ldots\ldots\ldots\ldots\ldots\ldots \quad (21d)$$

$$a_4 = \frac{h}{b} \quad \ldots\ldots\ldots\ldots\ldots\ldots \quad (21e)$$

and by the absolute values of h_s and $E I_L$. In this study, dimensionless ratios are used. These ratios are useful in design, because they define (1) the function of the lateral bracing in resisting the torsional deformations of a tower, and (2) the influences of changes in the number of struts in the tower, the values of E I and G J of the various members of the tower, and the height-to-width ratios of the towers.

The following sets of values are considered for the dimensionless ratios of Eq. 21:

$$r = 1.0;\ 2.0;\ 3.0;\ 4.0;\ 5.0 \quad \ldots\ldots\ldots\ldots \quad (22)$$

$$a_1 = 1.0;\ 2.0;\ 4.0;\ 6.0;\ 8.0 \quad \ldots\ldots\ldots\ldots \quad (23)$$

$$a_2 = 0.1;\ 0.3;\ 0.6;\ 1.0 \quad \ldots\ldots\ldots\ldots\ldots \quad (24)$$

and

$$a_3 = 0.1;\ 0.3;\ 0.6;\ 1.0 \quad \ldots\ldots\ldots\ldots\ldots \quad (25)$$

$$a_4 = 1.0;\ 2.0;\ 3.0;\ 4.0 \quad \ldots\ldots\ldots\ldots\ldots \quad (26)$$

These values are based on an inspection of the towers of the Golden Gate bridge, the first Tacoma Narrows bridge, the Lion's Gate bridge, and others. A limiting value of

$$r\,a_4 = 12 \quad \ldots\ldots\ldots\ldots\ldots\ldots \quad (27)$$

is selected for the height-to-width ratio of each hypothetical tower. With this limiting value in mind, the values of the r and a terms in Eqs. 22 to 26 define the characteristics of 1,360 different kinds of hypothetical towers.

Torsional Behavior of the Towers.—The torsional behavior of the hypothetical towers was determined by means of the analytical procedure given elsewhere.[5] A computer program was written for the procedure and the computations were performed by means of an IBM 701 digital computer.

The influences of the different variables on the values of

$$\frac{m_{x;01}}{M_y}, \frac{2\,m_{y;01}}{M_y}, \frac{b\,v_{z;01}}{M_y},$$

and

$$\frac{G\,J_{tow}}{E\,I_L}$$

are summarized in Figs 14 to 21. In these figures, representative values of r and a_1 and a_4 are considered. Furthermore, the values of $2\,m_{y;01}/M_y$ and $b\,v_{z;01}/M_y$ for a given tower are shown in the same figure, because

$$\frac{2\,m_{y;01}}{M_y} + \frac{b\,v_{z;01}}{M_y} = 1 \quad \ldots\ldots\ldots\ldots \quad (28)$$

is a requirement of statics for each tower.

The results of the computations are grouped in the figures to demonstrate the influence of a change in each variable on the torsional behavior of a tower. In each figure, three of the five variables (r and a_1 to a_4) are held constant as two are varied.

RESULTS FOR HYPOTHETICAL TOWERS

Figs. 14 and 15 show the effect of variations of a_1 and r, for two groups of towers, E and F. In Group E, the towers have a height-to-width ratio of 4:1; and in Group F a height-to-width ratio of 8:1. The values of a_2 and a_3 are the same for each group and are constant. (This does not mean that the values of the bending and torsional stiffnesses of the struts are a constant when a_1 is varied. Notations).

Figs. 14 and 15 show that

(1) The values of $m_{x;01}/M_y$ and $b\,v_{z;01}/M_y$ are increased by an increase in the values of a_1; whereas, the values of, $G\,J_{tow}/(E\,I_L)$ are decreased;
(2) The values of $m_{x;01}/M_y$ and $bv_{z;01}/M_y$ are increased by an increase in the value of r; whereas, the values of $G\,J_{tow}/(E\,I_L)$ are practically not affected; and
(3) The values of $m_{x;01}/M_y$ and $G\,J_{tow}/(E\,I_L)$ are influenced principally by a change in the value of a_1.

It is interesting to compare the torsional behaviors of towers which have r struts to those of similar towers which have no struts. For a tower without struts, the values of the moment and shear at the base of the tower, and the torsional rigidity, are given by

$$\left(\frac{m_{x;01}}{M_y}\right)_{\text{no struts}} = \frac{h_s}{b} \quad \ldots\ldots\ldots\ldots\ldots \quad (29)$$

$$\left(\frac{b\,v_{z;01}}{M_y}\right)_{\text{no struts}} = 1 \quad \ldots\ldots\ldots\ldots\ldots \quad (30)$$

$$\left(\frac{2\,m_{y;01}}{M_y}\right)_{\text{no struts}} = 0 \quad \ldots\ldots\ldots\ldots\ldots\ldots (31)$$

and

$$\left(\frac{G\,J_{tow}}{E\,I_L}\right)_{\text{no struts}} = \frac{3}{2}\left(\frac{b}{h_s}\right)^2 \quad \ldots\ldots\ldots\ldots (32)$$

Comparing the values that are obtained by means of Eqs. 29 to 32 with those of Figs. 14 to 21, a major change occurs in the behavior of a tower as soon as a strut of practical dimensions is introduced at the top of the tower. For ex-

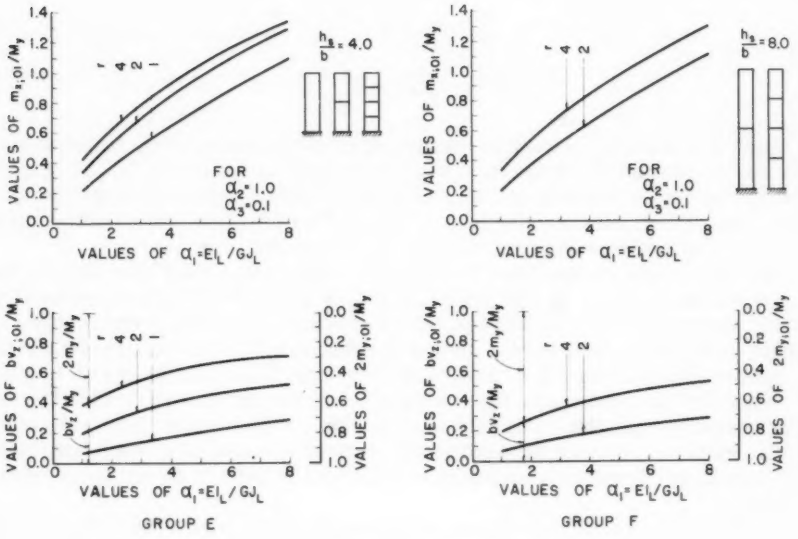

FIG. 14.—VARIATIONS IN NUMBER OF STRUTS

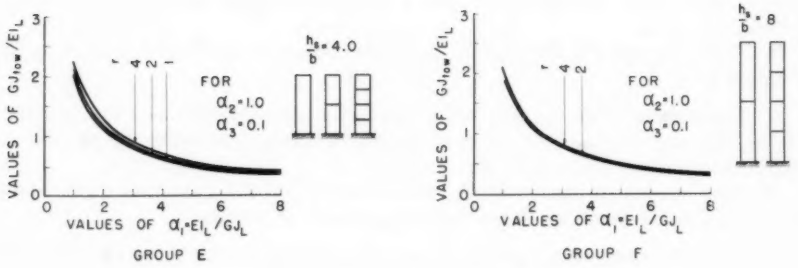

FIG. 15.—TORSIONAL RIGIDITIES OF GROUPS E AND F

ample, the torsional rigidity of a tower of Group E in Fig. 15 is from 4 to 35 times greater than that of a similar tower which has no struts. For a tower of Group F, the torsional rigidity is from 12 to 100 times greater than that of a similar tower which has no struts. In these and other examples, the increases that occur in the torsional rigidities are greatest for towers with small values of a_1. The values of $m_{x;01}/M_y$ and $b\, v_{z;01}/M_y$ are appreciably reduced in a tower as soon as the top strut is introduced. A reduction in the value of $b\, v_{z;01}$ is accompanied by an increase in the value of $2\, m_{y;01}/M_y$.

Briefly, the major change in the torsional behavior of a tower is a result of the requirements of continuity for a closed circuit. These requirements are given by

$$\sum \Delta \phi_x = 0 \quad \ldots\ldots\ldots\ldots\ldots\ldots \quad (33)$$

$$\sum \Delta \phi_y = 0 \quad \ldots\ldots\ldots\ldots\ldots\ldots \quad (34)$$

and

$$\sum x\, \Delta \phi_y - \sum y\, \Delta \phi_x = 0 \quad \ldots\ldots\ldots\ldots\ldots\ldots \quad (35)$$

in which $\Delta\phi_x$ and $\Delta\phi_y$ are angle-changes about the x- and y-axes, respectively. The angle-changes about the two axes are coupled by means of Eq. 35, and an interaction occurs between the torsional and flexural deformations of the legs and of the strut. Similar coupling or interaction effects occur in other kinds of structural systems in which bracing is introduced.

The top struts of the first Tacoma Narrows bridge were damaged by the torsional oscillations of the bridge (Parts b and c)[4] Further consideration should be given to the influence of the torsional rigidity of a tower on the resulting deflections of a bridge and on the response to torsional oscilliations. It appears (Part a)[4] that the fundamental torsional mode of a bridge is largely prevented by the resistance at the towers to a twist about their vertical axes. The following quotation (Part a)[4] is of interest: "The towers, however, offer much greater resistance to twisting than to bending parallel to the bridge axis and contribute therefore a material resistance to torsional oscilliations of the bridge."

In Figs. 16 and 17, the values of a_2 and a_3 are varied. The influences of these variations on the behavior of a tower are illustrated for two groups of towers designated as G and H. These groups are similar in certain respects to the two which are considered in Figs. 14 and 15. In Group G, the towers have two struts each and a height-to-width ratio of 4:1, and in Group H the towers have four struts each and a height-to-width ratio of 8:1. For both groups, $a_4 = 2.0$.

In Figs. 16 and 17, the effects of increases in the values of a_2 and a_3 are as follows:

(1) The values of $m_{x;01}/M_y$ are practically constant, whereas the values of $b\, v_{z;01}/M_y$ and $G J_{tow}/(E I_L)$ are slightly increased. The latter increases are biggest for towers with small values of a_1.

(2) The values of the statical relationships and the torsional rigidities of the towers are almost the same for both groups of towers.

The comparisons which are dealt with in Figs. 18 and 19 are of a different category from those dealt with in Figs. 14 to 17. In Figs. 18 and 19, the towers

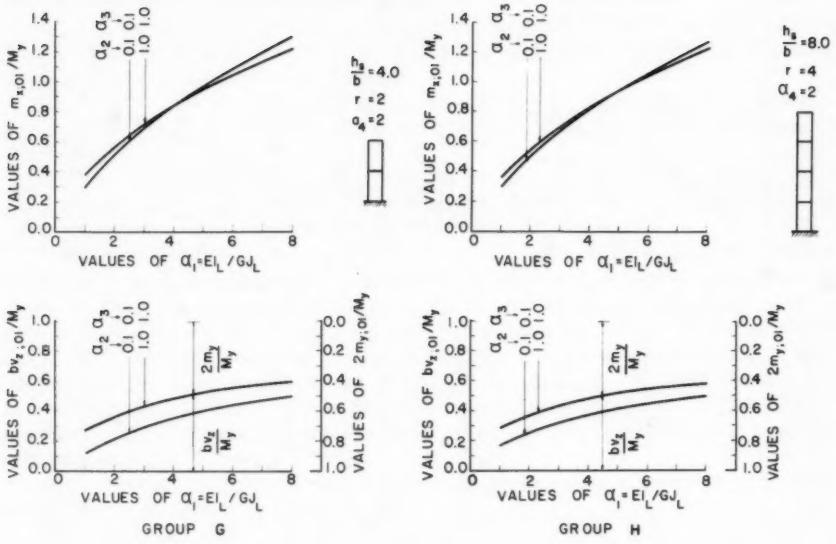

FIG. 16.—VARIATIONS IN STIFFNESSES OF STRUTS

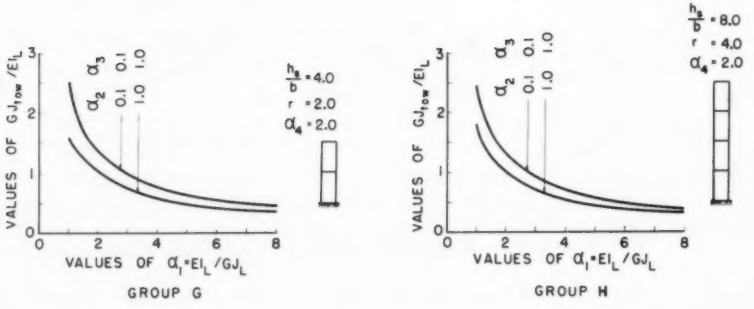

FIG. 17.—TORSIONAL RIGIDITIES OF GROUPS G AND H

are radially different in make-up and over-all dimensions. The values of r and of h_s/b are varied as the values of a_2, a_3, and a_4 are kept constant. The in-

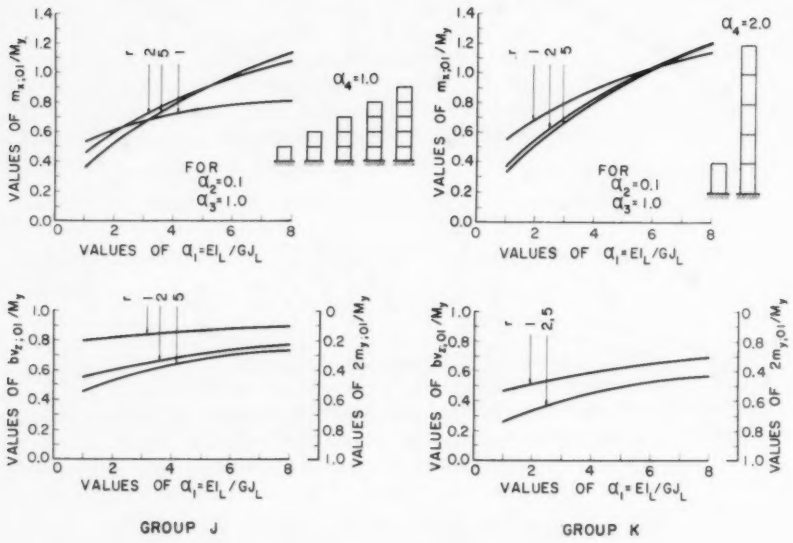

FIG. 18.—VARIATIONS IN HEIGHTS OF TOWERS

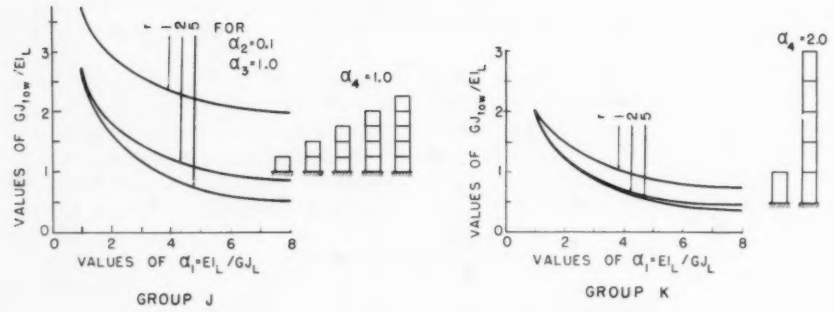

FIG. 19.—TORSIONAL RIGIDITIES OF GROUPS J AND K

fluences of these variations on the torsional behaviors of the towers are illustrated for two groups of towers, namely, Groups J and K. In Group J, the value of a_4 is 1.0, and in Group K the value of a_4 is 2.0.

In Figs. 18 and 19, the effect of changes in a_1 follows for each group of towers:

(1) The values of $m_{x;01}/M_y$ and $b\,v_{z;01}/M_y$ are increased by an increase in the value of a_1, whereas the values of $G\,J_{tow}/(E\,I_L)$ are decreased. For this relationship the value of r is constant.

(2) For a given value of a_1, the values of $m_{x;01}/M_y$, $b\,v_{z;01}/M_y$, $2\,m_{y;01}/M_y$, and $G\,J_{tow}/M_y$ are practically constant for towers with two or more struts.

(3) For a given value of a_1, the values of $m_{x;01}/M_y$, $b\,v_{z;01}/M_y$, $2\,m_{y;01}/M_y$, and $G\,J_{tow}/(E\,I_L)$ are generally different for the tower with one strut than they are for the towers with two or more struts.

The relationships in Figs. 18 and 19 can be used in comparing the values of the bending moments, twisting moments and shears at interior sections of a given tower. For example, consider the values of $m_{x;jk}/M_y$, $b\,v_{z;jk}/M_y$, and $2\,m_{y;jk}/M_y$ at an arbitrary section jk of the general hypothetical tower (Fig. 1(b)). Assume that the values of a_1 through a_4 are held constant. Figs. 18 and 19 indicate that the values of $m_{x;jk}/M_y$, $b\,v_{z;jk}/M_y$, and $2\,m_{y;jk}/M_y$ are practically the same for all sections jk which are two or more panels removed from the top of the tower. The results of other computations support this observation.

Figs. 18 and 19 indicate the need to examine more closely the torsional behaviors of towers with single struts.

The torsional behaviors of towers with single struts are illustrated in Figs. 20 and 21. They are illustrated for a group of towers (Group L) in which the values of a_1 and a_4 are varied and the values of a_2 and a_3 are held constant. The same kind of information is given in these figures as in the preceding figures. Additional information, however can be directly deduced from these figures because of the requirements of statics, which are

$$\frac{m_{x;10}}{M_y} = a_4 \frac{b\,v_{z;01}}{M_y} - \frac{m_{x;01}}{M_y} \quad \ldots\ldots\ldots\ldots\ldots (36)$$

and

$$\frac{m_{y;10}}{M_y} = \frac{m_{y;01}}{M_y} \quad \ldots\ldots\ldots\ldots\ldots\ldots (37)$$

for the moments at the tops of the legs, and

$$\frac{b\,v_{z;11}}{M_y} = \frac{2\,m_{y;01}}{M_y} \quad \ldots\ldots\ldots\ldots\ldots (38)$$

for the shears in the top struts. The moments at the ends of the top struts are the same as the corresponding moments at the tops of the legs.

Only the most important observations will be stated for towers which are similar to those of Group L. They are as follows:

(1) Practically every variable (a_1 through a_4) has an important influence on the values of the bending moments, twisting moments, and shears in the legs and top struts of the towers.

(2) In general, the values of $G\,J_{tow}/(E\,I_L)$ are decreased by an increase in the values of a_1. For a constant value of a_1, the values of $G\,J_{tow}/(E\,I_L)$

are practically constant when the value of a_4 exceeds about 3.0; otherwise, they are dependent on the value of a_4. Finally, the values of a_2 and a_3 have

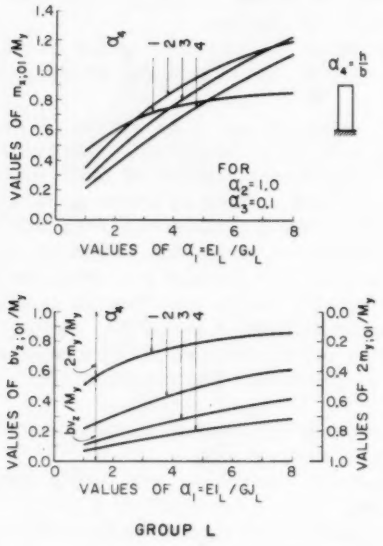

FIG. 20.—TOWERS WITH A SINGLE STRUT

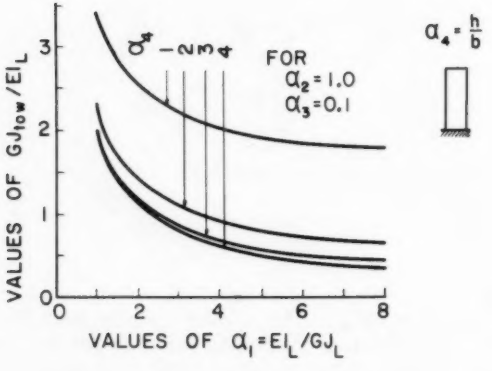

FIG. 21.—TORSIONAL RIGIDITIES OF GROUP L

little influence on the value of $G\,J_{tow}/(E\,I_L)$, except for small values of a_1. The reader is reminded that all values of a_1 through a_4 are assumed to be within practical ranges.

Statement (1) also holds for the top panel of a multi-strutted tower. In fact, the values of the bending moments, twisting moments, and shears in the top panel of a multi-strutted tower are approximately the same as if the panel were fixed at its base.

CONCLUSIONS

The preceding study illustrates the relative importance of different factors, and the approximations which can be made in determining the torsional behaviors of suspension bridge towers.

If desired, the method of analysis presented elsewhere,[5] can be adjusted to consider non-uniform distributions of moments of inertias and the effects of vertical loads on towers.

ACKNOWLEDGMENTS

Grateful acknowledgments are due to the late Bardy Cross, George S. Vincent, F. ASCE, and to the firms of Modjeski and Masters, and Ammann and Whitney, for furnishing the writers with information concerning the towers of the bridges used as examples in this paper.

Journal of the
STRUCTURAL DIVISION
Proceedings of the American Society of Civil Engineers

DEAD-LOAD STRESS IN MODEL DAMS BY METHOD OF INTEGRATION

By Jerome M. Raphael,[1] F. ASCE

SYNOPSIS

For massive structures such as dams, dead-load stresses form the most important fraction of the total stress in the body. Existing experimental methods that have been used to determine dead-load stresses in structural models are reviewed and evaluated. A new experimental technique termed the "method of integration" is described. The theoretical background of the test is described, the similitude factors are derived, description is given of a typical experiment, and types of results that may be expected are given. The method can be used to study alternative construction procedures to result in desired patterns of dead-load stress.

INTRODUCTION

In massive concrete structures, such as gravity dams, the forces due to dead weight constitute one of the most important loadings on the structure. Measurements of massive structures in service[2] have shown that stresses due to dead weight establish the predominating stress pattern, and that live-load stresses, due to water loading and temperature changes, modify this stress pattern. Furthermore, observations of actual structures have shown that construction procedures have a considerable effect on establishing the pattern of dead-load stresses.

Note.—Discussion open until February 1, 1962. To extend the closing date one month, a written request must be filed with the Executive Secretary, ASCE. This paper is part of the copyrighted Journal of the Structural Division, Proceedings of the American Society of Civil Engineers, Vol. 87, No. ST 6, August, 1961.

1 Prof. of Civ. Engrg., Univ. of California, Berkeley, Calif.

2 "The Development of Stresses in Shasta Dam," by Jerome M. Raphael, Transactions, ASCE, Vol. 118, 1953, p. 289.

Hence, when it was decided to perform an experimental stress analysis of a large and unusually shaped concrete dam, one of the prime objectives of the investigation was the development of a procedure for the determination of the dead-load stresses during construction and on completion of the structure. Although a number of procedures have been used in the past for the determination of dead-load stresses in completed structures, none showed the development of stresses in the dam taking into account construction procedures. It is believed that the method of integration developed to show the gradual accumulation

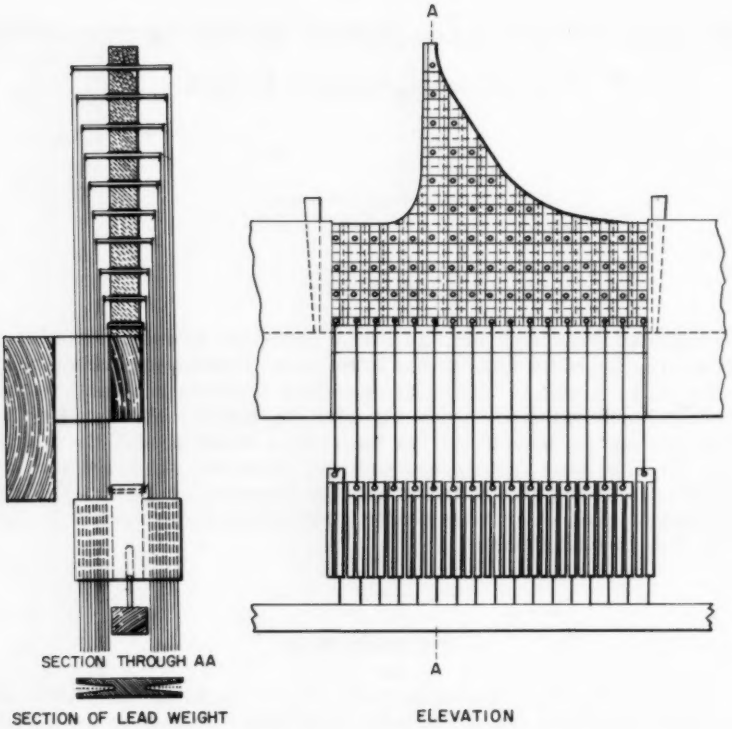

FIG. 1.—MODEL DAM SHOWING POSITIONS OF TUBES AND LINES FOR MEASURING

of stress has many points of superiority over other experimental methods. Before describing the method of integration, a brief historical sketch will be given of the development of experimental procedures for the determination of dead-load stresses.

METHOD OF APPLIED LOADS

The method of applied loads dates from the very beginnings of experimental stress analyses of dams. In the classic J. S. Wilson and William Gore exper-

iments[3] in Great Britain, reported in 1908, a rubber slab representing a typical section of a gravity dam together with part of its foundation was tested, as shown in Fig. 1. After dividing the cross section into a number of incremental areas, pins driven through the model at the center of mass of each subdivision were loaded with dead weights in proportion to the dead weight of each increment. Strains measured on the model before and after loading were used to determine stresses due to dead weight.

A variation of this method is used at the Istituto Sperimentale Strutture e Modelli[4] (ISMES) at Bergamo, Italy. Here, as shown in Fig. 2, the load is applied internally through rods anchored in the mass of the structure. The rods, in turn, are loaded either with dead weights, or tied into a mechanical system loaded with hydraulic jacks, shown in Fig. 3. If the profile of the dam model thus loaded is not too irregular, this internal loading system has the advantage of leaving the surface free for the application of strain gages. However, some local stress concentrations are bound to exist in the immediate vicinity of the anchoring devices and care must be taken to avoid strain measurements at this location.

METHOD OF INVERSION

The use of the method of inversion for the experimental determination of dead-load stresses in essentially two-dimensional models, has been described by the Laboratorio Nacional Engenharia Civil (LNEC).[5] In this method, a model of the structure is fabricated and fitted with strain gages. The difference is strains between the model in its upright and inverted position is measured. By inverting the model, a loading effect is produced which is equal to twice that of gravity. The sensitivity of this test can be increased by increasing the density and decreasing the modulus of elasticity of the model material. Fig. 4 shows the test setup used at LNEC on a model of a buttress dam. Considerable difficulty is experienced in attempting to utilize this method in a three-dimensional model of any size or complexity. Furthermore, unless the foundation is made so rigid that deformations are minimized on inverting the model, strains will be induced in a three-dimensional model, from the deformed foundation, which are unrelated to the normal gravity stresses. This might be a special weakness for utilizing this method in the testing of arch dams, because arches are quite sensitive to abutment deformations.

METHOD OF IMMERSION

M. A. Biot has shown[6] the analogy between the two-dimensional state of stress resulting from body-force loadings, such as the earth's gravitational

3 "Stresses in Dams: An Experimental Investigation by Means of India-Rubber Models," by J. S. Wilson and William Gore, Proceedings, I.C.E., Paper No. 3705, Vol. 172, Part 2, 1908.

4 "Materiaux pour Modèles Reduit et Installations de Charge," by E. Fumagelli, ISMES Publication No. 13, Report presented at the Internatl. Colloquium on Structural Models, Madrid, 1959.

5 "Analysis of Concrete Dams by Model Tests," by M. Rocha and J. L. Serafin, Communication No. C36, 5th Congress on Large Dams, Paris, 1955.

6 "Distributed Gravity and Temperature Loading in Two-Dimensional Elasticity Replaced by Boundary Pressures nad Dislocations," by M. A. Biot, Journal of Applied Mechanics, Vol. 2, 1955.

FIG. 2.—ANCHORS FOR DEAD LOAD HANGERS IN ARCH MODEL AT ISMES, BERGAMO

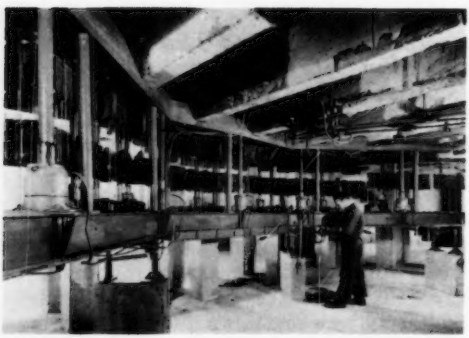

FIG. 3.—JACKS AND LINKAGE FOR APPLYING DEAD LOADS TO MODEL AT ISMES

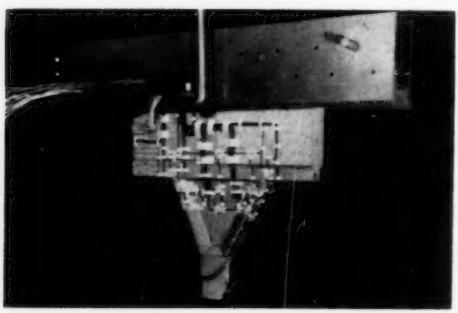

FIG. 4.—INVERTED MODEL OF BUTTRESS DAM BEING TESTED AT LNEC

pull on a structure, and the stress resulting from boundary loads. In this method, an accurately cut section of a gravity dam, together with part of its foundation, is inverted and lowered into a pool of mercury whose upper surface just touches the ground surface, as indicated in Fig. 5. Stresses at various points in the slice are then related to corresponding stresses in the prototype dam by use of Biot's similitude equations, which take into account the scale factor and the relative densities of the immersing fluid and the material of the dam. This method has been used in LNEC in Lisbon for finding the stress distribution in

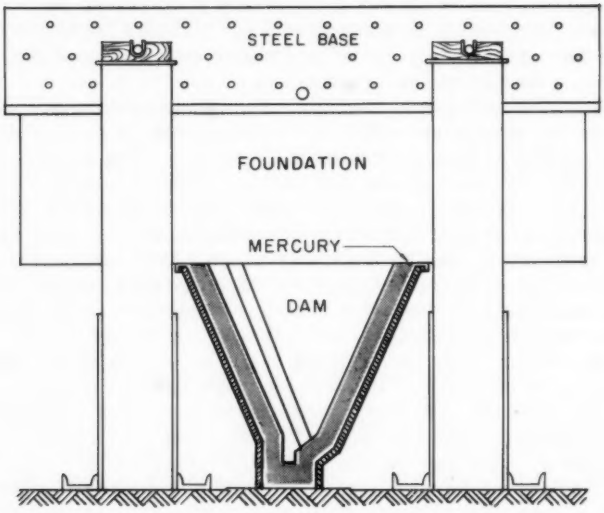

FIG. 5.—MODEL DAM IMMERSED IN MERCURY

a section of a gravity or of a buttress dam. Similar analogy has not been made for the three-dimensional state of stress.

CENTRIFUGAL METHOD

The principle of the centrifugal method for the experimental determination of dead-load stresses is the substitution of centrifugal forces for gravitational forces by rotating the model in a centrifuge.[7] This method has been used with considerable success in the Engineering Materials Laboratory of the University of California by H. D. Eberhart in two-dimensional photoelastic models of the cross sections of several gravity dams.[8] The model, made of a sheet of photoelastic material, was rotated at high speeds at elevated temperatures (200° F) for several hours until it reached thermal equilibrium. While maintaining con-

7 "The Stress Function and Photo-elasticity Applied to Dams," by J. H. A. Brahtz, Transactions, ASCE, No. 101, 1936.

8 "Analysis of Gravity Load Stresses by Photoelastic Methods," by J. J. Polivka, Proceedings, 16th Semi-Annual Eastern Photoelastic Conf., 1942.

stant rotation, temperatures were then reduced at the rate of 5° F per hr, until room temperature was reached. When the model was removed, it had frozen within it a stress pattern resulting from the equivalent of an increased gravitational field which could then be analyzed by photoelastic methods.

In another experiment,[9] A. J. Durelli, went a little further toward three-dimensional analysis. His experiment was concerned with the distribution of dead-load stresses in a single buttress of a massive head buttress dam. A model was cast using a photoelastic material of a single buttress together with part of its foundation. As soon as this casting had solidified, it was transferred to a centrifuge and rotated rapidly while curing progressed. At the end of the curing period, the model was removed with the stresses frozen within it. The model was then cut into two-dimensional slices, polished, and the stresses at various planes determined photoelastically.

Both of these test methods are excellent solutions for essentially two-dimensional problems. However, certain limitations must be recognized when extending this method to three-dimensional problems. The most serious difficulty is that while Poisson's ratio for rock and concrete lies generally in the range 0.15 - 0.20, Poisson's ratio for most plastics lies very close to 0.50. This wide disparity means that three-dimensional models made of plastic do not deform in all respects like the prototype, and that, as a consequence, the stresses are not distributed in a plastic model like those in the prototype. A second and less stringent limitation is that unlike gravity, centrifugal force is not constant throughout the model, but varies as the square of the radius from the center of rotation. Only by rotating a fairly small model on a long arm can the variation in the centrifugal field be held within feasible limits. A third limitation is that of size. Both centrifuges mentioned were designed to handle fairly small models. Difficulties can be anticipated in testing a model of a complex shape in sizes that can be handled by centrifuges. The aviation and missile industry has developed large centrifuges that make it possible to test fairly large plaster models having the proper Possion's ratio for three-dimensional analysis. However, the cost of equipment for such a test makes it unfeasible for the average experimental stress analysis.

METHOD OF CONSTRUCTION BY STAGES

A significant number of large concrete dams are constructed in stages, balancing the capacity of the reservoir with increasing hydrologic requirements. In this way construction costs are spread over a longer period of increasing demand rather than being concentrated at the beginning of the period, when the financial return is lower. Actually, in the larger sense all concrete dams are constructed by stages, since in each case definite controllable volumes of concrete are added as increments during construction.

The method of construction by stages was devised at the LNEC in studying how to increase the height of existing dams where it was required to know with precision the effect of the weight of the dam taking into account the construction

9 "Experimental Stress Analysis of the Bekhme Dam," by A. J. Durelli, Armour Research Foundation Final Report, Privately Issued for Harza Engineering Co., December, 1956.

sequence. J. L. Serafim and J. P. da Costa described[10] the philosophy of this testing method:

> "The various stages of construction of a dam correspond to an equivalent number of differently shaped soils and consequently the final state of stress in the solid will be the sum of all the states of stress resulting from each stage. This final state of stress is not equal to that which would be obtained if the structure were presumed to be built and loaded with its own weight in one operation; the greater the number of connections in the dam during the construction, the greater will the difference in the resulting state of stress be."

Proceeding from this basic philosophy, an experimental method was devised reversing the order of construction of a dam. A model was constructed of a plastic and fitted with strain gages. The model was then systematically cut down from the top by stages in a reverse order of the proposed construction sequence. Readings of the strain gages reflect the removal of the dead weight, and, by reversing this record, the gradual development of stress as construction proceeds can be followed easily. It can be seen that even with fairly high density model materials, the sensitivity of this type of test is not great because of the low general dead-load stress level in a model. It was to increase the sensitivity of dead-load tests that the method of integration described herein was devised.

METHOD OF INTEGRATION

Four of the five methods for dead-load testing described previously — applied loads, inversion, immersion, and centrifuging — had an important common defect. Any test in which a completely constructed model is suddenly endowed in its entirety with weight does not in the slightest degree reflect the incremental manner in which weight is added to the prototype structure, and the manner in which the structure gains its strength, and leads to erroneous conclusions as to the development of dead-load stresses in the dam as construction proceeds. The fifth method, the method of construction by stages, lacks the requisite sensitivity for accurate analysis.

The importance of the construction program in determining the distribution of stresses in a concrete dam has been demonstrated.[2] In studying a proposed design for a dam, question had been raised as to the behavior of the structure because of particularly large overhangs. Hence, a new experimental method was devised by which the stresses could be determined not only in the complete structure, but also at various stages of partial completion, following any given construction program. This method has been termed the "method of integration."

As finally developed, in the method of integration for the determination of dead-load stresses, the model is cut down by increments leaving a horizontal surface representing the top of a lift. On this surface, a uniform load is applied, of a magnitude great enough to cause a well-defined response in all the

10 "Methods and Materials for the Study of the Weight Stresses in Dams by Means of Models," by J. L. Serafin and J. P. da Costa, RILEM Internatl. Colloquium on Models of Structures, Madrid, June, 1959.

strain gages on the model. By using similitude factors, this is then related to the effect on the prototype dam of adding 1 ft of concrete at that elevation.

Thus, for every gage location there is available a record showing the stresses induced by adding 1 ft of concrete at successive elevations. This is a continuous function which can be integrated graphically or numerically to indicate the effect of successive stages of construction, including the dead load stresses in the complete dam. Thus, critical stages in the construction when dead-load stresses are a maximum which exceed the stress state in the complete dam will be indicated by study of a graph of stress versus height of dam.

SIMILITUDE FACTORS

The general considerations that apply to the derivation of the similitude factors used in the method of integration for determining dead stresses in dams

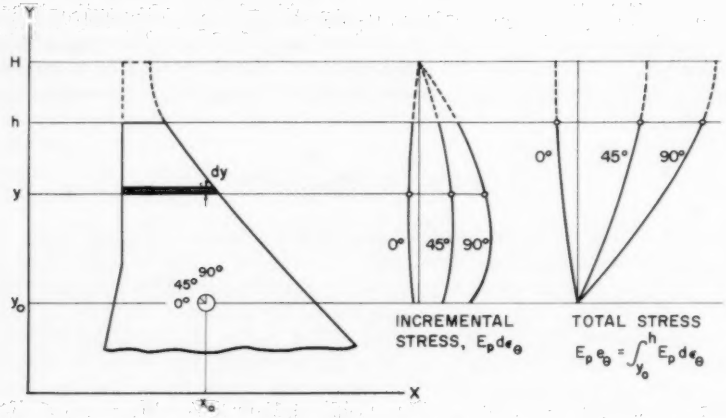

FIG. 6.—NOMENCLATURE FOR METHOD OF INTEGRATION

are shown in Fig. 6. As shown, the dam is to be constructed in horizontal lifts to a final elevation H. At an intermediate stage of construction, it will have reached elevation h. In testing, the model dam is cut down by stages to some elevation y. The similitude problem is to find the effect of the increment of height dy on the strains and stresses at location x_0, y_0.

For a geometrically similar model, the ratio of model length L_m to prototype length L_p is defined as

$$\lambda = \frac{L_m}{L_p} \quad \ldots\ldots\ldots\ldots\ldots\ldots \quad (1)$$

The ratio of the density of model loading γ_m to the density of prototype loading γ_p is defined as

$$g = \frac{\gamma_m}{\gamma_p} \quad \ldots\ldots\ldots\ldots\ldots\ldots \quad (2)$$

Thus, for a dead-load test of a model dam amde of a plaster weighing 40 pcf representing a prototype dam made of mass concrete weighing 155 pcf, the value of g is 0.26.

Expressed in these units, force then becomes $F = \gamma L^3$ and stress σ, which is force per unit area, becomes

$$\sigma = \frac{F}{L^2} = \frac{\gamma L^3}{L^2} = \gamma L \quad \ldots\ldots\ldots\ldots\ldots \quad (3)$$

Thus, the relationship of stresses between model and prototype can be shown to be

$$\frac{\sigma_m}{\sigma_p} = \frac{\gamma_m L_m}{\gamma_p L_p} = g\lambda \quad \ldots\ldots\ldots\ldots\ldots\ldots \quad (4)$$

Similitude factors for strain ϵ can be derived starting with the elastic stress-strain relationship:

$$\epsilon = \frac{\sigma}{E} \quad \ldots\ldots\ldots\ldots\ldots\ldots \quad (5)$$

in which E is the modulus of elasticity.

From Eqs. 3 and 5, one can write

$$\frac{\sigma_m}{\sigma_p} = \frac{\gamma_m L_m}{\gamma_p L_p} = \frac{E_m \epsilon_m}{E_p \epsilon_p} \quad \ldots\ldots\ldots\ldots\ldots \quad (6)$$

Consider a uniform load per unit area of w_{ym} to be applied at elevation y. If the dam is correspondingly increased in height at elevation y by the increment dy, then this will apply a stress γ_p dy at y.

If model and prototype are geometrically similar, and both have linear elastic properties, the ratio of the stress applied to the model to the stress applied to the prototype will be

$$\frac{w_{ym}}{\gamma_p \, dy} = \frac{E_m}{E_p} \frac{\epsilon_{ym}}{d\epsilon_{yp}} \quad \ldots\ldots\ldots\ldots\ldots\ldots \quad (7)$$

Thus, the incremental strain in the prototype caused by the incremental loading γ_p dy at y will be

$$d\epsilon_{yp} = \frac{E_m}{E_p} \frac{\gamma_p}{w_{ym}} \epsilon_{ym} \, dy \quad \ldots\ldots\ldots\ldots\ldots \quad (8)$$

It follows that the increment of stress in the prototype due to this incremental loading is

$$d\sigma_{yp} = E_p \, d\epsilon_{yp} = E_m \frac{\gamma_p}{w_{ym}} \epsilon_{ym} \, dy \quad \ldots\ldots\ldots\ldots\ldots \quad (9)$$

Thus, the stress in the prototype due to the dead-load when the dam is constructed to elevation h is the integrated effect of all the incremental loadings at y up to elevation h, or

$$\sigma_{hp} = \int_{y_0}^{h} d\sigma_{yp} = E_m \gamma_p \int_{y_0}^{h} \frac{\epsilon_{ym}}{w_{ym}} dy \quad \ldots\ldots\ldots (10)$$

and similarly for dead-load stress of the complete dam:

$$\sigma_{Hp} = E_m \gamma_p \int_{y_0}^{H} \frac{\epsilon_{ym}}{w_{ym}} dy \quad \ldots\ldots\ldots\ldots (11)$$

It will be noted that the model-loading factor w_{ym} is taken within the integral because it may vary with each elevation tested, and is thus a function of y.

In a typical test, a model was loaded uniformly with 1,500 lb of lead bricks applied to an area of 250 sq in. Thus, the increment of stress in the prototype corresponding to adding an increment of 1 ft of concrete to the dam was

$$d\sigma = \frac{E_m \gamma_p}{w_{ym}} \epsilon_{ym}\, dy = \frac{240{,}000 \times 158 \times 1}{\frac{1500 \times 144}{250}} \epsilon_{ym} \quad \ldots\ldots\ldots (12)$$

and

$$d\sigma = 0.044\ \epsilon_{ym} \quad \ldots\ldots\ldots\ldots (13)$$

where strains are measured in micro-inches per inch.

In testing, a model is cut down to definite elevations y convenient for analysis, and loaded heavily enough to give a well-defined response in the strain gages. Using the similitude factors contained in Eq. 9, curves of incremental stress versus loading at any elevation y can be plotted, as shown in Fig. 6.

The initial value of the curves cannot be determined experimentally, because of physical limitations, and it is necessary to compute the stresses at the gage elevation y_0 due to the effect of loading at that elevation. By Hooke's law

$$d\sigma_{90} = \frac{E_p}{1-\mu^2} \left(d\epsilon_{90} + \mu\, d\epsilon_0\right) \quad \ldots\ldots\ldots (14)$$

But $d\sigma_{90}$ is the applied load, equal to the density of the concrete of 158 pcf or -1.10 psi per ft of concrete. If μ is equal to 0.24, Eq. 14 reduces to

$$E_p\, d\epsilon_{90} = -1.04 - 0.24\, E_p\, d\epsilon_0 \quad \ldots\ldots\ldots (15)$$

Since the direction of this stress is known,

$$E_p\, d\epsilon_{90} + E_p\, d\epsilon_0 = 2\, E_p\, d\epsilon_{45} \quad \ldots\ldots\ldots (16)$$

For any strain gage rosette, Eqs. 15 and 16 must be satisfied, and all three strains must be consistent with the strains developed at adjacent points y.

With the incremental stress function completely defined, the stress at y_0 due to construction to height h can be found by graphical or numerical integration of the curves representing Eq. 10.

The principal stresses for any stage of construction can then be calculated in the usual fashion from the stresses along the individual directions shown on the curves for $E_p \epsilon_\theta$.

EXAMPLE

As an example of the use of the method of integration for determining the dead-load stresses in a dam, description will be given herewith of the procedures used to test the 1:200 model shown in Fig. 7. This is the central portion of one design proposed, but not used, for the 750-ft high, 5,000 ft long Oroville Dam,[11] after conditions at the dam site led to final decision to construct an embankment dam instead of the concrete dam on which this study is based. The model was constructed by casting a plaster-celite mixture in a rigid fiberglass mold on an extensive foundation assembled from prefabricated plaster-celite slabs. The central portion of the dam consists of an inclined arch which carries on it a pair of riding buttresses. The riding buttresses not only carry load into the flanks of the arch, but they stiffen the arch in an indeterminate fashion. It can be seen that in so indeterminate and complex a structure, experimental stress analysis has many advantages over a numerical procedure.

In the gravity loading test, a uniformly distributed load was applied to a series of horizontal surfaces, after all live-loading tests had been completed. This uniform load was approximated with lead bricks. At each elevation to be tested, the area of the exposed surface was measured, and divided by a planimeter into a number of equal smaller areas. The center of gravity of each of these small areas was then found, and the position for each lead brick carefully drawn, so that the weights were equally distributed. Between 50 and 70 lead bricks, each weighing 26 lb, were used for each load test. Thus the model supported nearly a ton of dead weight at various stages of the testing. The cut model with its dead weight in place is shown in Fig. 8. When a number of tiers of lead weights had to be used, sheets of paper were interposed between layers to increase the stability of the mass.

For this particular study, a uniform load was applied on six different horizontal sections, cut at even 100-ft elevations throughout the height of the model. Three identical tests were conducted at each elevation. Since all the lead bricks had to be placed by hand, it was found most expedient to load the model during the day, let it stand overnight, and then early the next morning, when all temperatures had been equalized and the air in the laboratory was still, a reading was taken of all strain gages with the dam in the loaded condition, the lead bricks removed, and a second series of readings taken of the unloaded model. Since the model progressively reduced in height during testing, the number of gages read for any test elevation was likewise reduced. Thus the time necessary to read the gages differed at each test elevation. However, using the test set up shown in Fig. 8, which was designed around the Fairchild RBI (Resis-

11 "Structural Model Investigations for Oroville Dam," by J. M. Raphael, Inst. of Engrg. Research, Univ. of California, Series 100, Issue 6, February, 1960.

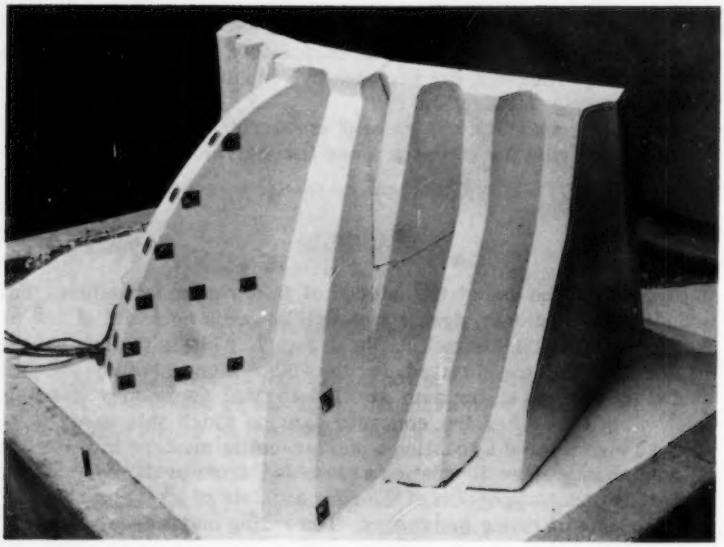

FIG. 7.—PLASTER MODEL OF CENTRAL SECTION OF MODEL OF OROVILLE DAM

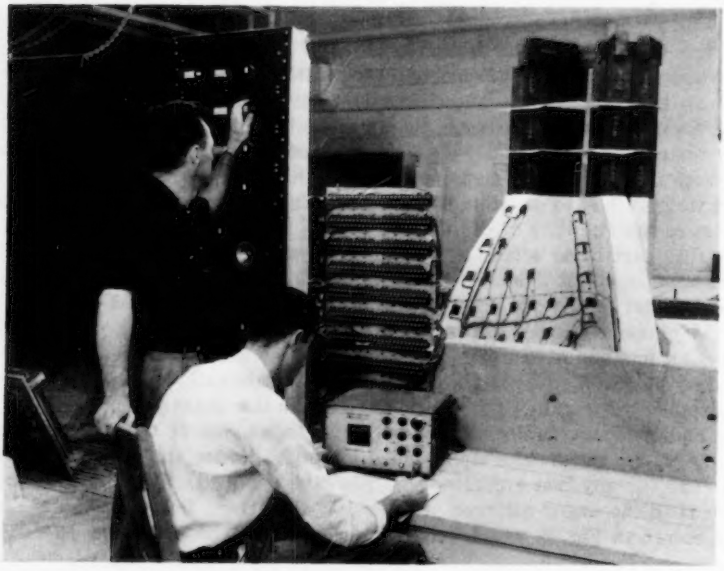

FIG. 8.—DEAD-LOAD TEST BY METHOD OF INTEGRATION AT UNIVERSITY OF CALIFORNIA

tance Bridge Indicator), 150 strain gages could be read in a period of 10 min without difficulty. It was found that model strains were sensitive to the exact placement of the uniform load, but an average of three tests tended to eliminate this error. Likewise, the use of the unloading cycle for strain measurements enabled more care to be taken with the exact placement of each lead brick, and tended further to reduce error from this cause.

DEAD-LOAD STRESSES

Fig. 9 shows the direction and magnitude of the principal dead-load stresses for the completed structure. It can be seen for that for the intrados, the principal compressive stresses increase gradually from top to bottom and that the directions are parallel to the boundaries upstream and downstream, varying gradually from face to face. For the extrados, the structural discontinuity introduced by the riding buttress is evidenced in higher compressive stresses near its lower boundary. Along the outstanding edge of the arch, the maximum compressive stresses increase from top to bottom. The considerable variation of the direction of these maximum principal stresses from the center line of the outstanding leg can be explained in part by twisting, shearing action at this boundary. Fairly high tensile stresses are found near the boundary of the arch and plug for both the extrados and intrados. Since these two structures were bonded together in the model at the arch-plug interface, a structural discontinuity proposed for the construction of the prototype would reduce or largely eliminate these tensile stresses.

Considerable speculation was raised as to the behavior of the main arch during construction. A glance at the downstream view of the dam shows the convergence of the sides of the arch as construction proceeds upwards, to the point where they overhang the base. In Fig. 10 some light is shed on the gradual development of the principal stresses for the intrados and extrados at the base as construction proceeds upwards. In Fig. 10, the intrados of the dam is shown at the left and the extrados at the right. Near the bottom foundation line, circles show the locations for which principal stresses were computed. Directly above each circle, and at elevations corresponding to the top elevation of the concrete at any particular time, the drawing shows the magnitude and direction of the principal stresses when concrete had reached that elevation. For example, for the farthest downstream location at the intrados, the maximum compressive principle stress was 135 psi when the dam was concreted to El. 400, 520 psi when construction had reached El. 700, and 600 psi when the dam was completed. It can be noted that the directions of the principal stress for the intrados change very little during the construction of the dam, and that the magnitudes increase gradually as construction progresses. However, for the extrados, there is considerable change in the direction of the principal stresses as construction proceeds upwards.

The gradual development of the vertical stress at the intrados and extrados is given in Fig. 11. Here, superimposed on an outline drawing of the intrados and extrados, are curves indicating the magnitude and sense of the vertical stress at any stage of construction, for various locations at El. 450 and along the base. Thus, the extreme left-hand curve at the bottom of the figure indicates the gradual increase of compressive vertical stress at the downstream end of the intrados from 0 to 400 psi as construction of the dam proceeds from the base to El. 906. At all locations at the base of the intrados the vertical

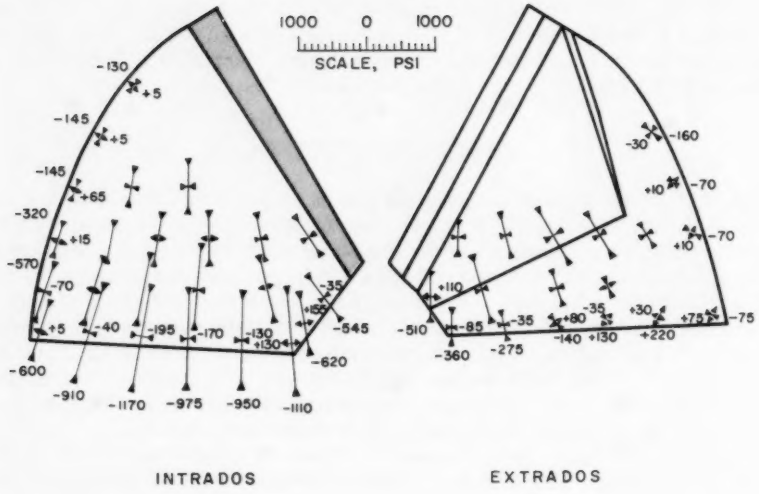

FIG. 9.—PRINCIPAL STRESSES DUE TO DEAD-LOAD

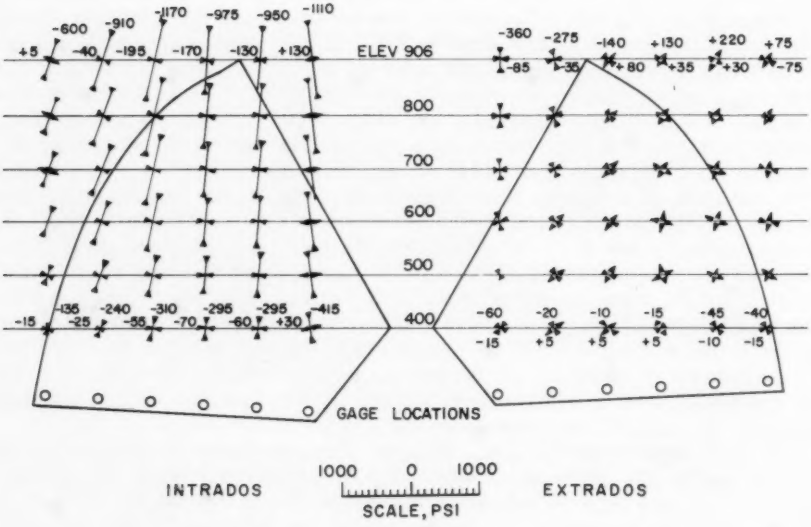

FIG. 10.—PRINCIPAL STRESSES AT BASE DUE TO DEAD-LOAD AT VARIOUS STAGES OF CONSTRUCTION

stress is compressive. Fig. 11 also indicates that the compression increases fairly rapidly until construction reaches about El. 700, and after that the increase is very slight. However, for the extrados, the curves indicate that the vertical stress is compressive at the upstream locations, tensile at the three downstream locations, and that it changes from tension to compression near the center of the extrados as construction passes El. 700.

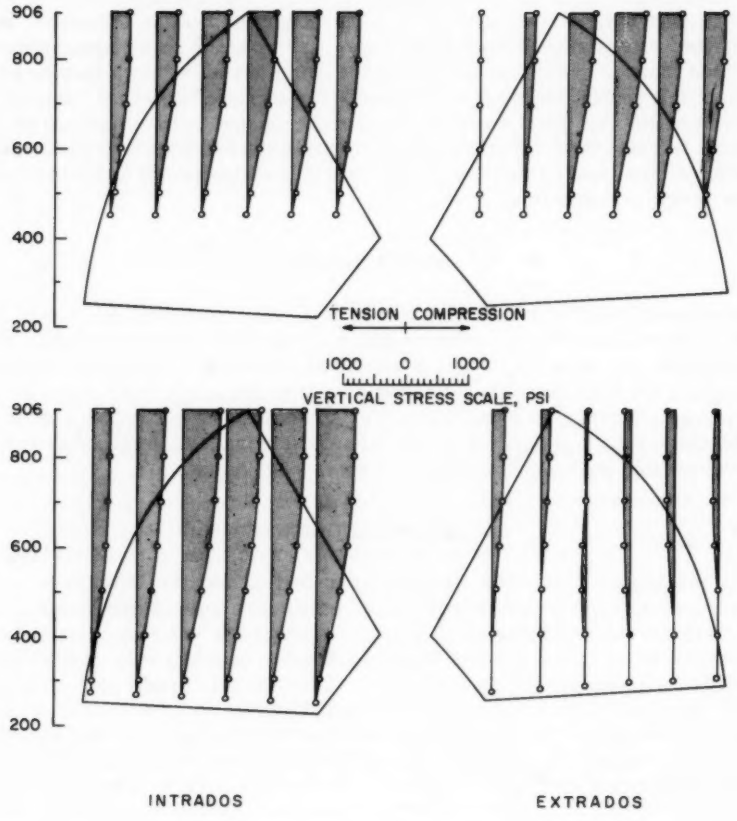

FIG. 11.—DEVELOPMENT OF VERTICAL STRESS DUE TO DEAD-LOAD

A slightly different picture is presented for the development of vertical stress at El. 450 due to construction of the dam. This information is shown on a set of curves at the top of Fig. 11. The effect of the weight of the vertical load from the buttress is readily apparent at El. 450. For this elevation, the vertical stresses are everywhere compressive for all stages of construction. The increase in stress is fairly uniform throughout the construction. Looking at Fig. 10 one can see that the vertical load coming down the riding buttress

causes heavy twisting in the arch below the junction of the riding buttress and the arch. Possibly a more gradual transition from riding buttress to arch might help make this stress picture more uniform below El. 450.

With so much tension shown at the base for the extrados, question might be raised as to the stability of the arch during construction. In evaluating the stability of the base, it was assumed that wherever tensile stresses existed, concrete could crack all the way back to zero stress. It was further assumed that if the concrete did crack, that the moment and thrust that caused the stresses would remain without redistribution to the remainder of the structure, which is a conservative assumption for the base. Having made these assumptions, it was found that for every cross-section for which stresses were measured, the resultant fell within the base, and it could thus be concluded that the arch was everywhere stable. This was not construed to mean that the method of construction in horizontal layers was best for this type of dam - another method involving sloped pours might very well result in considerably lessened tensile stress during construction.

CONCLUSIONS

A new method of experimental stress analysis, called the method of integration, is available for the determination of the dead-load stresses in dams. This method can be used to find the state of stress in a partially completed dam, and to evaluate the effect of different construction procedures on the dead load stress pattern remaining within the structure. This method should have considerable utility in predicting the behavior during and after construction of the overhanging portions of doubly curved, arched dams.

ACKNOWLEDGMENTS

The investigation reported herein was undertaken at the University of California in connection with an experimental stress analysis of one design of Oroville Dam for the Department of Water Resources of the State of California. Permission of the Department of Water Resources to publish the results of this investigation is gratefully acknowledged. Considerable credit should be given to J. L. Serafim of the Laboratorio Nacional Engenharia Civil of Lisbon and to Edward J. Wilson of the Engineering Materials Laboratory of the University of California whose discussions and speculations aided the writer in the development of this new method.

Journal of the
STRUCTURAL DIVISION
Proceedings of the American Society of Civil Engineers

GENERAL SOLUTION OF SPACE FRAMEWORKS

By Ignacio Martín,[1] A. M. ASCE, and José E. Hernández,[2]

SYNOPSIS

The solution of space frameworks with members in any direction, under any system of loads, in any direction, is established by applying the slope-defection-gyration method.[3] It provides a set of simultaneous equations that can be solved with relative ease by using the electronic computers now available.

The procedure presented herein can be extended to the approximate solution of plane or warped surface structure, concentrating the rigidity of sections of the structure in an arbitrary system of generatrices.

INTRODUCTION

The modern electronic computers provide the solution of complicated mathematical problems, and for that reason it is possible to solve sets of simultaneous equations that are established in structural analysis. This could be achieved without having to resort to methods of successive approximations that contributed so much to the progress of the structural analysis of continuous structures when the necessary elements to solve large sets of simultaneous equations were not available.

Note.—Discussion open until January 1, 1962. To extend the closing date one month, a written request must be filed with the Executive Secretary, ASCE. This paper is part of the copyrighted Journal of the Structural Division, Proceedings of the American Society of Civil Engineers, Vol. 87, No. ST 6, August, 1961.

[1] Partner, SACMAG of Puerto Rico, Inc., Cons. Engrs., San Juan, P. R.

[2] Struct. Asst., Saenz-Cancio-Martín-Gutiérrez, (SACMAG) ingenieros-arquitectos, Habana, Cuba.

[3] "Orthogonal Gridworks Loaded Normally to their Planes," by I. Martín and J. E. Hernández, Proceedings, ASCE, Vol. 86, No. ST 1, January, 1960.

The solution of a framework with members having any direction in space and under any system of loads can be attacked by establishing the flexural mo-

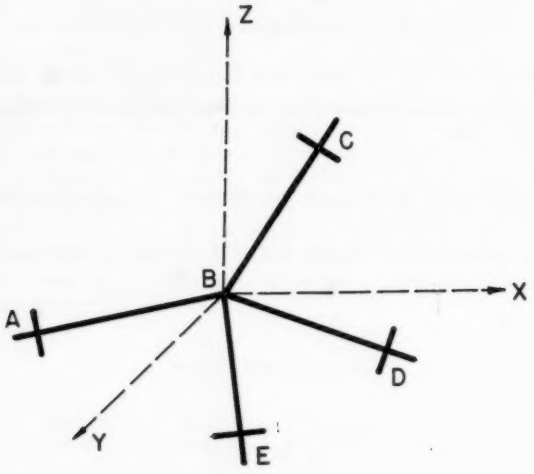

FIG. 1.

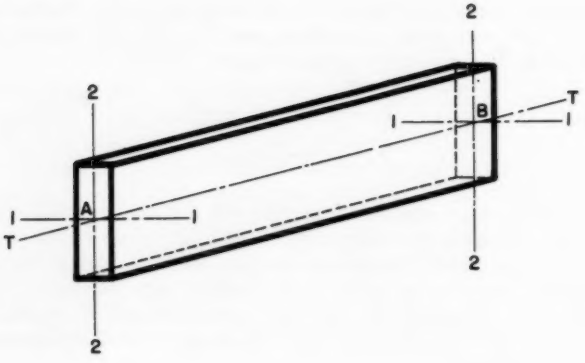

FIG. 2.

ment, torsional moment, and shear equations in the bar and the equilibrium equations of forces and moments in each joint.

Any warped surface under any system of loads, can be approximately solved by dividing the surface into a finite number of tangents in which the rigidity of

the tributary surface is concentrated, making the surface structure a framework structure.

DERIVATION OF THE SLOPE DEFLECTION-GYRATION-EQUATIONS

Notation.—The letter symbols adopted for use in this paper are defined and arranged alphabetically, for convenience of reference, in Appendix II.

Geometrical Relations.—A space joint B in which members AB, BC, BD, and BE coincide, as shown in Fig. 1, will be considered. An arbitrary cartesian system of coordinates will be used.

The direction of each bar is defined by its direction cosines a, b, and c, with respect to the system of cartesian coordinates selected.

Each joint is subjected to two types of deformations such as angular deformation and displacement. Both deformations can be considered as vectors, because an angular deformation can be defined as a vector with its axis coinciding with the axis of rotation. The deformation of joint B can be defined by its components:

$$\Delta_{BX} \qquad \theta_{BX}$$
$$\Delta_{BY} \qquad \theta_{BY}$$
$$\Delta_{BZ} \qquad \theta_{BZ}$$

If a member AB shown in Fig. 2 is considered, three axes can be defined: the torsion axis T-T, which is the longitudinal axis of the member; the principal axis of inertia 1-1; and the secondary axis of inertia 2-2. To systematize the procedure, the direction of the torsional axes of the bars can be determined by following the sequence of the letters assigned to the joints. Having done this, the direction of the principal (1) and secondary (2) flexural axes can be determined for each bar, so that the three axes T, 1, and 2 form a direction trihedron.

The direction cosines of each axis of the bar AB, are

$$a_{1AB} = a_{1BA} \cdots\cdots\cdots\cdots\cdots\cdots (1a)$$

$$b_{1AB} = b_{1BA} \cdots\cdots\cdots\cdots\cdots\cdots (1b)$$

$$c_{1AB} = c_{1BA} \cdots\cdots\cdots\cdots\cdots\cdots (1c)$$

and

$$a_{2AB} = a_{2BA} \cdots\cdots\cdots\cdots\cdots\cdots (2a)$$

$$b_{2AB} = b_{2BA} \cdots\cdots\cdots\cdots\cdots\cdots (2b)$$

$$c_{2AB} = c_{2BA} \cdots\cdots\cdots\cdots\cdots\cdots (2c)$$

and

$$a_{TAB} = a_{TBA} \cdots\cdots\cdots\cdots\cdots\cdots (3a)$$

$$b_{TAB} = b_{TBA} \cdots\cdots\cdots\cdots\cdots\cdots (3b)$$

$$c_{TAB} = c_{TBA} \cdots\cdots\cdots\cdots\cdots\cdots (3c)$$

The direction cosines comply with the following two conditions

$$a_{1AB}^2 + b_{1AB}^2 + c_{1AB}^2 = 1. \quad (4a)$$

$$a_{2AB}^2 + b_{2AB}^2 + c_{2AB}^2 = 1. \quad (4b)$$

$$a_{TAB}^2 + b_{TAB}^2 + c_{TAB}^2 = 1. \quad (4c)$$

and

$$\begin{vmatrix} a_{1AB} & b_{1AB} & c_{1AB} \\ a_{2AB} & b_{2AB} & c_{2AB} \\ a_{TAB} & b_{TAB} & c_{TAB} \end{vmatrix} = 1. \quad (5)$$

Sign Convention.—Consider bending and torsional moments, shear forces, and also deflections and rotations as vectors. Hence they all shall be positive or negative as they coincide with the positive or negative direction of axes T, 1, 2, or X, Y, Z.

When expressing moments in terms of deflections and rotations, these will be always considered positive and the moment will show the sign that corresponds.

Derivation of the Moment Equations.—Any system of loads applied to member AB can be decomposed into loads along the three bar axes, and torsional moments along axis T-T and flexural moments along axes 1-1 and 2-2 can be obtained.

The basic slope-deflection-gyration, Eqs. 3, can be applied to the torsional moments along axis T-T and the flexural moments along axes 1-1 and 2-2.

$$M_{1AB} = M_{F1AB} - k_{1AB}\left(1 + \beta_1\right)\frac{\Delta_{2A}}{|L_{AB}|} + k_{1AB}\left(1 + \beta_1\right)\frac{\Delta_{2B}}{|L_{AB}|} + k_{1AB}\,\theta_{1A} + \beta_1\, k_{1AB}\,\theta_{1B}. \quad (6a)$$

$$M_{1BA} = M_{F1BA} - k_{1BA}\left(1 + \beta_1'\right)\frac{\Delta_{2A}}{|L_{AB}|} + k_{1BA}\left(1 + \beta_1'\right)\frac{\Delta_{2B}}{|L_{AB}|} + \beta_1'\, k_{1BA}\,\theta_{1A} + k_{1BA}\,\theta_{1B}. \quad (6b)$$

$$M_{2AB} = M_{F2AB} + k_{2AB}\left(1 + \beta_2\right)\frac{\Delta_{1A}}{|L_{AB}|} - k_{2AB}\left(1 + \beta_2\right)\frac{\Delta_{1B}}{|L_{AB}|} + k_{2AB}\,\theta_{2A} + \beta_2\, k_{2AB}\,\theta_{2B}. \quad (7a)$$

$$M_{2BA} = M_{F2BA} + k_{2BA}\left(1 + \beta_2'\right)\frac{\Delta_{1A}}{|L_{AB}|} - k_{2BA}\left(1 + \beta_2'\right)\frac{\Delta_{1B}}{|L_{AB}|} + \beta_2'\, k_{2BA}\,\theta_{2A} + k_{2BA}\,\theta_{2B}. \quad (7b)$$

$$M_{TAB} = M_{FTAB} - k_{TAB}\,\theta_{TB} + k_{TAB}\,\theta_{TA}. \quad (8a)$$

and

$$M_{TBA} = M_{FTBA} + k_{TAB}\,\theta_{TB} - k_{TAB}\,\theta_{TA}. \quad (8b)$$

The moments corresponding to any other bar may be obtained by changing A to B and B to C in the preceding equations.

The following equations can be established for joints A and B, according to the geometry of the system:

$$\theta_{TA} = a_{TAB}\,\theta_{AX} + b_{TAB}\,\theta_{AY} + c_{TAB}\,\theta_{AZ} \quad \ldots\ldots \text{(9a)}$$

$$\theta_{TB} = a_{TBA}\,\theta_{BX} + b_{TBA}\,\theta_{BY} + c_{TBA}\,\theta_{BZ} \quad \ldots\ldots \text{(9b)}$$

$$\theta_{1A} = a_{1AB}\,\theta_{AX} + b_{1AB}\,\theta_{AY} + c_{1AB}\,\theta_{AZ} \quad \ldots\ldots \text{(10a)}$$

$$\theta_{1B} = a_{1BA}\,\theta_{BX} + b_{1BA}\,\theta_{BY} + c_{1BA}\,\theta_{BZ} \quad \ldots\ldots \text{(10b)}$$

$$\theta_{2A} = a_{2AB}\,\theta_{AX} + b_{2AB}\,\theta_{AY} + c_{2AB}\,\theta_{AZ} \quad \ldots\ldots \text{(11a)}$$

$$\theta_{2B} = a_{2BA}\,\theta_{BX} + b_{2BA}\,\theta_{BY} + c_{2BA}\,\theta_{BZ} \quad \ldots\ldots \text{(11b)}$$

$$\Delta_{1A} = a_{1AB}\,\Delta_{AX} + b_{1AB}\,\Delta_{AY} + c_{1AB}\,\Delta_{AZ} \quad \ldots\ldots \text{(12a)}$$

$$\Delta_{1B} = a_{1BA}\,\Delta_{BX} + b_{1BA}\,\Delta_{BY} + c_{1BA}\,\Delta_{BZ} \quad \ldots\ldots \text{(12b)}$$

$$\Delta_{2A} = a_{2AB}\,\Delta_{AX} + b_{2AB}\,\Delta_{AY} + c_{2AB}\,\Delta_{AZ} \quad \ldots\ldots \text{(13a)}$$

and

$$\Delta_{2B} = a_{2BA}\,\Delta_{BX} + b_{2BA}\,\Delta_{BY} + c_{2BA}\,\Delta_{BZ} \quad \ldots\ldots \text{(13b)}$$

It should be observed that the displacement component θ_{TB} along axis T-T does not have any influence in the torsional or flexural moments of member AB.

Similar equations can be established for all the other bars that coincide in joint B.

If the values obtained in Eqs. 9(a) to 13(b), inclusive, are substituted in Eqs. 6(a) to 8(b), inclusive, the following equations are:

$$M_{1BA} = M_{F1BA} - k_{1BA}\left(1 + \beta_1'\right)\frac{a_{2AB}\,\Delta_{AX} + b_{2AB}\,\Delta_{AY} + c_{2AB}\,\Delta_{AZ}}{|L_{AB}|} + k_{1BA}\left(1 + \beta_1'\right)\frac{a_{2BA}\,\Delta_{BX} + b_{2BA}\,\Delta_{BY} + c_{2BA}\,\Delta_{BZ}}{|L_{AB}|} + \beta_1'\,k_{1BA}\left(a_{1AB}\,\theta_{AX}\right) + b_{1AB}\,\theta_{AY} + c_{1AB}\,\theta_{AZ}\right) + k_{1BA}\left(a_{1BA}\,\theta_{BX} + b_{1BA}\,\theta_{BY} + c_{1BA}\,\theta_{BZ}\right) \quad \ldots\ldots \text{(14)}$$

$$M_{2BA} = M_{F2BA} + k_{2BA}\left(1 + \beta_2'\right)\frac{a_{1AB}\,\Delta_{AX} + b_{1AB}\,\Delta_{AY} + c_{1AB}\,\Delta_{AZ}}{|L_{AB}|} - k_{2BA}\left(1 + \beta_2'\right)\frac{a_{1BA}\,\Delta_{BX} + b_{1BA}\,\Delta_{BY} + c_{1BA}\,\Delta_{BZ}}{|L_{AB}|} + \beta_2'\,k_{2BA}\left(a_{2AB}\,\theta_{AX} + b_{2AB}\,\theta_{AY} + c_{2AB}\,\theta_{AZ}\right) + k_{2BA}\left(a_{2BA}\,\theta_{BX} + b_{2BA}\,\theta_{BY} + c_{2BA}\,\theta_{BZ}\right) \quad \ldots\ldots \text{(15)}$$

and

$$M_{TBA} = M_{FTBA} + k_{TBA}\left(a_{TBA}\,\theta_{BX} + b_{TBA}\,\theta_{BY} + c_{TBA}\,\theta_{BZ}\right) - k_{TBA}\left(a_{TAB}\,\theta_{AX} + b_{TAB}\,\theta_{AY} + c_{TAB}\,\theta_{AZ}\right) \quad (16)$$

If moments M_{1BA}, M_{2BA} and M_{TBA} are projected along the three cartesian axes, the following equations can be obtained:

$$M_{BAX} = a_{1AB}\,M_{1BA} + a_{2AB}\,M_{2BA} + a_{TAB}\,M_{TBA} \quad (17a)$$

$$M_{BAY} = b_{1AB}\,M_{1BA} + b_{2AB}\,M_{2BA} + b_{TAB}\,M_{TBA} \quad (17b)$$

and

$$M_{BAZ} = c_{1AB}\,M_{1BA} + c_{2AB}\,M_{2BA} + c_{TAB}\,M_{TBA} \quad (17c)$$

If the values obtained in Eqs. 14(a), 15(a), and 16(a) are substituted in Eqs. 17(a), 17(b), and 17(c), the following equations are

$$\begin{aligned}
M_{BAX} &= a_{1BA}\,M_{F1BA} + a_{2BA}\,M_{F2BA} + a_{TBA}\,M_{FTBA} \\
&- a_{1BA}\,a_{2BA}\,k_{1BA}\left(1+\beta_1'\right) + a_{2BA}\,a_{1AB}\,k_{2BA}\left(1+\beta_2'\right)\frac{\Delta_{AX}-\Delta_{BX}}{|L_{AB}|} \\
&- a_{1BA}\,b_{2AB}\,k_{1BA}\left(1+\beta_1'\right) + a_{2BA}\,b_{1AB}\,k_{2BA}\left(1+\beta_2'\right)\frac{\Delta_{AY}-\Delta_{BY}}{|L_{AB}|} \\
&- a_{1BA}\,c_{2AB}\,k_{1BA}\left(1+\beta_1'\right) + a_{2BA}\,c_{1AB}\,k_{2BA}\left(1+\beta_2'\right)\frac{\Delta_{AZ}-\Delta_{BZ}}{|L_{AB}|} \\
&+ a_{1BA}\,a_{1AB}\,k_{1BA}\left(\beta_1'\,\theta_{AX} + \theta_{BX}\right) \\
&+ a_{2BA}\,a_{2AB}\,k_{2BA}\left(\beta_2'\,\theta_{AX} + \theta_{BX}\right) \\
&+ a_{TBA}\,a_{TAB}\,k_{TBA}\left(-\theta_{AX} + \theta_{BX}\right) \\
&+ a_{1BA}\,b_{1AB}\,k_{1BA}\left(\beta_1'\,\theta_{AY} + \theta_{BY}\right) \\
&+ a_{2BA}\,b_{2AB}\,k_{2BA}\left(\beta_2'\,\theta_{AY} + \theta_{BY}\right) \\
&+ a_{TBA}\,b_{TAB}\,k_{TBA}\left(-\theta_{AY} + \theta_{BY}\right) \\
&+ a_{1BA}\,c_{1AB}\,k_{1BA}\left(\beta_1'\,\theta_{AZ} + \theta_{BZ}\right) \\
&+ a_{2BA}\,c_{2BA}\,k_{2BA}\left(\beta_2'\,\theta_{AZ} + \theta_{BZ}\right) \\
&+ a_{TBA}\,c_{TBA}\,k_{TBA}\left(-\theta_{AZ} + \theta_{BZ}\right) \quad (18a)
\end{aligned}$$

$$\begin{aligned}
M_{BAY} &= b_{1BA}\,M_{F1BA} + b_{2BA}\,M_{F2BA} + b_{TBA}\,M_{TBA} \\
&- \left[b_{1BA}\,a_{2AB}\,k_{1BA}\left(1+\beta_1'\right) + b_{2BA}\,a_{1AB}\,k_{2BA}\left(1+\beta_2'\right)\right]\frac{\Delta_{AX}-\Delta_{BX}}{|L_{AB}|}
\end{aligned}$$

$$- \left[b_{1BA}\, b_{2AB}\, k_{1BA} \left(1 + \beta_1'\right) + b_{2BA}\, b_{1AB}\, k_{2BA} \left(1 + \beta_2'\right) \right] \frac{\Delta_{AY} - \Delta_{BY}}{|L_{AB}|}$$

$$- \left[b_{1BA}\, c_{2AB}\, k_{1BA} \left(1 + \beta_1'\right) + b_{2BA}\, c_{1AB}\, k_{2BA} \left(1 + \beta_2'\right) \right] \frac{\Delta_{AZ} - \Delta_{BZ}}{|L_{AB}|}$$

$$+ b_{1BA}\, a_{1AB}\, k_{1BA} \left(\beta_1'\, \theta_{AX} + \theta_{BX}\right)$$

$$+ b_{2BA}\, a_{2AB}\, k_{2BA} \left(\beta_2'\, \theta_{AX} + \theta_{BX}\right)$$

$$+ b_{TBA}\, a_{TAB}\, k_{TBA} \left(-\theta_{AX} + \theta_{BX}\right)$$

$$+ b_{1BA}\, b_{1AB}\, k_{1BA} \left(\beta_1'\, \theta_{AY} + \theta_{BY}\right)$$

$$+ b_{2BA}\, b_{2AB}\, k_{2BA} \left(\beta_2'\, \theta_{AY} + \theta_{BY}\right)$$

$$+ b_{TBA}\, b_{TAB}\, k_{TBA} \left(-\theta_{AY} + \theta_{BY}\right)$$

$$+ b_{1BA}\, c_{1AB}\, k_{1BA} \left(\beta_1'\, \theta_{AZ} + \theta_{BZ}\right)$$

$$+ b_{2BA}\, c_{2AB}\, k_{2BA} \left(\beta_2'\, \theta_{AZ} + \theta_{BZ}\right)$$

$$+ b_{TBA}\, c_{TAB}\, k_{TBA} \left(-\theta_{AZ} + \theta_{BZ}\right) \quad \ldots\ldots\ldots\ldots\ldots\ldots\ldots\ldots (18b)$$

and

$$M_{BAZ} = c_{1BA}\, M_{F1BA} + c_{2BA}\, M_{F2BA} + c_{TBA}\, M_{FTBA}$$

$$- \left[c_{1BA}\, a_{2AB}\, k_{1BA} \left(1 + \beta_1'\right) + c_{2BA}\, a_{1AB}\, k_{2BA} \left(1 + \beta_2'\right) \right] \frac{\Delta_{AX} - \Delta_{BX}}{|L_{AB}|}$$

$$- \left[c_{1BA}\, b_{2AB}\, k_{1BA} \left(1 + \beta_1'\right) + c_{2BA}\, b_{1AB}\, k_{2BA} \left(1 + \beta_2'\right) \right] \frac{\Delta_{AY} - \Delta_{BY}}{|L_{AB}|}$$

$$- \left[c_{1BA}\, c_{2AB}\, k_{1BA} \left(1 + \beta_1'\right) + c_{2BA}\, c_{1AB}\, k_{2BA} \left(1 + \beta_2'\right) \right] \frac{\Delta_{AZ} - \Delta_{BZ}}{|L_{AB}|}$$

$$- c_{1BA}\, a_{1AB}\, k_{1BA} \left(\beta_1'\, \theta_{AX} + \theta_{BX}\right)$$

$$+ c_{2BA}\, a_{2AB}\, k_{2BA} \left(\beta_2'\, \theta_{AX} + \theta_{BX}\right)$$

$$+ c_{TBA}\, a_{TAB}\, k_{TBA} \left(-\theta_{AX} + \theta_{BX}\right)$$

$$+ c_{1BA}\, b_{1AB}\, k_{1BA} \left(\beta_1'\, \theta_{AY} + \theta_{BY}\right)$$

$$+ c_{2BA}\, b_{2AB}\, k_{2BA} \left(\beta_2'\, \theta_{AY} + \theta_{BY}\right)$$

$$+ c_{TBA}\, b_{TAB}\, k_{TBA} \left(-\theta_{AY} + \theta_{BY}\right)$$

$$+ c_{1BA}\, c_{1AB}\, k_{1BA} \left(\beta_1'\, \theta_{AZ} + \theta_{BZ}\right)$$

$$+ c_{2BA}\, c_{2AB}\, k_{2BA} \left(\beta'_2\, \theta_{AZ} + \theta_{BZ}\right)$$

$$+ c_{TBA}\, c_{TBA}\, k_{TBA} \left(-\theta_{AZ} + \theta_{BZ}\right) \ldots\ldots\ldots\ldots\ldots\ldots\ldots\ldots (18c)$$

If joint B is in equilibrium with respect to rotation, it is necessary that the sum of the moments along each axis should be equal to zero. If the effect of the moments produced by the relative displacements of the bars and the axial loads is considered, the equilibrium equations of the moments are

$$M_{BAX} + M_{BCX} + M_{BDX} + M_{\Delta BAX} + M_{\Delta BCX} + M_{\Delta BDX} + \ldots + m_{BX} = 0 \ldots\ldots\ldots\ldots (19a)$$

$$M_{BAY} + M_{BCY} + M_{BDY} + M_{\Delta BAY} + M_{\Delta BCY} + M_{\Delta BDY} + \ldots + m_{BY} = 0 \ldots\ldots\ldots\ldots (19b)$$

and

$$M_{BAZ} + M_{BCZ} + M_{BDZ} + M_{\Delta BAZ} + M_{\Delta BCZ} + M_{\Delta BDZ} + \ldots + m_{BZ} = 0 \ldots\ldots\ldots\ldots (19c)$$

In the usual case of framed structures, the moments due to the relative displacements of the bars and their axial loads can be disregarded, which reduces the equations to

$$M_{BAX} + M_{BCX} + M_{BDX} + \ldots\ldots m_{BX} = 0 \ldots\ldots\ldots (19d)$$

$$M_{BAY} + M_{BCY} + M_{BDY} + \ldots\ldots m_{BY} = 0 \ldots\ldots\ldots (19e)$$

and

$$M_{BAZ} + M_{BCZ} + M_{BDZ} + \ldots\ldots m_{BZ} = 0 \ldots\ldots\ldots (19f)$$

If the values of Eqs. 18(a), 18(b), and 18(c) are substituted in Eqs. 19(a), 19(b), and 19(c) and the procedure is repeated for all the other bars that coincide in joint B, three equations as a function of the linear and angular deformations can be obtained for each joint.

Derivation of the Shear Equations.—After determining the axes' directions for each bar, the equations for the shears along the T, 1, and 2 axes can be established, which for bar AB are

$$V_{2AB} = V^i_{2AB} - \frac{M_{1AB}}{|L_{AB}|} - \frac{M_{1BA}}{|L_{AB}|} \ldots\ldots\ldots\ldots (20a)$$

$$V_{2BA} = V^i_{2BA} + \frac{M_{1AB}}{|L_{AB}|} + \frac{M_{1BA}}{|L_{AB}|} \ldots\ldots\ldots\ldots (20b)$$

$$V_{1AB} = V^i_{1AB} + \frac{M_{2AB}}{|L_{AB}|} + \frac{M_{2BA}}{|L_{AB}|} \ldots\ldots\ldots\ldots (21a)$$

and

$$V_{1BA} = V^i_{1BA} - \frac{M_{2AB}}{|L_{AB}|} - \frac{M_{2BA}}{|L_{AB}|} \ldots\ldots\ldots\ldots (21b)$$

If the observer faces the plane in which the shears of the bars develop so that the axis perpendicular to that plane points towards him, the positive moments produce positive shears at the left end and negative shears at the right end.

Moments can be expressed as functions of their components along the three cartesian axes:

$$M_{1AB} = a_{1AB}\, M_{ABX} + b_{1AB}\, M_{ABY} + c_{1AB}\, M_{ABZ} \quad \ldots . (22a)$$

$$M_{1BA} = a_{1BA}\, M_{BAX} + b_{1BA}\, M_{BAY} + c_{1BA}\, M_{BAZ} \quad \ldots . (22b)$$

$$M_{2AB} = a_{2AB}\, M_{ABX} + b_{2AB}\, M_{ABY} + c_{2AB}\, M_{ABZ} \quad \ldots . (23a)$$

and

$$M_{2BA} = a_{2BA}\, M_{BAX} + b_{2BA}\, M_{BAY} + c_{2BA}\, M_{BAZ} \quad \ldots . (23b)$$

If the values of Eqs. 22(a) to 23(b), inclusive, are substituted in Eqs. 20(b) and 21(b), as a function of the direction cosines at end B, the following equations are

$$V_{2BA} = V^{i}_{2BA} + \frac{a_{1BA}\, M_{ABX} + b_{1BA}\, M_{ABY} + c_{1BA}\, M_{ABZ}}{|L_{AB}|} + \frac{a_{1BA}\, M_{BAX} + b_{1BA}\, M_{BAY} + c_{1BA}\, M_{BAZ}}{|L_{AB}|} \quad \ldots . (24)$$

and

$$V_{1BA} = V^{i}_{1BA} - \frac{a_{2BA}\, M_{ABX} + b_{2BA}\, M_{ABY} + c_{2BA}\, M_{ABZ}}{|L_{AB}|} - \frac{a_{2BA}\, M_{BAX} + b_{2BA}\, M_{BAY} + c_{2BA}\, M_{BAZ}}{|L_{AB}|} \quad \ldots . (25)$$

The components of the shear force along the three cartesian axes at end B, are

$$V_{BAX} = a_{1BA}\, V_{1BA} + a_{2BA}\, V_{2BA} \quad \ldots . (26a)$$

$$V_{BAY} = b_{1BA}\, V_{1BA} + b_{2BA}\, V_{2BA} \quad \ldots . (26b)$$

and

$$V_{BAZ} = c_{1BA}\, V_{1BA} + c_{2BA}\, V_{2BA} \quad \ldots . (26c)$$

If the values of V_{1BA} and V_{2BA} from Eqs. 24(a) and 25(a) are substituted in Eqs. 26(a), 26(b), and 26(c), the following equations are

$$V_{BAX} = a_{1BA}\, V^{i}_{1BA} + a_{2BA}\, V^{i}_{2BA} + \frac{a_{1BA}\, b_{2BA} - a_{2BA}\, b_{1BA}}{L_{BA}} \left(M_{ABX} + M_{BAX}\right) + \frac{a_{1BA}\, c_{2BA} - a_{2BA}\, c_{1BA}}{L_{BA}} \left(M_{ABZ} + M_{BAZ}\right) \quad \ldots . (27a)$$

$$V_{BAY} = b_{1BA}\, V^{i}_{1BA} + b_{2BA}\, V^{i}_{2BA} + \frac{b_{1BA}\, a_{2BA} - b_{2BA}\, a_{1BA}}{L_{BA}} \left(M_{ABX} + M_{BAX}\right) + \frac{b_{1BA}\, c_{2BA} - b_{2BA}\, c_{1BA}}{L_{BA}} \left(M_{ABZ} + M_{BAZ}\right) \quad \ldots\ldots (27b)$$

and

$$V_{BAZ} = c_{1BA}\, V^{i}_{1BA} + c_{2BA}\, V^{i}_{2BA} + \frac{c_{1BA}\, a_{2BA} - c_{2BA}\, a_{1BA}}{L_{BA}} \left(M_{ABX} + M_{BAX}\right) + \frac{c_{1BA}\, b_{2BA} - c_{2BA}\, b_{1BA}}{L_{BA}} \left(M_{ABY} + M_{BAY}\right) \quad \ldots\ldots (27c)$$

Similar equations can be obtained for V_{ABX}, V_{ABY} and V_{ABZ}, changing A to B and B to A. It must be noted carefully that in the preceding equations L_{BA} is negative, and the L_{AB} in the equations for V_{ABX}, V_{ABY}, and V_{BAZ} is positive.

M_{ABX}, M_{ABY}, M_{ABZ}, M_{BAX}, M_{BAY}, M_{BAZ}, can be substituted by their values as functions of the components of the linear and angular deformations along the three cartesian axes, found in equations of the type of Eqs. 17(a), 17(b), and 17(c). The components of shear force along the three cartesian axes will be expressed as a function of the components of the linear and angular deformations along the same axis.

If joint B is in equilibrium with respect to displacements, it is necessary that the sum of all forces along each axis should be equal to zero, so that the components along the three coordinate axes of the shears and the axial load along the T-axis of each bar concurring at joint B and the external loads applied at the joint should be equal to zero.

$$V_{BAX} + V_{BCX} + V_{BDX} + F_{BAX} + F_{BCX} + F_{BDX} + \ldots + P_{BX} = 0 \quad \ldots\ldots (28a)$$

$$V_{BAY} + V_{BCY} + V_{BDY} + F_{BAY} + F_{BCY} + F_{BDY} + \ldots + P_{BY} = 0 \quad \ldots\ldots (28b)$$

and

$$V_{BAZ} + V_{BCZ} + V_{BDZ} + F_{BAZ} + F_{BCZ} + F_{BDZ} + \ldots + P_{BZ} = 0 \quad \ldots\ldots (28c)$$

The values V_{BCX}, V_{BCY}, and V_{BCZ} may be obtained changing A to B and B to C in V_{ABX}, V_{ABY}, and V_{ABZ}, which are obtained as explained following Eqs. 27(a), 27(b), and 27(c).

Derivation of the Geometrical Equations.—With these equations, it is necessary to add the equations required by the geometric conditions of the struc-

ture which consist in making the difference of the deformations along the T-axis of each bar equal to the axial deformation of the same bar. These equations are

$$a_{TBA}\,\Delta_{BX} + b_{TBA}\,\Delta_{BY} + c_{TBA}\,\Delta_{BZ} - \left(a_{TAB}\,\Delta_{AX} + b_{TAB}\,\Delta_{AY} + c_{TAB}\,\Delta_{AZ}\right) = \Delta_{TBA} \quad \text{(29a)}$$

and

$$a_{TBC}\,\Delta_{BX} + b_{TBC}\,\Delta_{BY} + c_{TBC}\,\Delta_{BZ} - \left(a_{TCB}\,\Delta_{CX} + b_{TCB}\,\Delta_{CY} + c_{TCB}\,\Delta_{CZ}\right) = \Delta_{TBC} \quad \text{(29b)}$$

In the usual case of framed structures, the axial deformation of the bars can be disregarded, so that the equations are reduced to

$$a_{TBA}\,\Delta_{BX} + b_{TBA}\,\Delta_{BY} + c_{TBA}\,\Delta_{BZ} - \left(a_{TAB}\,\Delta_{AX} + b_{TAB}\,\Delta_{AY} + c_{TAB}\,\Delta_{AZ}\right) = 0 \quad \text{(29c)}$$

and

$$a_{TBC}\,\Delta_{BX} + b_{TBC}\,\Delta_{BY} + c_{TBC}\,\Delta_{BZ} - \left(a_{TCB}\,\Delta_{CX} + b_{TCB}\,\Delta_{CY} + c_{TCB}\,\Delta_{CZ}\right) = 0 \quad \text{(29d)}$$

Computation of the Design Moments and Shears.—Eqs. 19(c), 19(d), 19(e), 28(a), 28(b), 28(c), 29(c), and 29(d) are expressed as a function of the components along the three cartesian axes of the linear and angular deformations at joint B, and of the axial loads of the bars. Similar equations can be established for all the other joints. These equations can be solved simultaneously in order to obtain the values of the linear and angular deformations at each joint, and of the axial loads of the bars. As soon as the deformations and axial forces of the bars at each joint are obtained, the values of the flexural and torsional moments and shear forces can be obtained for each bar.

TABULAR PROCEDURE

For the purpose of systematizing the solution of the slope-deflection-gyration method, a set of tables has been prepared to permit methodical routine computations to be made before forming the equations, as this tends to avoid errors in these computations.

After the data have been entered in the tables, the filling-in can be done mechanically by assistants who need not be acquainted with the basic theory of the method.

The tables have been used to solve Examples I and II. In Example I a simplification for undisplaceable joint is used. In Example II all the tables are used.

SIMPLIFICATION OF TABLES

1. Undisplaceable Joint.—This case occurs when the bars that meet at the joint are so arranged that no movement of the joint is possible under load. It

is then only necessary to fill in Tables 1, 2-1 and 5 for that joint. This is the case of Example I, solved later.

Similar simplifications are possible for the cases of fixed joints in torsion, flexure, or supported ones, when undisplaceable.

2. Concentrated Loads at Joints Only.—In this case it is not necessary to fill in Tables 3 and 5.

3. Symmetrical Bar.—Here the matrices of the bar under consideration and the inverted bar in Tables 1 and 2 are identical.

4. Symmetrical Bar With Symmetrical Loads.—If symmetrical loads act on a symmetrical bar, the matrices of the bar considered and the inverted bar are equal in all the tables, as in Example II.

5. Symmetrical Structure with Symmetrical or Antimetric Loads.—In this case it is proven that the corresponding deformations are either equal, or equal with opposite signs, thus reducing the number of simultaneous equations.[3]

6. Triorthogonal Frame.—It is convenient in this case to make the coordinate axes parallel, respectively, to the torsion axes of the bars. By substituting the values of the direction cosines in Table 1 and filling in the other tables, the matrix of the system of slope-deflection-gyration equations is obtained, whose elements are explicitly expressed as functions of the rigidities and the transmission factors of each bar. The matrix is shown in Table 5.

7. Biorthogonal Frame Loaded Normally to Its Plane.—To obtain the matrix in this case[3] it is sufficient to consider the equilibrium of the moments with respect to the X and Y axes and the equilibrium of the shear with respect to the Z axis in Table 5, since the unknowns θZ, ΔX, and ΔY are equal to zero.

8. Biorthogonal Frame With Loads Within Its Plane.—In this case, only the moment equilibrium equation with respect to axis Z and the shear equilibrium equation with respect to axes X and Z are taken from Table 5. This simplification explicitly furnishes the matrix of the system of Maney's slope-deflection equations for the structure.

Simplifications 6, 7, and 8 refer to cases frequently met in practice. They can also be used to study the continuous systems of two or three dimensions. For that purpose these would be substituted by approximately equivalent orthogonal grids, concentrating the rigidities of the continuous system in the axes of the members of the grids.

CONCLUSIONS

1. The slope-deflection-gyration provides a mean to obtain the exact solution of space frameworks with members in any direction under any system of loads.

2. It is possible to prepare a program for an electronic computer following the tabular procedure outlined herein.

3. Other space structures, as warped surfaces can be solved approximately applying the slope-deflection-gyration method.

APPENDIX I.—EXAMPLES

Example E-1.—Undisplaceable Joint.—Consider the case presented by Fernandez Casado[4] of bars with uniform section AB, BC, and BD concurring at joint B, having fixed ends opposite to B (Fig. 3).

The position of the ends of the bars are indicated in Fig. 3.

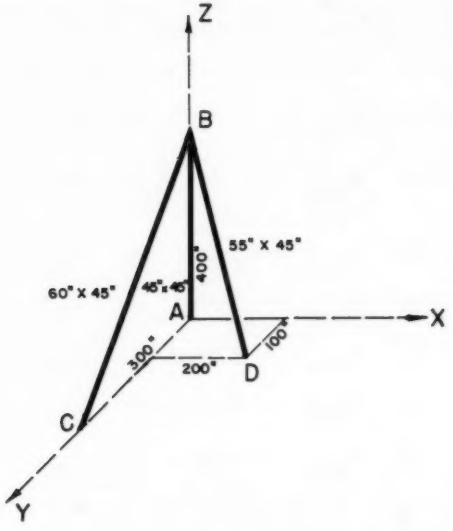

FIG. 3.

A moment is applied at joint B which can be expressed by its cartesian components as follows:

$$m_x = -3{,}000$$

$$m_y = 2{,}000$$

$$m_z = -1{,}000$$

Table E1 shows the values of the direction cosines, the relative rigidities and the computations to establish the following simultaneous equations:

$$3{,}343\ \theta_x - 244\ \theta_y + 262\ \theta_z - 3{,}000 = 0$$

4 "Cálculo de Estructuras Reticulares," by Fernández Casado, Quinta Edición, Editorial Dossat, Madrid, 1948.

$$- 244\,\theta_x + 2{,}759\,\theta_y + 458\,\theta_z + 2{,}000 = 0$$
$$262\,\theta_x + 458\,\theta_y + 1{,}054\,\theta_z - 1{,}000 = 0$$

their solution gives:

$$\theta_x = 0.750$$
$$\theta_y = -0.852$$
$$\theta_z = 1.135$$

Since the joint is undisplaceable, the displacement components do not exist.

By substituting the values previously obtained in the equations of the flexural and torsional moments and shears, the following results are obtained:

$M_{1BA} = 641$ in. lb $M_{1BC} = 1{,}215$ in. lb $M_{1BD} = 1{,}490$ in. lb

$M_{2BA} = -728$ in. lb $M_{2BC} = -2$ in. lb $M_{2BD} = 745$ in. lb

$M_{TBA} = 204$ in. lb $M_{TBC} = -341$ in. lb $M_{TBD} = -189$ in. lb

$V_{1BA} = -2.404$ lb $V_{1BC} = -3.645$ lb $V_{1BD} = -4.880$ lb

$V_{2BA} = 2.730$ lb $V_{2BC} = 0.006$ lb $V_{2BD} = -2.440$ lb

$V_{1AB} = 2.404$ lb $V_{1CB} = 3.645$ lb $V_{1DB} = 4.880$ lb

$V_{2AB} = -2.730$ lb $V_{2CB} = -0.006$ lb $V_{2DB} = 2.440$ lb

$F_{BA} = -11.791$ lb $F_{BC} = +4.211$ lb $F_{BD} = -12.525$ lb

The flexural moments at the ends of the bars opposite to joint B have one-half the value of the flexural moments of these bars at joint B. The torsional moments at the ends of the bars opposite joint B are equal in value to torsional moments of these bars at joint B.

The results obtained are equal to those found by Fernandez Casado[4] by the moment distribution method.

Example E-2.—Space Frame Stairway.—Fig. 4 shows a stairway with two unequal branches forming a 90° horizontal angle between them, without support at the common joint and fixed ends. The figure also indicates the plan, elevation, and cross section as well as the T-axis of the branches of the stairway.

The origin of coordinates coincides with joint B; the X-axis with the horizontal projection of AB; the Y-axis with the horizontal projection of BC, and the Z-axis with the vertical projection of BC. The coordinates of the stairway joints are:

A (- 3.40, 0, - 1.00)
B (0 , 0, 0)
C (0 , 7.35, 2.20)

The uniformly distributed load along both branches of the stairway is 2,060 kg per m.

Tables 1 to 4 inclusive show the computation of the elements of Table 5 which correspond to the slope-deflection-gyration equations.

In order to simplify the numerical computations, all the rigidities are shown in terms of the flexural principal rigidity of bar AB.

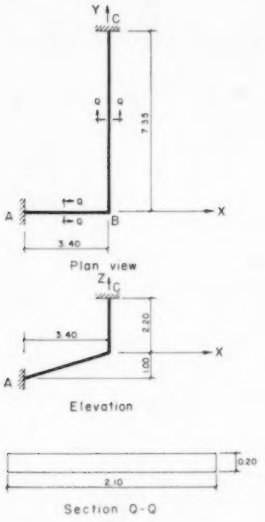

FIG. 4.

The following values are obtained by solving the slope-deflection-gyration equations of Table 5:

$$\theta_{BX} = -4{,}436.2 \qquad \Delta_{BX} = 3{,}980.1 \qquad F_{BA} = -5{,}127.5$$

$$\theta_{BY} = 179.9 \qquad \Delta_{BY} = 4{,}058.1 \qquad F_{BC} = -19{,}995$$

$$\theta_{BZ} = 612.44 \qquad \Delta_{BZ} = -13{,}569$$

Substituting the preceding amounts in Table 6 furnishes the values for the following design flexural and torsional moments (in kg. m):

$$M_{TAB} = 3{,}157.9 \qquad M_{TBC} = 124.0$$

$$M_{1AB} = -8{,}061.0 \qquad M_{1BC} = -6{,}769.5$$

$$M_{2AB} = -88{,}170.0 \qquad M_{2BC} = -12{,}376.0$$

$$M_{TBA} = 3{,}157.9 \qquad M_{TCB} = -124.0$$

$$M_{1BA} = -\ 3{,}671.0 \qquad M_{1CB} = 12{,}406.0$$

$$M_{2BA} = 13{,}240.0 \qquad M_{2CB} = -\ 26{,}037.0$$

If absolute values for rotations and deflections are desired, it is necessary to divide the relative values (obtained by solving the equations of Table 5) by the absolute value of flexural principal rigidity of bar AB, which is 3'322,000 Kgm. This way the following values are obtained:

$$\theta_{BX} = -\ .00134 \text{ radians} \qquad \Delta_{BX} = .120 \text{ cm}$$

$$\theta_{BY} = .0000542 \text{ radians} \qquad \Delta_{BY} = .122 \text{ cm}$$

$$\theta_{BZ} = .000184 \text{ radians} \qquad \Delta_{BZ} = -\ .408 \text{ cm}$$

The final moments, however, were obtained substituting directly in Table 6 the relative values of rotations and gyrations obtained by solving the equations of Table 5.

APPENDIX II.—NOTATION

a = direction cosine of a bar with respect to X-axis;

a_{1AB}, a_{2AB}, a_{TAB} = direction cosines on axes 1-1, 2-2 and T-T, respectively, of bar AB with respect to X-axis;

b = direction cosine of a bar with respect to Y-axis;

b_{1AB}, b_{2AB}, b_{TAB} = direction cosines on axes 1-1, 2-2 and T-T, respectively, of bar AB with respect to Y-axis;

c = direction cosine of a bar with respect to Z-axis;

c_{1AB}, c_{2AB}, c_{TAB} = direction cosines on axes 1-1, 2-2 and T-T, respectively, of bar AB with respect to Z-axis;

F_{BAX}, F_{BCX}, F_{BDX} = X-axis components of the axial forces of the bars that concur at joint B;

F_{BAY}, F_{BCY}, F_{BDY} = Y-axis components of the axial forces of the bars that concur at joint B;

F_{BAZ}, F_{BCZ}, F_{BDZ} = Z-axis components of the axial forces of the bars that concur at joint B;

k_{1AB} = flexural rigidity of bar AB at A, with respect to axis 1-1;

k_{2AB} = flexural rigidity of bar AB at A, with respect to axis 2-2;

k_{TAB} = torsional rigidity of bar AB, with respect to axis T-T;

k_{1BA} = flexural rigidity of bar AB at B, with respect to axis 1-1;

k_{2BA} = flexural rigidity of bar AB at B, with respect to axis 2-2;

$|L_{AB}|$ = length of bar AB, always considered positive;

L_{AB} = length of bar AB, with plus sign;

L_{BA} = length of bar AB, with minus sign;

M_{1AB}, M_{1BA} = resultant of bending moments of bar AB, at ends A and B, respectively, with respect to axis 1-1;

M_{2AB}, M_{2BA} = resultant of bending moments of bar AB, at ends A and B, respectively, with respect to axis 2-2;

M_{TAB}, M_{TBA} = resultant of torsion moments of bar AB, at ends A and B, respectively, with respect to axis T-T;

M_{BAX}, M_{BCX}, M_{BDX}, M_{BEX} = components of the resultant of bending moments of each bar concurrent at B, in a plane perpendicular to axis XX;

M_{BAY}, M_{BCY}, M_{BDY}, M_{BEY} = components of the resultant of bending moments of each bar concurrent at B, in a plane perpendicular to axis YY;

M_{BAZ}, M_{BCZ}, M_{BDZ}, M_{BEZ} = components of the resultant of bending moments of each bar concurrent at B, in a plane perpendicular to axis ZZ;

M_{F1AB}, M_{F1BA} = fixed end bending moments with respect to axis 1-1 of bar AB, at ends A and B, respectively;

M_{F2AB}, M_{F2BA} = fixed end bending moments with respect to axis 2-2 of bar AB, at ends A and B, respectively;

M_{FTAB}, M_{FTBA} = fixed end torsion moments with respect to axis T-T of bar AB, at ends A and B, respectively;

$M_{\Delta BAX}$, $M_{\Delta BCX}$, $M_{\Delta BDX}$ = bending moments at B, in a plane perpendicular to the X-axis, due to the relative displacements of the ends of the bars and the axial forces of the same bars, corresponding to the bars concurring at joint B. In the usual framed structures these values can be disregarded;

$M_{\Delta BAY}$, $M_{\Delta BCY}$, $M_{\Delta BDY}$, $M_{\Delta BAZ}$, $M_{\Delta BCZ}$, $M_{\Delta BDZ}$ = defined similarly to the previous case, and following the symbolism which corresponds in each case;

m_{BX} = external moment applied at joint B, in a plane perpendicular to axis XX;

m_{BY} = external moment applied at joint B, in a plane perpendicular to axis YY;

m_{BZ} = external moment applied at joint B, in a plane perpendicular to axis ZZ;

P_{BX}, P_{BY}, P_{BZ} = components along axes XX, YY, and ZZ, respectively, of the load applied at B;

V_{1AB} = shear at A of bar AB, on axis 1-1;

V_{1BA} = shear at B of bar AB, on axis 1-1;

V^i_{1AB}, V^i_{1BA} = isostatic shears on axis 1-1, due to the loads acting on bar AB, at A and B, respectively.

V_{2AB} = shear at A of bar AB, on axis 2-2;

V_{2BA} = shear at B of bar AB, on axis 2-2;

V^i_{2AB}, V^i_{2BA} = isostatic shear at A and B, respectively, on axis 2-2, due to the loads acting on bar AB;

V_{BAX} = component of resultant shear at B of bar AB, on axis XX;

V_{BAX}, V_{BCX}, V_{BDX}, V_{BEX} = components along axis XX of the resultant shear at B of the bars concurrent at B;

V_{BAY} = component of resultant shear at B of bar AB, on axis YY;

V_{BAY}, V_{BCY}, V_{BDY}, V_{BEY} = components along axis YY of the resultant shear at B of the bars concurrent at B;

V_{BAZ} = component of resultant shear at B of bar AB, on axis ZZ;

V_{BAZ}, V_{BCZ}, V_{BDZ}, V_{BEZ} = components along axis ZZ of the resultant shear at B of the bars concurrent at B;

β_1 = flexure transmission factor with respect to axis 1-1, from A to B, on bar AB;

β'_1 = flexure transmission factor with respect to axis 1-1, from B to A, on bar AB;

β_2 = flexure transmission factor with respect to axis 2-2, from A to B, on bar AB;

β'_2 = flexure transmission factor with respect to axis 2-2, from B to A, on bar AB;

Δ_{BX} = displacement of joint B, along axis XX;

Δ_{BY} = displacement of joint B, along axis YY;

Δ_{BZ} = displacement of joint B, along axis ZZ;

Δ_{1A} = displacement of joint A, along axis 1-1;

Δ_{1B} = displacement of joint B, along axis 1-1;

Δ_{2A} = displacement of joint A, along axis 2-2;

Δ_{2B} = displacement of joint B, along axis 2-2;

Δ_{TBA}, Δ_{TBC} = deformations along the T-axis of the bars concurring at joint B, due to axial loads F_{BA} and F_{BC}. For framed structures these values are negligible;

θ_{1A} = rotation of joint A, with respect to axis 1-1;

θ_{2A} = rotation of joint A, with respect to axis 2-2;

θ_{TA} = rotation of joint A, with respect to axis T-T;

θ_{1B} = rotation of joint B, with respect to axis 1-1;

θ_{2B} = rotation of joint B, with respect to axis 2-2;

θ_{TB} = rotation of joint B, with respect to axis T-T;

θ_{BX} = angular deformation of joint B in a plane perpendicular to axis XX;

θ_{BY} = angular deformation of joint B in a plane perpendicular to axis YY; and

θ_{BZ} = angular deformation of joint B in a plane perpendicular to axis ZZ.

TABLE 1.—EXAMPLE E1, ELASTIC CHARACTERISTICS OF BARS (JOINT = B)

		Bar = ____ L = ____				Bar = BA L = 400				Bar = BC L = 500				Bar = BD L = 458			
		T	1	2	Σ	T	1	2	Σ	T	1	2	Σ	T	1	2	Σ
1 1	a	a_T	a_1	a_2		0	1	0		0	1	0		.436	.447	.780	
	b	b_T	b_1	b_2		0	0	1		.6	0	.8		.218	-.894	.390	
	c	c_T	c_1	c_2		1	0	0		-.8	0	.6		-.873	0	.489	
	k	k_T	k_1	k_2		180	855	855		240	1620	911		224	1360	910	
	β	-1	β_1	β_2		-1	.5	.5		-1	.5	.5		-1	.5	.5	
	1+β	0	$1+\beta_1$	$1+\beta_2$		0	1.5	1.5		0	1.5	1.5		0	1.5	1.5	
	f=k(1+β)÷IL I	0	f_1	f_2		0	3.21	3.21		0	4.86	2.73		0	4.46	2.98	
1 2	a^2	a_T^2	a_1^2	a_2^2	Σa^2	0	1	0	1	0	1	0	1	.190	.200	.609	.999
	ab	$a_T b_T$	$a_1 b_1$	$a_2 b_2$		0	0	0		0	0	0		.095	-.400	.304	
	ac	$a_T c_T$	$a_1 c_1$	$a_2 c_2$		0	0	0		0	0	0		-.381	0	.381	
	b^2	b_T^2	b_1^2	b_2^2	Σb^2	0	0	1	1	.360	0	.640	1	.0475	.800	.152	1
	bc	$b_T c_T$	$b_1 c_1$	$b_2 c_2$		0	0	0		-.480	0	.480		-.190	0	.191	
	c^2	c_T^2	c_1^2	c_2^2	Σc^2	1	0	0	1	.640	0	.360	1	.762	0	.239	1.001
1 3	$k a^2$	$k_T a_T^2$	$k_1 a_1^2$	$k_2 a_2^2$	$\Sigma k a^2$	0	855	0	855	0	1620	0	1620	43	271	554	868
	kab	$k_T a_T b_T$	$k_1 a_1 b_1$	$k_2 a_2 b_2$	Σkab	0	0	0	0	0	0	0	0	21	-542	277	-244
	kac	$k_T a_T c_T$	$k_1 a_1 c_1$	$k_2 a_2 c_2$	Σkac	0	0	0	0	0	0	0	0	-85	0	347	262
	$k b^2$	$k_T b_T^2$	$k_1 b_1^2$	$k_2 b_2^2$	$\Sigma k b^2$	0	0	855	855	85	0	584	669	11	1086	138	1235
	kbc	$k_T b_T c_T$	$k_1 b_1 c_1$	$k_2 b_2 c_2$	Σkbc	0	0	0	0	-115	0	438	323	-42	0	177	135
	$k c^2$	$k_T c_T^2$	$k_1 c_1^2$	$k_2 c_2^2$	$\Sigma k c^2$	180	0	0	180	154	0	328	482	170	0	222	392
1 4	$\beta k a^2$	$\beta_T k_T a_T^2$	$\beta_1 k_1 a_1^2$	$\beta_2 k_2 a_2^2$	$\Sigma \beta k a^2$	0	427.5	0	427.5	0	810	0	810	-42.6	136	276.6	370
	βkab	$\beta_T k_T a_T b_T$	$\beta_1 k_1 a_1 b_1$	$\beta_2 k_2 a_2 b_2$	$\Sigma \beta kab$	0	0	0	0	0	0	0	0	-21.4	-272	138.3	155
	βkac	$\beta_T k_T a_T c_T$	$\beta_1 k_1 a_1 c_1$	$\beta_2 k_2 a_2 c_2$	$\Sigma \beta kac$	0	0	0	0	0	0	0	0	85.3	0	173.3	258.6
	$\beta k b^2$	$\beta_T k_T b_T^2$	$\beta_1 k_1 b_1^2$	$\beta_2 k_2 b_2^2$	$\Sigma \beta k b^2$	0	0	427.5	427.5	-86.4	0	291.5	205.1	-10.8	543	69.1	601.3
	βkbc	$\beta_T k_T b_T c_T$	$\beta_1 k_1 b_1 c_1$	$\beta_2 k_2 b_2 c_2$	$\Sigma \beta kbc$	0	0	0	0	115.2	0	218.7	333.9	42	0	87	129
	$\beta k c^2$	$\beta_T k_T c_T^2$	$\beta_1 k_1 c_1^2$	$\beta_2 k_2 c_2^2$	$\Sigma \beta k c^2$	-180	0	0	-180	-153.6	0	164	10.4	-170.7	0	108.7	-62

TABLE 2.—EXAMPLE E1

		Bar = ____ L = ____			Bar = BA L = 400			Bar = BC L = 500			Bar = BD L = 458		
	(K)	1	2	3	1	2	3	1	2	3	1	2	3
	1	$\measuredangle ka^2$	$\measuredangle kab$	$\measuredangle kac$	855	0	0	1620	0	0	868	−244	262
2 1	2	$\measuredangle kab$	$\measuredangle kb^2$	$\measuredangle kbc$	0	855	0	0	669	323	−244	1235	135
	3	$\measuredangle kac$	$\measuredangle kbc$	$\measuredangle kc^2$	0	0	180	0	323	482	262	135	392
	(β K)	1	2	3	1	2	3	1	2	3	1	2	3
	1	$\measuredangle\beta ka^2$	$\measuredangle\beta kab$	$\measuredangle\beta kac$	427.5	0	0	810	0	0	370	155	258.6
2 2	2	$\measuredangle\beta kab$	$\measuredangle\beta kb^2$	$\measuredangle\beta kbc$	0	427.5	0	0	205.1	333.9	155	601.3	129
	3	$\measuredangle\beta kac$	$\measuredangle\beta kbc$	$\measuredangle\beta kc^2$	0	0	−180	0	333.9	10.4	258.6	129	−62
	(G)	1	2	3	1	2	3	1	2	3	1	2	3
	1	$a_1 a_2$	$a_1 b_2$	$a_1 c_2$	0	1	0	0	8	.6	.349	.1745	.219
2 3	2	$b_1 a_2$	$b_1 b_2$	$b_1 c_2$	0	0	0	0	0	0	−.697	−.349	−.438
	3	$c_1 a_2$	$c_1 b_2$	$c_1 c_2$	0	0	0	0	0	0	0	0	0
	(H)	1	2	3	1	2	3	1	2	3	1	2	3
	1	$a_2 a_1$	$a_2 b_1$	$a_2 c_1$	0	0	0	0	0	0	.349	−.697	0
2 4	2	$b_2 a_1$	$b_2 b_1$	$b_2 c_1$	1	0	0	.8	0	0	.1745	−.349	0
	3	$c_2 a_1$	$c_2 b_1$	$c_2 c_1$	0	0	0	.6	0	0	.219	−.438	0
	(J) = (G)−(H)	1	2	3	1	2	3	1	2	3	1	2	3
	1	0	$a_1 b_2 - a_2 b_1$	$a_1 c_2 - a_2 c_1$	0	1	0	0	8	.6	0	−.5225	.219
2 5	2	$b_1 a_2 - b_2 a_1$	0	$b_1 c_2 - b_2 c_1$	1	0	0	.8	0	0	−.5225	0	−.438
	3	$c_1 a_2 - c_2 a_1$	$c_1 b_2 - c_2 b_1$	0	0	0	0	.6	0	0	.219	−.438	0
		Bar = ____ L = ____			Bar = BA L = 400			Bar = BC L = 500			Bar = BD L = 458		
	(K)+(β K)+(G)	1	2	3	1	2	3	1	2	3	1	2	3
	1	$\measuredangle\beta ka^2 + \measuredangle ka^2$	$\measuredangle\beta kab + \measuredangle kab$	$\measuredangle\beta kac + \measuredangle kac$	1282.5	0	0	2430	0	0	1238	−89	520.6
2 11	2	$\measuredangle\beta kab + \measuredangle kab$	$\measuredangle\beta kb^2 + \measuredangle kb^2$	$\measuredangle\beta kbc + \measuredangle kbc$	0	1282.5	0	0	874.1	656.9	−89	1836.3	264
	3	$\measuredangle\beta kac + \measuredangle kac$	$\measuredangle\beta kbc + \measuredangle kbc$	$\measuredangle\beta kc^2 + \measuredangle kc^2$	0	0	0	0	656.9	492.4	520.6	264	330
	(J, Q)	1	2	3	1	2	3	1	2	3	1	2	3
	1	0	0	0									
2 12	2	$J_{12} Q_{21}$	$J_{12} Q_{22}$	$J_{12} Q_{23}$									
	3	$J_{13} Q_{31}$	$J_{13} Q_{32}$	$J_{13} Q_{33}$									
	(J, R)	1	2	3	1	2	3	1	2	3	1	2	3
	1	0	0	0	0	0	0	0	0	0	0	0	0
2 13	2	$J_{12} R_{21}$	$J_{12} R_{22}$	$J_{12} R_{23}$	0	1282.5	0	0	699.3	525.5	46.6	−960	−138
	3	$J_{13} R_{31}$	$J_{13} R_{32}$	$J_{13} R_{33}$	0	0	0	0	394.1	295.4	114.0	57.8	72.4
	(J, Q)	1	2	3	1	2	3	1	2	3	1	2	3
	1	$J_{21} Q_{11}$	$J_{21} Q_{12}$	$J_{21} Q_{13}$									
2 14	2	0	0	0									
	3	$J_{23} Q_{31}$	$J_{23} Q_{32}$	$J_{23} Q_{33}$									
	(J, R)	1	2	3	1	2	3	1	2	3	1	2	3
	1	$J_{21} R_{11}$	$J_{21} R_{12}$	$J_{21} R_{13}$	1282.5	0	0	1944	0	0	−647	46.5	−272
2 15	2	0	0	0	0	0	0	0	0	0	0	0	0
	3	$J_{23} R_{31}$	$J_{23} R_{32}$	$J_{23} R_{33}$	0	0	0	0	0	0	−228	−115.7	−144.7

TABLE 2.—EXAMPLE E2—*CONTINUED*

		Bar = ____ L = ____			Bar = BA L = −3.54			Bar = BC L = +7.67			Bar = ____ L = ____		
	(K)	1	2	3	1	2	3	1	2	3	1	2	3
	1	Σka^2	Σkab	Σkac	9.4805	0	−29.669	.462	0	0			
2 1	2	Σkab	Σkb^2	Σkbc	0	1	0	0	4.5282	−13.939			
	3	Σkac	Σkbc	Σkc^2	−29.669	0	101.88	0	−13.939	46.933			
	(β K)	1	2	3	1	2	3	1	2	3	1	2	3
	1	$\Sigma\beta ka^2$	$\Sigma\beta kab$	$\Sigma\beta kac$	3.6708	0	−15.148	.231	0	0			
2 2	2	$\Sigma\beta kab$	$\Sigma\beta kb^2$	$\Sigma\beta kbc$	0	.5	0	0	1.7730	−7.1165			
	3	$\Sigma\beta kac$	$\Sigma\beta kbc$	$\Sigma\beta kc^2$	−15.148	0	50.849	0	−7.1165	23.423			
	(G)	1	2	3	1	2	3	1	2	3	1	2	3
	1	$a_1 a_2$	$a_1 b_2$	$a_1 c_2$	0	0	0	0	.287	−.959			
2 3	2	$b_1 a_2$	$b_1 b_2$	$b_1 c_2$	−.282	0	.961	0	0	0			
	3	$c_1 a_2$	$c_1 b_2$	$c_1 c_2$	0	0	0	0	0	0			
	(H)	1	2	3	1	2	3	1	2	3	1	2	3
	1	$a_2 a_1$	$a_2 b_1$	$a_2 c_1$	0	−.282	0	0	0	0			
2 4	2	$b_2 a_1$	$b_2 b_1$	$b_2 c_1$	0	0	0	.287	0	0			
	3	$c_2 a_1$	$c_2 b_1$	$c_2 c_1$	0	.961	0	−.959	0	0			
	(J) = (G, H)	1	2	3	1	2	3	1	2	3	1	2	3
	1	0	$a_1 b_2 - a_2 b_1$	$a_1 c_2 - a_2 c_1$	0	.282	0	0	.287	−.959			
2 5	2	$b_1 a_2 - b_2 a_1$	0	$b_1 c_2 - b_2 c_1$	−.282	0	.961	−.287	0	0			
	3	$c_1 a_2 - c_2 a_1$	$c_1 b_2 - c_2 b_1$	0	0	−.961	0	.959	0	0			
		Bar = ____ L = ____			Bar = BA L = −3.54			Bar = BC L = +7.67			Bar = ____ L = ____		
	(f, G)	1	2	3	1	2	3	1	2	3	1	2	3
	1	$f_1 a_1 a_2$	$f_1 a_1 b_2$	$f_1 a_1 c_2$	0	0	0	0	.025931	−.086648			
2 6	2	$f_1 b_1 a_2$	$f_1 b_1 b_2$	$f_1 b_1 c_2$	−.11949	0	.40720	0	0	0			
	3	$f_1 c_1 a_2$	$f_1 c_1 b_2$	$f_1 c_1 c_2$	0	0	0	0	0	0			
	(f_2 H)	1	2	3	1	2	3	1	2	3	1	2	3
	1	$f_2 a_2 a_1$	$f_2 a_2 b_1$	$f_2 a_2 c_1$	0	−13.174	0	0	0	0			
2 7	2	$f_2 b_2 a_1$	$f_2 b_2 b_1$	$f_2 b_2 c_1$	0	0	0	2.8625	0	0			
	3	$f_2 c_2 a_1$	$f_2 c_2 b_1$	$f_2 c_2 c_1$	0	44.894	0	−9.5650	0	0			
	(D) = (G) − (f_2 H)	1	2	3	1	2	3	1	2	3	1	2	3
	1	$f_1 a_1 a_2 - f_2 a_2 a_1$	$f_1 a_1 b_2 - f_2 a_2 b_1$	$f_1 a_1 c_2 - f_2 a_2 c_1$	0	+13.174	0	0	+.025931	−.086648			
2 8	2	$f_1 b_1 a_2 - f_2 b_2 a_1$	$f_1 b_1 b_2 - f_2 b_2 b_1$	$f_1 b_1 c_2 - f_2 b_2 c_1$	−.11949	0	+.40720	−2.8625	0	0			
	3	$f_1 c_1 a_2 - f_2 c_2 a_1$	$f_1 c_1 b_2 - f_2 c_2 b_1$	$f_1 c_1 c_2 - f_2 c_2 c_1$	0	−44.894	0	+9.5650	0	0			
	(N + N′)	1	2	3	1	2	3	1	2	3	1	2	3
	1	$N_{11} + N'_{11}$	$N_{12} + N'_{12}$	$N_{13} + N'_{13}$	0	+26.348	0	0	+.051862	−.17330			
2 9	2	$N_{21} + N'_{21}$	$N_{22} + N'_{22}$	$N_{23} + N'_{23}$	−23.898	0	+81.440	−5.7250	0	0			
	3	$N_{31} + N'_{31}$	$N_{32} + N'_{32}$	$N_{33} + N'_{33}$	0	−89.788	0	+19.130	0	0			
	(G) + (BK) + (K′)	1	2	3	1	2	3	1	2	3	1	2	3
	1	$\Sigma\beta ka^2 + \Sigma k'a^2$	$\Sigma\beta kab + \Sigma k'ab$	$\Sigma\beta kac + \Sigma k'ac$	13.151	0	−44.817	.693	0	0			
2 10	2	$\Sigma\beta kab + \Sigma k'ab$	$\Sigma\beta kb^2 + \Sigma k'b^2$	$\Sigma\beta kbc + \Sigma k'bc$	0	1.5	0	0	6.3012	−21.056			
	3	$\Sigma\beta kac + \Sigma k'ac$	$\Sigma\beta kbc + \Sigma k'bc$	$\Sigma\beta kc^2 + \Sigma k'c^2$	−44.817	0	152.73	0	−21.056	70.356			

TABLE 2.—EXAMPLE E2—*CONTINUED*

		Bar = ____ L = ____			Bar = BA L = -3.54			Bar = BC L = +7.67			Bar = ____ L = ____		
(K)-(B K)=0C		1	2	3	1	2	3	1	2	3	1	2	3
11	1	$\Sigma(\beta k a^2 + \Sigma k a^2$	$\Sigma(\beta k a b + \Sigma k a b$	$\Sigma(\beta k a c + \Sigma k a c$	13.151	0	−44.817	.693	0	0			
	2	$\Sigma(\beta k a b + \Sigma k a b$	$\Sigma(\beta k b^2 + \Sigma k b^2$	$\Sigma(\beta k b c + \Sigma k b c$	0	1.5	0	0	6.3012	−21.056			
	3	$\Sigma(\beta k a c + \Sigma k a c$	$\Sigma(\beta k b c + \Sigma k b c$	$\Sigma(\beta k c^2 + \Sigma k c^2$	−44.817	0	152.73	0	−21.056	70.356			
(J, Q)		1	2	3	1	2	3	1	2	3	1	2	3
12	1	0	0	0	0	0	0	0	0	0			
	2	$J_{12} Q_{21}$	$J_{12} Q_{22}$	$J_{12} Q_{23}$	0	4.23	0	0	1.8084	−6.0431			
	3	$J_{13} Q_{31}$	$J_{13} Q_{32}$	$J_{13} Q_{33}$	0	0	0	0	20.193	−67.471			
(J, R)		1	2	3	1	2	3	1	2	3	1	2	3
13	1	0	0	0	0	0	0	0	0	0			
	2	$J_{12} R_{21}$	$J_{12} R_{22}$	$J_{12} R_{23}$	0	4.23	0	0	1.8084	−6.0431			
	3	$J_{13} R_{31}$	$J_{13} R_{32}$	$J_{13} R_{33}$	0	0	0	0	20.193	−67.471			
(J_2 Q)		1	2	3	1	2	3	1	2	3	1	2	3
14	1	$J_{21} Q_{11}$	$J_{21} Q_{12}$	$J_{21} Q_{13}$	−3.7086	0	12.638	−.19889	0	0			
	2	0	0	0	0	0	0	0	0	0			
	3	$J_{23} Q_{31}$	$J_{23} Q_{32}$	$J_{23} Q_{33}$	−43.069	0	146.77	0	0	0			
(J_2 R)		1	2	3	1	2	3	1	2	3	1	2	3
15	1	$J_{21} R_{11}$	$J_{21} R_{12}$	$J_{21} R_{13}$	-3.7086	0	12.638	-.19889	0	0			
	2	0	0	0	0	0	0	0	0	0			
	3	$J_{23} R_{31}$	$J_{23} R_{32}$	$J_{23} R_{33}$	-43.069	0	146.77	0	0	0			
		Bar = ____ L = ____			Bar = BA L = -3.54			Bar = BC L = +7.67			Bar = ____ L = ____		
(J_2 Q)		1	2	3	1	2	3	1	2	3	1	2	3
16	1	$J_{31} Q_{11}$	$J_{31} Q_{12}$	$J_{31} Q_{13}$	0	0	0	.66459	0	0			
	2	$J_{32} Q_{21}$	$J_{32} Q_{22}$	$J_{32} Q_{23}$	0	−1.4415	0	0	0	0			
	3	0	0	0	0	0	0	0	0	0			
(J_2 R)		1	2	3	1	2	3	1	2	3	1	2	3
17	1	$J_{31} R_{11}$	$J_{31} R_{12}$	$J_{31} R_{13}$	0	0	0	.66459	0	0			
	2	$J_{32} R_{21}$	$J_{32} R_{22}$	$J_{32} R_{23}$	0	−1.4415	0	0	0	0			
	3	0	0	0	0	0	0	0	0	0			
(J Q)		1	2	3	1	2	3	1	2	3	1	2	3
18	1	$\Sigma(J_1 Q)^1$	$\Sigma(J_1 Q)^2$	$\Sigma(J_1 Q)^3$	0	4.23	0	0	22.001	−73.514			
	2	$\Sigma(J_2 Q)^1$	$\Sigma(J_2 Q)^2$	$\Sigma(J_2 Q)^3$	−46.778	0	159.41	−.19889	0	0			
	3	$\Sigma(J_3 Q)^1$	$\Sigma(J_3 Q)^2$	$\Sigma(J_3 Q)^3$	0	−1.4415	0	.66459	0	0			
(J R)		1	2	3	1	2	3	1	2	3	1	2	3
19	1	$\Sigma(J_1 R)^1$	$\Sigma(J_1 R)^2$	$\Sigma(J_1 R)^3$	0	4.23	0	0	22.001	−73.514			
	2	$\Sigma(J_2 R)^1$	$\Sigma(J_2 R)^2$	$\Sigma(J_2 R)^3$	−46.778	0	159.41	−.19889	0	0			
	3	$\Sigma(J_3 R)^1$	$\Sigma(J_3 R)^2$	$\Sigma(J_3 R)^3$	0	−1.4415	0	.66459	0	0			
(W)-(J Q)/ L		1	2	3	1	2	3	1	2	3	1	2	3
20	1	W_{11}	W_{12}	W_{13}	0	−.11949	0	0	2.8684	−9.5846			
	2	W_{21}	W_{22}	W_{23}	13.214	0	−45.031	−.025931	0	0			
	3	W_{31}	W_{32}	W_{33}	0	.40720	0	.086648	0	0			

TABLE 2.—EXAMPLE E2—*CONTINUED*

		Bar = ____ L = ____			Bar = BA L = −3.54			Bar = BC L = +7.67			Bar = ____ L = ____		
$(U_{ij}) = (J/N)/L$		1	2	3	1	2	3	1	2	3	1	2	3
21	1	U_{11}	U_{12}	U_{13}	0	−.11949	0	0	2.8684	−9.5846			
	2	U_{21}	U_{22}	U_{23}	13.214	0	−45.031	−.025931	0	0			
	3	U_{31}	U_{32}	U_{33}	0	.40720	0	.086648	0	0			
	$(J_1 N)$	1	2	3	1	2	3	1	2	3	1	2	3
22	1	0	0	0	0	0	0	0	0	0			
	2	$J_{12}(N+N')_{21}$	$J_{12}(N+N')_{22}$	$J_{12}(N+N')_{23}$	−.067392	0	+.22966	−1.64308	0	0			
	3	$J_{13}(N+N')_{31}$	$J_{13}(N+N')_{32}$	$J_{13}(N+N')_{33}$	0	0	0	−18.3456	0	0			
	$(J_2 N)$	1	2	3	1	2	3	1	2	3	1	2	3
23	1	$J_{21}(N+N')_{11}$	$J_{21}(N+N')_{12}$	$J_{21}(N+N')_{13}$	0	−7.4301	0	0	−.014884	+.049737			
	2	0	0	0	0	0	0	0	0	0			
	3	$J_{23}(N+N')_{31}$	$J_{23}(N+N')_{32}$	$J_{23}(N+N')_{33}$	0	−86.286	0	0	0	0			
	$(J_3 N)$	1	2	3	1	2	3	1	2	3	1	2	3
24	1	$J_{31}(N+N')_{11}$	$J_{31}(N+N')_{12}$	$J_{31}(N+N')_{13}$	0	0	0	0	+.049736	−.16620			
	2	$J_{32}(N+N')_{21}$	$J_{32}(N+N')_{22}$	$J_{32}(N+N')_{23}$	+.22966	0	−.78264	0	0	0			
	3	0	0	0	0	0	0	0	0	0			
	$(J N)$	1	2	3	1	2	3	1	2	3	1	2	3
25	1	$\Sigma(J_1 N)^1$	$\Sigma(J_1 N)^2$	$\Sigma(J_1 N)^3$	−.067392	0	+.22966	−19.98868	0	0			
	2	$\Sigma(J_2 N)^1$	$\Sigma(J_2 N)^2$	$\Sigma(J N)^3$	0	−93.716	0	0	−.014884	+.049737			
	3	$\Sigma(J_3 N)^1$	$\Sigma(J_3 N)^2$	$\Sigma(J_3 N)^3$	+.22966	0	−.78264	0	+.049736	−.16620			
		Bar = ____ L = ____			Bar = BA L = −3.54			Bar = BC L = +7.67			Bar = ____ L = ____		
$(S) = (JN)/L$		1	2	3	1	2	3	1	2	3	1	2	3
26	1	S_{11}	S_{12}	S_{13}	+.0190373	0	−.064676	−2.60608	0	0			
	2	S_{21}	S_{22}	S_{23}	0	+26.473	0	0	−.0019406	+.0064844			
	3	S_{31}	S_{32}	S_{33}	−.064876	0	+.22108	0	+.0064844	−.021669			

TABLE 3.—EXAMPLE E2

			Bar = _____ L = _____				Bar = BA L = -3.54				Bar = BC L = +7.67				Bar = _____ L = _____			
			M_r	aM_r	bM_r	cM_r	M_r	aM_r	bM_r	cM_r	M_r	aM_r	bM_r	cM_r	M_r	aM_r	bM_r	cM_r
		T	M_{rT}	$a_T M_{rT}$	$b_T M_{rT}$	$c_T M_{rT}$	0	0	0	0	0	0	0	0				
3	1	1	M_{r1}	$a_1 M_{r1}$	$b_1 M_{r1}$	$c_1 M_{r1}$	2150	0	2150	0	-10100	+10100	0	0				
		2	M_{r2}	$a_2 M_{r2}$	$b_2 M_{r2}$	$c_2 M_{r2}$	0	0	0	0	0	0	0	0				
3	2	$\sum$		M_a	M_b	M_c		0	2150	0		+10100	0	0				
3	3	$\sum + \sum'$		$M_a + M'_a$	$M_b + M'_b$	$M_c + M'_c$		0	0	0		0	0	0				
			V	aV	bV	cV	V	aV	bV	cV	V	aV	bV	cV	V	aV	bV	cV
		T																
3	4	1	V_1	$a_1 V_1$	$b_1 V_1$	$c_1 V_1$	0	0	0	0	0	0	0	0				
		2	V_2	$a_2 V_2$	$b_2 V_2$	$c_2 V_2$	3640	-1026.5	0	3498.0	7900	0	-2267.3	7576.1				
3	5	$\sum$		V_a	V_b	V_c		-1026.5	0	3498.0		0	-2267.3	7576.1				

TABLE 4.—EXAMPLE E2

			Bar = _____ L = _____			Bar = BA L = -3.54			Bar = BC L = +7.67			Bar = _____ L = _____		
		(J M)	1	2	3	1	2	3	1	2	3	1	2	3
		1	0	$J_{21}(M_a + M'_a)$	$J_{31}(M_a + M'_a)$	0	0	0	0	0	0			
4	1	2	$J_{12}(M_b + M'_b)$	0	$J_{32}(M_b + M'_b)$	0	0	0	0	0	0			
		3	$J_{13}(M_c + M'_c)$	$J_{23}(M_c + M'_c)$	0	0	0	0	0	0	0			
4	2	$\sum$	$(JM)^1$	$(JM)^2$	$(JM)^3$	0	0	0	0	0	0			
4	3	$\frac{\sum}{L}$	$\frac{(JM)^1}{L}$	$\frac{(JM)^2}{L}$	$\frac{(JM)^3}{L}$	0	0	0	0	0	0			
4	4	$\left[\sum\left(\frac{JM}{L}\right)^1\right] = 0$		$\left[\sum\left(\frac{JM}{L}\right)^2\right] = 0$		$\left[\sum\left(\frac{JM}{L}\right)^3\right] = 0$			These $(\sum)$ shall include all bars that converge in the common joint					

TABLE 3.—EXAMPLE E1—*CONTINUED*

		Bar = ____ L = ____			Bar = BA L = 400			Bar = BC L = 500			Bar = BD L = 458		
	$(J_s Q)$	1	2	3	1	2	3	1	2	3	1	3	3
2 16	1	$J_{1s} Q_{11}$	$J_{1s} Q_{12}$	$J_{1s} Q_{13}$									
	2	$J_{2s} Q_{21}$	$J_{2s} Q_{22}$	$J_{2s} Q_{23}$									
	3	0	0	0									
	$(J_s R)$	1	2	3	1	2	3	1	2	3	1	2	3
2 17	1	$J_{1s} R_{11}$	$J_{1s} R_{12}$	$J_{1s} R_{13}$	0	0	0	1458	0	0	271	-19.49	113.9
	2	$J_{2s} R_{21}$	$J_{2s} R_{22}$	$J_{2s} R_{23}$	0	0	0	0	0	0	39.0	-805	-115.8
	3	0	0	0	0	0	0	0	0	0	0	0	0
	$(J Q)$	1	2	3	1	2	3	1	2	3	1	2	3
2 18	1	$\Sigma(J_1 Q)^1$	$\Sigma(J_1 Q)^2$	$\Sigma(J_1 Q)^3$									
	2	$\Sigma(J_2 Q)^1$	$\Sigma(J_2 Q)^2$	$\Sigma(J_2 Q)^3$									
	3	$\Sigma(J_3 Q)^1$	$\Sigma(J_3 Q)^2$	$\Sigma(J_3 Q)^3$									
	$(J R)$	1	2	3	1	2	3	1	2	3	1	2	3
2 19	1	$\Sigma(J_1 R)^1$	$\Sigma(J_1 R)^2$	$\Sigma(J_1 R)^3$	0	1282.5	0	0	1093.4	820.9	160.6	-902.2	-65.6
	2	$\Sigma(J_2 R)^1$	$\Sigma(J_2 R)^2$	$\Sigma(J_2 R)^3$	1282.5	0	0	1944	0	0	-875	-69.2	-416.7
	3	$\Sigma(J_3 R)^1$	$\Sigma(J_3 R)^2$	$\Sigma(J_3 R)^3$	0	0	0	1458	0	0	310	-824.49	-1.9
	$(W)=(U Q)/L$	1	2	3	1	2	3	1	2	3	1	2	3
2 20	1	W_{11}	W_{12}	W_{13}									
	2	W_{21}	W_{22}	W_{23}									
	3	W_{31}	W_{32}	W_{33}									
		Bar = ____ L = ____			Bar = BA L = 400			Bar = BC L = 500			Bar = BD L = 458		
	$(U)=(U R)/L$	1	2	3	1	2	3	1	2	3	1	2	3
2 21	1	U_{11}	U_{12}	U_{13}	0	-3.21	0	0	2.19	1.64	2.24	-2.10	-.651
	2	U_{21}	U_{22}	U_{23}	-3.21	0	0	3.89	0	0	-1.775	-2.95	-1.311
	3	U_{31}	U_{32}	U_{33}	0	0	0	2.92	0	0	.677	-1.798	-.00414
	(J,N)	1	2	3	1	2	3	1	2	3	1	2	3
2 22	1	0	0	0									
	2	$J_{12}(N+N')_{21}$	$J_{12}(N+N')_{22}$	$J_{12}(N+N')_{23}$									
	3	$J_{13}(N+N')_{31}$	$J_{13}(N+N')_{32}$	$J_{13}(N+N')_{33}$									
	$(J_1 N)$	1	2	3	1	2	3	1	2	3	1	2	3
2 23	1	$J_{11}(N+N')_{11}$	$J_{11}(N+N')_{12}$	$J_{11}(N+N')_{13}$									
	2	0	0	0									
	3	$J_{13}(N+N')_{31}$	$J_{13}(N+N')_{32}$	$J_{13}(N+N')_{33}$									
	$(J_2 N)$	1	2	3	1	2	3	1	2	3	1	2	3
2 24	1	$J_{21}(N+N')_{11}$	$J_{21}(N+N')_{12}$	$J_{21}(N+N')_{13}$									
	2	$J_{22}(N+N')_{21}$	$J_{22}(N+N')_{22}$	$J_{22}(N+N')_{23}$									
	3	0	0	0									
	$(J N)$	1	2	3	1	2	3	1	2	3	1	2	3
2 25	1	$\Sigma(J_1 N)^1$	$\Sigma(J_1 N)^2$	$\Sigma(J_1 N)^3$									
	2	$\Sigma(J_2 N)^1$	$\Sigma(J_2 N)^2$	$\Sigma(J N)^3$									
	3	$\Sigma(J_3 N)^1$	$\Sigma(J_3 N)^2$	$\Sigma(J_3 N)^3$									

TABLE 5.—EXAMPLE E1, EQUATIONS (JOINT = B)

			Axial Forces			Common Joint= B						Joint=					
EQUATION	Equation Nº	INDEPENDENT TERM	F_{BA}	F_{BC}	F_{BD}	Δ_{Bx}	Δ_{By}	Δ_{Bz}	θ_{Bx}	θ_{By}	θ_{Bz}	$\Delta_{\_x}$	$\Delta_{\_y}$	$\Delta_{\_z}$	$\theta_{\_x}$	$\theta_{\_y}$	$\theta_{\_z}$
$\Sigma M_x=0$	1	3000							3343	-244	262						
$\Sigma M_y=0$	2	-2000							-244	2759	458						
$\Sigma M_z=0$	3	1000							262	458	1054						
$\Sigma V_x=0$	4		0	0	.436				+2.24	-3.12	+.989						
$\Sigma V_y=0$	5		0	.6	.218				-1.095	-2.95	-1.311						
$\Sigma V_z=0$	6		1	-.8	-.873				+3.597	-1.798	-.00414						
pr $\Delta_{\_}=0$	7																
pr $\Delta_{\_}=0$	8																
pr $\Delta_{\_}=0$	9																

TABLE 1.—EXAMPLE E2, ELASTIC CHARACTERISTICS OF BARS (JOINT = B)

		Bar = ____ L = ____				Bar = BA L = -3.54				Bar = BC L = +7.67				Bar = ____ L = ____			
		T	1	2	Σ	T	1	2	Σ	T	1	2	Σ	T	1	2	Σ
1 1	a	a_T	a_1	a_2		.961	0	-.282		0	-1	0					
	b	b_T	b_1	b_2		0	1	0		.959	0	-.287					
	c	c_T	c_1	c_2		.282	0	.961		.287	0	.959					
	k	k_T	k_1	k_2		772	1	110.25		.356	.462	51.0					
	β	-1	β_1	β_2		-1	.5	.5		-1	.5	.5					
	1+β	0	1+β_1	1+β_2		0	1.5	1.5		0	1.5	1.5					
	f=k(1+β)÷|L|	0	f_1	f_2		0	.42373	46.716		0	.090352	9.9739					
1 2	a^2	a_T^2	a_1^2	a_2^2	Σ a^2	.92352	0	.079524	1.0030	0	1	0	1				
	ab	$a_T b_T$	$a_1 b_1$	$a_2 b_2$		0	0	0		0	0	0					
	ac	$a_T c_T$	$a_1 c_1$	$a_2 c_2$		.27100	0	-.27100		0	0	0					
	b^2	b_T^2	b_1^2	b_2^2	Σ b^2	0	1	0	1	.91968	0	.082369	1.0020				
	bc	$b_T c_T$	$b_1 c_1$	$b_2 c_2$		0	0	0		.27523	0	-.27523					
	c^2	c_T^2	c_1^2	c_2^2	Σ c^2	.079524	0	.92352	1.0030	.082369	0	.91968	1.0020				
1 3	ka^2	$k_T a_T^2$	$k_1 a_1^2$	$k_2 a_2^2$	Σ ka^2	.71296	0	8.7675	9.4805	0	.462	0	.462				
	kab	$k_T a_T b_T$	$k_1 a_1 b_1$	$k_2 a_2 b_2$	Σ kab	0	0	0	0	0	0	0	0				
	kac	$k_T a_T c_T$	$k_1 a_1 c_1$	$k_2 a_2 c_2$	Σ kac	.20921	0	-29.878	-29.669	0	0	0	0				
	kb^2	$k_T b_T^2$	$k_1 b_1^2$	$k_2 b_2^2$	Σ kb^2	0	1	0	1	.32741	0	4.2008	4.5282				
	kbc	$k_T b_T c_T$	$k_1 b_1 c_1$	$k_2 b_2 c_2$	Σ kbc	0	0	0	0	.097982	0	-14.037	-13.939				
	kc^2	$k_T c_T^2$	$k_1 c_1^2$	$k_2 c_2^2$	Σ kc^2	.061393	0	101.82	101.88	.029323	0	46.904	46.933				
1 4	$\beta k a^2$	$\beta_T k_T a_T^2$	$\beta_1 k_1 a_1^2$	$\beta_2 k_2 a_2^2$	Σ βka^2	-.71296	0	4.3838	3.6708	0	.231	0	.231				
	β kab	$\beta_T k_T a_T b_T$	$\beta_1 k_1 a_1 b_1$	$\beta_2 k_2 a_2 b_2$	Σ β kab	0	0	0	0	0	0	0	0				
	β kac	$\beta_T k_T a_T c_T$	$\beta_1 k_1 a_1 c_1$	$\beta_2 k_2 a_2 c_2$	Σ β kac	-.20921	0	-14.939	-15.148	0	0	0	0				
	$\beta k b^2$	$\beta_T k_T b_T^2$	$\beta_1 k_1 b_1^2$	$\beta_2 k_2 b_2^2$	Σ βkb^2	0	.5	0	.5	-.32741	0	2.1004	1.7730				
	β kbc	$\beta_T k_T b_T c_T$	$\beta_1 k_1 b_1 c_1$	$\beta_2 k_2 b_2 c_2$	Σ β kbc	0	0	0	0	-.097982	0	-7.0185	-7.1165				
	βkc^2	$\beta_T k_T c_T^2$	$\beta_1 k_1 c_1^2$	$\beta_2 k_2 c_2^2$	Σ βkc^2	-.061393	0	50.91	50.849	-.029323	0	23.452	23.423				

TABLE 5.—EXAMPLE E2, EQUATIONS (JOINT = B)

			Axial Forces			Common Joint = B						Joint =					
EQUATION	Equation No.	INDEPENDENT TERM	F_{BA}	F_{BC}	F	Δ_{B_x}	Δ_{B_y}	Δ_{B_z}	θ_{B_x}	θ_{B_y}	θ_{B_z}	Δ_{-_x}	Δ_{-_y}	Δ_{-_z}	θ_{-_x}	θ_{-_y}	θ_{-_z}
$\Sigma M_x = 0$	1	-10100	0	0		0	13148	.086648	9.9425	0	-29.669						
$\Sigma M_y = 0$	2	-2150	0	0		+27430	0	+40720	0	5.5282	-13.939						
$\Sigma M_z = 0$	3	0	0	0		-9.5650	-44.894	0	-29.669	-13.939	148.81						
$\Sigma V_x = 0$	4	1026.5	.961	0		2.6251	0	-.064676	0	2.7489	-9.5846						
$\Sigma V_y = 0$	5	2267.3	0	.959		0	26.475	-.0064844	13.188	0	-45.031						
$\Sigma V_z = 0$	6	-11074.1	.282	.287		-.064876	-.0064844	.24275	.086648	.40720	0						
$pr_{BA} \Delta_{-}^{B} = 0$	7	0	0	0		.961	0	.282	0	0	0						
$pr_{BC} \Delta_{-}^{B} = 0$	8	0	0	0		0	.959	.287	0	0	0						
$pr\ \Delta_{-} = 0$	9																

TABLE 6.—EXAMPLE E2

		Bar = AB		L =	Bar = AB	L = +3.54		Bar = BC	L = +7.67		Bar =	L =		
	(θ)	1	2	3	1	2	3	1	2	3	1	2	3	
6 1	1	θ_{Ax}	θ_{Ay}	θ_{Az}	0	0	0	-4436.2	179.9	612.44				
	2	θ_{Bx}	θ_{By}	θ_{Bz}	-4436.2	179.9	612.44	0	0	0				
	(D)	T	1	2	T	1	2	T	1	2	T	1	2	
6 2	1	a_{TAB}	a_{1AB}	a_{2AB}	.961	0	-.282	0	-1	0				
	2	b_{TAB}	b_{1AB}	b_{2AB}	0	1	0	.959	0	-.287				
	3	c_{TAB}	c_{1AB}	c_{2AB}	.282	0	.961	.287	0	.959				
	(θ, D)	T	1	2	T	1	2	T	1	2	T	1	2	
6 3	1	$\theta_{Ax}\ a_{TAB}$	$\theta_{Ax}\ a_{1AB}$	$\theta_{Ax}\ a_{2AB}$	0	0	0	0	4436.2	0				
	2	$\theta_{Ay}\ b_{TAB}$	$\theta_{Ay}\ b_{1AB}$	$\theta_{Ay}\ b_{2AB}$	0	0	0	172.52	0	-51.631				
	3	$\theta_{Az}\ c_{TAB}$	$\theta_{Az}\ c_{1AB}$	$\theta_{Az}\ c_{2AB}$	0	0	0	175.77	0	587.33				
6 4	∑	θ_{TA}	θ_{1A}	θ_{2A}	0	0	0	348.29	4436.2	535.70				
	(θ_B D)	T	1	2	T	1	2	T	1	2	T	1	2	
6 5	1	$\theta_{Bx}\ a_{TAB}$	$\theta_{Bx}\ a_{1AB}$	$\theta_{Bx}\ a_{2AB}$	-4263.2	0	1251.0	0	0	0				
	2	$\theta_{By}\ b_{TAB}$	$\theta_{By}\ b_{1AB}$	$\theta_{By}\ b_{2AB}$	0	179.9	0	0	0	0				
	3	$\theta_{Bz}\ c_{TAB}$	$\theta_{Bz}\ c_{1AB}$	$\theta_{Bz}\ c_{2AB}$	172.71	0	588.55	0	0	0				
6 6	∑	θ_{TB}	θ_{1B}	θ_{2B}	-4090.5	179.9	1839.6	0	0	0				
	(Δ)	1	2	3	1	2	3	1	2	3	1	2	3	
6 7	1	Δ_{Ax}	Δ_{Ay}	Δ_{Az}	0	0	0	3980.1	4058.1	-13569				
	2	Δ_{Bx}	Δ_{By}	Δ_{Bz}	3980.1	4058.1	-13569	0	0	0				
	(Δ_B D)	T	1	2	T	1	2	T	1	2	T	1	2	
6 8	1		$\Delta_{Ax}\ a_{1AB}$	$\Delta_{Ax}\ a_{2AB}$		0	0		-3980.1	0				
	2		$\Delta_{Ay}\ b_{1AB}$	$\Delta_{Ay}\ b_{2AB}$		0	0		0	-1164.7				
	3		$\Delta_{Az}\ c_{1AB}$	$\Delta_{Az}\ c_{2AB}$		0	0		0	-13013				
6 9	∑		Δ_{1A}	Δ_{2A}		0	0		-3980.1	-14178				

TABLE 6.–EXAMPLE E2–*CONTINUED*

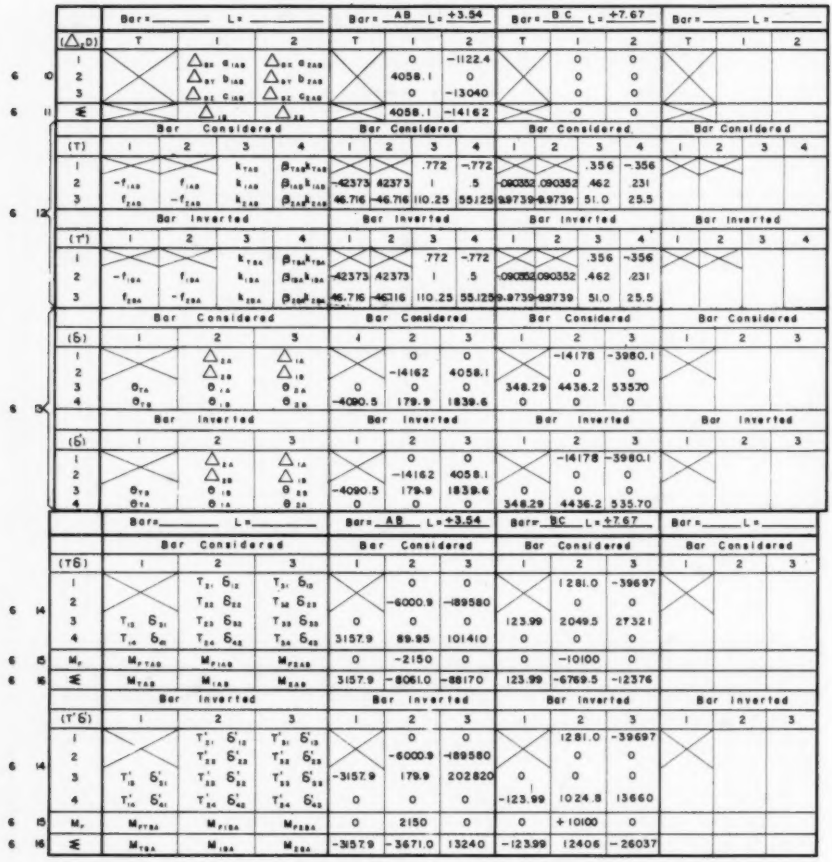

TABLE 7

Bar (1)	Length, in inches (2)	Section, in inches^2 (3)	I_1, in inches^4 (4)	I_2, in inches^4 (5)
AB	400	45 x 45	341,720	341,720
BC	500	60 x 45	810,000	455,625
BD	458	55 x 45	623,906	417,656

Journal of the
STRUCTURAL DIVISION
Proceedings of the American Society of Civil Engineers

GRID ANALYSIS BY THE REACTION DISTRIBUTION METHOD

By Irving Fader[1]

SYNOPSIS

The method of reaction distribution is a convenient approach in the solution of grid systems. Conventional methods of handling these systems usually result in the solution of involved equations subject to numerical errors. The reaction distribution method is a convergence process that is based on the stiffness characteristics of the members in the system. Reactions, moments, and deflections at each joint are obtainable by this method for all types of loading conditions. The numerical solution to various grid systems is given. To facilitate the presentation, a table of stiffness and carry-over relationships incorporating the scope of the spans used in the illustrative examples is included.

The important relationship of the converging series which greatly simplifies the distribution process, is established in these problems.

GENERAL ANALYSIS

Continuous beams are readily analyzed by the various methods available. It is assumed that the methods of consistent deformation, three moment theorem, slope-deflection and moment distribution, and so on, are familiar to the reader.

The solution of continuous beams on elastic supports or grid systems can be accomplished in the same manner by equating the joint compatibilities. The solution of these equations may be quite tedious, especially when several

Note.—Discussion open until January 1, 1962. To extend the closing date one month, a written request must be filed with the Executive Secretary, ASCE. This paper is part of the copyrighted Journal of the Structural Division, Proceedings of the American Society of Civil Engineers, Vol. 87, No. ST 6, August, 1961.

[1] Structural Engr., New York Naval Shipyard, Brooklyn, N. Y.

loading conditions enter in design considerations. The reaction distribution method offers a solution that is rather easy in application.

The basic approach is to initially introduce a rigid support at each joint that translates. The resulting continuous spans can thus be analyzed by using any of the available methods. The purpose in doing this is to obtain the reactions at these temporary supports. Due to joint translation, these reaction forces must be redistributed throughout the structure to maintain static equilibrium. Reaction distribution as the name implies is a method for accomplishing this result. Before the actual process is shown, fundamental expressions will be established.

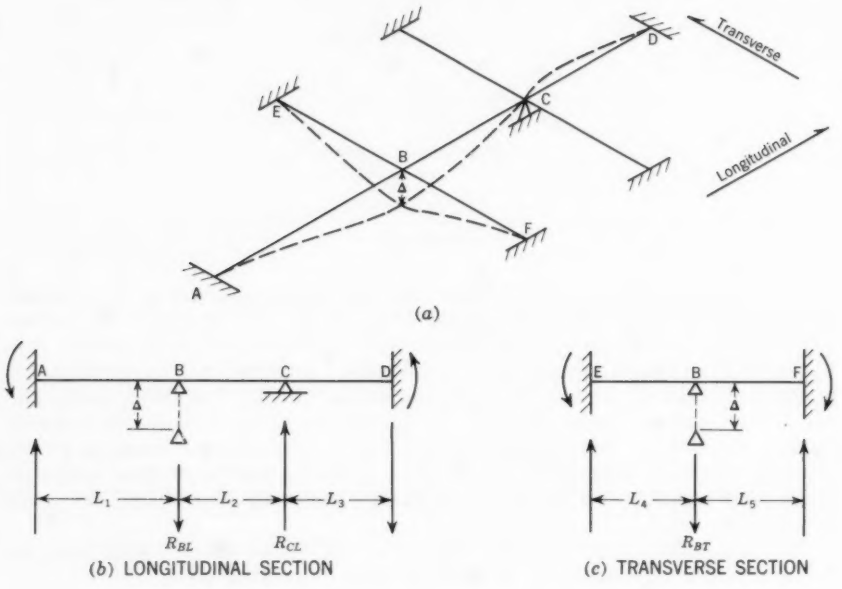

FIG. 1.

Fig. 1 (a) is a representation of a grid consisting of one longitudinal and two transverse members that interact at joints B and C. There is no superimposed loading on the system. A deflection (Δ) is induced at joint B and a temporary support is placed at joint C. Fig. 1 (b) isolates the longitudinal span. Fig. 1 (c) isolates the deflecting transverse span. The forces at joints B and C are indicated: R_{BL} is the longitudinal reaction at joint B; R_{BT} is the transverse reaction at joint B; R_{CL} is the longitudinal reaction at joint C.

Sign Convention.—The sign convention used in this presentation denotes all upward forces as positive. Moments causing tension on the bottom fiber are considered positive, downward deflection is positive.

Definitions.—Absolute translation stiffness, T, is defined as the force required to induce a deflection at the joint in question with translation prevented

at all the other joints. Relative translation stiffness is defined as the force required to induce a unit deflection at the joint in question with translation prevented at the other joints. Thus, from Fig. 1 (b) the longitudinal translation stiffness at joint B $\left[T_{BL}\right] = R_{BL}$ (a negative force) and from Fig. 1 (c) the transverse translation stiffness at joint B $\left[T_{BT}\right] = R_{BT}$.

Carry-over is defined as the forces induced at the unyielding joints when a deflection is induced at the joint in question. Therefore, in Fig. 1 (b) R_{CL} is the carry-over force. The ratio $\frac{R_{CL}}{R_{BL}}$ is termed as the carry-over factor from B to C.

Table 1 has been prepared giving stiffness and carry-over relationships for beams of constant EI and spans of equal length (Fig. 2).

Distribution factor (D.F.) is the percentage of force that is distributed in the longitudinal or transverse direction at the joint in question. Therefore, at joint B the longitudinal distribution factor

$$\left(D.F._L\right) = \frac{R_{BL}}{R_{BL} + R_{BT}} \quad \ldots\ldots\ldots\ldots\ldots \quad (1)$$

and the transverse distribution factor

$$\left(D.F._T\right) = \frac{R_{BT}}{R_{BL} + R_{BT}} \quad \ldots\ldots\ldots\ldots\ldots \quad (2)$$

For Case 1

$$T = \frac{-6\ E\ I\ \Delta}{L^3} = \sum D.R. \quad \ldots\ldots\ldots\ldots\ldots \quad (3a)$$

or

$$\Delta = \frac{\Sigma D.R.\ L^3}{6\ E\ I} \quad \ldots\ldots\ldots\ldots\ldots\ldots\ldots \quad (3b)$$

in which T is the translational stiffners, Δ denotes the deflection of a joint due to translation and D.R. refers to the distributed reaction. For Cases 2A and 2 B

$$T = \frac{-9.6\ E\ I\ \Delta}{L^3} = \Sigma\ D.R. \quad \ldots\ldots\ldots\ldots\ldots \quad (4a)$$

or

$$\Delta = \frac{-\Sigma\ D.R.\ L^3}{9.6\ E\ I} \quad \ldots\ldots\ldots\ldots\ldots\ldots\ldots \quad (4b)$$

For Cases 3 A and 3 C

$$T = \frac{-9.8571\ E\ I\ \Delta}{L^3} = \Sigma\ D.R. \quad \ldots\ldots\ldots\ldots \quad (5a)$$

or

$$\Delta = \frac{-\Sigma D.R.\ L^3}{9.8571\ E\ I} \quad \ldots\ldots\ldots\ldots\ldots\ldots\ldots \quad (5b)$$

For Case 3 B

$$T = \frac{-13.714286\ E\ I\ \Delta}{L^3} = \Sigma\ D.R. \quad \ldots\ldots\ldots\ldots \quad (6a)$$

or

$$\Delta = \frac{-\Sigma D.R.\ L^3}{13.714286\ E\ I} \quad \ldots\ldots\ldots\ldots\ldots\ldots \quad (6b)$$

For Case 4

$$T = \frac{-24\ E\ I\ \Delta}{L^3} = \Sigma\ D.R. \quad \ldots\ldots\ldots\ldots\ldots \quad (7a)$$

or

$$\Delta = \frac{-\Sigma\ D.R.\ L^3}{24\ E\ I} \quad \ldots\ldots\ldots\ldots\ldots\ldots \quad (7b)$$

For Cases 5A and 5B

$$T = \frac{-19.2\ E\ I\ \Delta}{L^3} = \Sigma D.R \quad \ldots\ldots\ldots\ldots\ldots \quad (8a)$$

or

$$\Delta = \frac{-\Sigma D.R.\ L^3}{19.2\ E\ I} \quad \ldots\ldots\ldots\ldots\ldots\ldots \quad (8b)$$

For Cases 6A and 6C

$$T = \frac{-18.85714285\ E\ I\ \Delta}{L^3} = \Sigma D.R. \quad \ldots\ldots\ldots \quad (9a)$$

or

$$\Delta = \frac{-\Sigma D.R.\ L^3}{18.85714285\ E\ I} \quad \ldots\ldots\ldots\ldots\ldots\ldots \quad (9b)$$

For Case 6B

$$T = \frac{-15\ E\ I\ \Delta}{L^3} = \Sigma D.R. \quad \ldots\ldots\ldots\ldots\ldots \quad (10a)$$

or

$$\Delta = \frac{-\Sigma D.R.\ L^3}{15\ E\ I} \quad \ldots\ldots\ldots\ldots\ldots\ldots \quad (10b)$$

Effect of Torsional Restraint.—In a system of interacting members, rotation at a joint causes bending on one member and torsion in the member at right angles to it. When I beams or other thin-walled members are used, it is reasonable to assume that the torsional resistence is negligible in comparison to the bending resistence. Therefore, torsional restraint is not considered in the analysis presented herein.

Reaction Distribution Process.— The first step in the process is to introduce rigid supports at the joints that are subject to translation. The resulting continuous spans are analyzed by any convenient method, thus determining the rigid reactions. The next step is to remove the temporary supports and allow translation. The supports are removed from one joint at a time. When the support is removed a force which is equal in magnitude but opposite in direction to the initial rigid reaction is acting on the system. This force is distributed in the longitudinal and transverse directions in accordance with the stiffness properties at the joint in question. The joint translation induces reactions at the other joints in the system, the magnitude and sign of which is determined by the carry-over factor. After distribution is accomplished at a joint, the rigid support is reintroduced thereby preventing any further joint translation. The process is repeated at each joint that is free to translate, thus completing one cycle of distribution. The forces that were carried over

TABLE 1.–TRANSLATION STIFFNESS AND CARRY OVER (CONSTANT EI; FIG. 2)

Case	R_1	R_2	R_3	R_4	R_5	M_1	M_2	M_3	M_4	M_5
1	-0.5T	T	-0.5T	——	——	0	-0.5TL	0	——	——
2A	-0.375T	T	-0.875T	+0.25T	——	0	-0.375TL	+0.25TL	0	——
2B	+0.25T	-0.875T	T	-0.375T	——	0	+0.25TL	-0.375TL	0	——
3A	- .369565T	T	- .956522T	+ .391304T	- .065217T	0	- .369565TL	+ .26087TL	- .065217TL	0
3B	+ .1875T	- .6875T	T	- .6875T	+ .1875T	0	+ .1875TL	- .3125TL	+ .1875TL	0
3C	- .065217T	+ .391304T	- .956522T	T	- .369565T	0	- .065217TL	+ .26087TL	- .369565TL	0
4	- .5T	T	- .5T	——	——	+ .25TL	- .25TL	+ .25TL	——	——
5A	- .5625T	T	- .6875T	+ .25T	——	+ .291667TL	- .270833TL	+ .166667TL	- .083333TL	——
5B	+ .25T	- .6875T	T	- .5625T	——	- .083333TL	+ .166667TL	- .270833TL	+ .291667TL	——
6A	- .5681818T	T	- .6363636T	+ .27272727T	- .0681818T	+ .2954545TL	- .272727TL	+ .1590909TL	- .0454545TL	+ .022727TL
6B	+ .3T	- .8T	T	- .8T	+ .3T	- .1TL	+ .2TL	- .3TL	+ .2TL	- .1TL
6C	- .0681818T	+ .27272727T	- .6363636T	T	- .5681818T	+ .022727TL	- .0454545TL	+ .1590909TL	- .272727TL	+ .2954545TL

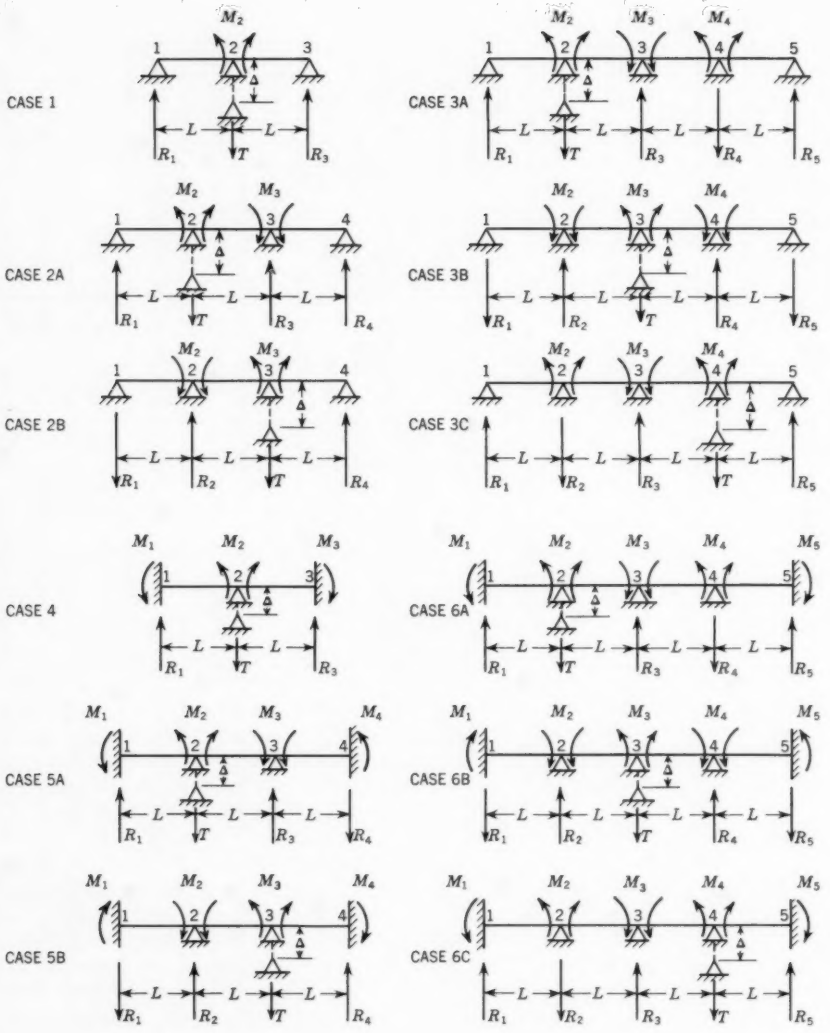
CASE 1
CASE 2A
CASE 2B
CASE 3A
CASE 3B
CASE 3C
CASE 4
CASE 5A
CASE 5B
CASE 6A
CASE 6B
CASE 6C

FIG. 2.

to each joint are now rigid reactions for the second distribution cycle. Again, the temporary support is removed to allow for distribution and carry-over and is then replaced. The distribution and carry-over cycles are repeated until there are no more forces to distribute. The system will then be in equilibrium. The final reaction at each joint is equal to the summation of all the rigid reactions and distributed reactions.

It is important to note that after each time a rigid reaction is distributed, the temporary support is immediately replaced at the joint. Therefore, only the distributed forces cause translation. The summation of the distributed forces (or distributed reactions) is the force that induced the joint translation and by definition is the absolute translation stiffness. The deflection at each joint can be easily obtained by equating the expression for stiffness (from Table 1) equal to the summation of the distributed reactions at the joint in question.

The complete process will be easily understood with the use of several illustrative problems that follow.

EXAMPLE ONE

Solution (Constant E I).—Initially place a rigid support at joint B. Because the 100 kip load is directly at joint B, it may be assumed to be in either the longitudinal or transverse span. Therefore assume 100 kip on the longitudinal beam.

Isolating each span in Fig. 3 with its superimposed loading yields the results indicated in Fig. 4.

From Table 1 Case (1 and 4)

$$\text{Relative } T_{\text{long.}} = \frac{-24I}{(L)^3} = \frac{-24I}{(10)^3} \times \frac{-(8)^3}{6I} = 2.048$$

$$\text{Relative } T_{\text{trans.}} = \frac{-6I}{(L)^3} = \frac{-6I}{(8)^3} \times \frac{-(8)^3}{6I} = 1.000$$

Thus,

$$\text{Longitudinal D.F.} = \frac{2.048}{3.048} = 0.671916$$

$$\text{Transverse D.F.} = \frac{1.000}{3.048} = 0.328084$$

To obtain distribution factors, it is more convenient to work with the relative rather than absolute stiffness factors. The stiffness expression is obtained from Table 1. For relative stiffness values, Δ is unity. The modulus of elasticity may be omitted if it is constant. It is usually more convenient to multiply these stiffness relationships by a value such that the minimum relative stiffness factor is unity.

The distribution factors and rigid support reactions are shown in Table 2. The summation of the rigid reactions at joint B is the total reaction to the temporary unyielding support (120 + 13.75 = 133.75). When the support is re-

TABLE 2.—REACTION DISTRIBUTION, EXAMPLE ONE

Joint B	Distribution Factor (D.F)	Rigid Reaction (R.R.)	Distributed Reaction (D.R.)	Carry Over (C.O.)	Balanced Reaction	Σ D. R.	ΔE I, in kip fps
(1)	(2)	(3)	(4)	(5)	(6)	(7)	(8)
Longitudinal	0.671916	+120.000	-89.8688	0	+30.1312	-89.8688	+3744.53
Transverse	0.328084	+ 13.750	-43.8812	0	-30.1312	-43.8812	+3744.53

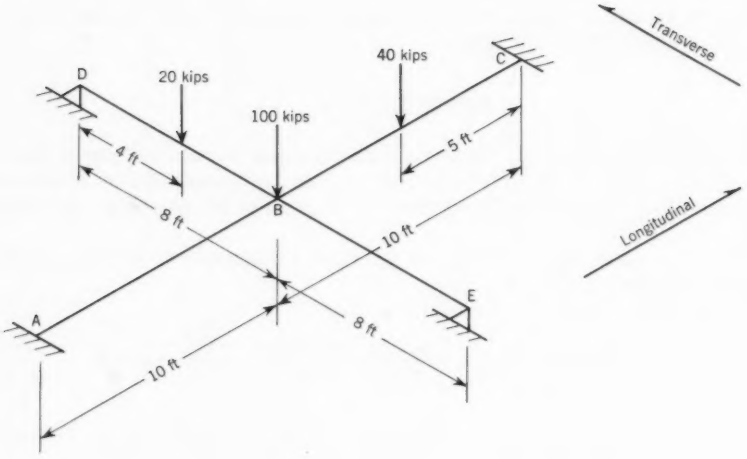

FIG. 3.

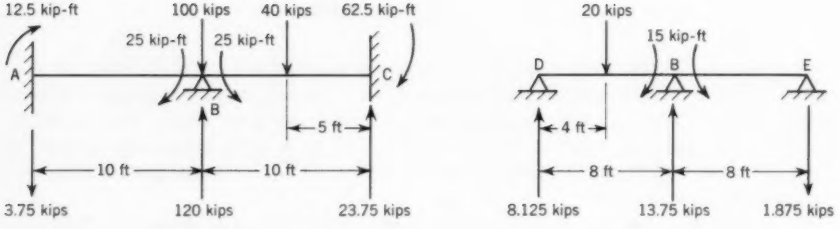

FIG. 4.

moved the joint will translate downward. The force inducing this deflection is therefore (- 133.75). This force is distributed in the longitudinal and transverse spans in accordance with the distribution factors. Therefore, the force (or distributed reaction) in the longitudinal direction is - 133.75 (0.671916) = -89.8688; the distributed reaction in the transverse direction is - 133.75 (0.328084) = - 43.8812. The joint is now balanced for the first cycle. Because all the other support points are turly rigid, no distribution takes place, consequently no other forces are induced at Joint B. Only one distribution cycle is necessary for this problem. The balanced reaction is equal to the summation of the rigid and distributed reactions. The deflection at Joint B is obtained by using the translation stiffness relationships given for Fig. 2 (Eqs. 3 through 10).

At Joint B (longitudinal)

$$T = \frac{-24\,EI\Delta}{L^3} \quad \ldots\ldots\ldots\ldots\ldots\ldots \quad (11a)$$

or

$$\Delta\,EI = \frac{-T\,L^3}{24} \quad \ldots\ldots\ldots\ldots\ldots\ldots \quad (11b)$$

Joint B (transverse)

$$T = \frac{-6\,EI\Delta}{L^3} \quad \ldots\ldots\ldots\ldots\ldots\ldots \quad (12a)$$

or

$$\Delta\,EI = \frac{-T\,L^3}{6} \quad \ldots\ldots\ldots\ldots\ldots\ldots \quad (12b)$$

ΣD.R. is the force that induced translation and is therefore equal to T. Therefore, at Joint B (longitudinal)

$$\Delta\,EI = \frac{-(89.8688)(10)^3}{24} = +\,3744.53 \text{ kip ft}^3 \downarrow$$

and at Joint B (transverse)

$$\Delta\,EI = \frac{-(43.8812)(8)^3}{6} = +\,3744.53 \text{ kip ft}^3 \downarrow$$

Since Σ D.R. at Joint B is known, the reaction components at each joint may be obtained by combining the initial value (the value obtained with the temporary rigid support) with the change in the component in question due to translation. This is shown in the following computations:

Final Joint Reaction Component = R. R. Component (Fig. 3)
+ (Σ D.R.) (carry-over factor; from Table 1) . . . . . (13)

Thus,

M_A = +12.5 + 0.25 (-89.8688)(10) = -212.172 kip ft

M_B (Long) = -25.0 + 0.25 | (10) = +199.672 kip ft

M_C = -62.5 + 0.25 | (10) = - 287.172 kip ft

R_A = -3.75 - 0.5 = +41.1844 kip

R_C = +23.75 -0.5 = +68.6844 kip

R_D = +8.125 -0.5 (-43.8812) = + 30.0656 kip

R_E = -1.875 -0.5 | = + 20.0656 kip

$M_{B(Tran)}$ = -15.0 -0.5 ↓ (8) = +160.525 kip ft

The final force diagram is shown in Fig. 5.

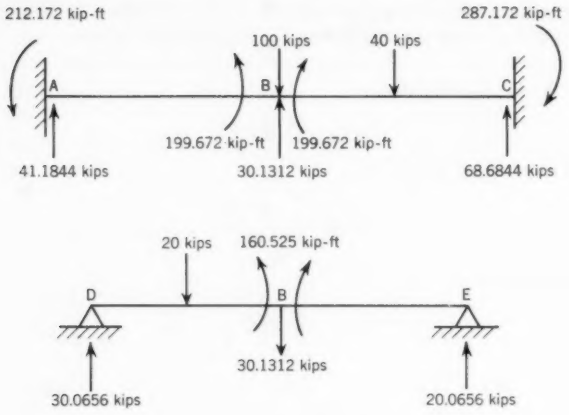

FIG. 5.

EXAMPLE TWO

For example two, assume constant E I, with the longitudinal span 10 ft long and the transverse spans 8 ft long (Fig. 6.).

For a grid with two or more deflecting joints, it is usually convenient to balance the system for a load at one joint at a time. In Fig. 6 a 100 kip load is placed at joint B. The system will be solved for this condition due to symmetry. The same solution will be obtained for a 100 kip load placed at joint C. For any superimposed loading condition the rigid reactions at these joints are determined and the system is balanced by taking ratios of these reactions to the solution for 100 kip at a joint.

From Table 1 Case 1 and 2

$$\text{Relative T (long.)} = -\frac{9.6\,I}{(10)^3} \times -\frac{(10)^3}{9.6\,I} = 1.000$$

$$\text{Relative T (trans.)} = -\frac{6\,I}{(8)^3} \times -\frac{(10)^3}{9.6\,I} = 1.2207$$

Longitudinal D. F. $\left(D.F._L\right)$ = 0.45031

Transverse D. F. $\left(D.F._T\right)$ = 0.54969

C.O. from B to C = C.O. from C to B = -0.875

Assume R.R. at Jt. B (long.) = $+100^k$

The reaction distributions for the joints that translate (B and C) are given in Table 3. It is not necessary to list all the other joints for there will not be any carry over from them to joints B and C. There will be, however, carry over from joints B and C to all the other joints. This is best accomplished after the joints are balanced, for the effect at any joint is determined by the summation of the forces that induce the change (ΣD.R.).

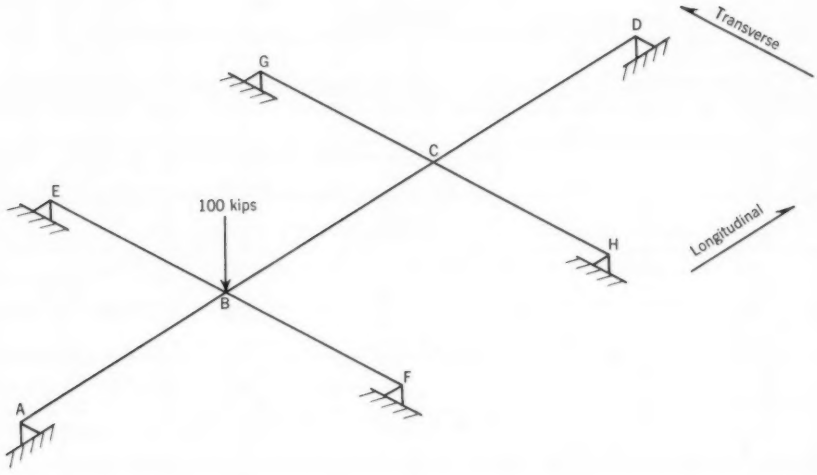

FIG. 6.

The rigid reaction at B longitudinal $(R.R._{BL})$ = 100 is listed. When the support at B is removed, the joint will translate downward; the force inducing this deflection is (- 100). This force is distributed at joint B in accordance with the distribution factors. Therefore, the distributed reaction at B (transverse) is

$$-100\ (0.54969) = -54.969$$

and the distributed reaction at B (longitudinal) is

$$-100\ (0.45031) = -45.031$$

Because there is no rigid reaction at joint C there is nothing to distribute for the first cycle, and consequently a zero carry-over. The temporary support is

reintroduced at joint B. Due to the first cycle distribution a longitudinal reaction is induced at joint C equal to the distributed reaction at joint B multiplied by the carry-over factor. Therefore, $R.R._{CL}$ for the second cycle is

$$-45.031 \times (-.875) = +39.402.$$

The distribution process is continued until nothing remains to be carried over. The summation of the rigid reactions and distributed reactions is listed

TABLE 3.—REACTION DISTRIBUTION FOR EXAMPLE 2

	Joint B		Joint C	
	Transverse	Longitudinal	Longitudinal	Transverse
D.F.	.54969	.45031	.45031	.54969
R.R.	0	+100.000	0	0
D.R.	-54.969	-45.031	0	0
C.O.	0	0	+39.402	0
D.R.	0	0	-17.743	-21.659
C.O.	0	+ 15.525	0	0
D.R.	-8.534	-6.991	0	0
C.O.	0	0	+6.117	0
D.R.	0	0	-2.755	-3.362
C.O.	0	+2.411	0	0
D.R.	-1.325	-1.086	0	0
C.O.	0	0	+0.950	0
D.R.	0	0	-0.428	-0.522
C.O.	0	+0.375	0	0
D.R.	-0.206	-0.169	0	0
C.O.	0	0	+0.148	0
D.R.	0	0	-0.067	-0.081
C.O.	0	+0.059	0	0
D.R.	-0.032	-0.027	0	0
C.O.	0	0	+.024	0
R.R.	0	0	-.011	-.013
C.O.	0	+.010	0	0
R.R.	-.005	-.005	0	0
C.O.	0	0	+.004	0
R.R.	0	0	-.002	-.002
C.O.	0	+.002	0	0
R.R.	-.001	-.001	0	0
ΣR.R.	0	+118.382	+46.645	0
ΣD.R.	-65.072	-53.310	-21.006	-25.639
Balanced Reaction	-65.072	+65.072	+25.639	-25.639
ΔEI	5552.8	5553.1	2188.1	2187.9

separately (Table 3) and combined to give the balanced reaction. It is necessary to have ΣD.R. separately in order to obtain the joint deflections. The

deflections are computed in the same manner shown in the previous example. At joint B longitudinal

$$\Delta EI = \frac{-TL^3}{9.6} \quad \frac{-(-53.31)(10)^3}{9.6} = +5553.1 \text{ kip ft}^3 \downarrow$$

at B transverse

$$\Delta EI = \frac{-TL^3}{6} = \frac{-(-65.072)(8)^3}{6} = +5552.8 \text{ kip ft}^3 \downarrow$$

At Joint C longitudinal

$$\Delta EI = \frac{-TL^3}{9.6} = \frac{-(-21.006)(10)^3}{9.6} = +2188.1 \text{ kip ft}^3 \downarrow$$

At C transverse

$$\Delta EI = \frac{-TL^3}{6} = \frac{-(-25.639)(8)^3}{6} = +2187.9 \text{ kip ft}^3 \downarrow$$

The reaction components at all the joints are obtained by using the carry over factors from Table 1 and ΣD.R. The computations are as follows:

$R_A = -.375\ (-53.31) + 0.25\ (-21.006) = +14.740$ kip

$R_D = +.25\ (-53.31) - 0.375\ (-21.006) = -5.450$ kip

M_B (long.) $= -.375\ (-53.31)\ (10) + 0.25\ (-21.006)\ (10) = +147.40$ kip ft

M_C (long.) $= +.25\ (-53.31)\ (10) - 0.375\ (-21.006)\ (10) = -54.50$ kip ft

$R_E = -0.5\ (-65.072) = +32.536$ kip $= R_F$

M_B (trans.) $= -0.5\ (-65.072)\ (8) = +260.288$ kip ft

$R_G = -0.5\ (-25.639) = +12.8195$ kip $= R_H$

M_C (trans.) $= -0.5\ (-25.639)\ (8) = +102.556$ kip ft

Alternate Solution.—A close inspection of the balancing cycle performed for the first solution shows that it is a converging geometric series of the form

$$S_n = a + ar + ar^2 + ar^n + ar^{n-1} \quad \ldots\ldots\ldots\ldots \quad (14)$$

Multiplying by $\frac{1-r}{1-r}$

$$S_n = \frac{a(1-r^n)}{1-r} = \frac{a}{1-r} - \frac{ar^n}{1-r} \quad \ldots\ldots\ldots\ldots \quad (15)$$

For $r < 1$

$$\lim_{n \to \infty} S_n = \frac{a}{1-r} \quad \ldots\ldots\ldots\ldots\ldots\ldots \quad (16)$$

$a = 100^k$

$r = [-\text{D.F. (long.) at point B}][\text{C.O. to C}][-\text{D.F. (long.) at point C}]$
$[\text{C.O. to B}] \quad \ldots\ldots\ldots\ldots\ldots\ldots \quad (17)$

$r = [(0-875)\ (0.43031)]^2 = 0.15525$

Thus

$$\Sigma \text{ R.R. at joint B (long.)} = \frac{100}{1 - .15525} = +118.378$$

ΣD.R. at joint B (trans.) = - 118.378 (.54969) = - 65.071

ΣD.R. at joint B (long.) = - 118.378 (.45031) = - 53.307

ΣR.R. at joint C (long.) = ΣDR. at JT. B (long.) x (- .875) = + 46.644

ΣD.R. at joint C (trans.) = - 46.644 (.54969) = - 25.640

Σ D.R. at joint C (long.) = - 46.644 (.45031) = - 21.004

Balanced Reaction B (trans.) = -65.071 Balanced Reaction C (trans.) = -25.640
Balanced Reaclton B (long.) = +65.071 Balanced Reaction C (long.) = +25.640

and

Δ E I at joint B (long.) = + 5552.8 Δ E I at C (long.) = 2187.9

Δ E I at joint B (trans.) = 5552.7 Δ E I at C (trans.) = 2187.9

The procedure of distributing reactions is greatly simplified by using this series form. The converging geometric series can be used to great advantage as will be shown in subsequent problems.

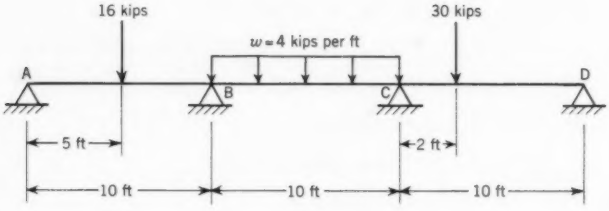

FIG. 7.

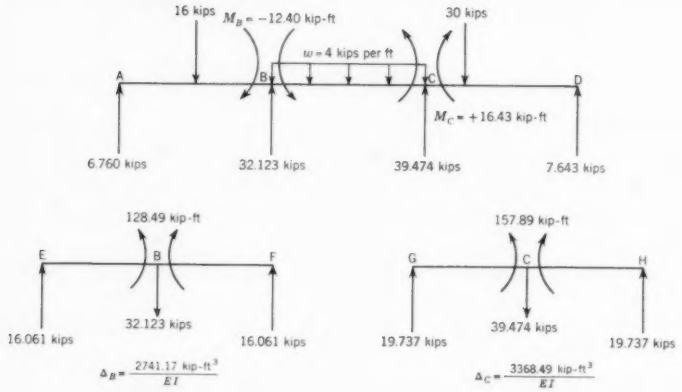

FIG. 8.

TABLE 4.—TABULATION OF BALANCED UNIT RIGID REACTIONS

	Balanced Reaction Components for $R.R._{BL} = +100$ kip	Balanced Reaction Components for $R.R._{CL} = +100$ kip
R_A, in kips	+14.740	-5.450
R_B (long.), in kips	+65.072	+25.639
R_B (trans.), in kip	-65.072	-25.639
R_C (long.)	+25.639	+65.072
R_C (trans.), in kip	-25.639	-65.072
R_D, in kip	-5.450	+14.740
M_B (long.), in kip ft	+147.40	-54.50
M_C (long.), in kip ft	-54.50	+147.40
R_E; R_F, in kip	+32.536	+12.8195
R_G; R_H, in kip ft	+12.8195	+32.536
M_B (trans.), in kip ft	+260.288	+102.556
M_C (trans.), in kip ft	+102.556	+260.288
Δ_B EI, in kip ft^3	+5552.8	+2187.9
Δ_C EI	+2187.9	+5552.8

TABLE 5.—SOLUTION OF ILLUSTRATIVE PROBLEM (FIG. 7)

	For Loading Rigid Supports	Balance For $RR_{BL} = 30.143$ kip	Balance For $RR_{CL} = 48.786$ kip	Final Reaction Component
R_A	+4.976	+4.443	-2.659	+6.760
R_{BL}	—	+19.615	+12.508	+32.123
R_{BT}	—	-19.615	-12.508	-32.123
R_{CL}	—	+7.728	+31.746	+39.474
R_{CT}	—	-7.728	-31.746	-39.474
R_D	+2.095	-1.643	+7.191	+7.643
M_{BL}	-30.24	+44.43	-26.59	-12.40
M_{CL}	-39.05	-16.43	+71.91	+16.43
R_E; R_F	0	+9.807	+6.254	+16.061
R_G; R_H	0	+3.864	+15.873	+19.737
M_{BT}	0	+78.46	+50.03	+128.49
M_{CT}	0	+30.91	+126.98	+157.89
Δ_B EI	0	1673.78	1067.39	2741.17
Δ_C EI	0	659.50	2708.99	3368.49

Illustrative Example.—The effect of a rigid reaction of + 100 kip at joint B has been computed. Due to the symmetry of the system, the same analysis will hold for a R.R. of + 100 kip at joint C. The results are given in Table 4. With this table it is possible to solve the system for any loading condition. The illustrative problem given in Fig. 7 is for loading on the longitudinal span as shown. There is no loading on the transverse spans. With temporary rigid supports at joints B and C the resultant continuous spans can be analyzed by any of the conventional methods. The reaction components for the superimposed loading condition are $R_A = +4.976$ kip, $R_B = +30.143$ kip, $R_C = +48.786$ kip, $R_D = +2.095$ kip, $M_B = -30.24$ kip ft, and $M_C = -39.05$ kip ft. The rigid reactions ($R.R._{BL} = +30.143$ kip and $R.R._{CL} = +48.786$ kip) must be distributed and the system solved. This is performed by applying the ratios of these rigid reactions to Table 4. The solution of the problem is given in Table 5 with final force diagrams shown in Fig. 8.

EXAMPLE THREE

For the structure noted in example 3 there is a constant EI and all spans are 10 ft long.

The grid in Fig. 9 will be solved for a 100 kip load at joint B. Due to symmetry similar solutions will be obtained for 100 kip loads at the other deflecting joints. For different conditions of superimposed loading the system can be solved in a manner similar to that shown in example 2.

Assume R.R. at joint "B" (long.) = +100 kip,
From Table 1 case 2.

$$\text{Rel. T (long.)} = \frac{-9.6\,I}{L^3}$$

$$\text{Rel. T (trans.)} = \frac{-9.6\,I}{L^3}$$

at each joint. Thus,

Longitudinal D.F. = 0.5

Transverse D.F. = 0.5

C.O. factor = - 0.875

Due to the nature of the distribution pattern shown in Table 6, after cycle 2, the carry over plus the distributed reaction at each joint equals zero. Therefore, the balanced reaction after cycle 2 is the final joint reaction. Final reactions at rigid supports and joint moments can easily be obtained by simple statics. Deflections at each joint can be determined by any of the conventional methods. However, if solution is desired by obtaining the summation of the distributed reactions at each joint, the distribution process must continue. The convergency factor is rather large so that many distribution cycles are necessary to complete the balancing. Convergence may be accomplished rapidly by using the geometric series used in example 2.

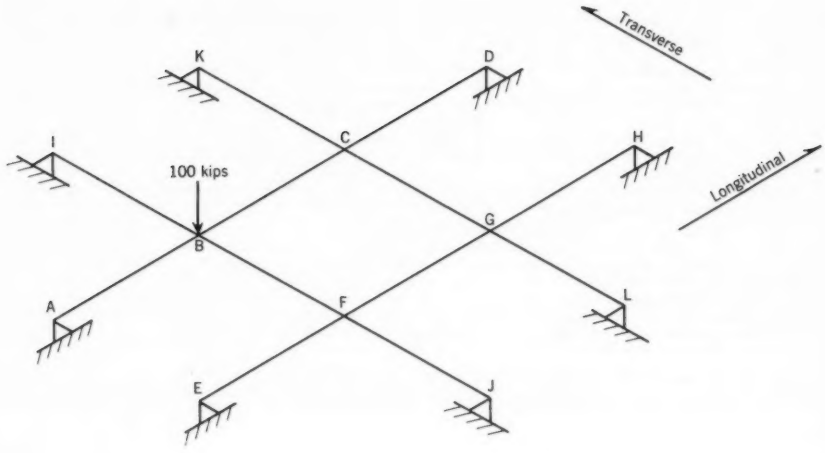

FIG. 9.

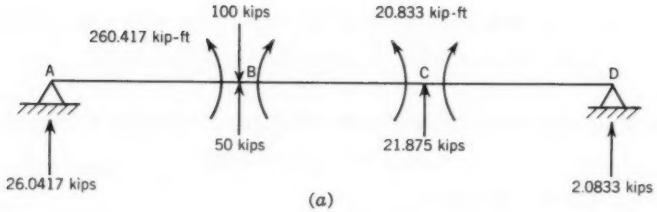

(a)

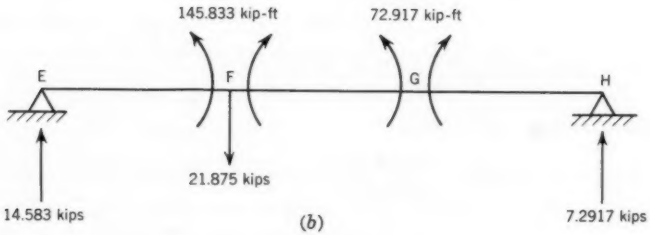

(b)

FIG. 10.

TABLE 6.—REACTION DISTRIBUTION

Joint F		Joint B		Joint C		Joint
Longi-tudinal	Transverse	Transverse	Longi-tudinal	Longi-tudinal	Transverse	Transverse
.5	.5	.5	.5	.5	.5	.5
0 0	0 0	0 -50	+100 -50	0 0	0 0	0 0
0 -21.875	+43.75 -21.875	0 0	0 0	+43.75 -21.875	0 -21.875	0 0
0 0	0 0	+19.140625 -19.140625	+19.140625 -19.140625	0 0	0 0	+19.140625 -19.140625
+16.74805 -16.74805	+16.74805 -16.74805	0 0	0 0	+16.74805 -16.74805	+16.74805 -16.74805	0 0
-21.875	+21.875	-50	+50	+21.875	-21.875	0

[a] Joints B and F are repeated in the chart to facilitate carry over.

Solution by Series.—Use is made of the limit expressed in Eq. 16

$$\lim_{n \to \infty} S_n = \frac{a}{1-r} \quad \ldots\ldots\ldots\ldots\ldots\ldots \quad (16)$$

After cycle 2 the distribution takes the form of a converging series. Thus

$$\Sigma \text{ D.R.} = \text{D.R. (cycle 1)} + \text{D.R. (cycle 2)} + \lim_{n \to \infty} S_n \quad \ldots\ldots \quad (18)$$

(from the balancing chart it can be seen that the convergency factor

$$r = (-0.875)^2 = (0.765625)$$

At Joint B [long. and trans.].

$$\Sigma \text{ D.R.} = -50 + 0 - \frac{19.140625}{1 - 0.765625} = -50 - 81.6667 = -131.6667$$

Thus,

$$\Delta B = \frac{131.6667\ (10)^3}{9.6\ EI} = \frac{13{,}715.2812 \text{ kip ft}^3 \downarrow}{EI}$$

At Joint C [long. and trans.].

$$\Sigma \text{ D.R.} = 0 - 21.875 - \frac{16.74805}{0.234375} = -21.875 - 71.4583 = -93.3333$$

and

$$\Delta C = \frac{93.3333\,(10^3)}{9.6\ EI} = \frac{9722.219 \text{ kip ft}^3 \downarrow}{EI}$$

At Joint G [long. and trans.].

$$\Sigma \text{ D.R.} = 0 + 0 - \frac{19.140625}{0.234375} = -81.6667$$

FOR EXAMPLE THREE

G	Joint F		Joint B		
Longitudinal	Longitudinal	Transverse	Transverse	Longitudinal	
.5	.5	.5	.5	.5	D.F.
0 0	0 0	0 0	0 -50	+100 -50	R.R. D.R. Cycle 1
0 0	0 -21.875	+43.75 -21.875	0 0	0 0	C.O. D.R. Cycle 2
+19.140625 -19.140625	0 0	0 0	+19.140625 -19.140625	+19.140625 -19.140625	C.O. D.R. Cycle 3
0 0	+16.74805 -16.74805	+16.74805 -16.74805	0 0	0 0	C.O. D.R. Cycle 4
0	-21.875	+21.875	-50	+50	Bal. React.

and

$$\Delta_G = \frac{81.6667(10)^3}{9.6\,EI} = \frac{8506.948 \text{ kip ft}^3}{EI} \downarrow$$

At Joint F [long. and trans.]

$$\Sigma \text{ D.R.} = -93.3333$$

and

$$\Delta_F = \frac{9722.219 \text{ kip ft}^3}{EI} \downarrow$$

Reactions at Rigid Supports and Joint Moments.—

$$R_A = -0.375(-131.6667) + 0.25(-93.3333) = +26.0417^{\text{kip}} = R_I$$

$$R_D = +0.25(-131.6667) - 0.375(-93.3333) = +2.0833^{\text{kip}} = R_J$$

$$M_B = +260.417 \text{ kip ft (long. and trans.)}$$

$$M_{C(\text{long.})} = +20.833 \text{ kip ft} = M_{F(\text{trans.})}$$

$$R_E = -0.375(-93.3333) + .25(-81.6667) = +14.5833 \text{ kip} = R_K$$

$$R_H = +0.25(-93.3333) - .375(-81.6667) = +7.2917 \text{ kip} = R_L$$

$$M_{F(\text{long.})} = +145.833 \text{ kip ft}$$

$$M_G = +72.917 \text{ kip ft. (long. and trans.)}$$

Final force diagrams are shown in Figs. 10(a) and 10(b). Member IBFJ is similar to member ABCD of Fig. 10(a) for which

$$\Delta_B = \frac{13{,}715.2812 \text{ kip ft}^3}{EI} \downarrow$$

and

$$\Delta_C = \frac{9722.219 \text{ kip ft}^3}{EI} \downarrow$$

Member KCGL is similar to member EFGH of Fig. 10(b) for which

$$\Delta_F = \frac{9722.219 \text{ kip ft}^3}{EI} \downarrow$$

and

$$\Delta_G = \frac{8506.948 \text{ kip ft}^3}{EI} \downarrow$$

EXAMPLE FOUR

Example four (Fig. 11) involves a grid with constant E I and all spans equal to 10 ft. Part A of this problem involves solving the grid in Fig. 11 for a 100 kip load at joint B and a similar analysis for a 100 kip load at joint D. Part B involves solving the grid for a 100 kip load at joint C. For different conditions of superimposed loading the system can be solved in a manner similar to that shown in example 2.

At Joints B and D, from Table 1 case 4, 6A, 6C

$$\text{Rel. } T_{(\text{long.})} = \frac{-18.85714285\, I}{L^3}$$

and

$$\text{Rel. } T_{(\text{trans.})} = \frac{-24\, I}{L^3}$$

Thus, longitudinal (D.F.) = 0.44 and transverse (D.F.) = 0.56; C.O. from B to C = - 0.636363; C.O. from B to D and D to B = + 0.272727.

At Joint C, from Table 1 Case 4 and 6B

$$\text{Rel. } T_{(\text{long.})} = \frac{-15\, I}{L^3}$$

$$\text{Rel. } T_{(\text{trans.})} = \frac{-24\, I}{L^3}$$

Thus, longitudinal (D.F.) = 0.38461538 and transverse (D.F.) = 0.61538462; C.O. from C to B and C to D = - 0.8.

Example 4 illustrates the distribution method when carry-over to several translating joints occurs in one direction. This problem differs from the previous ones in that carry-over to more than one joint must be considered in the balancing cycle (the same procedure applies).

The distributed longitudinal reaction at Joint B for a $R.R._{BL} = +100$ is in the first cycle of Table 7 (- 44). The carry-over to C (longitudinal) is - 44 (- 0.636363) = + 28.0 and to D (longitudinal) is - 44 (0.272727) = - 12.0. Since in the first cycle there are no other rigid reactions, this carry-over becomes the R.R. for the second cycle. The second cycle distribution indicated in the chart yields - 10.769 at C (longitudinal) and + 5.280 at D (longitudinal). The carry over to joint B (longitudinal) is the carry over from C (longitudinal) plus the carry-over from D (longitudinal); [- 10.769 (- 0.8) + 5.280 (+ 0.272727) = 8.615 + 1.44 = + 10.055.] The distributed reaction is - 10.055 (0.440) = -4.424. The remaining cycles are obtained in a similar manner, each time carrying over to all the translating joints.

It is noted that only the longitudinal span is indicated in the balancing chart. Because there is no transverse carry-over to the deflecting joints,

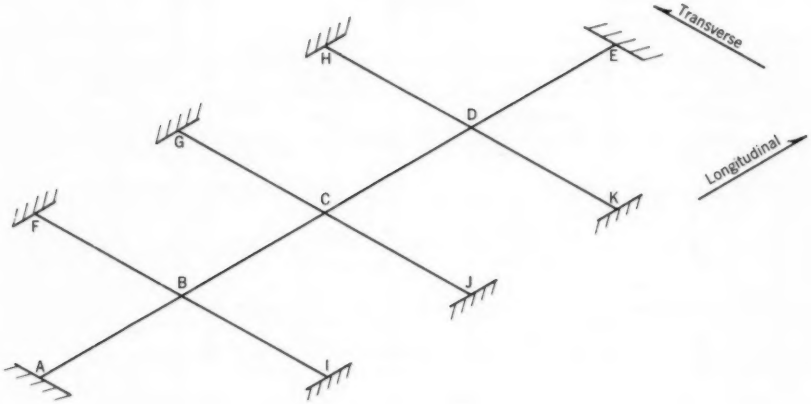
Transverse
Longitudinal
H
E
D
G
K
C
F
B
J
A
I

FIG. 11.

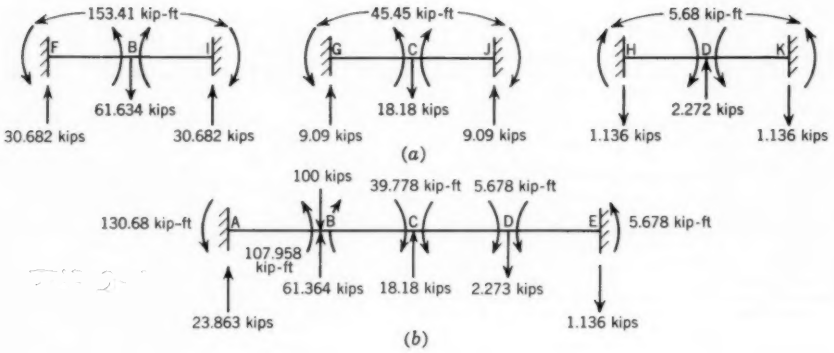
153.41 kip-ft
F
B
I
61.634 kips
30.682 kips
30.682 kips
45.45 kip-ft
G
C
J
18.18 kips
9.09 kips
9.09 kips
5.68 kip-ft
H
D
K
2.272 kips
1.136 kips
1.136 kips
(a)
100 kips
39.778 kip-ft
5.678 kip-ft
130.68 kip-ft
A
B
C
D
E
5.678 kip-ft
107.958 kip-ft
61.364 kips
18.18 kips
2.273 kips
23.863 kips
1.136 kips
(b)

FIG. 12.

TABLE 7.—REACTION DISTRIBUTION FOR EXAMPLE FOUR (PART A)[a,b]

	C.O.F.= -.636363 → C.O.F.= -0.8 ←		C.O.F.= -0.8 → -.636363 ←	+.272727 → +.272727 ←		
B (long.)		C (long.)		D (long.)	B (long.)	
0.440		0.38461538		0.440	0.440	long. D.F.
+100 -44.0		0 0		0 0	+100 -44.0	R.R. D.R.
0 0 0		+28.0 0 -10.769		0 -12.0 +5.280	0 0 0	C.O. D.R.
+1.440 +8.615 -4.424		0 -3.360 +1.292		+8.615 +0 -3.791	+1.440 +8.615 -4.424	C.O. D.R.
-1.034 -1.034 +0.910		+2.815 +2.412 -2.010		-1.034 -1.207 +0.986	-1.034 -1.034 +0.910	C.O. D.R.
+ .269 +1.608 -0.826		- .579 - .627 +0.464		+1.608 + .248 -0.817	+ .269 +1.608 -0.826	C.O. D.R.
- .223 - .371 +0.261		+ .526 + .520 -0.402		- .371 - .225 +0.262	- .223 - .371 +0.261	C.O. D.R.
+ .071 + .322 -0.173		- .166 - .167 +0.128		+ .322 + .071 -0.173	+ .071 + .322 -0.173	C.O. D.R.
- .047 - .102 +0.066		+ .110 + .110 -0.085		- .102 - .047 +0.066	- .047 - .102 +0.066	C.O. D.R.
+ .018 + .068 -0.038		- .042 - .042 +0.032		+ .068 + .018 -0.038	+ .018 + .068 -0.038	C.O. D.R.
- .010 - .026 + .016		+ .024 + .024 -0.018		- .026 - .010 +0.016	- .010 - .026 +0.016	C.O. D.R.
+ .004 + .014 - .008		- .010 - .010 +0.008		+ .014 + .004 -0.008	+ .004 + .014 -0.008	C.O. D.R.
- .002 - .006 + .004		+ .005 + .005 -0.004		- .006 - .002 +0.004	- .002 - .006 +0.004	C.O. D.R.
+ .001 + .003 - .002		- .003 - .003 +0.002		+ .003 + .001 -0.002	+ .001 + .003 -0.002	C.O. D.R.
+109.578		+29.542		-4.058	ΣR.R.	
-48.214		-11.362		+1.785	ΣD.R. (long.)	
+61.364		+18.180		-2.273	Balanced Longitudinal Reaction	
-61.364		-18.180		+2.272	ΣR.R. x [- Tran. D.F.] = ΣD.R.(Tr.) = Bal. Trans. Reac.	
+2556.8		+757.5		-94.7	ΔEI (long.), in kip ft^3	
+2556.8		+757.5		-94.7	ΔEI (trans.)	

[a] Assume rigid reaction at joint B (long.) = +100 kip.
[b] Joint B is repeated in balancing chart to facilitate carry-over process.

TABLE 8.—REACTION DISTRIBUTION FOR EXAMPLE FOUR (PART B)[a]

	-.636363 → -.8 ←		-.8 → -.636363 ←		+.272727 → +.272727 ←		
B (long.)		C (long.)		D (long.)		E (long.)	
0.440		.38461538		0.440		0.440	Long D.F.
0 0		+100 -38.462		0 0		0 0	R.R. D.R.
0 +30.770 -13.539		0 +0 0		+30.770 +0 -13.539		0 +30.770 -13.539	C.O. D.R.
-3.692 +0 +1.624		+2 (8.616) -6.628		0 -3.692 +1.624		-3.692 +0 +1.624	C.O. D.R.
+ .443 +5.302 -2.528		-2(1.033) +0.795		+5.302 + .443 -2.528		+ .443 +5.302 -2.528	C.O. D.R.
- .689 - .636 +0.583		+2 (1.609) -1.238		- .636 - .689 +0.583		- .689 - .636 +0.583	C.O. D.R.
+ .159 + .990 -0.506		-2 (0.371) +0.285		+ .990 + .159 -0.506		+ .159 + .990 -0.506	C.O. D.R.
- .138 - .228 +0.161		+2 (0.322) -0.248		- .228 - .138 +0.161		- .138 - .228 +0.161	C.O. D.R.
+ .044 + .198 -0.106		-2 (0.102) +0.078		+ .198 + .044 -0.106		+ .044 + .198 -0.106	C.O. D.R.
- .029 - .062 +0.040		+2 (0.067) -0.052		- .062 - .029 +0.040		- .029 - .062 +0.040	C.O. D.R.
+ .011 + .042 -0.023		-2 (0.025) +0.019		+ .042 + .011 -0.023		+ .011 + .042 -0.023	C.O. D.R.
- .006 - .015 +0.009		+2 (0.015) -0.012		- .015 - .006 +0.009		- .006 - .015 +0.009	C.O. D.R.
+ .002 + .010 -0.005		-2 (0.006) +0.005		+ .010 + .002 -0.005		+ .002 + .010 -0.005	C.O. D.R.
- .001 - .004 +0.002		+2 (0.003) -0.002		- .004 - .001 +0.002		- .001 - .004 +0.002	C.O. D.R.
0 + .002 -0.001		-2 (0.001) +0.001		+ .002 +0 -0.001		0 + .002 -0.001	C.O. D.R.
+32.473		+118.188		+32.473	ΣR.R.		
-14.289		-45.459		-14.289	ΣD.R. (long.)		
+18.184		+72.729		+18.184	Balanced Longitudinal Reaction		
-18.185		-72.731		-18.185	ΣR.R. x [Tr. D.F.] = ΣD.R. (Tr.) = Bal. Trans. Reac.		
+757.75		+3030.6		+757.75	ΔEI (long.), in kip ft^3		
+757.70		+3030.5		+757.70	ΔEI (trans.)		

[a] Assume rigid reaction at joint C (long.) = +100 kip

these transverse joints need not be listed. Its omission leads to a more convenient chart arrangement. ΣR.R. and ΣD.R. in the longitudinal direction are listed separately after which the balanced longitudinal reaction is obtained. The balanced transverse reaction is obtained by multiplying the negative of Σ R.R. at the joint in question by its transverse distribution factor. This is more convenient than distributing after each cycle. Because there is no carry-over to the translating joints in transverse direction ΣD.R. transverse = balanced transverse reaction. The value of Δ E I is then obtained by equating the values of ΣD.R. = T.

$$\Delta E I B \quad (\text{long.}) = \frac{-(-48.214)(10)^3}{18.85714285} = +2556.8 \text{ kip ft}^3 \downarrow$$

$$\Delta E I B \quad (\text{trans.}) = \frac{-(-61.364)(10)^3}{24} = +2556.8 \text{ kip ft}^3 \downarrow$$

$$\Delta E I C \quad (\text{long.}) = \frac{-(-11.362)(10)^3}{15} = +757.5 \text{ kip ft}^3 \downarrow$$

$$\Delta E I C \quad (\text{trans.}) = \frac{-(-18.18)(10)^3}{24} = +757.5 \text{ kip ft}^3 \downarrow$$

$$\Delta E I D \quad (\text{long.}) = \frac{-(+1.785)(10)^3}{18.85714285} = -94.7 \text{ kip ft}^3 \uparrow$$

$$\Delta E I D \quad (\text{trans.}) = \frac{-(+2.273)(10)^3}{24} = -94.7 \text{ kip ft}^3 \uparrow$$

Reactions at Rigid Supports and Joint Moments (Part A).—The reaction components at all the joints are obtained by multiplying the carry-over factors (from Table 1) by the forces that induced the change (ΣD.R.). Force diagrams are given in Figs. 12 (a) and 12 (b).

R_A = -0.5681818 [-48.214]	+0.3 [-11.362]	-0.0681818 [+1.785]	= +23.863 kip
R_E = -0.0681818	+0.3	-0.5681818	= -1.136 kip
M_A = +.2954545 (10)	-0.1 (10)	+.022727 (10)	= -130.680 kip ft
M_B = -.272727 (10)	+0.2 (10)	-.0454545 (10)	= +107.958 kip ft
M_C = +.1590909 (10)	-0.3 (10)	+.1590909 (10)	= -39.778 kip ft
M_D = -.0454545 (10)	+0.2 (10)	-.272727 (10)	= -5.678 kip ft
M_E = +.022727 (10)	-0.1 (10)	+.2954545 (10)	= +5.678 kip ft

Transverse Direction.—

R_F = -0.5 (-61.364) = +30.682 kip = R_I

M_F = +0.25 (10) = -153.410 kip ft M_I

M_B = -0.25 (10) = +153.410 kip ft

R_G = -0.5 (-18.180) = +9.09 kip R_J

M_G = +0.25 (10) = -45.45 kip ft = M_J

M_C = -0.25 (10) = +45.45 kip ft

$$R_H = -0.5\ (+2.272) = -1.136 \text{ kip} = R_K$$
$$M_H = +0.25\,(10) \Big| = +5.68 \text{ kip ft} = M_K$$
$$M_D = -0.25\,(10) \Big\downarrow = -5.68 \text{ kip ft}$$

Reactions at Rigid Supports and Joint Moments (Part B).—Part B of this example is solved in the same manner as part A. The balancing cycle is given

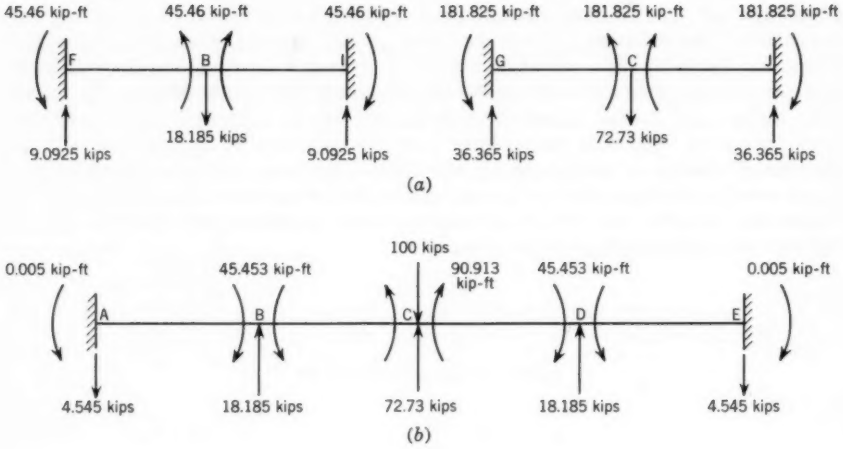

FIG. 13.

in Table 8 and final force diagrams in Figs. 13 (a) and 13 (b). The final force diagram for member HDK is similar to that for FBI of Fig. 12 (a).

$$R_A = -0.5681818\,[-14.289] + 0.3\,[-45.459] - 0.0681818\,[-14.289] = -4.545 \text{ kip}$$
$$R_E = -0.0681818 \Big| +0.3 \Big| -0.5681818 \Big| = -4.545 \text{ kip}$$
$$M_A = +.2954545\,(10) \Big| -0.1\,(10) \Big| +.022727\,(10) \Big| = -.005 \text{ kip ft}$$
$$M_B = -.272727\,(10) \Big| +0.2\,(10) \Big| -.0454545\,(10) \Big| = -45.453 \text{ kip ft}$$
$$M_C = +.1590909\,(10) \Big| -0.3\,(10) \Big| +.1590909\,(10) \Big| = +90.913 \text{ kip ft}$$
$$M_D = -.0454545\,(10) \Big| +0.2\,(10) \Big| -.272727\,(10) \Big| = -45.453 \text{ kip ft}$$
$$M_E = +.022727\,(10) \Big\downarrow -0.1\,(10) \Big\downarrow +.2954545\,(10) \Big\downarrow = -.005 \text{ kip}$$

Transverse Direction.—

$$R_F = -0.5\,(-18.185) = +9.0925 \text{ kip} = R_I$$
$$M_F = +.25\,(10) \Big| = -45.46 \text{ kip ft} = M_I$$
$$M_B = -.25\,(10) \Big\downarrow = +45.46 \text{ kip ft}$$

$R_G = -0.5\ (-72.73) = +36.365$ kip $= R_J$

$M_G = +.25\ (10) \Big| = -181.825$ kip ft $= M_J$

$M_C = -.25\ (10) \Big\downarrow = +181.825$ kip ft

CONCLUSIONS

This paper serves as an introduction to the method of reaction distribution. The examples contained herein demonstrate the use of the method. The greatest advantage of this method is that once understood it becomes a mechanical operation. The solution of grid systems is not limited to the types of spans given in Table 1. For different types of systems expressions for stiffness and carry-over would have to be developed. Grids with more interacting joints than those used in the illustrative problems can be solved. It can readily be seen, however, that the carry-over process becomes more complex with an increased number of translating joints. These systems can be subdivided into grids similar to those solved in this presentation and then combined for final balancing. It is felt that the analyses of the more complex grid systems should receive an independent presentation.

APPENDIX.—NOTATION

The notation used in this paper are presented here for convenience of reference and for the use of discussers:

C.O.	= carry over;
D.F.	= distribution factor;
$D.F._L$	= longitudinal distribution factor;
$D.F._T$	= transverse distribution factor;
D.R.	= distributed reaction;
E	= modulus of elasticity;
I	= moment of inertia;
M	= bending moment;
R	= reaction;
R_{BL}; R_{CL}; R_{DL}. . .	= longitudinal reactions;
R_{BT}; R_{CT}; R_{DT}. . .	= transverse reactions;
R.R.	= rigid reaction;
$R.R._{BL}$; $R.R._{CL}$; $R.R._{DL}$. . .	= longitudinal rigid reactions;

$R.R._{BT}$; $R.R._{CT}$; $R.R._{DT}$. . . = transverse rigid reactions;

T = translation stiffness;

T_{BL}; T_{CL}; T_{DL}. . . = longitudinal translation stiffnesses;

T_{BT}; T_{CT}; T_{DT}. . . = transverse translation stiffnesses; and

Δ = deflection of a joint due to translation.

Journal of the
STRUCTURAL DIVISION
Proceedings of the American Society of Civil Engineers

BENDING OF RECTANGULAR PLATES

By Mounir Badir,[1] M. ASCE

SYNOPSIS

A structural model that closely resembles the plate is described and analyzed for the purpose of solving problems of bending of rectangular plates numerically. The plate model consists of two groups of beams intersecting at right angles. Beams of one group are considered to be continuous over the beams of the other group, free to rotate at points of support and capable of resisting bending moments only. The twisting moments in the plate are carried by pairs of coil springs, connected parallel to the beams at points halfway between beam intersections. Loads are assumed to be concentrated at beam intersections. In comparison with solutions by first order finite differences or by other plate models, the procedure described herein has two main advantages: (1) the elastic surface, moments, etc., are obtained with a higher degree of accuracy, and (2) only a small number of simultaneous equations need to be solved.

INTRODUCTION

Object and Scope of the Investigation.—Since 1900, approximate numerical methods of analysis in the field of structural engineering became a necessity in order to avoid the complex mathematics involved in the solution of many problems by the formal analytical methods. Much research has been successfully conducted in this line by engineers, and definite numerical procedures

Note.—Discussion open until January 1, 1962. To extend the closing date one month, a written request must be filed with the Executive Secretary, ASCE. This paper is part of the copyrighted Journal of the Structural Division, Proceedings of the American Society of Civil Engineers, Vol. 87, No. ST 6, August, 1961.

[1] Asst. Prof. of Structural Engrg., Univ. of Alexandria, Egypt, U. A. R.

have been established for the solution of problems related to beams, columns, plates, and other elastic bodies.

The problem of bending of rectangular plates received great attention, and solutions are now obtainable by the finite difference method,[2] and by use of structural models.[3,4] In both approaches, it is required in general to solve a number of simultaneous linear equations. The accuracy of the results increases with the fineness of the division of the plate surface. Nevertheless, a rapidly increasing number of simultaneous equations will then have to be solved, and the solution becomes too complicated. The object of this investigation is to overcome this difficulty, that is, to reduce the amount of computations as much as possible, and at the same time obtain results with increased accuracy. This is obtained through analysis of a structural model which closely resembles the plate. The model and its analysis are described herein, and solutions are obtained for plates with simply supported, built-in, free, and elastically supported edges, as well as continuous plates. Plates with point supports can be also handled by this method without difficulty. The affect of Poisson's ratio on moments, deflections, etc., is considered at interior points, and at points on supported and free edges.

The analysis of the plate model is simple and yields results with a high degree of accuracy. In each case, the solution is obtained through analysis of two models, and the results are extrapolated. This procedure yields answers which are approximately 1% in error.

Generalized Scope.—The treatment by the presented structural model is general. It covers a broad scope of applicability, and it is not limited to bending of plates. By analogies, its application can be extended to boundary value problems in elasticity which involve the solution of Laplace's or Poisson's equations, as well as plane stress and plane strain problems which are usually solved by introduction of a stress function.

THE PLATE MODEL

Deflections and Moments of the Plate.—The elastic deformation of a laterally loaded plate is governed by the equation[5]

$$\frac{\partial^4 w}{\partial x^4} + 2\,\frac{\partial^4 w}{\partial x^2\,\partial y^2} + \frac{\partial^4 w}{\partial y^4} = \frac{p}{N} \quad \ldots\ldots\ldots\ldots (1)$$

in which, w is the deflection of the middle surface of the plate, p denotes the intensity of the applied load, $N = E\,t^3/\left[12\left(1 - \mu^2\right)\right]$ represents the flexural rigidity of the plate, E refers to the modulus of elasticity of the material, t is the thickness of the plate, and μ denotes Poisson's ratio.

2 "Numerical Computation of Buckling Loads by Finite Differences," by Mario G. Salvadori, Transactions, ASCE, Vol. 116, 1951, pp. 590-624.

3 "Deflections in Gridworks and Slabs," by Walter W. Ewell, Shigeo Okubo, and Joel I. Abrams, Transactions, ASCE, Vol. 117, 1952, pp. 869-890.

4 "Numerical Methods of Analysis in Engineering," Symposium presented at Illinois Inst. of Technology, at Chicago, in 1949; The MacMillan Co., New York, 1949, p. 142: "Numerical Methods of Analysis of Bars, Plates, and Elastic Bodies," by N. M. Newmark.

5 "Theory of Plates and Shells," by S. Timoshenko, McGraw-Hill Book Co., Inc., New York, 1940, p. 88.

The relation[6] between the bending moments M_x and M_y, the twisting moment M_{xy}, and the load p is given by

$$\frac{\partial^2 M_x}{\partial x^2} - 2\frac{\partial^2 M_{xy}}{\partial x\,\partial y} + \frac{\partial^2 M_y}{\partial y^2} = -p \quad \ldots\ldots\ldots\ldots (2)$$

Description of the Model.—To determine the structural model, consider the rectangular plate ABCD shown in Fig. 1(a), and imagine it to be divided into a number of strips by lines parallel to the sides of the plate. Lines like 1-1 and 2-2 divide the plate into strips extending in the x-direction, and lines like 2'-2' and 3'-3' divide it into strips parallel to the y-direction. The inner strips are all equal to λ in width, while the edge strips are only half as wide. These strips are represented in Fig. 1(b) as beams. Coil springs of length λ are connected at their ends to these beams at points half-way between their

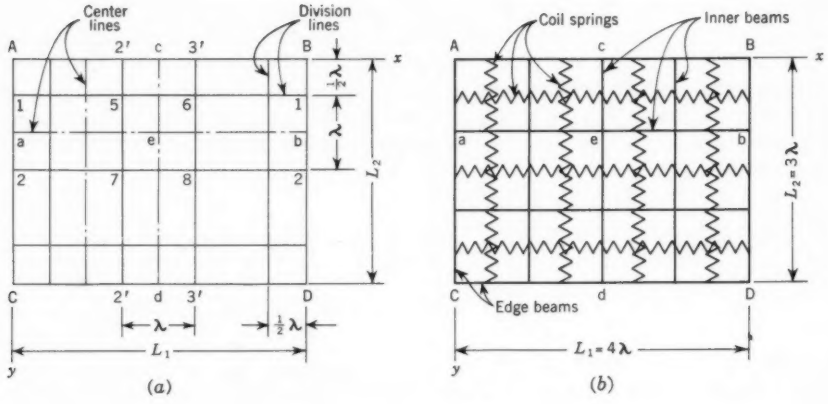

FIG. 1

intersections. The structure in Fig. 1(b) is the model of the plate in Fig. 1(a). Beams extending in one direction are considered to be continuous and freely supported by beams of the other direction. The load on a square area like 5-6-7-8 in common between the two intersecting beams ab and cd is considered as concentrated at their intersection point e. Similarly the load on rectangle 2'-3'-5-6 is replaced by a concentrated load at point c on the edge.

Elastic Properties and Deformations of the Model.—In order to describe the elastic behavior of the plate model, distinction is made between its two component parts, namely:

(A) the continuous beams extending in the x- and y-directions, which are considered to have only flexural rigidity, and

---

[6] Ibid., pp. 85-92.

(B) the coil springs which provide the tortional resistance of the plate model.

The load p, at an intersection point, is the sum of three portions p_x, p_y, and p_{xy} resisted, respectively, by bending of the x- and y- beams, and by torsion of coil springs. The "differential-difference" equation of the elastic surface of the plate model may be written, at an intersection point, in the form

$$\frac{\partial^4 w}{\partial x^4} + 2\left[\frac{\partial^4 w}{\partial x^2\,\partial y^2}\right] + \frac{\partial^4 w}{\partial y^4} = \frac{1}{N}\left(p_x + p_y + p_{xy}\right) = \frac{p}{N} \quad \ldots\ldots (3)$$

in which N is the flexural rigidity per unit width of the beams, when Poisson's ratio is zero.

In a similar manner the relation between load and moments is obtained

$$\frac{\partial^2 M'_x}{\partial x^2} - 2\left[\frac{\partial^2 M'_{xy}}{\partial x\,\partial y}\right] + \frac{\partial^2 M'_y}{\partial y^2} = -\,p \quad \ldots\ldots\ldots\ldots (4)$$

in which M'_x and M'_y are respectively the bending moments per unit width of x- and y- beams. The term M'_{xy} is the twisting moment in the coil springs. The two brackets in Eqs. 3 and 4 indicate that the inclosed terms are in difference form.

Eq. 4 can be rewritten in the form

$$P_o = P_x + P_y + P_{xy} = \left(p_x + p_y + p_{xy}\right)\lambda^2 = \left(-M'_{wx} + 2\,M'_{ox} - M'_{ex}\right)$$

$$+ \left(-M'_{sy} + 2\,M'_{oy} - M'_{ny}\right) + 2\left(M'_{wn} + 2\,M'_{es} - 2\,M'_{en} - 2\,M'_{ws}\right) \ldots (5)$$

in which P_o is the total load at point o. For example, M'_{ex} is the bending moment in the x-beam at point e distant λ from o to the east, and so on. For example, M'_{ws} is the twisting moment in the coil springs of the panel west-south of o, and so on.

The twisting moment in the coil springs of panel wn west-north of point o and the load P_{xy} at point o are given in terms of the deflections by the relations

$$M'_{wn} = \frac{N}{\lambda^2} \times \begin{array}{ccc} & +1 & -1 \\ & \boxed{\begin{array}{cc} nw & n \\ & wn \\ w & o \end{array}} & \\ -1 & & +1 \end{array} \quad \ldots\ldots\ldots\ldots (6)$$

and

$$P_{xy} = \frac{N}{\lambda^2} \times$$

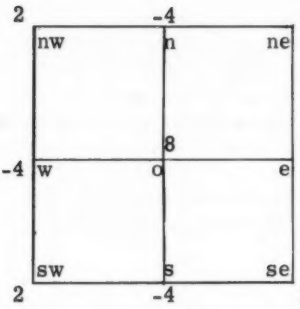

. . . . . (7)

in which the numbers are coefficients of the deflections at the intersection points. Eq. 7 also gives values of P_{xy} at o and the surrounding points for a unit deflection at o and zero elsewhere. In this case the twisting moments arising in the springs of the surrounding panels are

$$M'_{xy} = \frac{N}{\lambda^2} \times$$

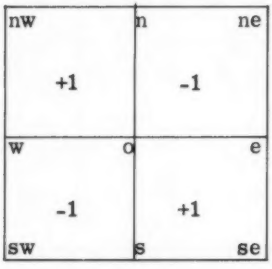

. . . . . (8)

Analogy Between Plate and Model.—The plant model is a representation of the plate by which it is possible to determine approximate deflections of the plate at a number of discrete points.

Comparison of Eqs. 1 and 3 shows the analogy between the differential equations for the elastic surface of the plate and its model, with exception of the second term of Eq. 3 which is in difference form. Nevertheless, with increasing number of intersection points, this term approaches the corresponding one of Eq. 1. The elastic surface of the model is therefore an approximation of the elastic surface of the plate itself, in case Poisson's ratio is zero. To determine the plant deflections when Poisson's ratio is different from zero, it is only necessary to substitute the proper value of N in the obtained deflections of the plate model.

Comparison of Eqs. 2 and 4 shows that the moments of the plate model represent the moments in the plate when Poisson's ratio is zero. The plate moments, shears, and reactive forces for any value of Poisson's ratio different from zero are obtained from model moments by use of the following relations. The plate moments

$$M_x = M'_x + \mu M'_y \quad \ldots\ldots\ldots\ldots\ldots\ldots (9)$$

$$M_y = M'_y + \mu M'_x \quad \ldots\ldots\ldots\ldots\ldots\ldots (10)$$

and

$$M_{xy} = (1-\mu)\, M'_{xy} \quad \ldots\ldots\ldots\ldots\ldots\ldots (11)$$

The shearing forces at sections of the plate located halfway between the beam intersection points are

$$Q_x = \frac{\partial M'_x}{\partial x} - \left[\frac{\partial M'_{xy}}{\partial y}\right] \quad \ldots\ldots\ldots\ldots\ldots\ldots (12a)$$

and

$$Q_y = \frac{\partial M'_y}{\partial y} - \left[\frac{\partial M'_{xy}}{\partial x}\right] \quad \ldots\ldots\ldots\ldots\ldots\ldots (12b)$$

These shearing forces are independent of μ, and hence are equal to the corresponding shearing forces of the plate model. The reactive forces at an intersection point on a supported edge of the plate are

$$V_x = \frac{\partial M'_x}{\partial x} - (2 - \mu)\left[\frac{\partial M'_{xy}}{\partial y}\right] \pm \frac{P}{\lambda} \quad \ldots\ldots\ldots\ldots (12c)$$

and

$$V_y = \frac{\partial M'_y}{\partial y} - (2 - \mu)\left[\frac{\partial M'_{xy}}{\partial x}\right] \pm \frac{P}{\lambda} \quad \ldots\ldots\ldots\ldots (12d)$$

in which P is the concentrated load at the intersection point of the model, which must not be overlooked in the computation of edge reactions. The positive sign of P is considered for points on the upper and left edges of the plate; the negative sign, for points on the lower and right edges. The plate corner reaction is given by

$$R_c = 2\, M_{xy} \equiv 2(1 - \mu) M'_{xy} \quad \ldots\ldots\ldots\ldots\ldots (12e)$$

The derivatives and differences of Eqs. 12 can be easily evaluated as will be shown later in the solved examples.

At a boundary, the beams of the plate model are made built-in, simply supported, continuous, elastically supported, or on point support where the plate is likewise supported. At free and elastically supported edges, the boundary conditions are more complicated, and special consideration is necessary so that the same general procedure may become applicable in such cases. Analysis of plates with free and elastically supported edges are presented subsequently.

ANALYSIS OF THE MODEL

Basic Model Unit.—Consider a square plate, length of side 2λ, and built-in along four edges. Fig. 2 shows the plate model with the coil springs removed

for convenience. Let the intersection point o undergo a downward unit deflection. Linearly varying bending moments are produced in the beams with magnitudes +6 N/λ^2 at o, and -6 N/λ^2 at ends w, n, e, and s. No moments are induced in the edge beams as a result of this displacement. The twisting moments in the coil springs are given by Eq. 8. Fig. 2 shows how these moments are registered. The bending moments are written above the x-beams, and on the west side of the y-beams. The twisting moments are scored at the centers of the panels. The numbers are all coefficients of N/λ^2. The necessary holding force at o is found by Eq. 5 to be 56 N/λ^2.

Method of Analysis.—Consider the plate model shown in Fig. 3, which is supported on its four edges. Let i represent points 1 to 9, and n be any one of these

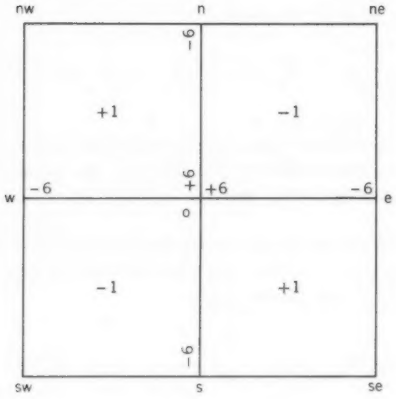

FIG. 2

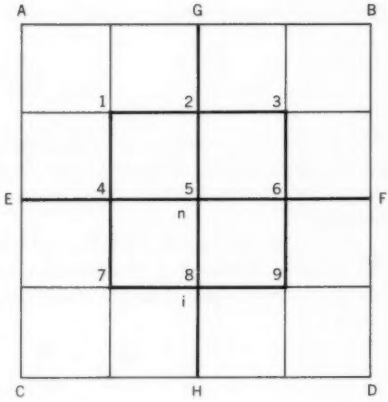

FIG. 3

points, for example, point 5. The analysis of the model may be summarized in the following steps:

(1) Allow a unit deflection $(w_n = 1)$ at only one intersection point (point n), the beams being locked against both rotation and deflection at all other intersection points.

(2) Determine the moments in the basic model unit (1-3-7-9) which has the deflected point at the center. The moments are as given in Fig. 2.

(3) Allow the beams to rotate. Distribute the unbalanced fixed end moments by moment distribution procedure. The twisting moments are not altered during this rotation.

(4) Determine the self-balanced system of holding forces $\left(R_{i,\ w_n=1}\right)$ using Eq. 5. Holding forces are only needed at intersection points on the x- and y-beams through the deflected point, and at the four diagonally adjacent points (1, 3, 7, and 9).

(5) Repeat steps 1 to 4 for all intersection points.

(6) Write an equation at every intersection point, stating that the sum of holding forces $\left(R_{n,w_i}\right)$ at the point, consistent with the true deflections $\left(w_i\right)$, must be equal to the applied load $\left(P_n\right)$, thus

$$\sum_{i=1,2,\ldots} w_i R_{n,w_i=1} = P_n \quad \ldots\ldots\ldots\ldots (13a)$$

The holding force at point (n) due to a unit deflection at point (i) is equal to the holding force at point (i) due to a unit deflection at point (n), that is

$$R_{n,w_i=1} = R_{i,w_n=1} \quad \ldots\ldots\ldots\ldots\ldots (13b)$$

Hence the "load-deflection equation" (Eq. 13(a)), becomes

$$\sum_{i=1,2,\ldots} w_i R_{i,w_n=1} = P_n \quad \ldots\ldots\ldots\ldots (14)$$

The result is a number of simultaneous equations equal to the number of unknown deflections. In view of the reciprocal relationship (Eq. 13(b)), the equations are of the normal type and can be conveniently solved by the "Doolittle Method."

(7) The moments, shears, and reactions of the plate are then obtained from the elastic surface of the model. The model moments are determined by superposition of the moments in step 3, thus at any point (n)

$$M'_{nx} = \sum_{i=1,2,\ldots} w_i M'_{nx,w_i=1} \quad \ldots\ldots\ldots\ldots (15a)$$

and

$$M'_{ny} = \sum_{i=1,2,\ldots} w_i M'_{ny,w_i=1} \quad \ldots\ldots\ldots\ldots (15b)$$

and in any panel wn, the twisting moment

$$M'_{wn} = \sum_{i=1,2,\ldots} w_i M'_{wn,w_i=1} \quad \ldots\ldots\ldots\ldots (15c)$$

Simplified Distribution Procedure.—Many computations for the distribution of the unbalanced moments in the beams can be eliminated by use of a direct distribution procedure. Consider the continuous beam AB, with equal spans λ, shown in Fig. 4(a). An unbalanced moment at support n can be distributed in the ratio of the stiffnesses K_a and K_b of the two continuous beams nA and nB. By the stiffness K_b, for example, is meant the moment at n required to produce a unit rotation of the beam nB at end n (Fig. 4(b)). The distributed moments are carried over to all the supports by use of carry-over factors in the different spans. The carry-over factor from support n to support 2' is $M_{2'}/M_n$; from 2' to 1', $M_{1'}/M_{2'}$; and so on (Fig. 4(c)). In this way an unbalanced moment is distributed and carried over to the ends of the beam through only one distribution.

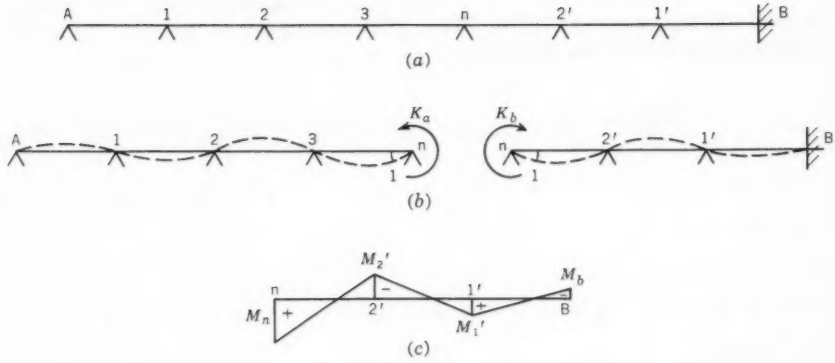

FIG. 4

	6	5	4	3	2	1	A	Commo factor
(1) Consistent moments:	−780	+209	−56	+15	−4	+1	0	
(2) Carry-over factors:		$-\frac{209}{780}$	$-\frac{56}{209}$	$-\frac{15}{56}$	$-\frac{4}{15}$	$-\frac{1}{4}$	0	
(3) Stiffnesses:	$\frac{4\,680}{1\,351}$	$\frac{627}{181}$	$\frac{336}{97}$	$\frac{45}{13}$	$\frac{24}{7}$	3		N/λ

(*a*) FAR END A HINGED

	6	5	4	3	2	1	A
(4) Consistent moments:	+1 351	−362	+97	−26	+7	−2	+1
(5) Carry-over factors:		$-\frac{362}{1\,351}$	$-\frac{97}{362}$	$-\frac{26}{97}$	$-\frac{7}{26}$	$-\frac{2}{7}$	$-\frac{1}{2}$
(6) Stiffnesses:	$\frac{1\,351}{390}$	$\frac{724}{209}$	$\frac{97}{28}$	$\frac{52}{15}$	$\frac{7}{2}$	4	N/λ

(*b*) FAR END A BUILT-IN

FIG. 5

Fig. 5 shows the stiffnesses and carry-over factors ready for use in the distribution procedure, in cases of beams with far ends hinged and built-in.

For illustration of the suggested simplification, consider the beam AB shown in Fig. 6(a). The stiffness of beam 2-A is found in line (6) of Fig. 5 under support 2, to be 7/2, and the stiffness of beam 2'-B is given in line (3) under support 2 as 24/7. Similarly the stiffness of beams 1-A and 3'-B, 3-A and 1'-B can be obtained. The rest of Fig. 6(a) is self explaining. The bending moment diagram is drawn in Fig. 6(b). The holding forces and the elastic line of the beam are shown in Fig. 6(c).

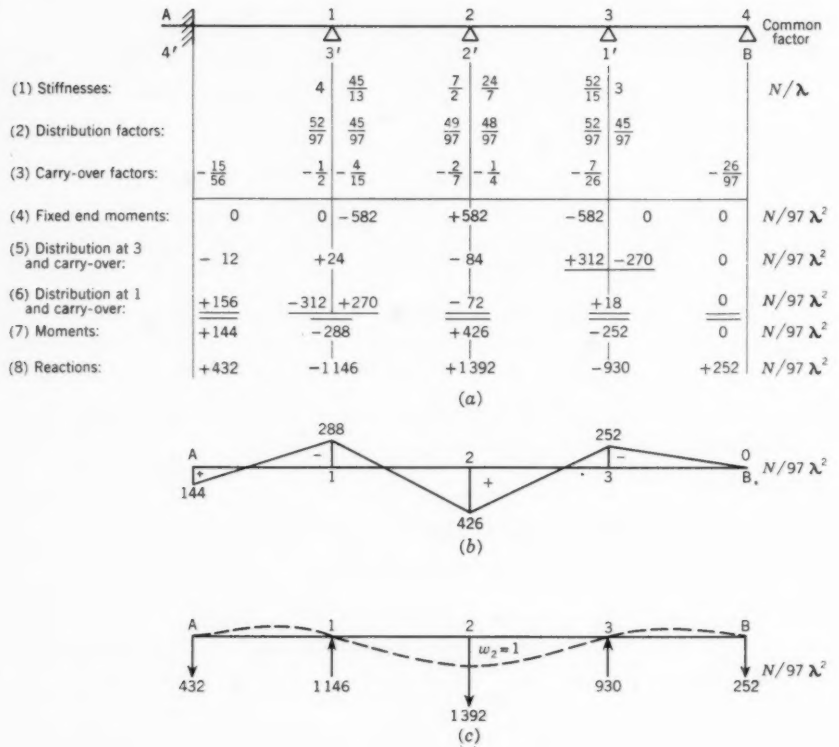

FIG. 6

If the plate model of Fig. 3 is built-in along edges AB and AC, and simply supported along the other two edges, the reactions of beam AB (Fig. 6(c)) would be the holding forces R_x and R_y accompanied with bending of beams EF and GH, produced by a unit deflection at point 5. The holding forces R_{xy} accompanied with twisting are obtained by Eq. 7. In Fig. 7(a) the holding forces are registered in lines (1), (2), and (3), and are added in line (4). In Fig. 7(b) are given the moments M'_x, M'_y, and M'_{xy}, registered in the same order described previously under the heading "Basic Model Unit."

Assuming a uniform loading of intensity p, the load-deflection equation (Eq. 14) can be written at points 5, thus

$$194\,w_1 - 1534\,w_2 + 194\,w_3 - 1534\,w_4 + 3560\,w_5 - 1318\,w_6 + 194\,w_7 - 1318\,w_8 + 194\,w_9 = 97\,\frac{p\,\lambda^4}{N} \quad \ldots(16a)$$

Noticing that in this case there is symmetry with respect to the diagonal line AD, the elastic surface is also symmetrical, hence

$$w_2 = w_4\,,\ w_3 = w_7\,,\ \text{and}\ w_6 = w_8 \quad \ldots\ldots\ldots\ldots(16b)$$

and Eq. 16(a) becomes

$$97\,w_1 - 1534\,w_2 + 194\,w_3 + 1780\,w_5 - 1318\,w_6 + 97\,w_9 = 48.5\,\frac{p\,\lambda^4}{N} \quad \ldots(16c)$$

Five other equations at points 1, 2, 3, 6, and 9 can be written and solved to determine the elastic surface of the model. In cases of symmetry, it is feasible

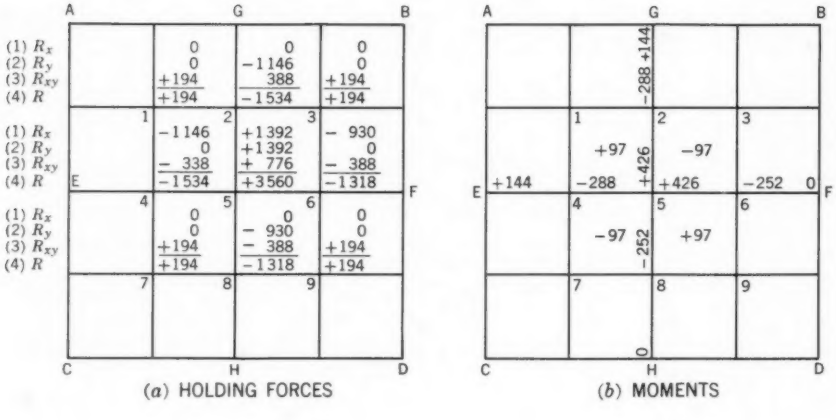

FIG. 7

to allow unit deflections at symmetrical points simultaneously, thus making it possible to deal with only a part of the model.

Holding Forces and Moments.—It was seen previously that the holding forces and moments of the model (Fig. 7) were obtained with great ease in a relatively short time, after the holding forces and moments of the beams (Figs. 6(b) and 6(c)) have been determined. In order to secure the same advantages in other cases, Table 1 has been prepared. It contains the results of analyses of several beams by the procedure previously described. The beams have continuous spans varying in number from two to six with combinations of simply

TABLE 1.—BENDING MOMENTS AND HOLDING FORCES IN MODEL BEAMS PRODUCED BY UNIT DEFLECTIONS AT INTERSECTION POINTS

Case	$\frac{L}{\lambda}$	Type[a] of Support at		Unit Deflection at Support	Holding Forces And Bending Moments At Support[b]							Common Factor
		Left End	Right End		1	2	3	4	5	6	7	
(1)	(2)	(3)	(4)	(5)	(6)							(7)
1. a	2	b	b	1	9	-6	3					N/λ^2
					15	-24	9					
b	2	b	b	2	-6	6	-6					N/λ^2
					-12	24	-12					
c	2	s	s	1	0	-3	0					$N/2\lambda^2$
					3	-6	3					
d	2	s	s	2	0	3	0					N/λ^2
					-3	6	-3					
e	2	b	s	1	30	-18	0					$N/7\lambda^2$
					48	-66	18					
f	2	b	s	2	-36	30	0					$N/7\lambda^2$
					-66	96	-30					
g	2	b	s	3	6	-12	0					$N/7\lambda^2$
					18	-30	12					
2. a	3	b	b	1	22	-14	4	-2				$N/5\lambda^2$
					36	-54	24	-6				
b	3	b	b	2	-28	26	-16	8				$N/5\lambda^2$
					-54	96	-66	24				
c	3	s	s	1	0	-8	2	0				$N/5\lambda^2$
					8	-18	12	-2				
d	3	s	s	2	0	18	-12	0				$N/5\lambda^2$
					-18	48	-42	12				
e	3	b	s	1	57	-36	9	0				$N/13\lambda^2$
					93	-138	54	-9				
f	3	b	s	2	-72	66	-36	0				$N/13\lambda^2$
					-138	240	-138	36				
g	3	b	s	3	18	-36	48	0				$N/13\lambda^2$
					54	-138	132	-48				
h	3	b	s	4	-3	6	-21	0				$N/13\lambda^2$
					-9	36	-48	21				
3. a	4	b	b	1	123	-78	21	-6	3			$N/28\lambda^2$
					201	-300	126	-36	9			
b	4	b	b	2	-78	72	-42	12	-6			$N/14\lambda^2$
					-150	264	-168	72	-9			
c	4	b	b	3	21	-42	63	-42	21			$N/14\lambda^2$
					63	-168	210	-168	63			
d	4	s	s	1	0	-45	12	-3	0			$N/28\lambda^2$
					45	-102	72	-18	3			

TABLE 1.—*CONTINUED*

Case	$\frac{L}{\lambda}$	Type[a] of Support at Left End	Type[a] of Support at Right End	Unit Deflection at Support	Holding Forces And Bending Moments At Support[b] 1	2	3	4	5	6	7	Common Factor
(1)	(2)	(3)	(4)	(5)	(6)							(7)
e	4	s	s	2	0	51	-36	9	0			$N/14\lambda^2$
					-51	138	-132	54	-9			
f	4	s	s	3	0	-36	60	-36	0			$N/14\lambda^2$
					36	-132	192	-132	36			
g	4	b	s	1	426	-270	72	-18	0			$N/97\lambda^2$
					696	-1038	432	-108	18			
h	4	b	s	2	-540	498	-288	72	0			$N/97\lambda^2$
					-1038	1824	-1146	432	-72			
i	4	b	s	3	144	-288	426	-252	0			$N/97\lambda^2$
					432	-1146	1392	-930	252			
j	4	b	s	4	-36	72	-252	354	0			$N/97\lambda^2$
					-108	432	-930	960	-354			
k	4	b	s	5	6	-12	42	-156	0			$N/97\lambda^2$
					18	-72	252	-354	156			
4. a	5	b	b	1	918	-582	156	-42	12	-6		$N/209\lambda^2$
					1500	-2238	936	-252	72	-18		
b	5	b	b	2	-1164	1074	-624	168	-48	24		$N/209\lambda^2$
					-2238	3936	-2490	1008	-288	72		
c	5	b	b	3	312	-624	930	-588	168	-84		$N/209\lambda^2$
					936	-2490	3072	-2274	1008	-252		
d	5	s	s	1	0	-336	90	-24	6	0		$N/209\lambda^2$
					336	-762	540	-144	36	-6		
e	5	s	s	2	0	762	-540	144	-36	0		$N/209\lambda^2$
					-762	2064	-1986	864	-216	36		
f	5	s	s	3	0	-540	906	-576	144	0		$N/209\lambda^2$
					540	-1986	2928	-2202	864	-144		
g	5	b	s	1	795	-504	135	-36	9	0		$N/181\lambda^2$
					1299	1938	810	-216	54	-9		
h	5	b	s	2	-1008	930	-540	144	-36	0		$N/181\lambda^2$
					-1938	3408	-2154	864	-216	36		
i	5	b	s	3	270	-540	804	-504	126	0		$N/181\lambda^2$
					810	-2154	2652	-1938	756	-126		
j	5	b	s	4	-72	144	-504	786	-468	0		$N/181\lambda^2$
					-216	864	-1938	2544	-1722	468		
k	5	b	s	5	18	-36	126	-468	660	0		$N/181\lambda^2$
					54	-216	756	-1722	1788	-660		
l	5	b	s	6	-3	6	-21	78	-291	0		$N/181\lambda^2$
					-9	36	-126	468	-660	291		
5. a	6	b	b	1	571	-362	97	-26	7	-2	1	$N/130\lambda^2$
					933	-1392	582	-156	42	-12	3	

TABLE 1.—*CONTINUED*

Case	$\frac{L}{\lambda}$	Type[a] of Support at		Unit Deflection at Support	Holding Forces And Bending Moments At Support[b]							Common Factor
		Left End	Right End		1	2	3	4	5	6	7	
(1)	(2)	(3)	(4)	(5)	(6)							(7)
b	6	b	b	2	-724	668	-388	104	-28	8	-4	$N/130\lambda^2$
					-1392	2448	-1548	624	-168	45	-24	
c	6	b	b	3	194	-388	578	-364	98	-28	14	$N/130\lambda^2$
					582	-1548	1908	-1404	588	-168	42	
d	6	b	b	4	-52	104	-364	572	-364	104	-52	$N/130\lambda^2$
					-156	624	-1404	1872	-1404	624	-156	
e	6	s	s	1	0	-209	56	-15	4	-1	0	$N/130\lambda^2$
					209	-474	336	-90	24	-6	1	
f	6	s	s	2	0	474	-336	90	-24	6	0	$N/130\lambda^2$
					474	1284	-1236	540	-144	36	-6	
g	6	s	s	3	0	-336	564	-360	96	-24	0	$N/130\lambda^2$
					336	-1236	1824	-1380	576	-144	24	
h	6	s	s	4	0	90	-360	570	-360	90	0	$N/130\lambda^2$
					-90	540	-1380	1860	-1380	540	-90	
i	6	b	s	1	5934	-3762	1008	-270	72	-18	0	$N/1351\lambda^2$
					9696	-14466	6048	-1620	432	-108	18	
j	6	b	s	2	-7524	6942	-4032	1080	-288	72	0	$N/1351\lambda^2$
					-14466	25440	-16086	6480	-1728	432	-72	
k	6	b	s	3	2016	-4032	6006	-3780	1008	-252	0	$N/1351\lambda^2$
					6048	-16086	19824	-14574	6048	-1512	252	
l	6	b	s	4	-540	1080	-3780	5934	-3744	936	0	$N/1351\lambda^2$
					-1620	6480	-14574	19392	-14358	5616	-936	
m	6	b	s	5	144	-288	1008	-3744	5862	-3492	0	$N/1351\lambda^2$
					432	-1728	6048	-14358	18960	-12846	3492	
n	6	b	s	6	-36	72	-252	936	-3492	4926	0	$N/1351\lambda^2$
					-108	432	-1512	5616	-12846	13344	-4926	
o	6	b	s	7	6	-12	42	-156	582	-2172	0	$N/1351\lambda^2$
					18	-72	252	-936	3492	-4926	2172	

[a] s denotes simple support; b, built-in support.
[b] Bending moments are written in upper lines; holding forces, in lower lines.

supported and built-in ends. Table 1 is useful in the analysis of plate models when L/λ is not more than 6, or 12 in cases of symmetry. The table has been prepared for inner beams of the model which have widths equal to λ, so that in case of edge beams with widths $\lambda/2$, the holding forces are only half the values given in the table.

Increased Accuracy by Extrapolation.—In general, accuracy of the results depends on the fineness of the chosen nets. Nevertheless it is feasible to use

less finely divided nets, and then extrapolate the results, although it becomes necessary to repeat the solution at least with two different nets. The extrapolation is made herein by the procedure suggested by L. F. Richardson.[7,8] In general the approximations k_i, k_j corresponding to meshes with n_i and n_j divisions are assumed to approach the true value k monotonically. The extrapolated value is then

$$k_{i,j} = k_j + \frac{1}{\left(\frac{n_j}{n_i}\right)^2 - 1} \left(k_j - k_i\right) \quad \ldots\ldots\ldots\ldots \quad (17)$$

PLATES SUPPORTED ALONG EDGES

Three plates supported along all the edges are now completely analyzed to illustrate the details and arrangement of the solution by the method described herein. The results are compared with those available by the formal analytical methods, in order to examine the accuracy of the procedure.

Uniformly Loaded Square Plate Simply Supported Along Four Edges.—Fig. 8 shows two models of the plate. In model a the length of side $L = 2\lambda$; in model b, $L = 4\lambda$. In model a (Fig. 8(a)) the deflection at the center point 1 has to be determined. Figs. 9(a) and 9(b) show, respectively, the holding forces and moments consistent with a unit deflection at point 1 as obtained from Table 1 case 1d. The holding force at point 1 must be equal to the applied load, hence the load-deflection equation (Eq. 14) gives

$$20\, w_1 \frac{N}{\lambda^2} = p\lambda^2 \quad \ldots\ldots\ldots\ldots\ldots\ldots \quad (18a)$$

from which the center deflection of the plate is

$$w_1 = 0.05 \frac{p\lambda^4}{N} = 0.003125 \frac{p L^4}{N} \quad \ldots\ldots\ldots\ldots \quad (18b)$$

and the center moments are

$$M'_{1x} = M'_{1y}\, 3\, w_1 \frac{N}{\lambda^2} = 0.0375\, p L^2 \quad \ldots\ldots\ldots\ldots \quad (18c)$$

and the twisting moment in panel 1A, for example, is

$$M'_{1A} = w_1 \frac{N}{\lambda^2} = 0.0125\, p L^2 \quad \ldots\ldots\ldots\ldots \quad (18d)$$

---

7 "The Approximate Arithmatical Solution by Finite Differences of Physical Problems Involving Differential Equations, with an Application to the Stresses in a Masonry Dam," by L. F. Richardson, Philosophical Transactions, Royal Soc. of London, Series 210A, 1910.

8 "Numerical Computation of Buckling Loads by Finite Differences," by Mario G. Salvadori, Transactions, ASCE, Vol. 116, 1951, Eq. 41, p. 608.

For $\mu = 0.30$, the plate deflection and moments are

$$w_1 = 0.003125 \times 12 \ (1 - 0.09) \frac{p L^4}{E t^3} = 0.03412 \frac{p L^4}{E t^3} \quad \ldots\ldots(19a)$$

$$M_{1x} = M_{1y} = 0.0375 \ (1 + 0.30) \ p L^2 = 0.04875 \ p L^2 \quad \ldots\ldots(19b)$$

and

$$M_{1A} = M_{1D} = - M_{1B} = - M_{1C} = (1 - 0.30) \times 0.0125 \ p L^2$$

$$= 0.00875 \ p L^2 \quad \ldots\ldots(19c)$$

The model and plate moments are shown in Fig. 10. The shear Q_y at middle section of beam 1-G is obtained from the moments of Fig. 10(a) by use of Eq. 12(b)

$$Q_{y,1-G} = \left[(0.0375 - 0) - (-0.0125 - 0.0125)\right] p L^2 \times \frac{2}{L} = 0.125 \ p L \quad \ldots\ldots(19d)$$

and to find the shear Q_y at G, the effect of concentrated load $0.125 \ p L^2$ at G is added, hence

$$Q_{y,G} = 0.125 \ p L + 0.125 \ p L^2 \times \frac{2}{L} = 0.375 \ p L \quad \ldots\ldots(19e)$$

and the reaction V_y at G is determined from Eq. 12(d), hence

$$V_{y,G} = \left[(0.0375 - 0) - (2-0.30)(-0.0125 - 0.0125) + 0.125\right] p L^2 \times \frac{2}{L} = 0.41 \ p L \quad \ldots\ldots(19f)$$

From Eq. 12(e), the concentrated reaction at each corner is

$$R_c = 2 \times 0.00875 \ p L^2 = 0.0175 \ p L^2 \quad \text{(downward)} \quad \ldots\ldots(19g)$$

In model b (Fig. 8(b)), the deflections at only three points must be determined, in view of symmetry. The holding forces and moments consistent with unit deflections at the intersection points are obtained from Table 1, cases 3e and 3f. Case 3e however requires a modification in order to account for symmetry. Unit deflections at the two quarter points are allowed simultaneously. The holding forces and moments can be readily obtained by superposition. Details of analysis of models b are omitted for briefness, but the results of analyses by plate model a and b are summarized in Table 2, extrapolated and compared with the corresponding values given by S. Timoshenko. In models a and b, $n_a=2$ and $n_b=4$, and the extrapolated value in Eq. 17 becomes

$$k_{a,b} = k_b + \frac{1}{3}\left(k_b - k_a\right) \quad \ldots\ldots\ldots\ldots\ldots \quad (20)$$

The results given in Table 2 columns (2) and (3) are extrapolated in column (4). The exact values obtained by Timoshenko are given[9] in column (5). Com-

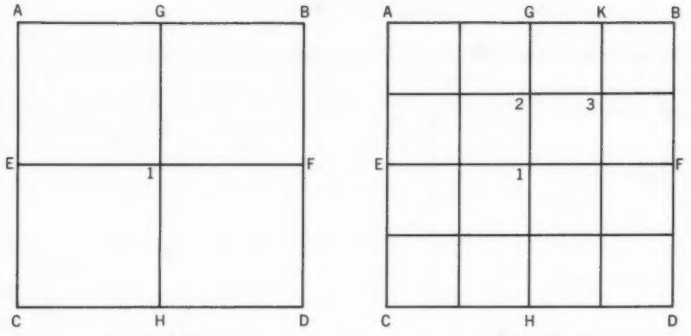

(*a*) MODEL a (*b*) MODEL b

FIG. 8

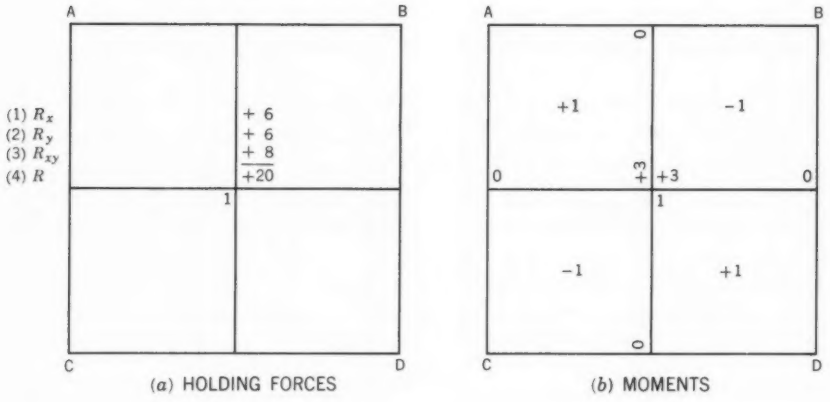

(*a*) HOLDING FORCES (*b*) MOMENTS

FIG. 9

parison of columns (4) and (5) shows the close agreement between the values obtained by analysis of the suggested plate model and the exact values. For example, the center deflection and center moment are, respectively, 1.6% and

9 "Theory of Plates and Shells," by S. Timoshenko, McGraw-Hill Book Co., Inc., New York, 1940, p. 133, Table 5.

0.4% of the exact values. The small number of equations which need to be solved and the high degree of accuracy of the results witness the powerfulness of the procedure.

Uniformly Loaded Square Plate Built-in Along Four Edges.—In general, more divisions are needed in the analysis of plates with built-in edges than in

TABLE 2.—UNIFORMLY LOADED SQUARE PLATE SIMPLY SUPPORTED ALONG FOUR EDGES (μ = 0.30)

Item (1)	Results by Model a (2)	Results by Model b (3)	Extrapolation of Results (4)	Results by Timoshenko (5)	Common Factor (6)
Center Deflection, w_{max}	0.03412	0.04229	0.045	0.0443	pL^4/Et^3
Center Moment, M_{max}	0.04875	0.04793	0.0477	0.0479	pL^2
Shear at Mid-edge, Q_{max}	0.375	0.35	0.342	0.338	pL
Reaction at Mid-edge, V_{max}	0.41	0.42	0.423	0.42	pL
Corner Reaction, R_c	0.0175	0.0448	0.054	0.065	pL^2

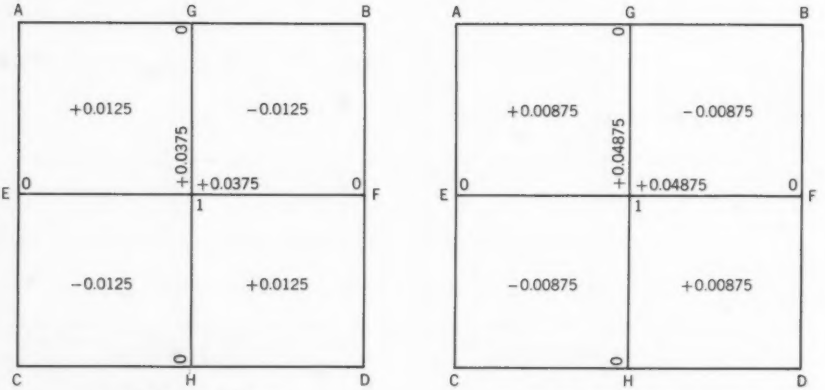

FIG. 10

case of plates with simply supported edges, if results with the same degree of accuracy are desired. For this reason the two plate models a and b shown in Fig. 11, with sides L = 4 λ and L = 6 λ, respectively, are considered.

In model a it is necessary to determine the deflections at points 1, 2, and 3; in model b, at points 1 to 6. Details of the analysis of models a and b are omitted for briefness, but the results are given in Table 3, in columns (2) and (3). These results are extrapolated in column (4), and compared with the exact values of column (5).

TABLE 3.—UNIFORMLY LOADED SQUARE PLATE BUILT-IN ALONG FOUR EDGES, ($\mu = 0.30$)

Item	Results by Model a	Results by Model b	Extrapolation of Results	Results by Timoshenko	Common Factor
(1)	(2)	(3)	(4)	(5)	(6)
Center Deflection, w_{max}	0.01474	0.01429	0.01393	0.0138	$pL^4/(Et^3)$
Center Moment, positive M_{max}	0.02652	0.02457	0.02301	0.02275	pL^2
Mid-edge Moment, negative M_{max}	-0.04445	-0.0482	-0.0512	-0.0513	pL^2

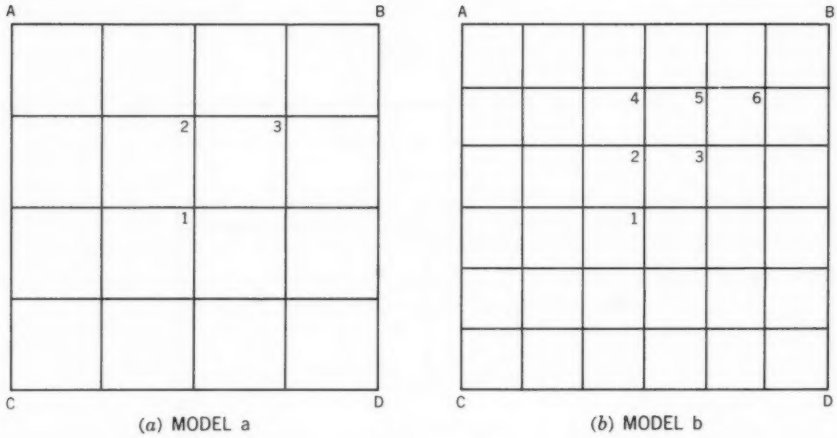

FIG. 11

Comparison of Table 3 columns (4) and (5) shows the outstanding agreement between the values obtained by the suggested procedure and the exact values.

Uniformly Loaded Continuous Plate, Simply Supported Along All Edges and Along Intermediate Supports.—The procedure is also applicable to continuous plates. For examining, the degree of accuracy of the results the plate shown in Fig. 12(a) is analyzed, and only the results of the analysis are presented herein. The plate is simply supported along the edges and also along interme-

TABLE 4.—UNIFORMLY LOADED CONTINUOUS PLATE, SIMPLY SUPPORTED ALONG ALL EDGES AND ALONG INTERMEDIATE SUPPORTS, ($\mu = 0.30$)

Position (1)	Item (2)	Results by Model a (3)	Results by Model b (4)	Extrapolation of Results (5)	Common Factor (6)
Center of Middle Span, (point 1)	Deflection, w_1	0.001525	0.0018	0.001433	pL^4/N
	Moment, M_{1x}	0.0451	0.0363	0.0334	pL^2
	Moment, M_{1y}	0.0302	0.0248	0.023	pL^2
Middle of Intermediate Support (point 3)	Moment, M_{3x}	-0.0426	-0.0672	-0.0754	pL^2
	Moment, M_{3y}	-0.01278	-0.02016	-0.02262	pL^2
Center of Side Span (point 5)	Deflection, w_5	0.002325	0.00282	0.002985	pL^4/N
	Moment, M_{5x}	0.047	0.0417	0.0399	pL^2
	Moment, M_{5y}	0.0395	0.0361	0.035	pL^2

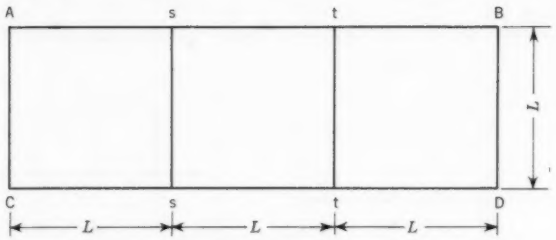

(*a*) PLATE

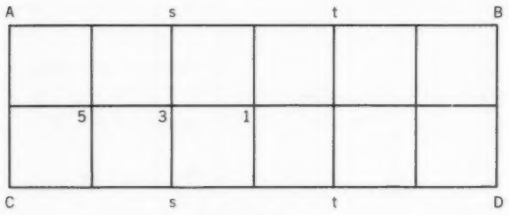

(*b*) MODEL a

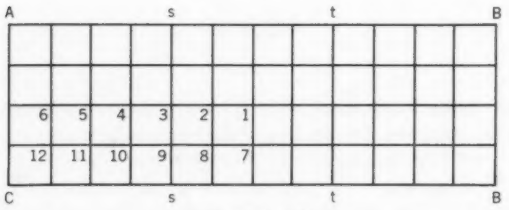

(*c*) MODEL b

FIG. 12

diate supports ss and tt, forming three square spans of length L. For a uniform loading, only one quarter of the plate need to be considered in view of symmetry. Two models a and b in which $L = 2\lambda$ and $L = 4\lambda$ as shown in Figs. 12(b) and 12(c) are analyzed. In model a the deflections at point 1 and 5 are the only two unknowns. In model b, the deflections at ten points must be determined. The deflection at points 3 and 9 on support ss is zero. The load-deflection equations in both cases can be readily determined by use of Table 1 as previously described.

The moments and deflections at the center of the middle span (point 1), at the middle of the intermediate support (point 3), and at the center of the side span (point 5) as obtained by analysis of models a and b are summarized and extrapolated in Table 4. The moment at the middle of the intermediate support is $-0.0754\ p\ L^2$. The magnitude of the same moment as given by Timoshenko[10] is $-0.0763\ p\ L^2$. The two values are in good agreement.

PLATES WITH FREE EDGES

Boundary Conditions.—It was shown in the general solution of plates supported on all edges that the effect of Poisson's ratio can be disregarded in determining the elastic surface of the plate model. This is, however, not possible in case of plates with free edges, because the boundary conditions are somewhat more involved. For example at a free edge extending in the x-direction, the boundary conditions are

$$M_y = 0 \quad \ldots\ldots\ldots\ldots\ldots\ldots (21a)$$

and

$$V_y = 0 \quad \ldots\ldots\ldots\ldots\ldots\ldots (21b)$$

in which M_y and V_y are as given by Eqs. 10 and 12(d). If the general procedure is followed, the moment M_y' is zero and the plate moment M_y will not vanish at the free edge, resulting in residual moments $\mu\, M_x'$. But if the procedure is modified, by adding the couples

$$M_y' = -\,\mu\, M_x' \quad \ldots\ldots\ldots\ldots\ldots\ldots (22)$$

at the free edge, then boundary condition (Eq. 21(a)) is satisfied. In this case

$$M_x = \left(1 - \mu^2\right) M_x' \quad \ldots\ldots\ldots\ldots\ldots\ldots (23)$$

Similarly, if the effect of Poisson's ratio is disregarded until the deflection surface is determined, residual reactive forces of magnitude $\mu \left[\frac{\partial M_{xy}'}{\partial x}\right]$ will arise at the free edge of the plate. Hence reactive forces of magnitude

---

10 "Theory of Plates and Shells," by S. Timoshenko, McGraw-Hill Book Co., Inc., New York, 1940, pp. 234–237.

$$V''_y = -\mu \left[\frac{\partial M'_{xy}}{\partial x}\right] \quad \ldots\ldots\ldots\ldots\ldots\ldots (24)$$

must be added at the free edge in order to annul these residuals.

In the analysis of the model, the couples M'_y produce additional moments in the y-beams, which can be readily determined by use of carry-over factors of Fig. 5. These moments, in turn, require additional holding forces R'_y at the intersection points. The reactive forces V''_y also require additional holding forces R''_y at points on the free edge only, which may be evaluated from the relation

$$R''_y = -\mu\lambda \left[\frac{\partial M'_{xy}}{\partial x}\right] \quad \ldots\ldots\ldots\ldots\ldots\ldots (25)$$

Similar conclusions are made by consideration of a free edge parallel to the y-axis. In this case additional couples

$$M'_x = -\mu M'_y \quad \ldots\ldots\ldots\ldots\ldots\ldots (26a)$$

and additional reactive forces

$$V''_x = -\mu \left[\frac{\partial M'_{xy}}{\partial y}\right] \quad \ldots\ldots\ldots\ldots\ldots\ldots (26b)$$

are applied at the free edge, and the additional holding forces R'_x and R''_x are obtained as previously described.

The holding forces R''_x and R''_y can be conveniently determined by use of the "multi-operator" shown in Fig. 13 in which the coefficients of the twisting moments M'_{xy} are given. The operator in this form is applicable for all points on free edges extending in the direction n-s or w-e, as well as corner points on two free edges. The operator is placed on the model with point o on the edge point, and parts of the operator lying outside the model are disregarded.

Uniformly Loaded Rectangular Plate Simply Supported on Three Edges, the Fourth Edge Free.—Consider a rectangular plate, sides L and L_1, with one edge L free, the other edges simply supported. And let the ratio $L/L_1 = 2$, and $\mu = 0.30$.

Fig. 14 shows two models a and b of the plate, in which $L = 2\lambda$ and $L = 4\lambda$, respectively. Fig. 15 shows the moments and the holding forces in model a produced by a unit deflection at intersection point 1. In Fig. 15(a) the moments in the edge beam AB are given in line (1) as obtained from Table 1, case 1d. The zero moments in y-beam 1-E are written in column (1). In column (2) the additional couple $M'_y = -0.30 \frac{3N}{\mu^2} = -0.90 \frac{N}{\lambda^2}$ at point 1 and zero at point E is given. The total moments are given in column (3). In Fig. 15(b) the holding force at point 1 is computed as usual in lines (1), (2), and (3). In line (4), the additional holding force R'_y is given. In line (5), the additional hold-

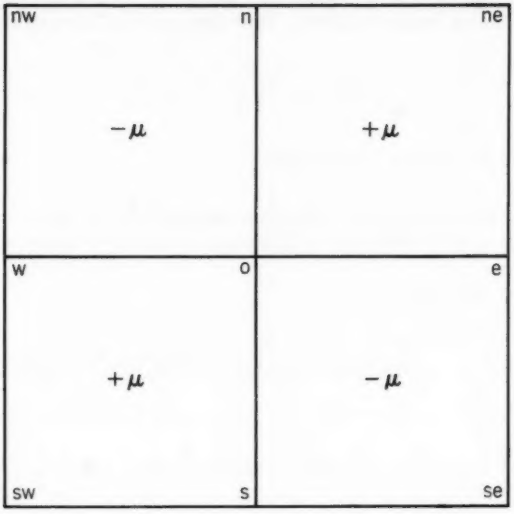

FIG. 13

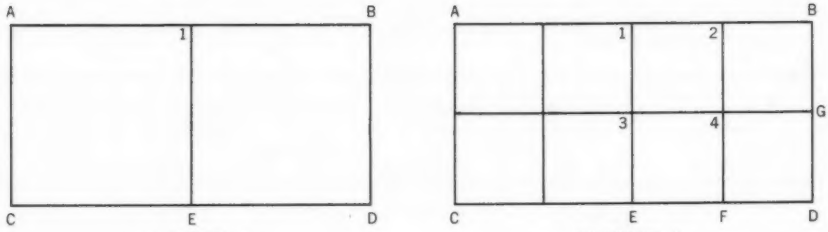

(*a*) MODEL a (*b*) MODEL b

FIG. 14

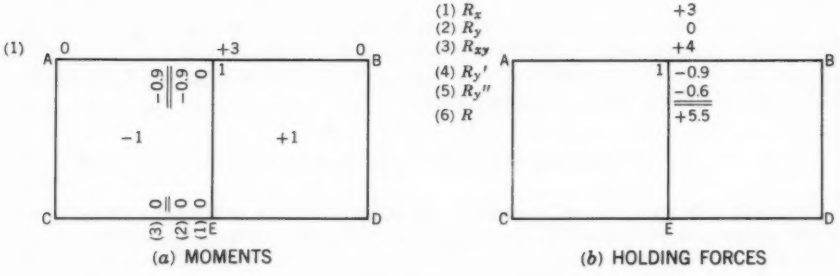

(*a*) MOMENTS (*b*) HOLDING FORCES

FIG. 15

ing force R_y'' by use of the operator of Fig. 13 is presented. In line (6) the sum of these forces is determined. Now the load-deflection equation (Eq. 14) gives

$$5.5\ w_1 \frac{N}{\lambda^2} = 0.5\ p\lambda^2 \quad \ldots\ldots\ldots\ldots\ldots\ldots (27a)$$

from which the deflection of the plate

$$w_1 = p\frac{\lambda^4}{11\ N} = \frac{p\ L^4}{176\ N} = 0.062\ \frac{p\ L^4}{E\ t^3}, \quad \ldots\ldots\ldots\ldots\ldots\ldots (27b)$$

and the bending moment

$$M'_{1x} = 3\ w_1 \frac{N}{\lambda^2} = 0.06818\ p\ L^2, \quad \ldots\ldots\ldots\ldots (27c)$$

from which

$$M_{1x} = (1 - 0.09)\ 0.06818\ p\ L^2 = 0.062\ p\ L^2 \ldots\ldots\ldots (27d)$$

In model b the deflection at four points only must be determined in view of symmetry. The analysis of the model is omitted. In Table 5 the maximum deflection and bending moment (at point 1) as obtained by analysis of models a and b are given, extrapolated and compared with the results given by Timoshenko.[11] Comparison of the values given in columns (4) and (5) of the table shows the outstanding agreement between the results as obtained by analysis of the plate models and by Timoshenko.

TABLE 5.—UNIFORMLY LOADED RECTANGULAR PLATE SIMPLY SUPPORTED ALONG THREE EDGES, THE FOURTH EDGE FREE ($L/L_1 = 2$, $\mu = 0.30$)

Item	Results by Model a	Results by Model b	Extrapolation of Results	Results by Timoshenko	Common Factor
(1)	(2)	(3)	(4)	(5)	(6)
Maximum Deflection, w_1	0.062	0.0737	0.0776	0.0775	pL^4/Et^3
Maximum Bending Moment, M_{1x}	0.062	0.0603	0.0597	0.060	pL^2

ELASTICALLY SUPPORTED PLATES

Boundary Conditions.—Consider a rectangular plate in which one or more of its edges are supported by elastic beams, and assume that these beams re-

[11] "Theory of Plates and Shells," by S. Timoshenko, McGraw-Hill Book Co., Inc., New York, 1940, p. 219, Table 28.

sist only bending moments. The boundary conditions at an edge parallel to the x-axis are

$$M_y = 0 \quad \ldots\ldots\ldots\ldots\ldots\ldots\ldots\ldots (28a)$$

and

$$V_y = - p_{bx} \quad \ldots\ldots\ldots\ldots\ldots\ldots\ldots (28b)$$

in which P_{bx} is the reactive force transmitted from the plate to the supporting beam which undergoes the same deflection as the edge of the plate, such that

$$p_{bx} = H\left(\frac{\partial^4 w}{\partial x^4}\right) \quad \ldots\ldots\ldots\ldots\ldots\ldots\ldots (29)$$

in which H is the flexural rigidity of the supporting beam.

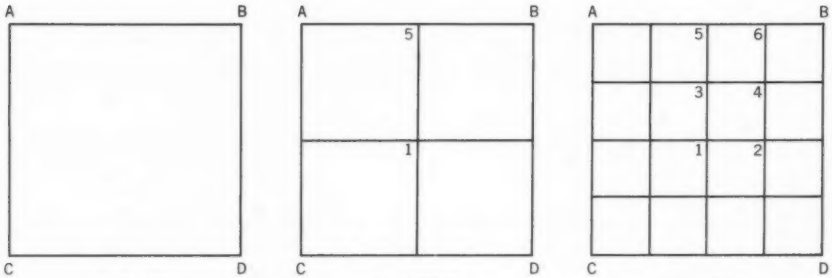

(*a*) PLATE (*b*) MODEL a (*c*) MODEL b

FIG. 16

The conditions given by Eqs. 28 are similar to the boundary conditions at a free edge of the plate Eqs. 21. As explained previously, here again additional couples M'_y (Eq. 22) and additional reactive forces (Eq. 24) must be applied at the edge of the plate model, in order to avoid residuals at the edge of the plate. To find the moments and holding forces consistent with a unit deflection at any intersection point of the model, first the moments and holding forces are obtained as if the edge were free. To the holding forces thus obtained, the forces R_{bx} necessary to hold the supporting beam in its deflected form must be added. These latter forces can be obtained from Table 1 if N in the common factor is replaced by $N_b = H/\lambda$. And to find the supporting beam moments, produced by unit deflections, from the table, N is replaced by H in the common factor.

Uniformly Loaded Square Plate Simply Supported Along Two Opposite Edges and the Other Two Edges Elastically Supported.—Consider the square plate ABCD (Fig. 16(a)), side of length L, simply supported along edges AC and BD, and supported along edges AB and CD by two elastic beams. Let the beams

have flexural rigidity H such that H/(NL) = 2, and μ = 0.30. The plate is uniformly loaded. Figs. 16(b) and 16(c) show two plate models a and b, in which L = 2 λ and L = 4 λ, respectively.

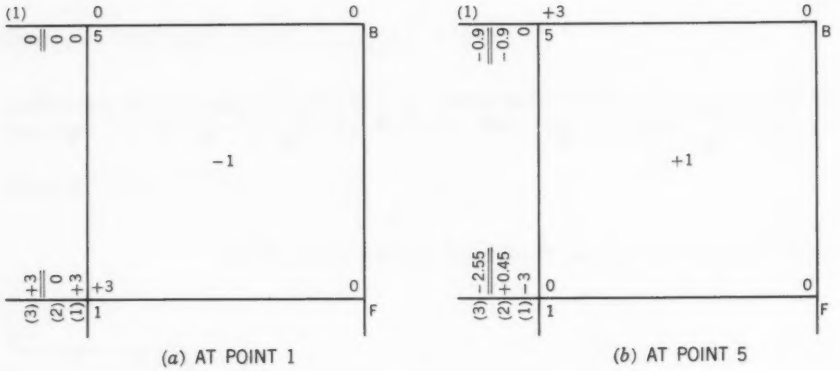

FIG. 17

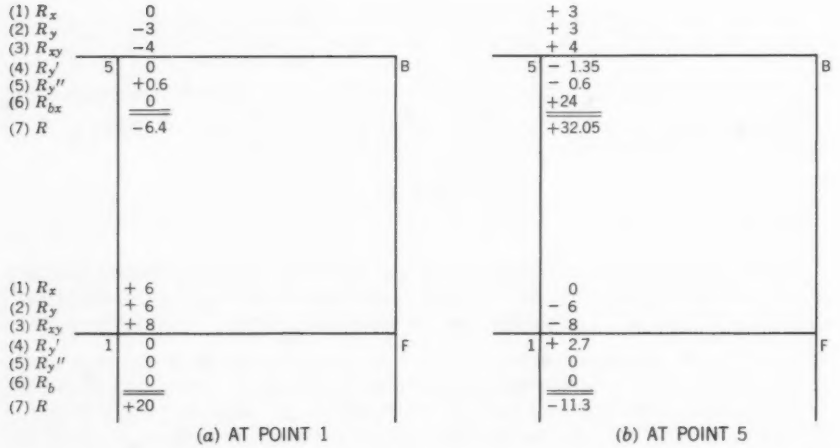

FIG. 18

In model a the deflections at the two points 1 and 5 must be determined. Fig. 17 shows the moments produced in the model by unit deflections at these points, as obtained from Table 1, cases 1c and 1d. The moments are registered in the same order described previously. Fig. 18 shows the holding forces cor-

responding to these unit deflections. The forces given in lines (1) to (5) have the same significance as explained previously. In line (6) the forces R_{bx} which are obtained from Table 1, case 1d, and $N_b = H/\lambda = 2\,H/L = 4\,N$ are written. The holding forces in lines (1) to (6) are added in line (7).

Th load-deflection equations (Eqs. 13(a)) at points 1 and 5 are

$$20\ \ w_1 - 11.3\ \ w_5 = 1\ \ \frac{p\,\lambda^4}{N} \quad \ldots\ldots\ldots\ldots (30a)$$

and

$$-\ 6.4\ w_1 + 32.05\ w_5 = 0.5\ \frac{p\,\lambda^4}{N} \quad \ldots\ldots\ldots\ldots (30b)$$

The solution of these equations give the plate deflections

$$w_1 = 0.066294\ \frac{p\,\lambda^4}{N} = 0.0041434\ \frac{p\,L^4}{N} = 0.04525\ \frac{p\,L^4}{E\,t^3} \quad \ldots\ldots (31a)$$

and

$$w_5 = 0.028839\ \frac{p\,\lambda^4}{N} = 0.0018024\ \frac{p\,L^4}{N} = 0.01968\ \frac{p\,L^4}{E\,t^3} \quad \ldots\ldots (31b)$$

from which the plate model moments are obtained, using Eqs. 15, hence at point 1

$$M'_{1x} = 3\ w_1\ \frac{N}{\lambda^2} = 0.04972\ p\ L^2 \quad \ldots\ldots\ldots\ldots (32a)$$

and

$$M'_{1y} = \left(3\ w_1 - 2.55\ w_5\right)\frac{N}{\lambda^2} = 0.03133\ p\ L^2 \quad \ldots\ldots\ldots (32b)$$

The plate moments are obtained from the model moments by use of Eqs. 9, 10, and 11, hence

$$M_{1x} = 0.05912\ p\ L^2 \quad \ldots\ldots\ldots\ldots\ldots (33a)$$

and

$$M_{1y} = 0.04625\ p\ L^2 \quad \ldots\ldots\ldots\ldots\ldots (33b)$$

Analysis of model b is made in the same way, and deflections at points 1 to 6 are determined. The analysis however is omitted for briefness, but the results are given herein. Table 6 contains the results as obtained by analysis of models a and b and extrapolation of these results, as well as the results computed by the writer from the general solution given by Timoshenko.[12] The agree-

12 "Theory of Plates and Shells," by S. Timoshenko, McGraw-Hill Book Co., Inc., New York, 1940, Article 43, Eqs. (f), (g), (h), on p. 221; Article 29, Eqs. of M_x and M_y on p. 130.

TABLE 6.—UNIFORMLY LOADED SQUARE PLATE SIMPLY SUPPORTED ALONG TWO OPPOSITE EDGES AND ELASTICALLY SUPPORTED ALONG THE OTHER TWO EDGES ($\mu = 0.30$)

Item (1)	Results by Model a (2)	Results by Model b (3)	Extrapolation of Results (4)	Results by Timoshenko (5)	Common Factor (6)
Center Deflection, w_1	0.04525	0.05523	0.05856	0.05893	pL^4/Et^3
Center Moment, M_{1x}	0.05912	0.05827	0.05799	0.05814	pL^2
Center Moment, M_{1y}	0.04625	0.04514	0.04477	0.04501	pL^2

ment between the results in columns (4) and (5) of Table 6 shows the high degree of accuracy of the results as obtained by the presented procedure.

COMPARISON OF ACCURACY

For comparison of accuracy of the results obtained by use of the plate model, complete analysis by the first order finite difference procedure was made in the case of three of the previously analyzed plates, namely:

(a) Uniformly loaded square plate, simply supported along four edges;
(b) Uniformly loaded square plate, built-in along four edges; and
(c) Uniformly loaded rectangular plate, simply supported along three edges, the fourth edge free.

Table 7 shows the exact values and the percentage error in the extrapolated results as obtained by both procedures. It is noted from column (9) of the table that, with exception of the center deflection of the simply supported square plate, the deflections and moments have a higher degree of accuracy when obtained by analysis of the plate model. In this exceptional case, however, the error is only 1.58%. In case of the square plate built-in along the four edges, although the number of simultaneous equations involved in the solution by the plate model is less than in the solution by the finite difference procedure, the obtained deflection and moments are more accurate by analysis of the plate model.

Comparison is also made herein between the results as obtained by analysis of the plate model and by grid analogy[13] presented by Walter W. Ewell, F. ASCE, Shigeo Okubo, and Joel I. Abrams, A. M. ASCE. In case of a square plate built-in along the four edges and uniformly loaded, the deflection of the grid joint nearest to the center of the plate in a grid with 9 by 9 divisions is approximately 2.7% in error. The analysis involves the solution of ten simul-

13 "Deflections in Gridworks and Slabs," by Walter W. Ewell, Shigeo Okubo, and Joel I. Abrams, Transactions, ASCE, Vol. 117, 1952, Table 3, p. 887.

TABLE 7.—COMPARISON OF ACCURACY OF RESULTS OBTAINED BY ANALYSIS OF PLATE MODEL AND BY FIRST ORDER FINITE DIFFERENCE PROCEDURE

Item and Procedure	Results				Extrapolation of Results	"Exact" Values	Common Factor	Error Percent
	L = 2λ	L = 4λ	L = 6λ	L = 8λ				
(1)	(2)	(3)	(4)	(5)	(6)	(7)	(8)	(9)
(A) Uniformly Loaded Square Plate Simply Supported Along Four Edges ($\mu = 0.30$)								
Center Deflection,								
Plate Model	0.03412	0.04229	—	—	0.045	0.0443	$\frac{pL^4}{Et^3}$	1.58
Finite Difference	0.04266	0.04389	—	—	0.0443	0.0443		—
Center Moment,								
Plate Model	0.04875	0.04793	—	—	0.0477	0.0479	pL^2	0.42
Finite Difference	0.04063	0.04557	—	—	0.0472	0.0479		1.46
(B) Uniformly Loaded Square Plate Built-in Along Four Edges ($\mu = 0.30$)								
Center Deflection,								
Plate Model	—	0.01474	0.01429	—	0.01393	0.01376	$\frac{pL^4}{Et^3}$	1.24
Finite Difference	—	0.01966	—	0.01565	0.01428	0.01376		3.78
Center Moment,								
Plate Model	—	0.02652	0.02457	—	0.02301	0.02275	pL^2	1.14
Finite Difference	—	0.02465	—	0.02363	0.02329	0.02275		2.37
Mid-edge Moment,								
Plate Model	—	-0.04455	-0.0482	—	-0.0512	-0.0513	pL^2	0.2
Finite Difference	—	-0.0386	—	-0.0475	-0.0505	-0.0513		1.56
(C) Uniformly Loaded Rectangular Plate Simply Supported Along Three Edges, the Fourth Edge Free ($\mu = 0.30$)								
Max. Deflection,								
Plate Model	0.062	0.0737	—	—	0.0776	0.0775	$\frac{pL^4}{Et^3}$	0.13
Finite Difference	0.0739	0.0763	—	—	0.0771	0.0775		0.52
Max. Moment,								
Plate Model	0.062	0.0603	—	—	0.0597	0.060	pL^2	0.5
Finite Difference	0.0492	0.0567	—	—	0.0592	0.060		1.35

taneous linear equations obtained after a lengthy process of moment and torque distribution. By analysis of the plate model, the error in the extrapolated value

of the center deflection is only 1.24%. The analysis involves the solution of a set of three and another set of six simultaneous linear equations.

CONCLUSIONS

The results of analysis of the structural plate model presented herein for the purpose of solving problems of laterally loaded rectangular plates justify the following conclusions:

(1) The procedure is general. It is applicable in cases of plates with simply supported, built-in, free, and elastically supported edges, as well as continuous plates. Plates with point supports, though not considered in the investigation, can be conveniently handled by the same procedure.

(2) The procedure is simple. It is only necessary to replace the plate by a structural model with a small number of intersection points. For example, it is sufficient to divide a uniformly loaded square plate, with edge conditions other than built-in, into 2 by 2 and 4 by 4 divisions and extrapolate the results. In case the edges are built-in, it is recommended to choose more divisions, for example, models with 4 by 4 and 6 by 6 divisions, in order to describe the elastic surface of the plate with enough accuracy. The number of simultaneous equations involved in the solution are thus reduced to a minimum, and answers are obtained in a short time.

(3) The procedure yields results with a high degree of accuracy. In the problems solved herein, errors as low as 0.13% and 0.2% are obtained, and the highest error is 1.58%. Results of analysis by use of the structural model are more accurate than those obtained by the finite difference method. Investigation of the built-in square plate justifies the same conclusion, although the number of divisions in the analysis of the structural model is smaller than in the solution by finite differences.

(4) The procedure can be extended for use by means of analogies in many problems in elasticity, such as boundary value problems which are governed by Laplace's or Poisson's equations, as well as plane stress and plane strain problems usually solved by introduction of a stress function.

Journal of the
STRUCTURAL DIVISION
Proceedings of the American Society of Civil Engineers

FURTHER STUDIES OF THE STRENGTH OF BEAM-COLUMNS

By Robert L. Ketter,[1] A.M. ASCE

SYNOPSIS

To afford a larger number of "exact solutions" for comparison with approximate interaction curve expressions, this paper presents the results of a continuing investigation of the ultimate carrying capacity of beam-columns. Two basically different loading conditions have been examined, and the results have been presented in interaction curve form.

The first of the assumed loading conditions is that of a column subjected to an axial thrust and end moments M_0 and βM_0. The values of β that have been considered are +1.0, +0.5, 0, -0.5 and -1.0. The maximum strengths of columns subjected to lateral loads applied at their center-line sections have also been determined.

In all cases it has been assumed that the member is an "as-rolled" wide-flange shape that is subjected to bending moments in the plane of its web. It has further been assumed that the member is constrained to deform only in the plane of the web. Failure is therefore characterized by "excessive bending" in the plane of the applied moments.

For the case in which the imposed moments result in a double curvature type of deformation, the possibility of "unwinding" and thereby failing in a

Note.—Discussion open until January 1, 1962. To extend the closing date one month, a written request must be filed with the Executive Secretary, ASCE. This paper is part of the copyrighted Journal of the Structural Division, Proceedings of the American Society of Civil Engineers, Vol. 87, No. ST 6, August, 1961.

[1] Prof. and Chmn., Dept. of Civ. Engrg., Univ. of Buffalo, Buffalo, N. Y.

single curvature mode exists. A method for the examination of this situation is discussed and the presented interaction curves include this possibility.

INTRODUCTION

A structural member subjected to an axial thrust plus an increasing magnitude of bending moment, due either to end-moments or lateral loads, will in the initial stage resist the imposed loading in a purely elastic manner. However, a certain magnitude of these loads, which corresponds to initial yielding, will be reached. Thereafter, the deformational response of the member increases at an ever-increasing rate. The maximum carrying capacity is reached when the member continues to deform at no increase in applied loading.

Analytical solutions to the problem of determining the strength of such members have, in the strictest sense, followed one of two approaches. The

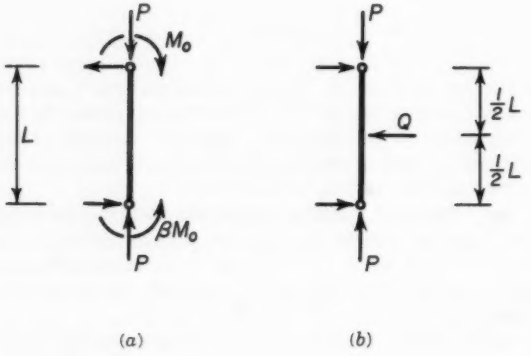

FIG. 1.—CONDITIONS OF LOADING

first of these is based on the reasoning that a lower bound to the actual collapse load can be realized by using the elastic limit value. Since the mathematics of obtaining such a solution are straightforward, there is much to recommend this procedure. However, certain fundamental objections to such an approach exist. First, the exact amount of the reserve in strength above the predicted proportional limit load is a variable, unknown quantity. Second, most "as-rolled" and all "as-welded" members contain residual stresses. These initial stresses may have large maximum values, and the assumption of an abnormally low value for the range of proportionality would therefore be required. For that case in which the maximum "locked-in" stress equals the yield stress (a condition that can exist in certain built-up, welded members), the strict elastic limit solution would predict a zero carrying capacity, since the member has theoretically "failed" prior to load application.

The second method of solution requires the determination of the actual load-deformational response of the member to an imposed, increasing loading system. Curvature values, which in the inelastic range depend on both the magnitudes of the axial thrust and the bending moment at the section in question,[2] are graphically or numerically integrated to define the true deflected shape. The bending moments, however, depend on these deflections. A trial-and-error procedure starting from a known moment-curvature relationship and an assumed deflection is therefore usually required.[3] This general approach, originally proposed by T. von Karmán, Hon. M. ASCE, has much in its favor, since the true problem is considered. It should be noted, however, that solutions by this method are time consuming.

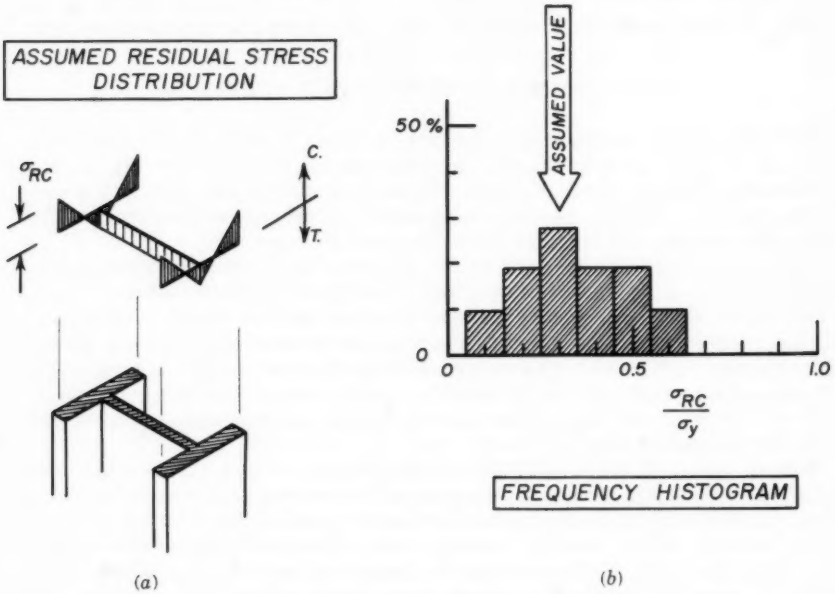

FIG. 2.—ASSUMED RESIDUAL STRESS PATTERN

To facilitate the work of the designer and specification writer, considerable attention during the past decade has been focused on the development of ap-

2 "Plastic Deformation of Wide-Flange Beam-Columns," by R. L. Ketter, E. L. Kaminsky, and L. S. Beedle, Transactions, ASCE, Vol. 120, 1955, p. 1028.

3 "Columns Under Combined Bending and Thrust," by T. V. Galambos and R. L. Ketter, Proceedings, ASCE, Vol. 85, No. EM 2, April, 1959.

proximate "interaction equations."[4,5,6,7,8] In general these have been obtained by fitting "acceptable types of curves" to available test results. Comparisons were also made against the few "exact solutions" that were available.

The purpose of this paper is to present the results of additional computations of "exact solutions" of ultimate carrying capacity and thereby afford a more complete spectrum against which proposed, approximate, interaction equations can be compared. Two basically different types of loading condition have been studied and these are shown diagrammatically in Fig. 1. In Fig. 1(a), a column of length L is presumed to be subjected to an axial thrust, P, and end moments, M_o at the upper end and βM_o at the lower end. The values of β that have been considered are +1.0, +0.5, 0, -0.5 and -1.0 in which β producing a single curvature type of deformation is considered positive. (The interaction curves for the cases β = +1.0 and 0 are reproduced from another publication.[3]) The maximum strengths of columns subjected to lateral loads applied at their center-line sections (Fig. 1(b)) have also been determined.

DEVELOPMENT OF INTERACTION CURVES

The wide-flange cross-sectional shape is to be considered throughout this study. It is assumed that bending moments are applied about the major axis of this cross-section and that deformations occur only in the plane of the web of the member. Failure, as considered herein, is therefore characterized by "excessive bending" in the plane of the applied moments.

The stress-strain properties of the material are presumed to be ideally elastic-plastic; that is, there is initially a linear range where stress is proportional to strain, followed by a region of constant yield stress. The cross-section in question is assumed to contain the symmetrical residual stress pattern shown in Fig. 2(a). The maximum compressive residual stress, σ_{RC}, has been chosen equal to $0.3\sigma_y$, in which σ_y is the yield stress of the material. This is consistent with measured values of cooling residual stresses as shown in the histogram[9] of Fig. 2(b).

Having assumed the magnitude and distribution of the residual stress and the stress-strain properties of the material, it is now possible to define for a given cross-sectional shape the basic relationships that exist in the inelastic range between thrust, bending moment, and curvature. This was done elsewhere[2] for the 8 WF 31 shape and those relationships will be assumed in this study. It should be noted that the P-M-ϕ relationships assume that the full

4 "Strength Analysis of Eccentrically-Loaded Columns," by F. R. Shanley, Report 54-57, Dept. of Engrg., Univ. of California, May, 1954.

5 "Lateral Buckling of Eccentrically Loaded I- and H- Section Columns," by H. N. Hill and J. W. Clark, Proceedings, First Natl. Congress of Applied Mechanics, ASME, 1951, p. 407.

6 "Recherches sur le Flambement de colonnes en acier A 37, a profil en double Te, sollicitees obliquement," by F. Campus and C. Massonnet, Comptes Rendus de Recherches, IRSIA, April, 1956.

7 "The Stanchion Problem in Framed Structures Designed According to Ultimeate Carrying Capacity," by M. R. Horne, Proceedings, Institution of Civ. Engrs., Part III, Vol. 5, No. 1, April, 1956, p. 105.

8 "Guide to Design Criteria for Metal Compression Members," Column Research Council of Engrg. Foundation, Ann Arbor, Mich., 1960.

9 "The Influence of Residual Stress on the Strength of Structural Members," by R. L. Ketter, Proceedings, Seventh Tech. Session, Column Research Council, 1957.

magnitude of the axial thrust is first applied and while it is held constant, bending moments are increased to their maximum valves. A definite loading history is therefore prescribed.

Elastic Limit Solution.—For completeness and for future comparisons, it is desirable to include at this stage, before discussion of the development of the ultimate strength curves, the elastic limit solutions for the first of the two loading conditions shown in Fig. 1. In Appendix I, it is shown that for the case where no residual stresses are present, the following algebraic interaction relationship exists:

$$\frac{P}{P_y} + \frac{M_o}{M_y}\ (\zeta) = 1.0 \quad \ldots\ldots\ldots\ldots\ldots\ldots\ (1)$$

in which

$$\zeta = \sec \zeta\left(\frac{x}{L}\right) \quad \ldots\ldots\ldots\ldots\ldots\ldots\ (2)$$

$$\beta = \frac{\cos \zeta\left(1 - \frac{x}{L}\right)}{\cos \zeta\left(\frac{x}{L}\right)} \quad \ldots\ldots\ldots\ldots\ldots\ldots\ (3)$$

and

$$\zeta = \pi\sqrt{\frac{P}{P_E}} \quad \ldots\ldots\ldots\ldots\ldots\ldots\ (4)$$

The modifying factor ζ of Eq. 1, as defined by Eqs. 2, 3 and 4, is a function only of the ratios P/P_E and β. The corresponding curves are given in Fig. 3.

To obtain the curves shown in Fig. 3, it is first necessary to determine for given values of P/P_E and β the location of the section of maximum moment (and therefore maximum stress). This is obtained from Eq. 3. Knowing this location; that is, knowing x/L from Eq. 3, the modifying or "amplifying" factor, ζ, is obtained from Eq. 2. If Eq. 3 has no solution in the range $0 \leq x \leq L$, the maximum stress occurs at the end of the member and the amplification factor equals one.

If $M_o = 0$, two possible solutions exist. The first of these follows directly from Eq. 1; the maximum axial thrust, P, equals the yield thrust, P_y. The second possible solution corresponds to that case in which the amplification factor, ζ, approaches infinity. Here, the maximum axial thrust is the Euler buckling load for the pin-ended member.

Ultimate Carrying Capacity Solution.—The method of solution used in the investigation of the ultimate carrying capacity of a given member and loading is the same as that used in another paper.[3] It is essentially as follows: The member is sub-divided into eight equal segments as shown in Fig. 4(a). A constant value of axial thrust is assumed. In addition, a value of the end moment, M_o, is also selected for investigation. Deflection values, based on a consideration of the elastic response of the member to the assumed loading or on information obtained from previous inelastic calculations, are assumed at each of the various division points along the member. Using these, moments at the several points are computed, and from the M-P-ϕ relationship discussed previously, corresponding curvature values are established. If these curvatures are numerically integrated twice, new deflection values are obtained. These will not necessarily be equal to those originally assumed and additional trials may be required.

The previously described process would be repeated for successively increasing values of the end moment. This would make possible the definition of

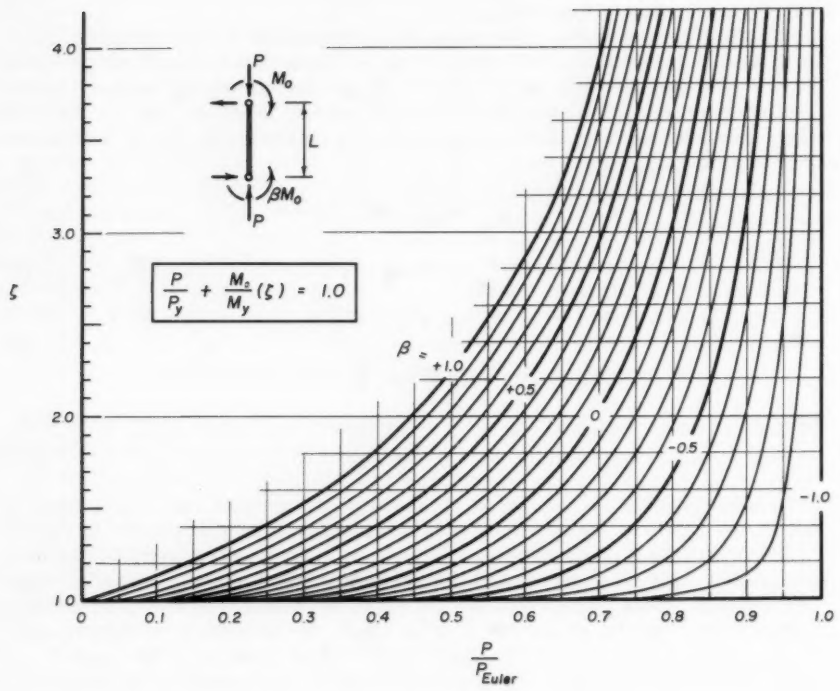

FIG. 3.—ELASTIC LIMIT INTERACTION SOLUTION

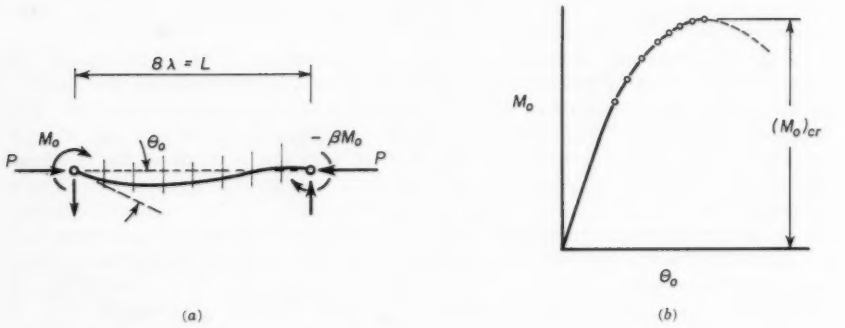

FIG. 4.—METHOD OF SOLUTION USED IN DETERMINING ULTIMATE STRENGTH

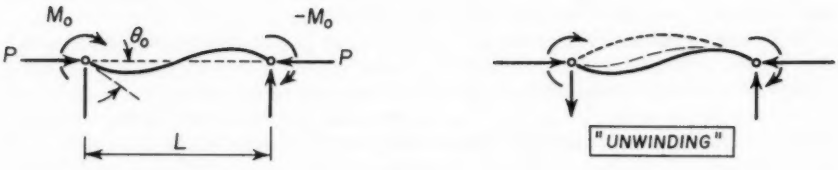

FIG. 5.—DOUBLE CURVATURE LOADING

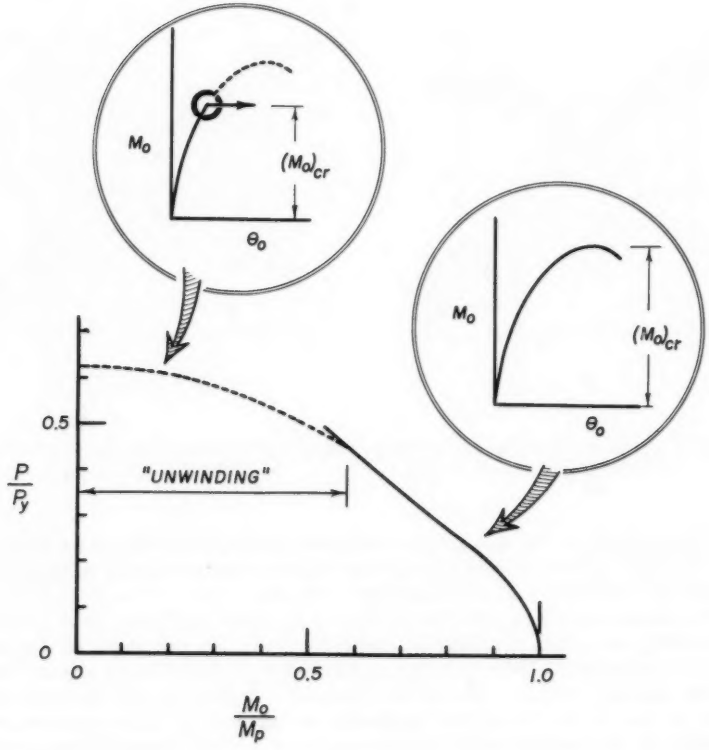

FIG. 6.—BEHAVIOR OF A MEMBER LOADED IN DOUBLE CURVATURE

the load-deformational response of the member; e.g., the relationship between the end-moment and end-slope could be plotted as shown in Fig. 4(b). From this diagram, the ultimate moment (for that particular chosen length of member and assumed axial thrust) would be determined.

The total process described in the preceding paragraph would be repeated for other assumed values of constant axial thrust. For each of these there would be corresponding critical values of the applied end moment. A curve of these solutions could be plotted in which axial thrust would be the ordinate and the ultimate end-bending moment would be the abscissa. Such a curve will be referred to as an "ultimate strength interaction curve" and will be the form for presentation of the results of this study.

With the exception of that particular case for which $\beta = -1.0$ (the double curvature case) the numerical process described previously for solving the ultimate strength problem is stable for all values of end bending moment less than the ultimate. For that particular loading condition, however, the possi-

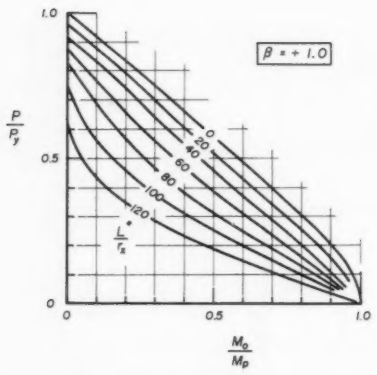

FIG. 7.—ULTIMATE STRENGTH INTERACTION CURVES ($\beta = +1.0$)

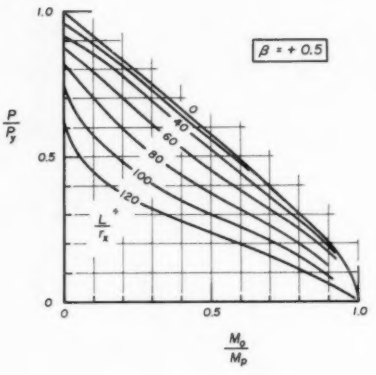

FIG. 8.—ULTIMATE STRENGTH INTERACTION CURVES ($\beta = +0.5$)

bility exists that at certain lesser values of axial thrust or end bending moment, or both, the deflection pattern may degenerate into one of single curvature with the member suddenly "failing" (Fig. 5).

In the elastic range, a solution to the "unwinding" problem can be obtained by examining, at any given stage of applied loading, the response of the member to an infinitesimally small first mode deformational disturbance. For an assumed ideally elastic, pin-ended member, a shift in the location of the section of zero moment and the beginning of "unwinding" will occur when the magnitude of the applied axial thrust reaches the "first mode-Euler buckling load," P_E.

The "real member" in question will not "fail" in the elastic range. For the actual situation in which the member is partially yielded, it is necessary to examine the response of the member to a single curvature type of virtual disturbance at each increasing value of M_O. (This process is described in

detail in Appendix II where sample calculations are given.) In certain ranges, the member will unwind prior to reaching the "double curvature mode—excessive bending—ultimate carrying capacity." This is illustrated in Fig. 6.

The ultimate strength interaction curves for the cases in which the member is subjected to axial thrust plus the combinations of end bending moments discussed earlier are given in Figs. 7 to 11. For that situation where the member is subjected to a centrally applied lateral load in addition to the axial thrust, the solutions are shown in Fig. 12.

In the strictest sense these curves apply only to 8 WF 31 members that contain the residual stress pattern shown in Fig. 2(b). Furthermore, the yield point of the material was assumed to be 33 kips per sq in. With regard to the first of these restrictive conditions, it may be said that the 8 WF 31 has one of the lowest of the shape factors. It would therefore be expected that strength predictions on the basis of these solutions should be conservative. For members having material properties essentially the same as those of the ideally

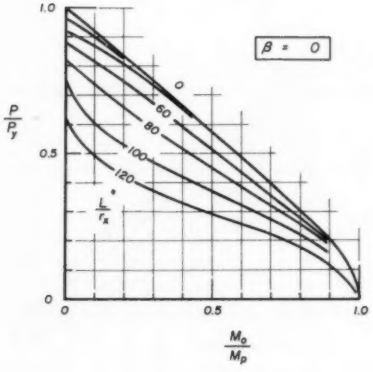

FIG. 9.—ULTIMATE STRENGTH INTERACTION CURVES ($\beta = 0$)

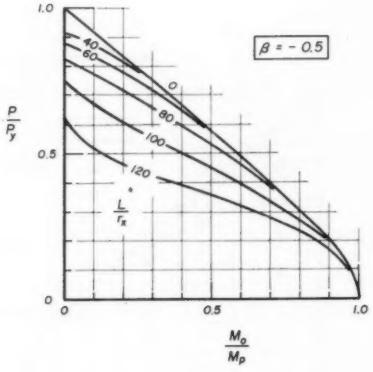

FIG. 10.—ULTIMATE STRENGTH INTERACTION CURVES ($\beta = -0.5$)

elastic-plastic type, but having a yield strength other than 33 kips per sq in., the slenderness ratio will need to be modified to allow the use of these charts. A modification according to Eq. 5 is considered to be adequate.

$$\left(\frac{L}{r}\right)_{\text{Adjusted}} = \left(\frac{L}{r}\right)_{\text{Actual}} \sqrt{\frac{(\sigma_y)_{\text{Actual}}}{33}} \quad \ldots\ldots\ldots (5)$$

COMMENT

It is not the intent of this paper to justify the adequacy of the numerical integration procedure. Therefore, no comparisons with test results will be

given. It should be noted, however, that such studies have been made[3,10,11] for the cases $\beta = +1.0$ and 0.

Another publication[12] discusses the various approximate interaction expressions that have been and are now being considered. For the case where $\beta = +1.0$, two general forms are listed:[5,6,8]

$$\frac{P}{P_{ult}} + \frac{\left(\frac{M_o}{M_{ult}}\right)}{\left(1 - \frac{P}{P_E}\right)} = 1.0 \quad \ldots\ldots\ldots\ldots\ldots\ldots (6)$$

and[3,11,13]

$$\frac{P}{P_y}\left[\alpha_1 + \alpha_2\left(\frac{P}{P_y}\right)\right] + \left(\frac{M_o}{M_{ult}}\right) = 1.0 \quad \ldots\ldots\ldots\ldots (7)$$

As shown elsewhere,[10] either of these expressions adequately represents the "exact solution."

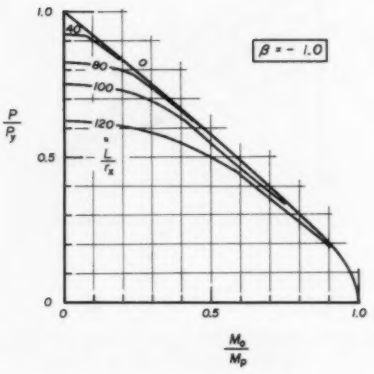

FIG. 11.—ULTIMATE STRENGTH INTERACTION CURVES ($\beta = -1.0$)

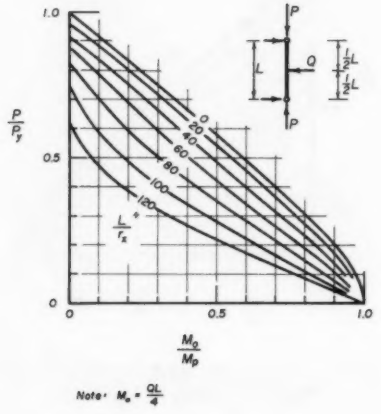

FIG. 12.—ULTIMATE STRENGTH INTERACTION CURVES (CONCENTRATED LATERAL LOAD)

For $\beta \neq 1.0$, it has been suggested that an "equivalent uniform moment factor" be defined. Based on lateral buckling considerations, C. E. Massonnet, F. ASCE, has suggested, for the case in which maximum moment occurs within the span, the expression given as

10 "Stability Considerations in the Design of Steel Columns," by C. Massonnet, Proceedings, ASCE, Vol. 85, No. ST 7, September, 1959.

11 "ASCE-WRC Commentary on Plastic Design - Compression Members," Proceedings, ASCE, Vol. 86, No. EM 1, January, 1960.

12 "Guide to Design Criteria for Metal Compression Members," Column Research Council of Engrg. Foundation, Ann Arbor, Mich., Chapter 5.

13 "Plastic Design in Steel," A.I.S.C., New York, N. Y., 1959.

$$M_{Equivalent} = M_o \sqrt{0.3\left(1 + \beta^2\right) + 0.4\,\beta} \quad \ldots\ldots\ldots (8)$$

G. Winter, F. ASCE, has recommended[8] the substitution of 0.29 and 0.42 in place of 0.3 and 0.4, respectively, in Eq. 8. Horne, using a somewhat different approach has obtained[7] results similar to Massonnet's.

For the β values considered herein, Table 1 gives[14] the modification factors that correspond to each of the studies referred to previously.

For the case in which the maximum moment occurs at the end of the member, Massonnet[10] has suggested the following second, limiting, interaction relationship:

$$\frac{M_o}{M_p} = (1.18)\left(1 - \frac{P}{P_y}\right) \quad \ldots\ldots\ldots\ldots (9)$$

It should be noted that a double standard has therefore been proposed, in which the equation predicting the least M_o/M_p is correct for that particular case.

TABLE 1.—MODIFICATION FACTORS

	β				
	+1.0	+0.5	0	-0.5	-1.0
$\frac{M_{Equ}}{M_o}$ (Horne)	1.000	0.762	0.565	0.429	0.391
$\frac{M_{Equ}}{M_o}$ (Massonnet)	1.000	0.759	0.548	0.416	0.447

From the interaction curves of Figs. 7 to 11, it is possible to compute the equivalent bending moment factor for the "as-rolled" 8 WF 31 section constrained to bend in the plane of its web. It should be observed, however, that such comparisons contain four dimensionless parameters instead of the two used by Massonnet and Horne. That is,

$$\frac{M_{Equ}}{M_o} = f\left(\beta, \frac{P}{P_y}, \frac{L}{r}\right) \quad \ldots\ldots\ldots\ldots (10)$$

It is also possible to combine the axial thrust and slenderness terms and thereby obtain a form more easily compared with the elastic solution.

$$\frac{M_{Equ}}{M_o} = g\left(\beta, \frac{P}{P_y}, \frac{P}{P_E}\right) \quad \ldots\ldots\ldots\ldots (11)$$

Three values of P/P_y have been selected for illustration: $P/P_y = 0.2$, 0.4 and 0.6. In Fig. 13 β is plotted as the abscissa, M_{Equ}/M_o as the ordinate, and various P/P_E values as the "cross-curves."

14 "Guide to Design Criteria for Metal Compression Members," Column Research Council of Engrg. Foundation, Ann Arbor, Mich., Table 5.3, p. 80.

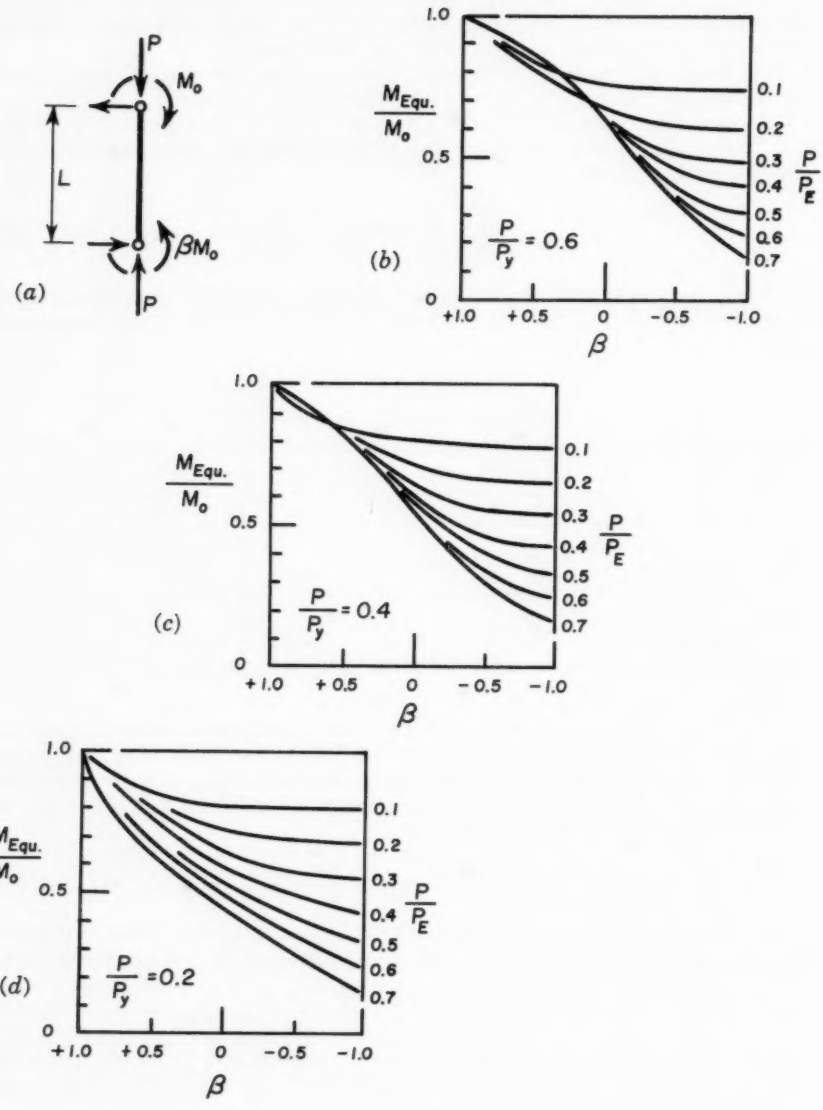

FIG. 13.—EQUIVALENT MOMENT FACTORS

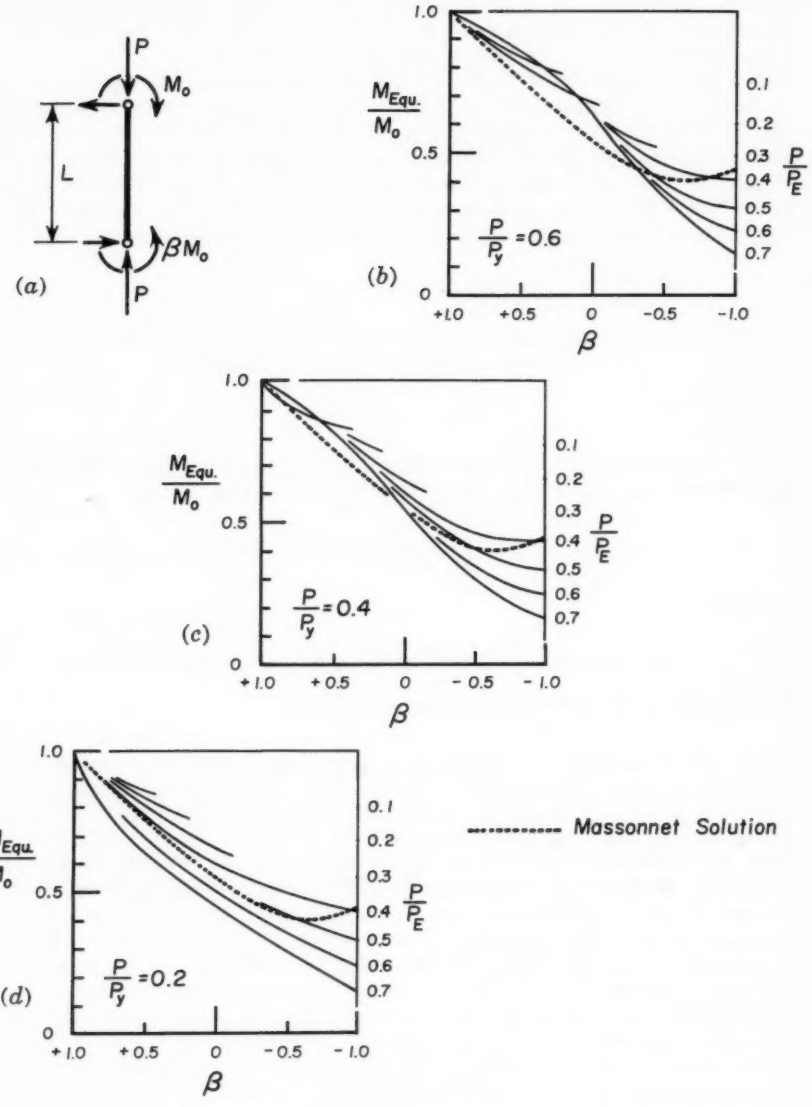

FIG. 14.—COMPARISON OF EQUIVALENT MOMENT FACTORS WITH MASSONNET'S SOLUTION

Probably the most important indication brought out by Fig. 13 is that, if a single standard is required for the full range of definition of the equivalent moment, then the ratio P/P_E is a major factor in determining the equivalent moment expression. It is as significant as the factor β. Of somewhat lesser importance is the influence of P/P_y. It should be noted, however, that as P/P_y becomes larger, its influence is more pronounced.

If a double standard is used, the region of influence of the ratio P/P_E can be reduced. A comparison of Massonnet's equivalent moment expression (Eq. 8) with the values given in Fig. 13 is shown in Fig. 14. Only that range which requires the use of the equivalent moment has been included. That is, for smaller values of P/P_E and β, the strength of a given member as predicted by the Massonnet procedure would be governed by Eq. 9 rather than by Eqs. 6 and 8. This region has been excluded in the comparison.

APPENDIX I.—DETERMINATION OF ELASTIC LIMIT INTERACTION EQUATION (NO RESIDUAL STRESS)

For the member in question (Fig. 15), Timoshenko[15] has shown that the deflection at any section "x" along the length of the member is

$$y = \frac{M_o}{P}\left[\frac{\text{Sin } k(L-x) + \beta \text{ Sin } (k\,x)}{\text{Sin } (k\,L)} - 1 + \left(\frac{x}{L}\right)(1-\beta)\right] \quad \ldots\ldots (12)$$

in which

$$k\,L = \zeta = \pi\sqrt{\frac{P}{P_E}} \quad \ldots\ldots\ldots\ldots\ldots (13)$$

The moment at the corresponding section is then

$$M = M_o\left[\frac{\text{Sin } \zeta\left(1 - \frac{x}{L}\right) + \beta \text{ Sin } \zeta\left(\frac{x}{L}\right)}{\text{Sin } \zeta}\right] \quad \ldots\ldots\ldots (14)$$

Since the maximum stress will be reached at the section of maximum moment, it is first necessary to define the location of the critical section. That is,

$$\frac{\partial M}{\partial x} = \frac{\partial}{\partial x}\left[\text{Sin } \zeta\left(1 - \frac{x}{L}\right) + \beta \text{ Sin } \zeta\left(\frac{x}{L}\right)\right] = 0 \quad \ldots\ldots\ldots (15)$$

which gives

$$\beta = \frac{\text{Cos } \zeta\left(1 - \frac{x}{L}\right)}{\text{Cos } \zeta\left(\frac{x}{L}\right)} \quad \ldots\ldots\ldots\ldots\ldots (16)$$

15 "Theory of Elastic Stability," by S. Timoshenko, New York, N. Y., McGraw-Hill Book Co., 1936, p. 12, Eq. 23.

Substituting Eq. 16 in Eq. 14 gives

$$M_{max} = M_o \left(\sec \zeta \frac{x}{L}\right) \quad \ldots\ldots\ldots\ldots\ldots \quad (17)$$

The interaction relationship is therefore

$$\frac{P}{P_y} + \frac{M_{max}}{M_y} = 1.0 \quad \ldots\ldots\ldots\ldots\ldots \quad (18)$$

or

$$\frac{P}{P_y} + \frac{M_o}{M_y} \left(\sec \zeta \frac{x}{L}\right) = 1.0 \quad \ldots\ldots\ldots\ldots \quad (19)$$

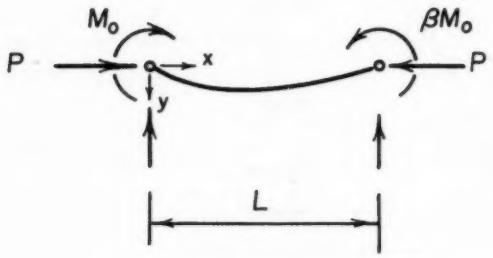

FIG. 15.—GENERAL LOADING CONDITION

APPENDIX II.—INSTABILITY DUE TO "UNWINDING"

The member and loading condition in question is that shown in Fig. 16(b). The problem is to determine that particular value of (M_o/M_y) for which the magnitude of the imposed axial thrust and the amount of yielding is sufficient to allow a shift in the point of zero moment (initially assumed to be at the centerline section).

To solve this problem it will be assumed that at the stage of loading in question the member is subjected to a virtual, deformational disturbance of the single curvature type. The tangent to the moment-curvature relationship for any particular value of moment represents the instantaneous resistance of the member to an increasing moment. Where moments decrease, the full elastic value is effective. At each of the various points along the length of the member, it is therefore possible to define the effective stiffness. With this information, Newmark's procedure for determining the buckling load can be directly applied.[16] "Unwinding" will occur when the critical axial thrust thus computed equals that applied to the member.

16 "Numerical Procedures for Computing Deflections, Moments, and Buckling Loads," Transactions, ASCE, Vol. 108, 1943, p. 1161.

Fig. 17 is an indication of the degree of accuracy obtained. The member in question is the same as that considered in Fig. 16. The end moment is the

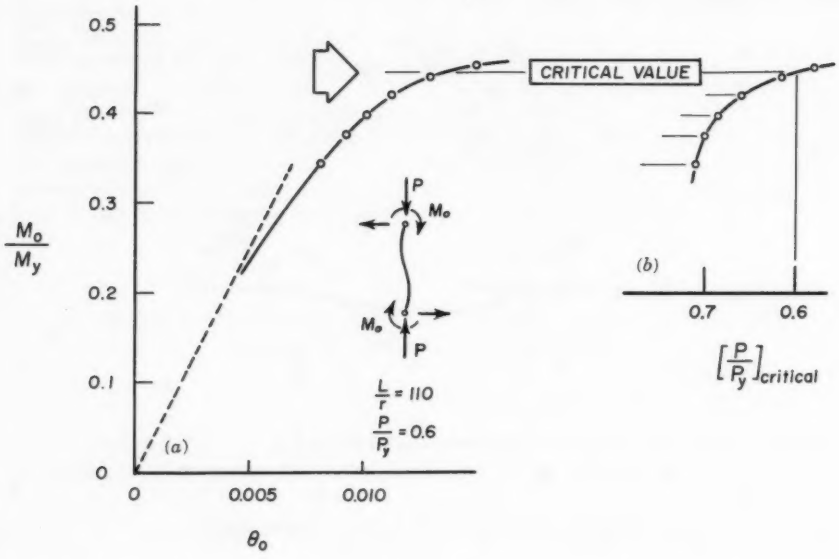

FIG. 16.—DETERMINATION OF THE CRITICAL LOADING ASSOCIATED WITH UNWINDING

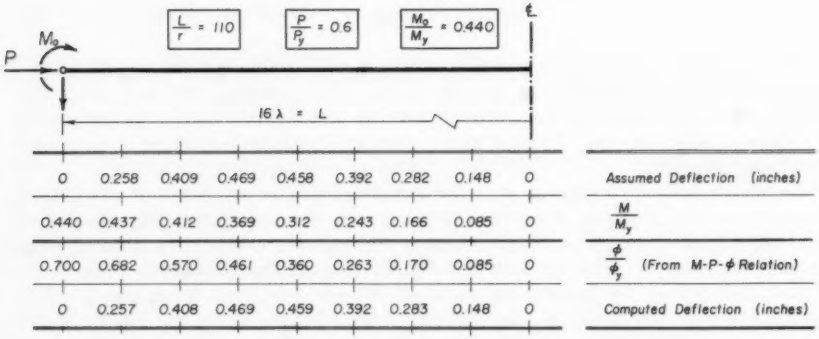

FIG. 17.—INDICATION OF THE DEGREE OF ACCURACY USED IN THE COMPUTATIONS

one closest to that which causes instability. Fig. 18 summarizes the numerical work associated with the calculation of the critical thrust value. For the given

slenderness ratio, the eight division spacing, σ_y = 33 kips per sq in. and E = 30,000 kips per sq in.,

$$\left(\frac{P}{P_y}\right)_{critical} = 57.7 \left(\frac{\text{Assumed Deflection}}{\text{Calculated Deflection}}\right) \quad \ldots\ldots\ldots \quad (20)$$

Therefore, for the member considered:

$$0.612 \leq \left(\frac{P}{P_y}\right)_{critical} \leq 0.617 \quad \ldots\ldots\ldots\ldots \quad (21)$$

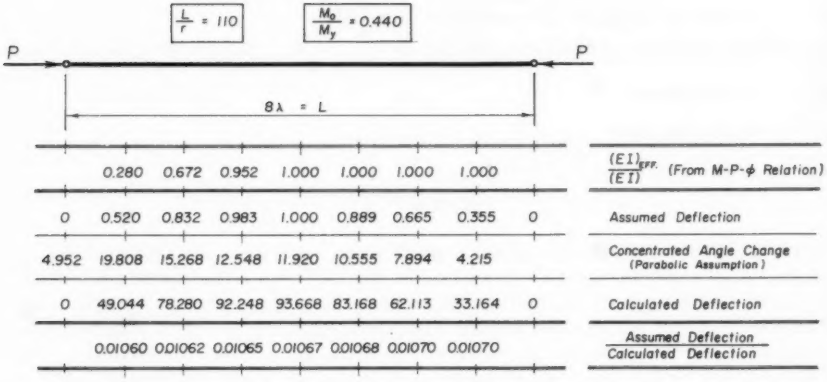

FIG. 18.—SUMMARY OF THE COMPUTATIONS REQUIRED IN THE DETERMINATION OF THE CRITICAL THRUST ASSOCIATED WITH UNWINDING

APPENDIX III.—NOMENCLATURE

The following symbols have been adopted for use in this paper:

- A = area of cross-section;
- E = Young's Modulus of Elasticity;
- I = moment of inertia;
- L = length of member;
- M = bending moment;
- M_o = applied moment at end of member;
- M_p = fully plastic moment under pure moment;
- M_y = initial yield moment under pure moment;
- M_{Equ} = equivalent uniform moment in a beam-column;

P = axial thrust;

P_y = axial load corresponding to compressive yielding stress over entire section;

P_E = Euler buckling load $\left(\frac{\pi^2 E I}{L^2}\right)$;

Q = lateral load;

r = radius of gyration;

r_x = radius of gyration about the strong axis;

α = non-dimensional parameters;

β = ratio of applied end moments (Fig. 1);

θ_o = end rotation;[5]

ϕ = curvature;

σ = stress; and

σ_y = yield stress.

Journal of the
STRUCTURAL DIVISION
Proceedings of the American Society of Civil Engineers

STRENGTH OF PLATE GIRDERS IN BENDING

By Konrad Basler,[1] A.M. ASCE, and Bruno Thürlimann,[2] M. ASCE

FOREWORD

An investigation of welded plate girders was conducted at Lehigh University during the years 1957 to 1960. The objective of this project was to determine the static carrying capacity of transversely stiffened plate girders. The study was grouped into an experimental and a theoretical phase, and the results of the experiments were published as a Welding Research Council Bulletin.

The theoretical considerations are presented as a series of three papers, covering first the bending strength (this paper), then the shear strength (in the October 1961 Journal of the Structural Division), and finally the interaction between bending and shear (in the October 1961 Journal of the Structural Division).

Note.—Discussion open until January 1, 1962. Separate discussions should be submitted for the individual papers in this symposium. To extend the closing date one month, a written request must be filed with the Executive Secretary, ASCE. This paper is part of the copyrighted Journal of the Structural Division, Proceedings of the American Society of Civil Engineers, Vol. 87, No. ST 6, August, 1961.

[1] Consultant, Egg b. Zürich, Switzerland; formerly Res. Asst. Prof., Lehigh Univ., Bethlehem, Pa.

[2] Prof. of Civ. Engrg., Federal Inst. of Tech., Zürich, Switzerland; formerly Res. Prof., Lehigh University, Bethlehem, Pa.

SYNOPSIS

An analysis is presented of the static load-carrying capacity of plate girders subjected to bending. First, the phenomenon of "web buckling" is discussed to explain the discrepancy between actual behavior (1)[3] and theory. Following this is an analysis of the bending strength of plate girders. Finally, an attempt is made to interpret the findings as a design concept.

INTRODUCTION

In the design of plate girders the tendency is to arrange as much material as possible in the extreme fibers. By keeping the web area as small as possible, the lever arm of the internal forces is maximized and with it the carrying capacity. In the past web buckling has been set as a limitation to this tendency towards an optimum utilization of the material. Consequently, considerable effort has been spent in establishing web buckling values (2), (3), (4).

The conventional plate-buckling theory predicts the load intensity under which a plane plate subjected to edge stresses deflects out of its plane. The formulation of the problem is the same as that for a column, and, as a result, the same word "buckling" is used to describe the phenomenon in a plate. Because the computed column-buckling value gives an adequate measure of the strength of a column, it was natural to consider that a web-buckling value is of equal significance. Such an assumption is not true. The strength of a plate can exceed its buckling limit, and this additional margin of strength is termed "postbuckling strength" (5).

[3] Numerals in parentheses refer to corresponding items in Appendix II.

The existence of postbuckling strength has been pointed out ever since buckling values were computed, and, as a consequence, a somewhat smaller factor of safety was applied to web buckling than that used for primary column buckling. What should be the value of this factor of safety? In order to clarify this problem the plate-girder investigation at Lehigh University (Bethlehem, Pa.) was started.

The experiments (1) demonstrated that the concept of expressing the postbuckling strength of a girder as a certain percentage of the web-buckling strength is untenable and should be replaced by a strength prediction which considers the influence of the flanges and transverse stiffeners on the overall carrying capacity. The strength of girders with respect to bending is the subject of this paper.

Notation.—The letter symbols adopted for use in this paper are defined where they first appear, in the illustrations or in the text, and are arranged alphabetically, for convenience of reference, in Appendix III.

WEB BUCKLING

It is the purpose of this section to explain the behavior of a plate when strained beyond the buckling limit.

Phenomenon of Web Buckling.—A rectangular plate subjected to edge thrust is shown in Fig. 1(a). For a given edge-displacement pattern the strain ϵ_a expresses the applied deformation and Y is a nondimensionalized measure of the plate deflection out of its plane at a particular location. Assuming completely elastic behavior of the material, the result of the linear buckling theory that is commonly used can thus be illustrated by Fig. 1(b). The plate remains plane for all positive values of the applied strain ϵ_a (tension), and also for a limited range of negative strains (compression). However, the theory predicts that at a certain critical compressive strain, ϵ_{cr}, the path in this X-Y diagram bifurcates. The plate must then bulge out of its plane. This phenomenon is referred to as plate-buckling and the corresponding load is termed the plate-buckling load or critical load.

The actual behavior differs radically from that predicted by the linear buckling theory because initial plate imperfections are present. With the help of Fig. 1(c) this contradiction will be explained. In Fig. 1(c) the relation between the applied deformation, $X = \epsilon_a/|\epsilon_{cr}|$, and the resulting plate deflection, Y, is again plotted, assuming that the plate has a small initial deflection of the magnitude Y_i as shown for X = 0. Discussing first the upper half of Fig. 1(c), it is clearly seen that only the strain-deflection path of a perfectly plane plate exhibits a bifurcation point of equilibrium, and that the sudden rate of increase of plate deflection disappears with increasing initial deflections. These initial imperfections need not be very large to completely obscure the buckling behavior. The majority of the tests conducted at Fritz Engineering Laboratory on shop fabricated, welded plate girders furnished web-deflection curves of the type shown for $Y_i = 1$ or $Y_i = 0.5$. Webs of riveted girders (6) have, in general, smaller initial distortions and may lead to a path more like the curve for $Y_i = 0.2$. In aluminum girders the relative initial imperfections are even smaller due to the fact that the lower modulus of elasticity requires a sturdier web to furnish the same critical stress as an equivalent steel

girder. Therefore, a more pronounced rate of increase of web deflections can be expected such as indicated (7) by the curve for $Y_i = 0.05$. Curves which come consistently closer to the singular case $Y_i = 0$ seem to be obtainable only in carefully conducted laboratory tests on isolated aluminum plates (8).

The conclusion is that, in general, a web-buckling load cannot be observed on a full scale, shop fabricated plate girder built of steel, because the transition from the pre-buckling into the post-buckling range is not accompanied by a sudden increase in deflection. Thus, concerning the behavior of the web, there appears no reason why the computed web-buckling strain should not be exceeded in a plate girder under working load.

Fig. 1(c) also indicates that, in cases where postbuckling strains are tolerated, an effort to cold straighten the web of a slender girder in the shop would be ineffective since the order of magnitude of the final deflections is almost independent of the initial deflections.

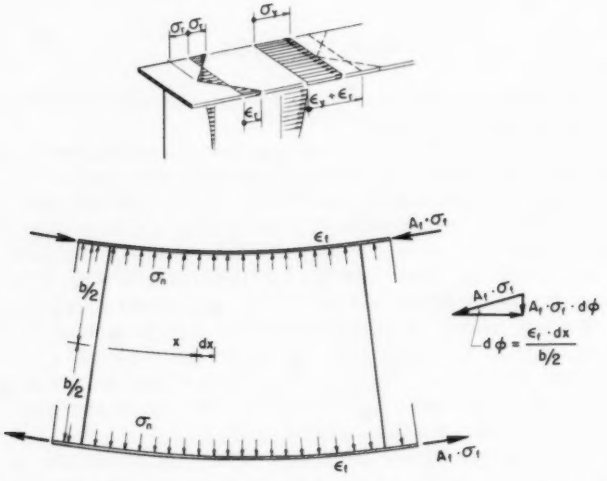

FIG. 1.—PLATE DEFLECTION, Y, VERSUS APPLIED EDGE STRAIN, X

By using von Kármán's nonlinear differential equations for plates (9), several investigators have derived similar plate deflection curves for special cases (10),(11),(12),(13). Fig. 1(c), however, is simply the plot of

$$-Y^2 + Y_i^2 + \frac{Y_i}{Y} = X + 1 \quad \ldots\ldots\ldots\ldots\ldots\ldots (1)$$

in which X is $\epsilon_a/|\epsilon_{cr}|$, a measure of the applied deformation, Y_i represents the initial plate deflection, and Y is the resulting plate deflection. The plate deflections Y_i and Y are nondimensionalized in terms of the plate thickness and a constant which depends on the shape of the deflection. Eq. 1 was derived (14) by assuming that the deflected configuration grows under load without changing its shape and by neglecting the influence of the membrane shear stresses. It

should be further pointed out that the branches resulting in negative values of Y (lower half of Fig. 1 (c)) are also equilibrium positions for the plate under the stated assumptions. If the plate could be brought to a position on the dashed branches which are unstable equilibrium positions, it could then snap to either side of the reference plane and stabilize there. This is the so-called canning effect.

Web Participation under Bending.—Having analyzed the lateral deformations of a plate when strained beyond the buckling limit, an explanation is now given as to how the deflected web participates in carrying part of the moment applied to the girder. Of all the stresses in the web only the membrane stresses in the longitudinal direction of the beam give rise to a bending moment about the girder's neutral axis. Therefore, reference is only made to these stresses or equivalent strains in the subsequent material.

As an example, measured web deflections and membrane stresses are shown in Fig. 2, plotted against the outline of the cross section and the elevation of the particular test girder from which the data were observed (1). The membrane strains were obtained by averaging the strain readings on both sides of the web. The strains or stresses—depending on the scale used—are plotted for three different bending moments. These moments are expressed in terms of the yield moment M_y, which is the moment initiating nominal yielding according to ordinary beam theory. The test data corresponding to a particular applied moment are connected by straight lines. Thus, the stress distribution over the entire girder depth can be visualized and compared with the predictions of beam theory, predictions which are also plotted in thin lines for each of the three moment values.

The initial distortions in this cross section and the additional web deflections under the three moment values appear on the left-hand side of Fig. 2. How the stresses are related to the web deflections becomes apparent when a longitudinal web strip, which extends over the panel length, is considered. It is readily seen that an axial shortening can be "digested" not only by straining alone, but also by lateral deflection of the web. Thus, strips in the compression range (upper portion of Fig. 2) avoid carrying their full share of axial stress, as shown quite clearly in Fig. 2.

This modified stress distribution could be estimated using the method on which the derivation of Eq. 1 is based. However, because it would depend on the initial distortions which are quite random, an assumption as to the resulting stress distribution will be made rather than to the shape and magnitude of the initial web distortions. It will be assumed that the contribution of the compressed web portion may be disregarded except for an effective strip along the compression flange (Fig. 3(c)). This leads to the effective-width concept as already used in existing specifications (15), (16).

There exists little information on the effective compressive strip in plates subjected to edge displacements similar to those of webs of bending girders. But it seems safe to assume that at ultimate load at least the same effective strip width can be expected as for a thin plate under uniform edge compression, namely about 30 t for mild steel.

ULTIMATE BENDING MOMENT

It is seen from the previous material that the attainment of the web-buckling load does not constitute failure of a plate girder. When will a plate

girder subjected to bending fail? Obviously, not before one of the framing members around a web panel fails, because only then will the deflected web be unable to burden the framing members with that portion of the bending moment which it alone cannot resist. In a symmetrically proportioned plate girder subjected to bending, the static carrying capacity is reached when the compression flange fails—barring brittle fracture. Therefore, this section, which analyzes the static strength of plate girders subjected to bending, will be concerned with the bracing and proportioning of the compression flange.

In order to classify the different buckling types, the compression flange may be considered as an isolated column. With regard to buckling, such a column has three degrees of freedom: it can buckle laterally, torsionally, or in the vertical direction. This is pictured in Fig. 3(b) where the three arrows

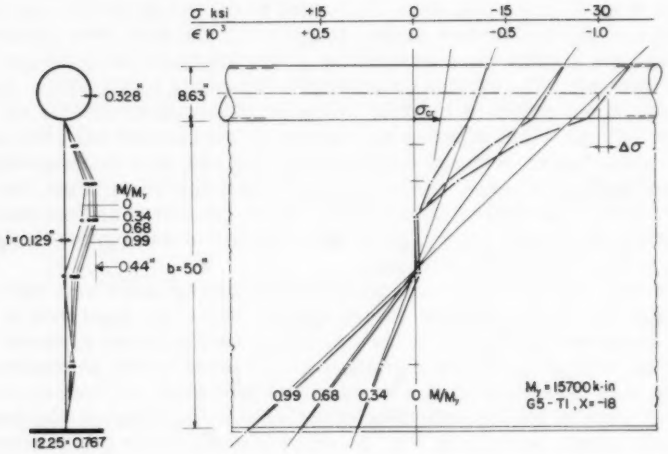

FIG. 2.—MEASURED STRESSES AND WEB DEFLECTIONS

show the three directions of motion. In Fig. 3(a) the notation to be used later is also defined.

Vertical Buckling of the Flange.—If the compression flange possessed rigidity in all directions, it could be the lone carrier of the compressive force. Together with the tension-flange force this would provide the resisting bending moment. This concept is realized in a truss. A plate girder of I-shaped cross section could act the same way provided the web were able to brace continuously the compression flange which otherwise lacks rigidity in the web direction. Since the required bracing stiffness is small, the danger of compression-flange failure in the vertical direction is limited to high web slenderness ratios. By setting an upper limit to the web slenderness parameter $\beta = b/t$, it should be possible to arrive at a design concept which is unaffected by this type of failure. To establish such a limit will require a number of simplifying assumptions which are discussed herein.

In the process of bending, curvature gives rise to transverse flange-force components which cause a uniform compressive stress σ_n on the upper

and lower edges of the web. This is indicated in Fig. 4 where the reaction stresses σ_n needed to keep the flanges in equilibrium are shown. If the plate were subjected to stresses of this kind only, failure of the web would occur similar to that of an Euler column under a stress intensity

$$\sigma_n = \sigma_{cr} = \frac{\pi^2 E}{12(1 - \nu^2)} \frac{t^2}{b^2} \quad \ldots\ldots\ldots\ldots\ldots (2)$$

Actually, the plate is also subjected to longitudinal stresses as pictured in Fig. 2. Assuming that the adverse influence of the compressive stresses in the longitudinal direction is offset by the tension in this direction, and that the influence of yield penetration into the web at high flange strains is offset by the restraint offered to the thin web by the flange, the value given above can be considered as an estimate of the web's resistance against vertical buckling of the flange.

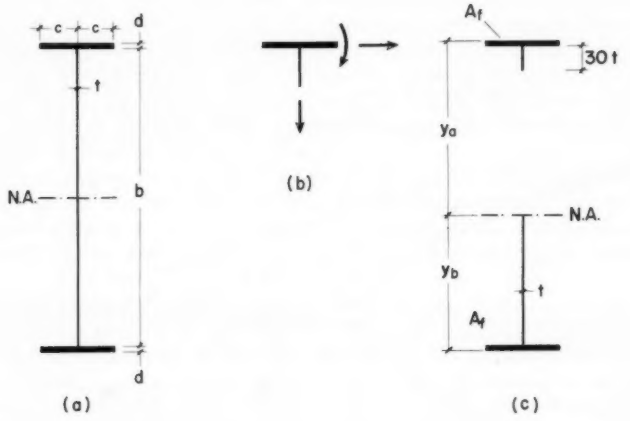

FIG. 3.—(a) NOTATION, (b) BUCKLING MODES OF THE COMPRESSION FLANGE, AND (c) EFFECTIVE GIRDER CROSS SECTION

Over the length dx the transverse component of the flange force amounts to $A_f \sigma_f \frac{2 \epsilon_f}{b} dx$, where σ_f is the flange stress and ϵ_f the flange strain. To prevent vertical buckling it is required that the applied force be smaller than the resisting force, and this leads to

$$\frac{b}{t} < \sqrt{\frac{\pi^2 E}{24(1 - \nu^2)} \frac{A_w}{A_f} \frac{1}{\sigma_f \epsilon_f}} \quad \ldots\ldots\ldots\ldots (3)$$

This slenderness limit depends somewhat on the ratio of web area to flange area, $A_w/A_f = \rho$. In general, this ratio of area is not below 0.5. In order to prescribe an upper limit for b/t applicable within the range of practical design, Eq. 3 can be used assuming a minimum value of 0.5 for A_w/A_f. If it is required that every flange fiber reaches yield stress before failure, then a

flange force $A_f \sigma_y$ is obtained. To fulfil this condition the flange strain must be somewhat greater than the yield strain $\epsilon_y = \sigma_y/E$ because an elimination of residual stresses σ_r requires a strain of $\epsilon_f = (\sigma_y + \sigma_r)/E$, as sketched in Fig. 4. Under these assumptions and by substituting known numerical values, Eq. 3 can be written as

$$\frac{b}{t} < \frac{0.48\ E}{\sqrt{\sigma_y\ (\sigma_y + \sigma_r)}} \quad \ldots\ldots\ldots\ldots\ldots\ldots\ (4)$$

and amounts to $b/t < 360$ for mild steel where $\sigma_y = 33$ ksi and σ_r is assumed to be 16.5 ksi.

Although this derivation for web-slenderness limitation appears somewhat crude, it agrees fairly well with the test observations, points out the parameters involved, and establishes a relationship between them. Eq. 4 indicates

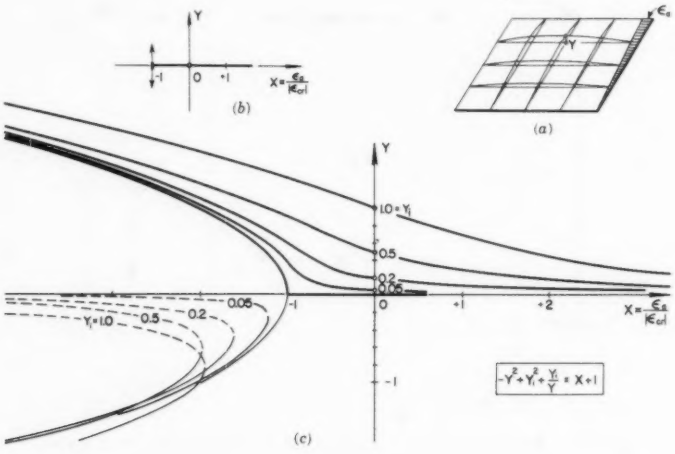

FIG. 4.—VERTICAL BUCKLING

that a girder built of high-strength steel will require a lower b/t limit than one made of mild steel. This is due to the fact that the flange force and curvature can increase in proportion to the higher yield stress, thus giving rise to a larger vertical force component. For a girder built of low-alloy high-strength steel with a minimum yield point of 50 ksi and σ_r again assumed to be 16.5 ksi, the web-slenderness ratio should not exceed 250.

This vertical failure of the compression flange was observed (1) in a test on a girder whose web-slenderness ratio was $\beta = 388$, web-to-flange area ratio $A_w/A_f = 0.68$, and whose flange strain ϵ_f was slightly more than the yield strain ϵ_y. The experiments also included a girder with a tubular compression flange, a cross section of which appears in Fig. 2. It differed from

the one mentioned previously only in the shape of the compression flange. Regardless of the amount of strain imposed, this girder could not be made to fail in this manner. In this case the flange was a self-supporting element with respect to vertical buckling and needed no bracing by the web. Therefore, it can be concluded that the stated limit for the web-slenderness parameter is conservative for all those girders whose flanges provide a certain degree of vertical rigidity, such as in riveted girders with flange angles.

It must be pointed out that girders which are loaded not only at points of transverse stiffening, but at intermediate points as well, require webs sturdier than stipulated by Eq. 4. This will also be the case in curved compression flanges, such as those sometimes used over interior supports of continuous girders.

Lateral Buckling.—Lateral buckling of beams has been analyzed thoroughly (16),(17). The topic is taken up again only in order to derive and justify a design concept especially applicable to plate girders.

In an effort to arrive at a simple design formula the paper by K. de Vries (18) is probably the most significant. In the discussion which it provoked (19) it was pointed out, especially by G. Winter, that there should be not one but a pair of formulas, each one applicable when the other becomes unnecessarily restrictive. It was generally agreed that the first of these could be the one proposed by de Vries, which depends only on the parameter of (span length x girder depth) ÷ (flange width x flange thickness). This formula, $\sigma_{cr}(v)$, appears in the upper left corner of Fig. 5.

It is the objective of this section to show that the second formula of the pair expresses the concept that the lateral buckling stress $\sigma_{cr}(w)$ is that of a column whose effective cross section is composed of the compression flange and one sixth of the web. This concept is pictured in the upper right corner of Fig. 5.

Relation Between St. Venant Torsion and Warping Torsion.—Since the papers by Timoshenko (2) were published in the early 1900's, it has been recognized that the resistance of an I-beam against lateral buckling consists of two parts: St. Venant torsion and warping torsion, often referred to as pure torsion and flange bending torsion. The St. Venant part is due to twisting of each component plate where the angle of twist gives rise to a shear stress flow as pictured in the left of Fig. 5. The sum of the torques due to this stress flow is the St. Venant torsional resistance considered in the accepted analysis of lateral-torsional buckling of beams. The warping contribution, shown on the right side of Fig. 5, is due to lateral bending of the flange plates and will be discussed in detail subsequently.

In order to reflect these two parts, the expression for the critical bending moment is rewritten between the two sketches of Fig. 5 as expression (a). The assumptions under which it can be transformed into expression (b) of Fig. 5 are shown in Appendix I, where the two approximate formulas appear as the equivalents of these two terms. The first term takes only St. Venant torsion into account, the second only warping; hence the symbols $\sigma_{cr}(v)$ and $\sigma_{cr}(w)$, respectively.

From expression (c) in Fig. 5 it is seen that the relation between these three stresses is the same as that existing between the sides of a right triangle. The length of the hypotenuse represents the correct critical stress, whereas the two sides indicate the prediction by each formula alone. Therefore, a conservative estimate of the lateral buckling stress is obtained if

either approximation formula is used alone. When either of the two values $\sigma_{cr}(v)$ or $\sigma_{cr}(w)$ is predominant, the other can be neglected, since the length of the hypothenuse is only slightly more (in no case more than 41%) than that of the longer leg alone.

It has been (18) convincingly demonstrated that for hot-rolled beam sections the $\sigma_{cr}(v)$ expression applies. However, in plate girders the warping torsion is generally the governing factor and the design should be based on the aforementioned column concept. This is seen from Fig. 6, where the critical buckling stress of a plate girder is plotted against the slenderness ratio of a column whose effective cross section is composed of the compression flange and one-sixth of the web. By assuming that the flange thickness is related to the web thickness, the stress resulting from the formula $\sigma_{cr}(v)$ and the exact critical stress $\sigma_{cr}(v, w)$ can be plotted in the same coordinate system. This is done for a flange to web thickness ratio of 3 and various web slenderness ratios. As seen, the exact lateral-torsional buckling stress

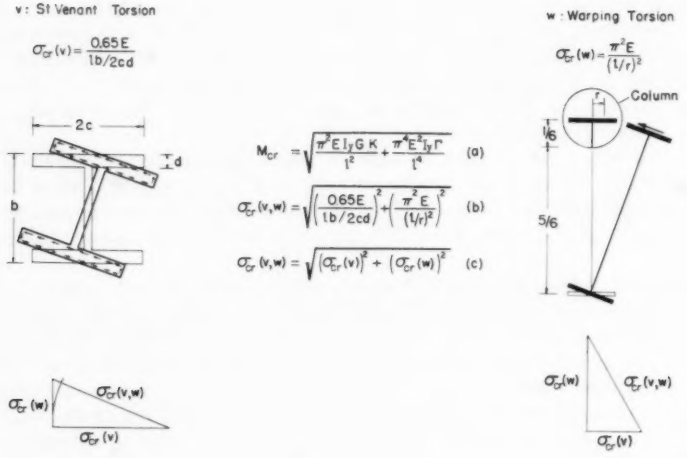

FIG. 5.—LATERAL BUCKLING

$\sigma_{cr}(v, w)$, considering both warping and St. Venant torsion, exceeds the simple column prediction only slightly for a web slenderness ratio $\beta = 200$ and even less for higher values of β.

As seen from the test results to be discussed herein under the heading "Design Considerations: Correlation with Test Results" the experimental program was confined to a low range of column slenderness ratios, from $l/r = 15$ to 40, that is, $\lambda = 0.16$ to 0.42.

Physical Interpretation of Warping Torsion.—Analyzing the mode of buckling from the lateral-torsional buckling equations, it can be shown that, for the case of negligible St. Venant torsion, the rotation of the cross section occurs around the tension flange. With the notation defined in Fig. 7(a), the buckling mode of a beam under pure bending and with simply supported ends

can thus be expressed as

$$w(x, y) = w_o \frac{2y + b}{2b} \cos \frac{\pi x}{l} \quad \ldots\ldots\ldots\ldots (5)$$

in which w_o is the maximum deflection of the top flange at centerline of the span and normal to the web plane. The lateral force component of the compression flange is equal to $\sigma_f A_f \frac{d^2 w_a}{dx^2}$. This overturning force is held in equi-

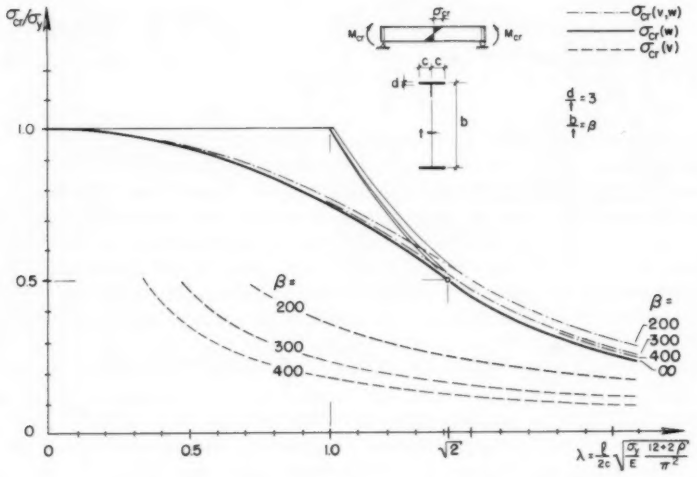

FIG. 6.—LATERAL BUCKLING STRESSES FOR GIRDERS WITH SLENDER WEBS

librium by the bending resistance of the compression flange, $E I_f \frac{d^4 w_a}{dx^4}$. Thus

$$E I_f \frac{d^4 w_a}{dx^4} + \sigma_f A_f \frac{d^2 w_a}{dx^2} = 0 \quad \ldots\ldots\ldots\ldots (6)$$

Inserting $w(x, y = b/2)$ in this differential equation yields

$$\sigma_{cr} = \frac{\pi^2 E}{(l/r)^2} \quad \ldots\ldots\ldots\ldots\ldots (7)$$

with $r = \sqrt{I_f/A_f}$. This is simply the lateral-buckling stress of the compression flange plate. The tension flange has neither a stabilizing nor a detrimental effect since it remains undeflected in the lateral direction and, as stipulated,

St. Venant torsion is neglected. However, the stresses in the web also create a lateral force component which amounts to

$$q = \sigma\, t\, \frac{d^2w}{dx^2} \quad \ldots\ldots\ldots\ldots\ldots\ldots (8)$$

per unit depth and is pictured in Fig. 7. Lacking rigidity in the lateral direction, the web certainly burdens the two flanges with the resultant lateral forces

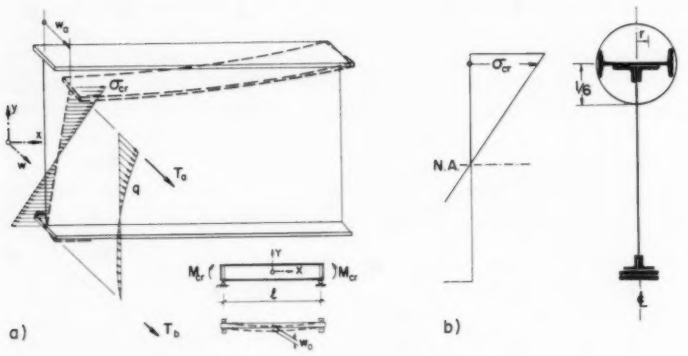

FIG. 7.—LATERAL FORCE COMPONENTS OF WEB

T_a and T_b. These two reactions are

$$T_a = \frac{1}{b} \int_{-b/2}^{+b/2} q\left(y + \frac{b}{2}\right) dy = \frac{1}{6}\, A_w\, \sigma_f\, \frac{d^2w_a}{dx^2} \quad \ldots\ldots (9a)$$

and

$$T_b = \frac{1}{b} \int_{-b/2}^{+b/2} q\left(\frac{b}{2} - y\right) dy = 0 \quad \ldots\ldots\ldots\ldots (9b)$$

That T_b is zero could have been concluded from the vanishing tension-flange deflection. To the lateral force component of the compression flange, however, is to be added the web contribution (Eq. 9a) and the equilibrium condition now becomes

$$E\, I_f\, \frac{d^4w_a}{dx^4} + \sigma_f\left(A_f + \frac{1}{6}\, A_w\right) \frac{d^2w_a}{dx^2} = 0 \quad \ldots\ldots\ldots (10a)$$

resulting in

$$\sigma_{cr}(w) = \frac{\pi^2 E}{l^2} \frac{I_f}{A_f + \frac{1}{6} A_w} \quad \ldots\ldots\ldots\ldots (10b)$$

or

$$\sigma_{cr}(w) = \frac{\pi^2 E}{\left(\frac{l}{r}\right)^2} \quad \ldots\ldots\ldots\ldots\ldots (10c)$$

with

$$r = \sqrt{\frac{I_f}{A_f + \frac{1}{6} A_w}} \quad \ldots\ldots\ldots\ldots\ldots (10d)$$

which is the expression derived in Appendix I. It should be noted that the critical stress represents the stress at the centroid of the compressed element furnishing the lateral rigidity, thus it is not the extreme fiber stress.

From the previous derivation it can readily be seen what modification of Eqs. 10 would be needed if the stress distribution over the girder depth differs from the assumed linear one. For example, a stress distribution similar to that of the full plastic moment necessitates taking into account one quarter of the web area instead of one sixth. For a stress distribution as pictured by the plotted points of Fig. 2, a value smaller than $A_w/6$ would result. Since the influence of the web on lateral buckling is small compared to that of the flange, it is justified to use the average value of one sixth, corresponding to the linear stress distribution, also for the other extreme cases.

If the girder cross section differs somewhat from the doubly symmetric I-shape, the neutral axis may shift from the mid-depth of the web. In plate girders this effect is generally limited in extent, and thus it is not necessary to change the equivalent web portion of $b\,t/6 = A_w/6$ to a more precise value. Of much greater importance for profiles without double symmetry is the fact that compression and tension flanges have unequal lateral rigidities, an example of which is shown in Fig. 7(b). From the physical interpretation it becomes clear that in this case of negligible St. Venant torsion only the lateral rigidity of the compression flange is of significance. Therefore, $\sigma_{cr}(w)$ as given in Eqs. 10b and c should apply fairly well to all plate girders with symmetry about the vertical axis. To check this, reference can be made to an excellent survey on simplified lateral buckling formulas recently assembled (17). In Figs. 5 to 8 of that paper the lateral-buckling stresses as obtained by various approximate formulas applied to unsymmetrical I-sections are compared with the rigorous solution (Eq. 1 of that paper). This comparison indicates that the formula $\sigma_{cr}(v)$ does not provide a good approximation to the exact value for the case of $l = 300$ in. According to the previously discussed relation between $\sigma_{cr}(v)$ and $\sigma_{cr}(w)$, it should be expected that $\sigma_{cr}(w)$ would apply more adequately. That this is the case is shown in Appendix I, where Figs. 7 and 8 of the previously cited paper (17) are reproduced as Fig. 13.

Because the phenomenon of lateral buckling if St. Venant torsion is neglected is simply one of lateral buckling of the compression flange, the buckling curves used in the inelastic range must be those of weak axis buckling of wide

flange type columns. It can be concluded (20) that, depending whether the girder is welded or riveted, the critical stress in the inelastic range must be significantly different. In order to avoid too great a differentiation, it is recommended (16) that the basic column curve be used, which represents an average of the extreme transition curves in a stress versus slenderness diagram, pending further research on this problem. It is suggested that this basic

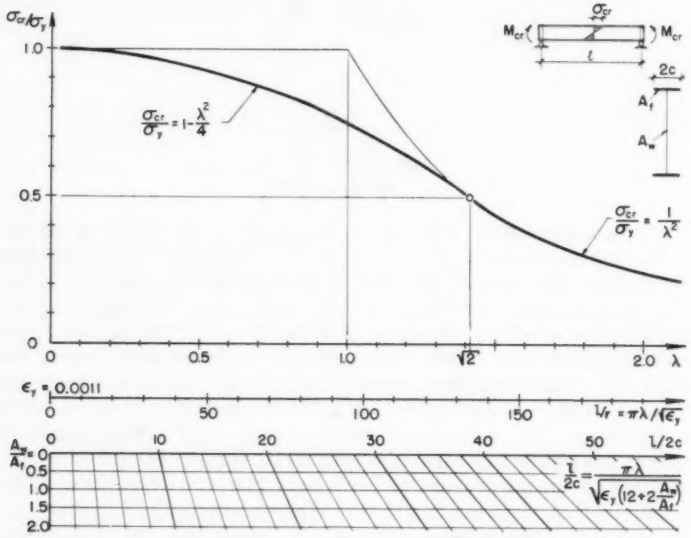

FIG. 8.—LATERAL BUCKLING CURVE, $\sigma_{cr(w)}$

column curve be used for lateral buckling of plate girders analyzed with the warping torsion concept:

$$\frac{\sigma_{cr}}{\sigma_y} = 1 - \frac{\lambda^2}{4} \quad \ldots\ldots\ldots\ldots\ldots\ldots (11a)$$

for $0 < \lambda < \sqrt{2}$,

$$\frac{\sigma_{cr}}{\sigma_y} = \frac{1}{\lambda^2} \quad \ldots\ldots\ldots\ldots\ldots\ldots (11b)$$

for $\lambda > \sqrt{2}$, with

$$\lambda = \frac{l}{r}\sqrt{\frac{\epsilon_y}{\pi^2}} = l\sqrt{\frac{\epsilon_y}{\pi^2}\,\frac{A_f + \frac{1}{6}A_w}{I_f}} \quad \ldots\ldots\ldots (12)$$

The curve of Eqs. 11 is plotted in Fig. 8. First the standard slenderness ratio λ, which makes the plot independent of yield stress, is used for the abscissa scale. Next the scale for the parameter l/r, valid only for $\epsilon_y = \sigma_y/E = 33/30{,}000 = 0.0011$, is shown. Finally, the old established parameter "buck-

ling length to flange width" is presented. This lowest abscissa scale is applicable only if the shape of the compression flange is a rectangle.

Preservation of Shape.—The derivation of the general lateral buckling expression (Eq. 23 in Appendix I) is based on the assumption that the shape of the girder cross section is preserved at the instant of buckling. The validity of this assumption becomes uncertain for plate girders with high web-slenderness ratios and in cases where the transverse stiffeners are not fitted to the tension flange. However, this uncertainty concerns only the St. Venant torsion part since it is dependent on an undeformed cross section whose component plates are assumed to be forced through the same angle of twist. If, for example, the joint between the tension flange and web were pinned, the torsional constant K in Eq. 23 would reduce to about one-half the value for a rigid joint, (exactly one half if the web's contribution in Σ b $t^3/3$ is neglected), and a reduction in "critical" stress, $\sigma_{cr}(v)$, of almost 30% would result. The derivation of $\sigma_{cr}(w)$ in Eqs. 10, however, is not affected at all. Since warping torsion in a plate girder is the predominant contribution to lateral stability, a deformation of profile shape has but little effect on the resulting buckling stress and an analysis on the basis of $\sigma_{cr}(w)$ alone is a conservative one in all cases.

Recalling that at the tension flange side no shear transfer in the lateral direction is needed (Eq. 9b), and having shown that a preservation of the right angle between tension flange and web is not essential, a theoretical confirmation is obtained of the test evidence that transverse stiffeners may be cut short for a limited distance at the side of the tension flange (21).

Torsional Buckling of the Flange Plate.—The analysis of the three modes of failure is simplified in that it does not recognize the dependence of the different failure modes on each other. It was correct to single out vertical buckling, because it occurs in a direction of symmetry. However, when torsional buckling of the compression flange is treated independently of lateral buckling, it is an unconservative simplification.

If all restraint on the flange from the web is neglected, the case reduces to buckling of a long, hinged plate under pure edge compression at its ends. Hence, the only parameter on which the flange plate buckling stress depends is the ratio of outstanding width to plate thickness, c/d. In Fig. 9, the critical flange stress is plotted as a function of this parameter and λ. The quantity λ is a dimensionless parameter defined subsequently. In the inelastic range the curve is obtained by assuming (22) that the onset of strain-hardening of flange plate is at $\lambda = 0.45$, that compressive residual stress of $\sigma_y/2$ ($\lambda = \sqrt{2}$) exists, and that the transition curve is tangent to the curves at these two points. Then the analytical expressions of the buckling curve are

$$\frac{\sigma_{cr}}{\sigma_y} = 1 - 0.53(\lambda - 0.45)^{1.36} \quad \ldots\ldots\ldots\ldots (13a)$$

for $0.45 < \lambda < \sqrt{2}$,

$$\frac{\sigma_{cr}}{\sigma_y} = \frac{1}{\lambda^2} \quad \ldots\ldots\ldots\ldots\ldots\ldots (13b)$$

for $\lambda > \sqrt{2}$, with

$$\lambda = \frac{c}{d}\sqrt{\frac{12(1 - \nu^2)\epsilon_y}{\pi^2 k}} \quad \ldots\ldots\ldots\ldots\ldots (14)$$

and a plate buckling coefficient (3) k = 0.425. Assuming a yield strain ϵ_y = 33/30,000 = 0.0011, the critical stress can be expressed in terms of the plate slenderness c/d as shown on the second abscissa scale in Fig. 9.

Above the computed buckling limit the strength of any plate is, in general, made up of two parts. First, a favorable rearrangement of forces where elements adjacent to the plate participate, and second, the plate's own post-buckling strength. The first part is not significant for the flange plate of a girder with a thin web. For the second, Winter concludes (23) that only for an outstanding flange of more than about thirty times the flange thickness can a sizable effect of post-buckling strength be expected. In such a range the ultimate stresses are less than one half of the yield stress, thus it is of little interest in the design of plate girders. Therefore, it is recommended that the post-buckling strength be ignored completely (as is the established practice in the design of cold-formed light-gage steel structures (15).

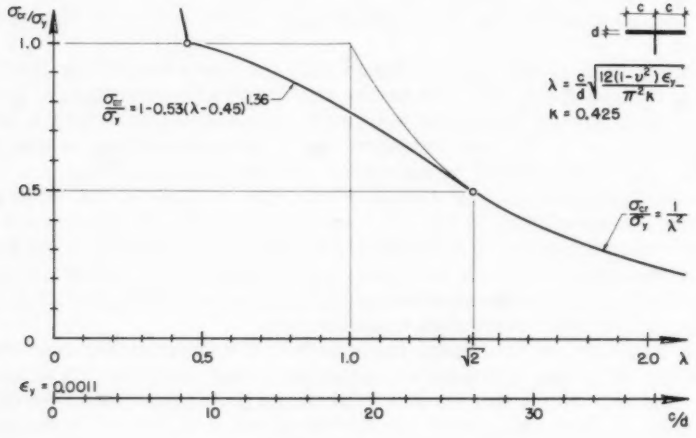

FIG. 9.—TORSIONAL BUCKLING OF THE FLANGE PLATE

As described previously (1), a test girder was built with an extremely wide flange (c/d = 24). Its ultimate load exceeded the computed critical flange buckling stress by about 10%. The flange distortions of such a structure approach magnitudes under which serviceability is impaired prior to reaching the ultimate load.

In designing plate girders, the compression flange should be made as wide as possible to increase its lateral rigidity and its lateral buckling strength. But if this is done in excess, torsional buckling of the flange plate will replace lateral buckling at a lower ultimate stress.

In order to eliminate torsional buckling as a primary cause of failure, the critical stress of the flange plate given by Eqs. 13, should exceed that of

lateral buckling given by Eqs. 11, resulting in

$$\frac{l}{c} > \frac{2.9}{\sqrt{1 + \frac{1}{6}\frac{A_w}{A_f}}} \frac{c}{d} \quad \ldots\ldots\ldots\ldots\ldots\ldots (15a)$$

for elastic range, $\frac{c}{d} > 26$, and

$$\frac{l}{c} > \frac{80}{\sqrt{1 + \frac{1}{6}\frac{A_w}{A_f}}} \left(0.053\,\frac{c}{d} - 0.45\right)^{0.68} \quad \ldots\ldots\ldots (15b)$$

for inelastic range, $\frac{c}{d} < 26$. This correlation between c/d and l/c is plotted in Fig. 10. As indicated, in the condition

$$\frac{2c}{d} \leq 12 + \frac{1}{2c} \quad \ldots\ldots\ldots\ldots\ldots\ldots (15c)$$

(that is, a flange width-to-thickness ratio not exceeding 12 plus the ratio of lateral-buckling length to flange width) would exclude the possibility of tor-

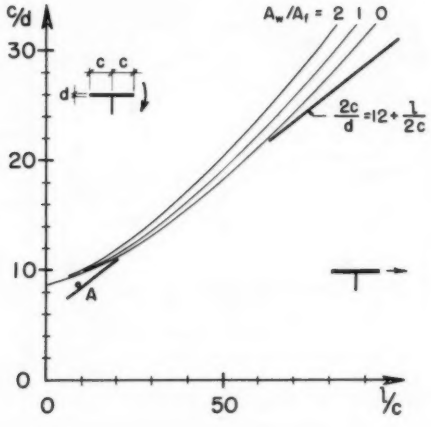

FIG. 10.—BOUNDARY BETWEEN LATERAL AND TORSIONAL BUCKLING OF FLANGE

sional buckling as a primary cause of failure for girder sections under uniform bending. Should it be desirable to exceed this limit for the flange width-to-thickness ratio, Eq. 15c could be used to find an equivalent column length with which the critical stress is found from the basic column curve, Fig. 8.

This procedure of eliminating plate buckling by specifying the plate-slenderness ratio as a function of the column slenderness ratio has been recommended (16). Inserting the appropriate values into Eq. 3.3b of Ref. 16 results in exactly the expression given for the elastic range, Eq. 15a.

The curves in Fig. 10 for the inelastic range are dependent on the assumption of the transition curves. As noted previously, values for plates and columns have been established (22) for the onset of strain hardening (l/r = 16.5,

c/d = 8.5 for σ_y = 33 ksi). This is plotted as point A in Fig. 10. If the column curve used would take strain hardening into account, the curves of Fig. 10, which form the boundary between torsional and lateral buckling, would necessarily pass through this point A.

DESIGN CONSIDERATIONS

Ultimate Bending Stresses.—Although the strength prediction of a girder segment subjected to pure bending appears to be simple because only three possible types of compression-flange buckling have to be considered, there are still some difficulties in specifying admissible compressive-flange stresses. This is due to the presence of four independent parameters which influence the result, namely l/r, c/d, A_w/A_f, and b/t. Whereas the first two essentially control lateral and torsional buckling of the compression flange, the two latter parameters also influence the ultimate bending moment to a certain degree.

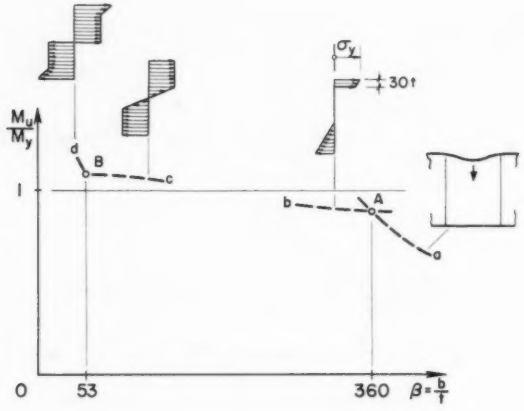

FIG. 11.—ULTIMATE BENDING MOMENT VERSUS WEB SLENDERNESS

A slender web burdens the flanges with the stresses which the web cannot resist. This leads to an increase of the compressive flange stresses above the nominally computed values.

Assuming first that the flange is prevented from buckling laterally or torsionally, the predicted ultimate bending moment M_u is indicated in Fig. 11 as a function of the web-slenderness parameter β and is expressed nondimensionally in terms of the yield moment M_y. At very high web slenderness ratios, vertical buckling of the flange would take place before the extreme fiber stress reached the yield stress, curve a. Curve b indicates the strength furnished if the yield stress in the compression flange could be reached, assuming that a width of the compressed portion of the web equal to only 30t were effective. As the web slenderness ratio is decreased along curve c the

stress pattern would eventually approach point B, corresponding to the full plastic moment. According to Fig. 8 (22), strain hardening could take place when $\beta < 53$, because the web could endure an edge strain of more than 12 ϵ_y without the occurrence of inelastic instability. A moment equal to the full plastic value can be developed when $\epsilon_f \leq 12\ \epsilon_y$ and strain-hardening can commence, hence $M_u > M_p$ when $\epsilon_f > 12\ \epsilon_y$. Thus, the ultimate moment will exceed or at least equal the plastic moment at $\beta < 53$.

Rather than to speculate on the course of this transition from the established intersections A and B in Fig. 11, a straight line may be considered to represent with sufficient accuracy the strength predictions in the range of web slenderness ratios $0 < \beta < 360$. Fig. 12 is thus drawn assuming that a plastic moment is reached at $\beta = 53$ and an effective width of 30 t is available at $\beta = 360$. Of greater importance than the exact shape of the transition curve

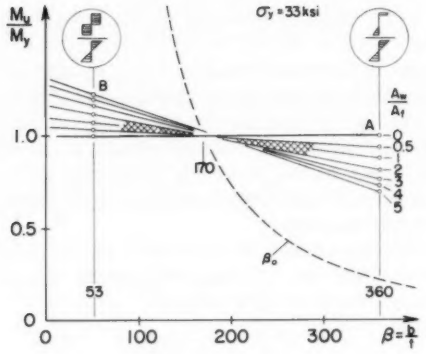

FIG. 12.—ULTIMATE BENDING MOMENT AS INFLUENCED BY THE PARAMETERS b/t AND A_w/A_f

is the fact that the ultimate bending moment M_u depends also on a "shape factor," $\rho = A_w/A_f$, the ratio of web to flange area, as is born out in Fig. 12. The range of A_w/A_f in which most plate girders are built is cross-hatched. Details of computation for this figure are shown in Appendix I.

If the information in Fig. 12 is to be expressed analytically it can be done conveniently in the form

$$\frac{M_u}{M_y} = 1 - C(\beta - \beta_o) \quad \ldots\ldots\ldots\ldots\ldots\ldots \quad (16)$$

in which the coefficient C is the slope of a line in Fig. 12 and β_o the intersecting abscissa of $M_u/M_y = 1$ and the same line. The constant C could be expressed as in Eq. 17a, but since most plate girders are built in the range $A_w/A_f < 2$, the simpler Eq. 17b may be used:

$$C = \frac{1}{300 + 1200\ \frac{A_f}{A_w}} \quad \ldots\ldots\ldots\ldots\ldots\ldots (17a)$$

and

$$C = 0.005 \frac{A_w}{A_f} \quad \ldots\ldots\ldots\ldots\ldots\ldots (17b)$$

Assuming that the stress computation would be made with the usual section-modulus concept, the nominal ultimate bending stress σ_u would equal M_u/S, where S is the section modulus. Since $M_y/S = \sigma_y$, $M_u/M_y = \sigma_u/\sigma_y$. Thus, Eq. 16 can also be written as

$$\sigma_u = \sigma_y \left[1 - 0.0005 \frac{A_w}{A_f} (\beta - \beta_o)\right] \ldots\ldots\ldots\ldots (18a)$$

The expression as written assumes that instability of the compression flange does not influence the carrying capacity. It is convenient to incorporate the influence of lateral or torsional buckling simply by replacing σ_y with the respective critical stress σ_{cr},

$$\sigma_u = \sigma_{cr} \left[1 - 0.0005 \frac{A_w}{A_f} (\beta - \beta_o)\right] \ldots\ldots\ldots\ldots (18b)$$

But, unlike the case in the plastic range, there cannot be an increase of the nominal ultimate bending stress when elastic instability occurs because a stress distribution similar to that for the plastic moment will not take place. In order to keep the concept simple it is proposed to use Eq. 18b only for the range of web-slenderness ratios where $\beta > \beta_o$, namely in the post-buckling range where a linear stress distribution according to Navier-Bernoulli would be an unconservative assumption.

Defining the post-buckling range as one where the nominally computed bending stress σ is greater than the critical web stress (3), the limiting value of value of b/t (β_o) can be expressed as follows:

No flange restraint:

$$\sigma = \sigma_{cr} = 23.9 \frac{\pi^2 E}{12(1 - \nu^2)} \left(\frac{t}{b}\right)^2 \longrightarrow \frac{b}{t} = 4.6\sqrt{\frac{E}{\sigma}} \quad \ldots\ldots (19a)$$

Full flange restraint:

$$\sigma = \sigma_{cr} = 39.6 \frac{\pi^2 E}{12(1 - \nu^2)} \left(\frac{t}{b}\right)^2 \longrightarrow \frac{b}{t} = 6.0\sqrt{\frac{E}{\sigma}} \quad \ldots\ldots (19b)$$

Conforming to the existing United States specifications an intermediate value is suggested,

$$\beta_o = 5.7\sqrt{\frac{E}{\sigma}} \quad \ldots\ldots\ldots\ldots\ldots\ldots (20)$$

which gives $\beta_o = 170$ when $\sigma = \sigma_y = 33$ ksi, Fig. 12, and 140 for a yield stress equal to 50 ksi.

In this way, the influence of the two parameters A_w/A_f and b/t would be restricted in the ordinary plate-girder design to a range of high web-slenderness ratios where a reduction of the allowable compressive flange stress is indicated. The reduction, in percentage, of the nominally computed flange stress σ can generally be expressed as given subsequently in Eq. 21a, the limits of which are obtained from Eqs. 4 and 20. For A7 steel Eq. 21b gives the highest possible reduction, while for a low-alloy high-strength

structural steel with a yield point of 50 ksi Eq. 21c would apply:

Nominal Bending Stress, in ksi	Bending Stress Reduction, in %	Valid for
σ	$0.05\frac{A_w}{A_f}\left(\beta - 5.7\sqrt{\frac{E}{\sigma}}\right)$	$5.7\sqrt{\frac{E}{\sigma}} < \beta < \frac{0.48\ E}{\sqrt{\sigma_y(\sigma_y + \sigma_r)}}$ ..(21a)
33	$0.05\frac{A_w}{A_f}(\beta - 170)$	$170 < \beta < 360$ .....(21b)
50	$0.05\frac{A_w}{A_f}(\beta - 140)$	$140 < \beta < 250$ .....(21c)

Correlation with Test Results.—The expressions which have been presented for computing ultimate load can be substantiated by the results of nine tests carried out on five different plate girders. The girders and the tests have been described (1). In Table 1 some of the girder properties are summarized.

TABLE 1.—SUMMARY OF BENDING TESTS ON WELDED PLATE GIRDERS

GIRDER		G1	G2	G3	G4	G5
(dimensions in inches, yield stress in kips/in²)	2c/d	20.56/0.427, σ_y=35.4	12.19/0.769, σ_y=38.6	Ø8.62/0.328, σ_y=35.5	12.16/0.774, σ_y=37.6	Ø8.62/0.328, σ_y=35.5
	b/t	50.00/0.270	50.00/0.270	50.00/0.270	50.00/0.129	50.00/0.129
	2c/d	12.25/0.760	12.19/0.774	12.19/0.770	12.19/0.765	12.25/0.767
$\frac{I}{e_a}$ [in³]		14,380 / 25.9	14,940 / 25.9	16,220 / 28.9	13,420 / 25.7	14,710 / 28.9
TEST		T1	T1 T2	T1 T2	T1 T2	T1 T2
Parameters	l_k	100	100 50	100 50	100 50	100 50
	l/r	19	32 16	39 19	30 15	36 18
	2c/d	48	16	–	16	–
	b/t	185	185	185	388	388
	A_w/A_f	1.5	1.4	1.6	0.7	0.8
Ult. Loads	P_u^{th}	73	141 145	126 130	118 121	106 109
	P_u^{ex}	81	135 144	130 136	118 125	110 124
P_u^{ex}/P_u^{th}		1.11	0.96 0.99	1.03 1.05	1.00 1.03	1.04 1.14
FAILURE MODES						

Below the cross section the section modulus is given as the ratio of the moment of inertia, I, to the distance from the neutral axis to the extreme compression flange fiber, e_a. The effective lateral-buckling lengths, l_k, are chosen as 100 in. in tests T1 and 50 in. in tests T2, although the actual bracing distances were 75 and $37\frac{1}{2}$ in., respectively. The determination of these values was explained in Sec. 2.5 of Ref. 1, where the failure modes are described. The radius of gyration is computed as $r = \sqrt{I/A}$ where A is the sum of the compression flange area and one sixth of the web area and I is the moment of inertia of this area about the vertical axis of symmetry.

The yield stresses of the compression flanges, listed to the right of the respective cross sections in Table 1, are somewhat above the value of 33 ksi

which was used to fix some of the abscissa scales in Figs. 8 and 9. Nevertheless, for the slenderness ratios involved the error in using these figures, as plotted, is negligible.

Girder G1.—With a slenderness ratio of the compression flange as low as 19 and a flange width-to-thickness ratio as high as 48, torsional buckling must be the governing failure cause. Referring to Fig. 9 when c/d = 24, $\sigma_{cr} = 0.56\ \sigma_y = 0.56 \times 35.4 = 19.8$ ksi. This stress need not be further reduced in accordance with Eq. 21a since this expression applies only to web slenderness ratios $\beta = b/t$ in excess of $\beta_o = 5.7\sqrt{E/\sigma} = 5.7 \times \sqrt{30{,}000/19.8} = 222$. Hence $\sigma_u = \sigma_{cr}$ and $M_u = \sigma_u I/e_a = 19.8 \times 14{,}380/25.9 = 11{,}000$ kip-in. For a moment arm of 150 in., $P_u^{th} = M_u/150$ in. = 73 kips. As shown in Table 1, $P_u^{ex} = 81$ kips giving a ratio of experimental to ultimate load of 1.11.

Girder G2, Test T1.—Substituting the value of c, d, and l, it is found that Eq. 15c holds. Thus torsional failure should not be the buckling mode of the flange. Entering Fig. 8 either at l/r = 32, or 1/2 c = 8 with $A_w/A_f = 1.4$, results in $\sigma_{cr} = 0.97\ \sigma_y = 0.97 \times 38.6 = 37.5$ ksi. With $\beta_o = 5.7\sqrt{E/\sigma} = 5.7\sqrt{30{,}000/37.5} = 161$, the reduction in accordance with Eq. 21a becomes $0.05 \times 1.4(185-161) = 2\%$. Hence, $M_u = 0.98 \times 37.5 \times 14{,}940/25.9 = 21{,}200$ kip-in. and $P_u^{th} = 21{,}200/150$ in. = 141 kips. This would be compared with the observed ultimate load of 135 kips.

Girder G2, Test T2.—Eq. 15c shows that the mode of failure can be either lateral or torsional buckling. The curves for lateral as well as torsional buckling (Figs. 8 and 9) furnish $\sigma_{cr} = \sigma_y$. With the 2% reduction according to Eq. 21a, it results in $M_u = 0.98 \times 38.6 \times 14{,}940/25.9 = 21{,}800$ kip-in., $P_u^{th} = 21{,}800/150$ in. = 145 kips.

Girder G3, Test T1.—With an 1/r = 39, Fig. 8 furnishes $\sigma_{cr} = 0.96\ \sigma_y = 0.96 \times 35.5 = 34.1$ ksi. Reduced 1% according to Eq. 21a, $\sigma_u = 33.7$ ksi. As pointed out under the heading "Ultimate Bending Moment: Lateral Buckling" the stress should be computed at the centroid of the compressive element which provides the lateral rigidity. This was not done in the previous cases where the distance of the extreme fiber, e_a, is very closely equal to the one of the flange controid. But for girders G3 and G5 e_a is taken as the distance from the neutral axis to the center of the tubular compression flange: $M_u = 33.7 \times 16{,}200/28.9 = 18{,}900$ kip-in., $P_u^{th} = 18{,}900/150$ in. = 126 kips. Of course, a tubular flange has a very significant torsional stiffness. But with a lateral buckling stress equal to 96% of the yield stress, considering the torsional stiffness would at most increase the ultimate moment by 4%.

Girder G3, Test T2.—$\sigma_{cr} = 0.99\ \sigma_y = 0.99 \times 35.5 = 35.1$ ksi. With 1% reduction, $\sigma_u = 34.8$ ksi, $M_u = 34.8 \times 16{,}220/28.9 = 19{,}500$ kip-in., $P_u^{th} = 19{,}500/150$ in. = 130 kips.

Girder G4, Test T1.—The girder failed by lateral buckling. According to Fig. 8, $\sigma_{cr} = 0.98\ \sigma_y = 0.98 \times 37.6 = 36.8$ ksi, $\beta_o = 163$. Reduction: $0.05 \times 0.70(388-163) = 8\%$. Hence, $\sigma_u = 0.92 \times 36.8 = 33.8$ ksi, $M_u = 33.8 \times 13{,}420 \div 25.7 = 17{,}700$ kip-in., $P_u^{th} = 17{,}700/150$ in. = 118 kips.

Girder G4, Test T2.—$M_u = 0.92\sigma_y I/e_a = 0.92 \times 37.6 \times 13{,}420/25.7 = 18{,}100$ kip-in., $P_u^{th} = 18{,}100/150$ in. = 121 kips.

Girder G5.—Computation similar to that for girder G3 gives:

Test T1: $M_u = 0.97\ \sigma_y(1-0.09)I/e_a = 34.4 \times 0.91 \times 14{,}710/28.9 = 15{,}900$ kip-in., $P_u^{th} = 15{,}900/150$ in. = 106 kips.

Test T2: $M_u = 0.99\ \sigma_y(1-0.09)I/e_a = 35.1 \times 0.91 \times 14{,}710/28.9 = 16{,}300$ kip-in., $P_u^{th} = 16{,}300/150$ in. = 109 kips.

The last test result, G5-T2, exceeds the predicted considerably because the actual 1/r ratio was so small that the flange could strain-harden. This is also borne out with the load versus centerline deflection diagram shown in Fig. 2.9 in Ref. 1. If the analysis were based on a column curve which takes strain-hardening into account (Ref. 20, Fig. 27) this discrepancy would be reduced.

All of these design considerations have been concerned with the ultimate compressive flange stresses. From these stresses the ultimate bending moment was computed. Except for the possibility of a brittle fracture, vertical, torsional, or lateral buckling of compression flange will always be the cause of failure under a statically loaded and symmetrically proportioned plate girder. Two facts contribute to this. First, it is the web portion adjacent to the compression flange which, through its insufficient participation of membrane stresses, causes an overstress of the compression flange. Second, if two equal members are subjected to axial forces of equal magnitude but opposite signs, it is the compression member which fails first because of instability. Only in the case of girders with smaller tension flange area than compression flange area is it possible that the ultimate moment, predicted from one or more of the three different types of compression flange failures discussed, could not be reached. In such a case, it is suggested that the ultimate moment be taken as

$$M_u = \sigma_y \frac{I}{e_b} \quad \ldots\ldots\ldots\ldots\ldots\ldots \quad (22)$$

ACKNOWLEDGMENTS

This investigation has been carried out at Fritz Engineering Laboratory, Lehigh Univ., Bethlehem, Pennsylvania of which William J. Eney is the Head. The Director of the Laboratory is Lynn S. Beedle.

Sponsored jointly by the Amer. Inst. of Steel Constr., the U. S. Dept. of Commerce - Bur. of Public Roads, the Pennsylvania Dept. of Highways, and the Welding Research Council, the research project at Lehigh Univ. was guided by the "Welded Plate Girder Committee" whose members were:

E. L. Erickson,	U. S. Dept. of Commerce - Bur. of Public Roads, Chairman
A. Amirikian,	Bur. of Yards and Docks, U. S. Navy
Lynn S. Beedle,	Lehigh Univ.
Karl de Vries,	Bethlehem Steel Co.
F. H. Dill,	American Bridge Div., U. S. Steel Corp.
E. R. Estes,	Florida Steel Corp.
G. F. Fox,	Howard, Needles, Tammen & Bergendoff
J. A. Gilligan,	U. S. Steel Corp.
LaMotte Grover,	Air Reduction Sales Co.
T. R. Higgins,	Amer. Inst. of Steel Constr.
W. H. Jameson,	Bethlehem Steel Co.
C. D. Jensen,	Pennsylvania Dept. of Highways
Knud Jensen,	Pennsylvania Dept. of Highways
Bruce G. Johnston,	Univ. of Michigan
K. H. Koopman,	Welding Research Council
George W. Lamb,	Consulting Bridge & Struct. Engr. (deceased)
W. M. McLean,	Dravo Corp.

N. W. Morgan,	U. S. Dept. of Commerce - Bur. of Public Roads
W. H. Munse,	Univ. of Illinois
E. J. Ruble,	Assn. of Amer. Railroads
J. E. South,	Pennsylvania Railroad Co.
R. M. Stuchell,	Pittsburgh-Des Moines Steel Co.
Bruno Thürlimann,	Federal Inst. of Tech., Switzerland
Neil Van Eenam,	U. S. Dept. of Commerce - Bur. of Public Roads
J. Vasta,	Bur. of Ships, Navy Dept.
George Winter,	Cornell Univ.
W. Spraragen,	Welding Research Council

The Committee members' constructive criticism is gratefully acknowledged. Special thanks are due Messrs. T. R. Higgins and W. A. Milek of the Amer. Inst. of Steel Constr., and Lynn S. Beedle and B. T. Yen of Lehigh Univ. for their careful review of the manuscript.

APPENDIX I.

Derivation of $\sigma_{cr}(v)$ and $\sigma_{cr}(w)$.—For the subsequent derivations it is assumed that the lever arm between the flange centroids and the distance between the extreme fibers can be put equal to the web depth b. The notation is defined both in Fig. 3(a) and in Appendix III. The expression for the critical moment of a beam of span l with simply supported ends is (3):

$$M_{cr} = \frac{\pi}{l}\sqrt{E\, I_y\, G\, K}\,\sqrt{1 + \pi^2\, E\, \Gamma / l^2 G\, K} \quad \ldots\ldots\ldots \quad (23)$$

With

I_y = girder's moment of inertia about weak axis $= \frac{2}{3}\, A_f\, c^2$

K = torsional constant $= \frac{1}{3}\left(2\, c\, d^3 + b\, t^3 + 2\, c\, d^3\right) = \frac{1}{3}\, A_f \left(2\, d^2 + \frac{A_w}{A_f}\, t^2\right)$

Γ = warping constant $= \frac{1}{4}\, I_y\, b^2 = \frac{1}{6}\, A_f\, b^2\, c^2$

G = shear modulus $= \frac{E}{2(1+\nu)}$

S = section modulus $= b\, A_f \left(1 + \frac{1}{6}\, \frac{A_w}{A_f}\right)$

and

$$\sigma_{cr} = \frac{M_{cr}}{S} = \sqrt{\underbrace{\frac{\frac{\pi^2\, E^2}{18(1+\nu)}}{\frac{l^2\, b^2}{d^2\,(2\,c)^2}}}_{A} \cdot \underbrace{\frac{1 + \frac{t^2}{2\, d^2}\, \frac{A_w}{A_f}}{\left(1 + \frac{1}{6}\, \frac{A_w}{A_f}\right)^2}}_{B} + \underbrace{\frac{\pi^4\, E^2}{l^4}}_{C} \cdot \underbrace{\frac{c^4}{\left(3 + \frac{1}{2}\, \frac{A_w}{A_f}\right)^2}}_{D}} \quad \ldots \quad (24)$$

The fraction B in Eq. 24 can be put equal to one. This is the case if the flange thickness d is about 1.2 times the web thickness t, and in all the cases

where the web area is negligible compared with the flange area, $A_w/A_f \sim 0$. Then the remainder A in the first term is the square of $\sigma_{cr}(v)$ (Fig. 5), because the numerator equals $(0.65\ E)^2$ using Poisson's ratio $\nu = 0.3$.

The radius of gyration r of the equivalent column composed of the compression flange and one sixth of the web is defined as $r^2 = I/A$, with

$$I = \frac{d(2\,c)^3}{12} \quad \ldots\ldots\ldots\ldots\ldots\ldots \quad (25)$$

and

$$A = A_f + \frac{1}{6}\,A_w = 2\,c\,d\left(1 + \frac{1}{6}\,\frac{A_w}{A_f}\right) \ldots\ldots\ldots\ldots \quad (26)$$

Hence,

$$\frac{r^2 = c^2}{\left(3 + \frac{1}{2}\,\frac{A_w}{A_f}\right)} \quad \ldots\ldots\ldots\ldots\ldots\ldots \quad (27)$$

The expression D in Eq. 24 can thus be interpreted as r^4, and the product of fraction C and fraction D is simply the square of $\sigma_{cr}(w)$ introduced with Fig. 5.

Ratio M_u/M_y.—With the notation defined in Fig. 3, the abbreviations $A_w = b\,t$, $\rho = A_w/A_f$, $\eta_a = y_a/b$, $\eta_b = y_b/b$, and the assumption that the flange thickness is infinitely small, the computation is as shown below:

Point A, b/t = 360.—

Neutral axis:
$$A_f\,y_b + t\,y_b\,\frac{y_b}{2} = A_f(b - y_b) + \frac{b}{12}\,t\left(\frac{23}{24}\,b - y_b\right) \ldots\ldots \quad (28)$$

$$\eta_b = \sqrt{\frac{1}{6} + \frac{7}{3\,\rho} + \frac{4}{\rho^2}} - \left(\frac{1}{12} + \frac{2}{\rho}\right) \ldots\ldots\ldots\ldots \quad (29)$$

Moment of inertia:

$$I = A_f\,y_b^2 + \frac{1}{3}\,y_b^3\,t + A_f(b - y_b)^2 + \frac{b}{12}\,t\left(\frac{23}{24}\,b - y_b\right)^2 \ldots\ldots \quad (30)$$

Section modulus:

$$S_a = \frac{I}{y_a} = \frac{A_f\,b}{1 - \eta_b}\left[\eta_b^2 + \frac{\rho}{3}\,\eta_b^3 + (1 - \eta_b)^2 + \frac{\rho}{12}\left(\frac{23}{24} - \eta_b\right)^2\right] \ldots \quad (31)$$

Ultimate moment:
$$M_u = \sigma_y\,S_a \quad \ldots\ldots\ldots\ldots\ldots\ldots \quad (32)$$

Yield moment:
$$M_y = \sigma_y\,b\,A_f\left(1 + \frac{\rho}{6}\right) \ldots\ldots\ldots\ldots\ldots \quad (33)$$

hence

$$\frac{M_u}{M_y} = \frac{\eta_b^2 + \frac{\rho}{3}\,\eta_b^3 + (1 - \eta_b)^2 + \frac{\rho}{12}\left(\frac{23}{24} - \eta_b\right)^2}{(1 - \eta_b)\left(1 + \frac{\rho}{6}\right)} \quad \ldots\ldots \quad (34)$$

Point B, b/t = 53.—

Plastic moment:
$$M_p = \sigma_y\,A_f\,b\left(1 + \frac{\rho}{4}\right) \ldots\ldots\ldots\ldots\ldots \quad (35)$$

with $M_u = M_p$

$$\frac{M_u}{M_y} = \frac{M_p}{M_y} = \frac{1 + \frac{\rho}{4}}{1 + \frac{\rho}{6}} \quad (= f = \text{"shape factor"}) \quad \ldots \quad (36)$$

Resulting in:	Value of ρ	$\beta = 360$ η_b	$\beta = 360$ M_u/M_y	$\beta = 53$ M_u/M_y
	0	0.500	1.00	1.00
	1/2	0.481	0.94	1.04
	1	0.466	0.89	1.07
	2	0.444	0.82	1.12
	3	0.430	0.77	1.17
	4	0.417	0.74	1.20
	5	0.413	0.70	1.23

The simplifying assumption of infinitely small flange thickness affects the result M_u/M_y only slightly, since both numerator and denominator are affected in the same way and thus cancel possible errors to a large extent. The

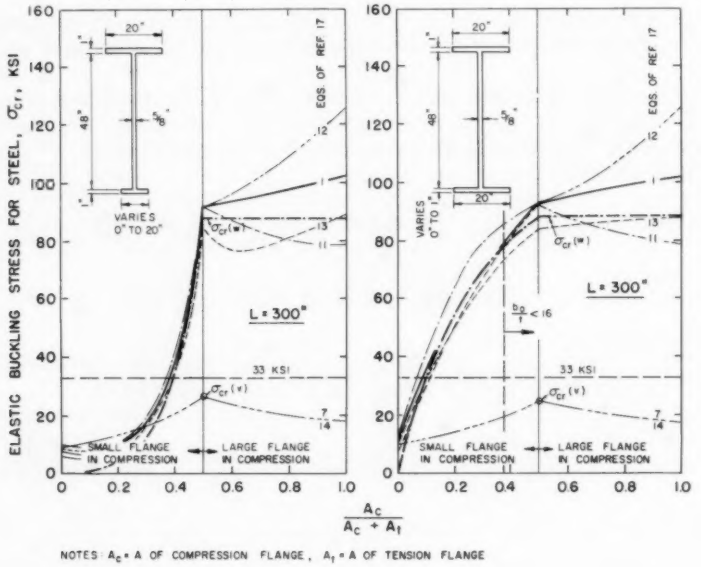

FIG. 13.—LATERAL BUCKLING STRESS $\sigma_{cr}(w)$ COMPARED WITH EXPRESSIONS OF REF. 17

same remark applies to cross sections which differ somewhat from the double symmetric I shape. Furthermore, the foregoing ratios M_u/M_y change little in the ranges of high web slenderness ratios β. Therefore, a value $\beta = 360$ appears to be appropriate also for other ratios of A_w/A_f, even though this limit of 360 is derived for $A_w/A_f = 0.5$ only.

Lateral Buckling of Unsymmetrical I-Sections.—The radius of gyration, considering the compression flange (2 c x d) and one sixth of the web (b t/6)

as a column, is

$$r^2 = \frac{I}{A} = \frac{2c^3 d}{3(2cd + bt/6)} \quad \ldots\ldots\ldots\ldots \quad (37)$$

For the example outlined in Fig. 13:

$$\sigma_{cr}(w) = \frac{\pi^2 E}{\left(\frac{l}{r}\right)^2} = \frac{9.86 \times 30{,}000}{300 \times 300} \; r^2 = 2.2 \; \frac{c^3 d}{2cd + 5} \left[\text{ksi}\right] \quad \ldots\ldots \quad (38)$$

Using the abbreviation $\kappa = \frac{A_c}{A_c + A_t}$, that is, $A_c = \frac{\kappa}{1 - \kappa} A_t$, or $cd = \frac{10\kappa}{1 - \kappa}\left[\text{in}^2\right]$,

Case $d = 1$ in., $c = \frac{10}{1 - \kappa}$ [in.], $\sigma_{cr}(w) = \frac{440\kappa^3}{(1 - \kappa)^2 (1 + 3\kappa)} \left[\text{ksi}\right]$ .... (39)

Case $c = 10$ in., $d = \frac{\kappa}{1 - \kappa}$ [in.], $\sigma_{cr}(w) = \frac{440\kappa}{1 + 3\kappa} \left[\text{ksi}\right]$ ..... (40)

These critical stresses apply for $0 < \kappa < 1/2$, while for $1/2 < \kappa < 1$, σ_{cr} is is equal to the value for $\kappa = 1/2$ as plotted in Fig. 13.

APPENDIX II.—REFERENCES

---

1. "Web Buckling Tests on Welded Plate Girders," by K. Basler, B. T. Yen, J. A. Mueller, and B. Thürlimann, Bulletin No. 64, Welding Research Council, New York, 1960.
2. "Theory of Elastic Stability," by S. Timoshenko, McGraw-Hill Book Co., Inc., New York, 1936.
3. "Buckling Strength of Metal Structures," by F. Bleich, McGraw-Hill Book Co., Inc., New York, 1952.
4. "Ausbeulen," by C. F. Kollbrunner, und M. Meister, Springer-Verlag, Berlin, Göttingen und Heidelberg.
5. "Post-Buckling Strength of Plates in Steel Design," by G. Winter, I.A.B.S.E., F. Rep., 1952, p. 268.
6. "Test of a Riveted Plate Girder with a Thin Web," by D. D. Vasarhelyi, J. C. Taylor, N. C. Vasishth, and C. Y. Yuan, Proceedings, ASCE, Vol. 86, No. ST10, October, 1960.
7. "Observations on the Behavior of Aluminum Alloy Test Girders," by R. L. Moore, Transactions, ASCE, Vol. 112, 1947, pp. 901-920.
8. "Versuchsbericht über das Ausbeulen der auf einseitigen, gleichmässig und ungleichmässig verteilten Druck beanspruchten Platten," by F. Stüssi, C. F. Kollbrunner, and M. Walt, Inst. f. Baust. a.d. E.T.H., Mitt. Nr. 25, Verlag Leemann, Zurich, 1951.

9. "Encyklopädie der Mathematischen Wissenschaften," by T. von Kármán, Vol. IV, 1910, p. 349.

10. "Effect of Small Deviations from Flatness on the Effective Width and Buckling of Plates in Compression," by P. C. Hu, E. E. Lundquist, and S. B. Batdorf, N.A.C.A., T.N. 1124, 1946.

11. "Behavior of Buckled Rectangular Plates under the Action of Shearing Forces," by St. Bergmann, Institution of Structural Engrg. and Bridge Bldg., Rep., Stockholm, 1948.

12. "Le voilement des plaques planes sollicitées dans leur plan," by C. Massonnet, A.I.P.C., Rap. f., 3e Congrès, Liège, Belgique, septembre, 1948, pp. 291-300.

13. "Compressive Buckling of Stiffened Plates," by B. H. Falconer, and J. C. Chapman, Engineer, Vol. 195, 1953, pp. 789,882.

14. "Strength of Plate Girders," by K. Basler, Ph. D. Dissertation, Mic. 59-6958, University Microfilms, Inc., Ann Arbor, Mich., October, 1959.

15. "Specification for the Design of Light Gage Steel Structural Members," Light Gage Cold-Formed Steel Design Manual, American Iron and Steel Inst., New York, 1956.

16. "Guide to Design Criteria for Metal Compression Members," Column Research Council, Univ. of Michigan, Ann Arbor, Mich., 1960.

17. "Lateral Buckling of Beams," by J. W. Clark, and H. N. Hill, Proceedings, ASCE, Vol. 86, No. ST7, July, 1960.

18. "Strength of Beams as Determined by Lateral Buckling," by K. de Vries, Transactions, ASCE, Vol. 112, 1947, pp. 1245-1271.

19. Discussion by G. Winter, D. B. Hall, T. R. Higgins, N. Van Eenam, H. N. Hill, H. D. Hussey, H. G. Brameld, E. H. Gaylord, O. G. Julian, and K. de Vries, of "Strength of Beams as Determined by Lateral Buckling," by K. de Vries, Transactions, ASCE, Vol. 112, 1947, pp. 1272-1320.

20. "Basic Column Strength," by L. S. Beedle and L. Tall, Proceedings, ASCE, Vol. 86, No. ST7, July, 1960.

21. "Plate Girder Research," by K. Basler and B. Thürlimann, Proceedings, AISC Natl. Engrg. Conf., 1959.

22. "On Inelastic Buckling in Steel," by G. Haaijer and B. Thürlimann, Proceedings, ASCE, Vol. 84, No. EM2, April, 1958.

23. "Strength of Thin Steel Compression Flanges," by G. Winter, Transactions, ASCE, Vol. 112, 1947, p. 527.

APPENDIX III.—NOMENCLATURE

A = area;

b = depth of girder;

c = half of flange width;

d = thickness of flange;

E = modulus of elasticity (30,000 ksi);

e = distance from neutral axis to extreme fiber;

f = shape factor M_p/M_y;

I = moment of inertia corresponding to r;

k = buckling coefficient;

l = buckling length of a column;

M = bending moment;

P = load on test girders (defined in Fig. 1.1 of Ref. 1);

r = radius of gyration (in lateral direction, by considering compression flange and one sixth of the web as column cross section);

S = section modulus;

t = thickness of web;

w = deflection perpendicular to the plane of the web;

X = ratio of applied strain to critical strain;

Y = nondimensionalized plate deflection;

β = ratio of web depth to web thickness = b/t;

ϵ = strain;

λ = normalized slenderness ratio;

υ = Poisson's ratio (= 0.3);

ρ = ratio between web and flange area = A_w/A_f;

σ = normal stress;

Subscripts or Superscripts:

a = above;

b = below;

cr = critical;

ex = experimental;

f = compression flange;

i = initial;

r = residual;

th = theoretical;

u = ultimate;

w = web; and

y = yielding.

Journal of the
STRUCTURAL DIVISION
Proceedings of the American Society of Civil Engineers

DISCUSSION

Note.—This paper is a part of the copyrighted Journal of the Structural Division, Proceedings of the American Society of Civil Engineers, Vol. 87, No. ST 6, August, 1961.

VARIOUS INSTABILITY MODES OF THE FIXED BASE COLUMN[a]

Closure by Donald A. Sawyer

DONALD A. SAWYER,[6] A. M., ASCE.—Larson has pointed out the writer's inaccuracy in terminology by correctly distinguishing between a "rocker" and a "roller." His derivation of the fundamental buckling load for the true roller case has extended the scope of the paper. It may be observed that an eccentric "frictionless" roller would not be permissible because any tilt of the top of the column would cause a tangential force on the roller. Fortunately, friction always exists to some degree and eccentric rollers could be tolerated in practice. It would be interesting to study the significance of friction for this case with particular attention paid to the minimum requirements for friction under various magnitudes of eccentricity.

With regard to the applicability of Eq. 34 to lift slab conditions, the writer wishes to take issue with Larson. Larson states that Eq. 34 describes a structure in which there is no lateral movement of the slab during buckling and in which there is clearance between the slab collar and the column. The writer maintains that if a condition of zero sway of the slab will result in a smaller buckling load, then the system will accommodate itself to this lower buckling mode. With respect to the clearance requirement, practical reasons dictate that a small clearance be provided, as Larson states later in his discussion. The initial buckling would occur in the small gap. After this initial buckling had closed the gap, however, a different condition would exist for which Larson's point would apply. Actually, this is an academic point, because the most critical stage of the lift occurs either at the start of the lift or at the conclusion depending on how adequately the slab is restrained from sidesway. Eq. 34 would apply to an intermediate stage of greater strength.

Larson's summary of pertinent lift slab column problems is very valuable and should serve as a starting point for further studies.

Chinn has shown that an alternate approach to the derivation of the controlling equations can be made. This approach is aptly demonstrated by his four examples that verify the answers obtained by the writer. This verification is appreciated.

Several discussions by letter offered additional references on the subject of structures loaded by links. E. C. Hartmann, F. ASCE, was kind enough to furnish an additional reference[7] as did R. L. Ketter, M. ASCE.[8] R. Dabrowski

---

[a] July, 1960, by Donald A. Sawyer (Proc. Paper 2544).

[6] Asst. Prof., Univ. of Florida, Gainesville, Fla.

[7] "Buckling of Struts: Two Cases Giving Abnormally Low Loads," by H. L. Cox and D. L. R. Bailey, Engineering, March 14, 1952, p. 340.

[8] Stahlbau, Ein Handbuch fur Studium und Praxis, Vol. 1, Verlags-GMBH, Koln, 1956.

sent a copy of another reference[9] which is concerned with frames loaded by positive and negative links. Finally, Bruce Johnston, F. ASCE, wished to point out that his lectures at the University of Florida gave reference to a series of letters and other data published in Engineering News Record.[10-14] The general nature of these additional references reinforces the writer's original statement that the link-loaded column has appeared rather obscurely in the literature.

9 "Knicksicherheit des Portalrahmens bei eintretender Richtungsanderung im Lastangriff," by R. Dabrowski, Der Bauingenieur, Vol. 35, No. 5, 1960, p. 178.

10 "Bridge Collapse Traced to Rockers," Anonymous, Engineering News-Record, June 19, 1952, p. 28.

11 "Learning from Accidents," Editorial, Engineering News-Record, July 3, 1952, p. 128.

12 "How Careless!," by A. K. Wetzig, Engineering News-Record, July 17, 1952, p. 10, Reader Comment.

13 "Controversial Rocker," by T. P. Young, Engineering News-Record, July 24, 1952, p. 10, Reader Comment.

14 "Was Viaduct Support Stable?," by R. M. Boynton, Engineering News-Record, August 7, 1952, p. 7, Reader Comment.

DYNAMIC RESPONSE OF ELASTO-PLASTIC FRAMES[a]

Closure by Joseph Penzien

JOSEPH PENZIEN,[6] M. ASCE.—As pointed out by Eremin the elasto-plastic characteristics of secondary components such as walls, partitions, stair wells, and so forth, as well as their stiffness and strength characteristics provide the apparent ability of many existing structures to withstand strong motion earthquakes. This important point was, of course, a general conclusion reached by Blume in a previous paper.[3]

Eremin has expressed interest in a "repeated stress-strain loop that resulted from a dynamic vibrating force" and has raised the question regarding recovery time of steel when strained plastically. It is interpreted by the writer that he is concerned with time-effects on the stress-strain properties of steel. These effects as reported in the literature can be important if strain rates are sufficiently high. The time between repeated stress-strain loops can be estimated approximately from the elastic response of a low damped single degree system to a random type of input such as used in this investigation. Such response is an oscillation near its own natural frequency that has an amplitude envelope and phasing that change in a random fashion. When plastic deformation is allowed in the system, the time interval between repeated stress-strain loops will become somewhat larger depending on the degree of plastic deformation allowed. If one is studying the dynamic response of a specific structure or element that has sufficiently high frequency response characteristics, then time effects on stress-strain properties of materials cannot always be ignored. In the general investigation reported by the writer no attempt was made to allow for such effects because the primary purpose of the investigation was to show the gross effect that inelastic deformations have on dynamic response.

Eremin's comment regarding the effect of damping on dynamic stresses in his comparison of the results in Figs. 5 to 12 with the results in Fig. 13 appears perhaps to be a misinterpretation of these results. First, it must be understood that the forcing function used in obtaining the results of Figs. 5 to 12 was the El Centro ground acceleration whereas the forcing function used in obtaining the results of Fig. 13 was a harmonic forcing function whose frequency coincided exactly with the natural frequency of the system. Secondly, the abscissa in Figs. 5 to 12 represents period T whereas in Fig. 13 it represents the strength ratio θ. In each case (in which $\lambda = 0$), it is observed that the maximum response must reach a sufficiently high level over the elastic response so that the energy fed into the system can be absorbed. This observation as well as others are considered to be consistent throughout Figs. 5 to 13.

---

[a] July, 1960, by Joseph Penzien (Proc. Paper 2545).

[6] Assoc. Prof. of Civ. Engrg., Univ. of California, Berkeley, Calif.

Blume has discussed the importance of separating the amount of attenuation received from viscous damping and inelastic deformation. This separation can be done in all cases even for those cases involving damping at 0.05, 0.10, and 0.15 of critical, because Curves No. 2 in Figs. 8, 10, and 12 also represent those cases of an infinite yield point with damping of 0.05, 0.10, and 0.15 of critical, respectively. Therefore, it is to be observed that these curves show the attenuation due to viscous damping only and that Curves 2 through 4 in Figs. 5 through 7 show the attenuation due to inelastic deformations only. The attenuation shown by most of the remaining curves includes that due to both viscous damping and inelastic deformation.

The writer is in complete agreement with Blume's excellent appraisal of the needs for future research, both analytical and experimental, in the general field of inelastic response of structures to strong-motion earthquakes. Many answers are still needed before the structural designer can properly consider the possiblity of having inelastic deformations in earthquake resistant structures.

Errata.—On page 85, in the second part of Eq. 8, $\ddot{U}\tau$ should be changed to $\ddot{\bar{U}}\tau$. On page 92, in the seventh line preceding CONCLUSIONS, u_{go}/ω^2 should be changed to $\ddot{u}_{go}/\omega^2$. On page 94, in line 1, Housner should be changed to Houser.

FREEZING AND THAWING EFFECTS ON PRESTRESSED CONCRETE[a]

Closure by M. J. Gutzwiller and F. E. Musleh

M. J. GUTZWILLER,[13] M. ASCE, and F. E. MUSLEH,[14] A. M. ASCE.—It should be pointed out that all of the mixes were designed to have an air content of 4% ± 2%. The main purpose of the tests was not to compare the durability of the different strengths of concrete but rather to examine the effect of the prestressing on the durability of a particular strength of concrete, namely 5,000 psi. The results of the 5,000 psi plain concrete versus the 5,000 psi prestressed concrete, as tabulated in Table 3 and Table 4, clearly show that the durability was increased by the prestressing.

The results shown in Table 3 do show, as pointed out by Kunze, that the 3,000 psi plain concrete (if specimen D-2 was omitted) has a higher durability factor than the 5,000 psi plain concrete, or 5,000 psi prestressed concrete. The writers feel that the data obtained in this study are too limited to draw a general conclusion on comparison of concrete durability of different mixes. Within the range of variables in this experiment, it can be said that the richer mix showed a slightly higher rate of deterioration than the leaner mix.

---

[a] October, 1960, by M. J. Gutzwiller and F. E. Musleh (Proc. Paper 2633).
[13] Prof. of Structural Engrg., Purdue Univ., Lafayette, Ind.
[14] Design Engr., Pierce, Gruber and Beam, Inc., Indianapolis, Ind.

FLOW GRAPHS IN STRUCTURAL ANALYSIS[a]

Closure by Kurt H. Gerstle

KURT H. GERSTLE,[8] M. ASCE.—Thanks are extended to Su for his interesting comments. A review of electrical engineering literature shows various practical applications of the proposed technique in that field; it is hoped that applications may also be forthcoming in the field of structural mechanics.

---

[a] October, 1960, by Kurt H. Gerstle (Proc. Paper 2634).
[8] Assoc. Prof. of Civ. Engrg., Univ. of Colorado, Boulder, Colo.

CONCEPTS OF STRUCTURAL SAFETY[a]

Discussion by George B. Begg, Jr.

GEORGE B. BEGG,[32] JR., M. ASCE.—This paper has contributed valuable insights into the sociotechnical problems in structural safety confronting the present-day designer. Brown strongly develops the need of integrating broad economic viewpoints with the technical approach to structural-design assumptions. To admit and welcome a dialogue with participants from disciplines other than the design office, university, and testing laboratory is a long overdue innovation. However, this writer doubts that the question is currently as "open" as the author infers in his paragraphs on "Structural Life."

Brown suggests that the design of a static structure may be approached on either the "definite life span" or "monumental" basis. Limiting comment to the design of buildings and hydraulic structures, the writer has seldom observed the definite life span as operative nor does there seem to be any gathering demand for it in the future.

To document this position the writer would like to discuss the problem of vertical extensions in buildings in which no such provisions were contemplated in the original design. The unprovided for vertical extension is deliberately chosen because of the great demands it makes on concepts of structural safety. In a more subtle, but just as real, way it offers considerable challenge to the definite life span assumption.

Many large design offices are frequently requested to prepare feasibility studies on proposed vertical extensions to existing buildings. Such studies require the combined appraisal of the architect, mechanical engineer, estimator, and structural engineer. From a structural viewpoint the request essentially inquires, "Can we put one, two, or three stories on this structure for such and such live loads?" Usually the structural engineer is told by those concerned with the operation and funding of the project that the vertical extension is functionally the only desired area and if we cannot have it there we probably cannot afford it.

Confining structural comments to the context of this paper, several features reoccur in these feasibility studies:

Age of Structure.—The buildings under consideration most often fall in the 20 yr to 50 yr old age bracket. This means that they are experiencing the author's "fatigue, wear, and corrosion [that] necessitates a definite life to a structure." Thus, whereas the vertical extension is modern, the base struc-

---

[a] December, 1960, by C. B. Brown (Proc. Paper 2678).

[32] Chf., Design and Investigation Sect., Structural Engrg. Branch, Pub. Buildings Service, Washington, D. C.

ture is often groaning under the service of years with the accompanying increasing maintenance and decreasing productivity.

The Design-Functional Records of the Structure.—In this area let us consider a specific design office. The Public Buildings Service (and its predecessor agencies) is over 100 yr old. As a matter of policy, and vindicated by experience, the structural engineering records have always been maintained at a high degree of completeness - perhaps unequalled in any other structural design office. Therefore, in a feasibility study we can utilize the original design computations, working drawings, field reports made during construction, and building management history in reaching our conclusions. However, in employing these extensive documents, the ability to understand the existing structure is often limited by:

a. Conflicting Data.—The results of a design computation may be contradicted by the requirements of the contract drawing.

b. Operational History.—The design assumptions and execution often appear satisfactory, but a building superintendent can be continuously reporting extensive but unanalyzed cracks and deflections.

c. Absence of Original Design Team.—Computations and drawings that were crystal clear to a designer preparing them 30 yr ago, can confuse a later investigator, particularly where a vital assumption was not explicitly recorded. The absence of the original design team is pertinent to this discussion because it precludes any documented position on the proposed life span of the structure.

Investigator - Client Relationship.—Two important ground rules governing feasibility studies should be recognized herein. The first is that such studies are invariably limited in time - with the resulting value judgments on what to investigate and how far. The second rule to remember is that the structural engineer is usually not the dominant voice in the final decision - nor should he be. Generally, the client asks what he thinks is a simple question only to receive a very complex answer or a series of countering questions. And the answer or the questions rarely have a unified note. When confronted by a positive answer from his architect, mechanical engineer, and estimator the client is hardly in the right psychological mood to follow "definite life span" theorizing from his structural engineer. In those cases in which the structural engineer is swimming against the tide, it is usually necessary to pursue a factual but simplified argument aimed at the common denominator, for example "the existing foundation system will not accept even a minor part of the new loads that will result from the proposed extension."

The preceding review of vertical extensions in the advanced life of a building leads to some questions. A similar group of questions would have emerged if remodeling instead of extension had been developed. The writer is convinced that the answers to the following questions are either implicitly stated in Brown's paper or naturally grew out of it:

1. Safety.—How do we provide for safety in a structure that is substantially altered late in its operational life? Or again, what modification of variables as developed in the discussion of the ratio and probability methods is required for a vertical extension that uses new materials and stresses and is executed by a new design team but rests on an old structure that was not designed for it? And what probability of such occurrance should be assigned in a new design?

2. The Definite Life Span Assumption.—Can a definite life span design hope to compete with the monumental design in building in the future? Will the client agree (except in an unusual speculative case) to a building that is designed to be replaced in a specific number of years? Why should we look for a leveling-off of the current practice of vertical and horizontal extensions plus remodeling? If the public in general is to participate in judging the design assumption, what type of preliminary agreement on terminology and premises must the design team agree on? Should the architect or the engineer be the moderator in the developing dialogue?

LATERAL INELASTIC BUCKLING OF TIED ARCHES[a]

Discussion by M. Gregory

M. GREGORY.[9]—The author has presented an interesting paper on the lateral inelastic buckling of a tied arch. It is quite permissible to make a Southwell Plot on the observed lateral deflections in the inelastic range. An upward curving line is expected, as shown in Fig. 6, but how one should interpret the inverse slope of this curve (and it varies considerably from one end of the curve to the other) in terms of the critical load, is difficult to say. If it is realized that the tangent-modulus critical load is a property of an inelastic structure possessing no initial imperfections either of form or of loading, one would expect some agreement between the critical load and the practical behavior of the structure under load only if its imperfections were extremely small, in fact much smaller than in the case of a linearly elastic structure. This is why the test specimens had to be "of greater perfection than is necessary with those that buckle in the elastic range." One should not expect agreement in practical cases, though it is interesting to note some small measure of agreement when imperfections are minimized, as the author has carefully shown.

The author would agree that it should not be thought that the tangent-modulus critical load furnishes a solution to all inelastic instability problems. It is still a critical load, a property of the perfect structure. The problem of the practical structure is much more difficult and intractable. It is basically a problem of strain configuration (as is indeed emphasized even in the philosophy one uses in discussing the relevance of the tangent modulus). To obtain vital fundamental information on this problem it would be useful to measure strains at critical points as the arch is loaded, in order to know which portion of the stress-strain curve applied at any stage of the loading.

---

[a] January, 1961 by Chin Fung Kee (Proc. Paper 2704).

[9] Senior Lecturer in Civ. Engrg., Univ. of Tasmania; Nuffield Foundation Fellow visiting the Univ. of Cambridge, Cambridge, England.

SAFETY, RELIABILITY AND STRUCTURAL DESIGN[a]

Discussion by Jack R. Benjamin and Theodore C. Zsutty

JACK R. BENJAMIN,[10] M. ASCE, and THEODORE C. ZSUTTY[11] —This most interesting paper contains many general concepts of great value in structural engineering. The paper is concerned with important aspects of the mathematical theory of probability. It must be understood that decisions cannot be rationally made purely on the theory of probability. Two equally important additional bodies of theory must be considered. First, the statistical nature of the problem must be solved. This involves the values of parameters, fit of distributions, hypothesis tests, and forecasting concepts, among other items. Finally, the making of rational decisions demands the use of decision theory. Probability supplies the initial mathematical framework, statistics interprets nature, and decision theory adds value concepts.

In probability studies it must be emphasized that if R and S are random variables, ν and P_F are also random variables. The computation of a mean, $\bar{\nu}$, Fig. 2, is only the first step. The variance of ν and associated P_F is actually more critical in the decision analysis than the characteristic long run value. Finally, real structures involve many modes of behavior each with its own ν and P_F. These structures can be designed to a constant ν or a constant P_F. The two designs differ significantly. It can be readily shown that constant P_F may involve widely varying load factors throughout the structure. Thus current load factors, based on judgment, cannot possibly yield a structure with constant probability of failure unless it is a simple beam under one loading condition. Even two independent loads applied to a simple beam demands two different load factors to maintain a constant probability of failure. The differences in the variances of the loads and resistance are responsible for the phenomena.

The first basic question of how to determine a realistic probability distribution of load must be resolved. The log-normal distribution for loads is convenient for computation purposes, but it has certain characteristics that restrict its use in real situations. First, the distribution is limited at zero load rather than at a constant dead load of major magnitude. The "Weibull distribution" might be used to overcome this difficulty. Second, the tail of the log-normal is very extensive; a consition that gives forecasts of very large loads. Elements of control always exist with man-made loads and, thus, forecasting from sample data for these loads into regions of low probability is hazardous indeed. A similar difficulty applies also to extreme value distributions when small data samples, are used to estimate the parameters of the distribution. The small data sample has basic limitations of description such that the accu-

[a] March, 1961, by A. M. Freudenthal (Proc. Paper 2764).

[10] Prof. of Structural Engrg., Stanford Univ., Stanford, Calif.

[11] Asst. Prof. of Civ. Engrg., San Jose State College, San Jose, Calif.

rate estimation of parameters required for forecasting is not possible. Also, the variance of a forecast is made up of the population variance plus the sampling variance of estimated value. The sampling variance increases as the magnitude of the forecasted load increases beyond the range of values in the data simple. Until these variances are considered and confidence limits established, the equations, charts, and tables given in terms of theoretical distributions will remain as exercises in mathematics without practical use. It should be noted that ν and P_F are forecasts.

The second basic question of how to determine the distribution of structural resistance has a better chance of being answered because many test records of resistance of structural elements are available. In order to use probability of failure as a basis for design it will be necessary to have a formula that will predict some central value such as the mean of the resistance of a structural element and that has a known probability distribution of the population of resistance values about this central value. The confidence intervals of the predicted central value and the distribution parameters should also be known. It is doubtful whether any of the present formulas for resistance accurately predict a central value, and if it is even more doubtful if anything is accurately known about the distribution of actual values about the predicted value. If records of a large number of widely varied tests of resistance of a structural element are available, one way of obtaining the required formula is by the empirical methods of multiple regression analysis and dimensional analysis. In the event that empirical methods prove to be the only way of obtaining the formulas for resistance, then a large program of testing, guided by the principles of experimental design, will be required for nearly all structural elements. In conjunction with this program, studies are required to determine the variation and covariation of member dimensions and strengths due to workmanship errors.

The implication that the probability distribution of resistance of a structural element is the same as that of the material of which it is composed may be highly erroneous in practical cases. For example, the ultimate moment of an under-reinforced concrete beam is quite insensitive to large variations of its concrete cylinder strength. Even if the concrete strength has an extremal distribution due to poor quality control, there is no reason to believe that the ultimate moment resistance has the same extremal distribution. Similarly there is no justification to assume that a steel beam, which contains many residual fabrication stresses and points of stress concentration, would have a distribution of plastic moment resistance the same as that of a yield strength specimen of the same steel. In general, each structural element may have a distribution of resistance that differs from that of tests of its base material or materials.

The author is to be congratulated on his continued pioneering effort. The writers believe insufficient data are presently available to allow rational structural design using statistical concepts. However, it is time that the long-range educational process toward this goal be initiated; this paper is an outstanding step in that direction.

PROCEEDINGS PAPERS

The technical papers published in the past year are identified by number below. Technical-division sponsorship is indicated by an abbreviation at the end of each Paper Number, the symbols referring to: Air Transport (AT), City Planning (CP), Construction (CO), Engineering Mechanics (EM), Highway (HW), Hydraulics (HY), Irrigation and Drainage (IR), Pipeline (PL), Power (PO), Sanitary Engineering (SA), Soil Mechanics and Foundations (SM), Structural (ST), Surveying and Mapping (SU), and Waterways and Harbors (WW), divisions. Papers sponsored by the Department of Conditions of Practice are identified by the symbols (PP). For titles and order coupons, refer to the appropriate issue of "Civil Engineering." Beginning with Volume 82 (January 1956) papers were published in Journals of the various Technical Divisions. To locate papers in the Journals, the symbols after the paper number are followed by a numeral designating the issue of a particular Journal in which the paper appeared. For example, Paper 2703 is identified as 2703(ST1) which indicates that the paper is contained in the first issue of the Journal of the Structural Division during 1961.

VOLUME 86 (1960)

AUGUST: 2564(SM4), 2565(EM4), 2566(ST8), 2567(EM4), 2568(PO4), 2569(PO4), 2570(HY8), 2571(EM4), 2572(EM4), 2573(EM4), 2574(SM4), 2575(EM4), 2576(EM4), 2577(HY8), 2578(EM4), 2579(PO4), 2580 (EM4), 2581(ST8), 2582(ST8), 2583(EM4)[c], 2584(PO4)[c], 2585(ST8)[c], 2586(SM4)[c], 2587(HY8)[c].

SEPTEMBER: 2588(IR3), 2589(IR3), 2590(WW3), 2591(IR3), 2592(HW3), 2593(IR3), 2594(IR3), 2595(IR3), 2596 (HW3), 2597(WW3), 2598(IR3), 2599(WW3), 2600(WW3), 2601(WW3), 2602(WW3), 2603(WW3), 2604(HW3), 2605(SA5), 2606(WW3), 2607(SA5), 2608(ST9), 2609(SA5)[c], 2610(IR3), 2611(WW3)[c], 2612(ST9)[c], 2613(IR3)[c], 2614(HW3)[c].

OCTOBER: 2615(EM5), 2616(EM5), 2617(ST10), 2618(SM5), 2619(EM5), 2620(EM5), 2621(ST10), 2622(EM5), 2623(SM5), 2624(EM5), 2625(SM5), 2626(SM5), 2627(EM5), 2628(EM5), 2629(ST10), 2630(ST10), 2631(PO5)[c], 2632(EM5)[c], 2633(ST10), 2634(ST10), 2635(ST10)[c], 2636(SM5)[c].

NOVEMBER: 2637(ST11), 2638(ST11), 2639(CO3), 2640(ST11), 2641(SA6), 2642(WW4), 2643(ST11), 2644(HY9), 2645(ST11), 2646(HY9), 2647(WW4), 2648(WW4), 2649(WW4), 2650(ST11), 2651(CO3), 2652(HY9), 2653(HY9), 2654(ST11), 2655(HY9), 2656(HY9), 2657(SA6), 2658(WW4), 2659(WW4)[c], 2660(SA6), 2661(CO3), 2662(CO3), 2663(SA6), 2664(CO3)[c], 2665(HY9)[c], 2666(SA6)[c], 2667(ST11)[c].

DECEMBER: 2668(ST12), 2669(IR4), 2670(SM6), 2671(IR4), 2672(IR4), 2673(IR4), 2674(ST12), 2675 (EM6), 2676(IR4), 2677(HW4), 2678(ST12), 2679(EM6), 2680(ST12), 2681(SM6), 2682(IR4), 2683(SM6), 2684(SM6), 2685(IR4), 2686(EM6), 2687(EM6), 2688(EM6), 2689(EM6), 2690(EM6), 2691(EM6)[c], 2692 (ST12), 2693(ST12), 2694(HW4)[c], 2695(IR4)[c], 2696(SM6)[c], 2697(ST12)[c].

VOLUME 87 (1961)

JANUARY: 2698(PP1), 2699(PP1), 2700(HY1), 2701(SA1), 2702(SU1), 2703(ST1), 2704(ST1), 2705(SU1), 2706 (HY1), 2707(HY1), 2708(HY1), 2709(PO1), 2710(HY1), 2711(HY1), 2712(ST1), 2713(HY1), 2714(PO1), 2715 (ST1), 2716(HY1), 2717(SA1), 2718(SA1), 2719(SU1)[c], 2720(SA1)[c], 2721(ST1), 2722(PP1)[c], 2733(PO1)[c], 2724 (HY1)[c], 2725(ST1)[c].

FEBRUARY: 2726(WW1), 2727(EM1), 2728(EM1), 2729(WW1), 2730(WW1), 2731(EM1), 2732(SM1), 2733(WW1), 2734(SM1), 2735(EM1), 2736(EM1), 2737(PL1), 2738(PL1), 2739(PL1), 2740(PL1), 2741(EM1), 2742(ST2), 2743(EM1), 2744(WW1), 2745(WW1), 2746(SM1), 2747(WW1), 2748(EM1), 2749(WW1), 2750(WW1)[c], 2751 (EM1)[c], 2752(SM1)[c], 2753(PL1)[c], 2754(ST2)[c], 2755(PL1).

MARCH: 2756(HY2), 2757(IR1), 2758(AT1), 2759(CO1), 2760(HY2), 2761(IR1), 2762(IR1), 2763(HY2), 2764 (ST3), 2765(HY2), 2766(HW1), 2767(SA2), 2768(CO1), 2769(IR1), 2770(HY2), 2771(SA2), 2772(HY2), 2773 (CO1), 2774(AT1), 2775(IR1), 2776(HY2), 2777(HY2), 2778(SA2), 2779(ST3), 2780(HY2), 2781(HY2)[c], 2782 (HW1)[c], 2783(SA2)[c], 2784(CO1), 2785(CO1)[c], 2786(IR1)[c], 2787(ST3)[c], 2788(AT1)[c], 2789(HW1).

APRIL: 2790(EM2), 2791(SM2), 2792(SM2), 2793(SM2), 2794(SM2), 2795(SM2), 2796(SM2), 2797(SM2), 2798 (EM2), 2799(EM2), 2800(EM2), 2801(EM2), 2802(ST4), 2803(EM2)[c], 2804(SM2)[c], 2805(ST4)[c].

MAY: 2806(SA3), 2807(WW2), 2808(HY3), 2809(WW2), 2810(HY3), 2811(WW2), 2812(HY3), 2813(WW2), 2814(HY3), 2815(WW2), 2816(HY3), 2817(HY3), 2818(SA3), 2819(WW2), 2820(SA3), 2821(WW2), 2822 (WW2)[c], 2823(HY3), 2824(SA3), 2825(HY3), 2826(SA3)[c], 2827(HY3)[c].

JUNE: 2828(SM3), 2829(EM3), 2830(EM3), 2831(IR2), 2832(SM3), 2833(HW2), 2834(IR2), 2835(EM3), 2836 (IR2), 2837(IR2), 2838(SM3), 2839(SM3)[c], 2840(IR2)[c], 2841(HW2)[c], 2842(EM3)[c], 2843(ST5), 2844(ST5), 2845 (ST5), 2846(ST5)[c].

JULY: 2847(PO2), 2848(SU2), 2849(HY4), 2850(PO2), 2851(HY4), 2852(PO2), 2853(SU2), 2854(HY4), 2855 (PO2), 2856(PO2), 2857(PO2), 2858(SA4), 2859(SU2), 2860(SA4), 2861(PO2), 2862(SA4), 2863(HY4), 2864 (HY4), 2865(HY4), 2866(HY4), 2867(HY4), 2868(PO2)[c], 2869(SA4)[c], 2870(SU2)[c], 2871(HY4), 2872(HY4)[c], 2873(SU2), 2874(SA4).

AUGUST: 2875(WW3), 2876(WW3), 2877(WW3), 2878(SM4), 2879(ST6), 2880(EM4), 2881(SM4), 2882(EM4), 2883(WW3), 2884(EM4), 2885(SM4), 2886(WW3), 2887(EM4), 2888(WW3), 2889(AT2), 2890(AT2), 2891 (AT2), 2892(AT2), 2893(AT2), 2894(AT2), 2895(AT2), 2896(AT2), 2897(AT2), 2898(AT2), 2899(AT2), 2900 (AT2), 2901(AT2), 2902(SM4), 2903(ST6), 2904(ST6), 2905(SM4), 2906(ST6), 2907(EM4), 2908(ST6), 2909 (EM4), 2910(ST6), 2911(EM4), 2912(SM4), 2913(ST6), 2914(WW3)[c], 2915(ST6)[c], 2916(EM4)[c], 2917(SM4)[c].

c. Discussion of several papers, grouped by divisions.

AMERICAN SOCIETY OF CIVIL ENGINEERS

OFFICERS FOR 1961

PRESIDENT

GLENN W. HOLCOMB

VICE-PRESIDENTS

Term expires October 1961:
CHARLES B. MOLINEAUX
LAWRENCE A. ELSENER

Term expires October 1962:
DONALD H. MATTERN
WILLIAM J. HEDLEY

DIRECTORS

Term expires October 1961:
THOMAS J. FRATAR
EARL F. O'BRIEN
DANIEL B. VENTRES
CHARLES W. BRITZIUS
WAYNE G. O'HARRA
FRED H. RHODES, JR.
N. T. VEATCH

Term expires October 1962:
ELMER K. TIMBY
SAMUEL S. BAXTER
THOMAS M. NILES
TRENT R. DAMES
WOODROW W. BAKER
BERNHARD DORNBLATT

Term expires October 1963:
ROGER H. GILMAN
HENRY W. BUCK
EARLE T. ANDREWS
C. MERRILL BARBER
JOHN D. WATSON
HARMER E. DAVIS

PAST PRESIDENTS

Members of the Board

FRANCIS S. FRIEL
FRANK A. MARSTON

EXECUTIVE SECRETARY
WILLIAM H. WISELY

TREASURER
E. LAWRENCE CHANDLER

ASSISTANT SECRETARY
DON P. REYNOLDS

ASSISTANT TREASURER
LOUIS R. HOWSON

PROCEEDINGS OF THE SOCIETY

HAROLD T. LARSEN
Manager of Technical Publications

PAUL A. PARISI
Editor of Technical Publications

MARVIN L. SCHECHTER
Associate Editor of Technical Publications

IRVIN J. SCHWARTZ
Assistant Editor of Technical Publications

COMMITTEE ON PUBLICATIONS

THOMAS M. NILES, *Chairman*

WAYNE G. O'HARRA, *Vice-Chairman*

BERNHARD DORNBLATT
HENRY W. BUCK
JOHN D. WATSON
HARMER E. DAVIS